Optimal Operation of Industrial Batch Crystallizers

A Nonlinear Model-based Control Approach

Ali Mesbah

Cover design: Ardavan Khorsand

OPTIMAL OPERATION OF INDUSTRIAL BATCH CRYSTALLIZERS

A Nonlinear Model-based Control Approach

PROEFSCHRIFT

ter verkrijging van de graad van doctor
aan de Technische Universiteit Delft,
op gezag van de Rector Magnificus prof. ir. K.C.A.M. Luyben,
voorzitter van het College voor Promoties,
in het openbaar te verdedigen op

vrijdag 10 december 2010 om 10:00 uur

door

Ali MESBAH

scheikundig ingenieur
geboren te Tehran, Iran

Dit proefschrift is goedgekeurd door de promotor:
Prof. dr. ir. P. M. J. Van den Hof

Copromotor: Dr. ir. H. J. M. Kramer

Samenstelling promotiecommisie:

Rector Magnificus,	voorzitter
Prof. dr. ir. P. M. J. Van den Hof,	Technische Universiteit Delft, promotor
Dr. ir. H. J. M. Kramer,	Technische Universiteit Delft, copromotor
Prof. ir. O. H. Bosgra,	Technische Universiteit Delft
Prof. ir. J. Grievink,	Technische Universiteit Delft
Prof. dr. ir. A. C. P. M. Backx,	Technische Universiteit Eindhoven
Prof. dr. Z. K. Nagy,	Loughborough University, UK
Dr. ir. S. K. Bermingham,	Process Systems Enterprise Ltd, UK

Ir. A. E. M. Huesman heeft als begeleider in belangrijke mate aan de totstandkoming van het proefschrift bijgedragen.

This dissertation has been completed in partial fulfillment of the requirements of the dutch institute of systems and control (disc) for graduate studies.

The work presented in this thesis was financially supported by SenterNovem, Dutch Ministry of Economic Affairs, within the CryPTO project (EUREKA / IS-project E! 3458 / IS043074).

ISBN: 978-90-9025844-7

Printed in the Netherlands by CPI Wöhrmann Print Service

To my parents, may I always be so fortunate as to be so loved...

Acknowledgments

Looking back at the past four years, I feel deeply indebted to many people, in one way or another, for their encouragement and advice. Without this support, the successful completion of this thesis would surely have been impossible.

First, I wish to thank my supervisors Paul Van den Hof, Herman Kramer, and Adrie Huesman for their friendship and guidance. I am grateful to you for the numerous fruitful discussions we had in the course of past years. I greatly appreciate the freedom I was given to carry out my PhD research. Adrie, I heavily relied on your constructive pieces of advice, which were always put in an understandable form. Herman, I wish to thank you for your readiness to discuss problems of any kind. Your sense of humor turned the 'bumpy road' of my research into a memorable experience. Paul, I particularly owe you for shedding light on my scientific quest. You taught me 'what research really means', for which I will always remain thankful to you.

I would also like to express my sincere gratitude to other people who made this work possible. I am grateful to my predecessor Alex Kalbasenka, whose support during the first few months of my PhD research allowed me to get a good grasp of the project. I wish to thank Jeffrey Landlust for the insightful discussions and also his assistance in real-time implementation of the controllers. I am thankful to Jobert Ludlage, Cornè Versteeg, Matthias Rauls, Johan Grievink, and Sean Bermingham for our regular technical meetings, which were very beneficial to my PhD research. I am greatly indebted to Professor Zoltan Nagy from Loughborough University for providing me with the opportunity of having a productive collaboration. Finally, the special thanks goes to my colleagues and the support staff at DCSC and P&E, particularly the fellow crystallization team members: Richard, Widya, Somnath, Ana, and Marco.

Last but not least, I wish to thank my ever best friends, Peyman, Mohammad, and Ali, for their encouragement throughout these years; and my parents and sister for their unconditional love and support.

Ali Mesbah
Delft, November 2010

Contents

1 CHAPTER

Introduction

The process of scientific discovery is, in effect, a continual flight from wonder.

Albert Einstein

Optimal operation of industrial batch crystallizers is becoming a prerequisite for fulfilling the stringent requirements of the consumer-driven market of high value-added crystalline products. Control of batch crystallizers has received substantial attention in academia as well as industry. Recent developments in measurement and computing technologies have led to ample opportunities for optimal operation of batch crystallizers. After introducing the principles of batch crystallization, this chapter presents a short review on the state-of-the-art in control of these processes. Subsequently, the primary challenges in control of industrial batch crystallizers are addressed. This essentially builds up the platform to formulate the problem statement dealt with throughout this thesis. The chapter is concluded with the outline of this thesis.

1.1 Batch crystallization

Crystallization is the formation of a material in the solid state, where the molecules are arranged in a regular pattern (Larsen et al. 2006). The crystalline material is formed from a fluid phase, making crystallization a core separation and purification technology in major sectors of chemical process industries. The merits of crystallization lie in producing high purity products in one processing step at relatively mild process conditions. In addition, crystallization processes require a relatively low level of energy consumption.

The vast majority of crystallization operations are performed in batch mode. Batch processes are most suitable when the production volumes are low, when isolation is necessary, e.g., for sterility or safety, and when frequent changeovers

are required (Srinivasan et al. 2003). With the stringent regulations and requirements in manufacturing of crystalline products, there has been a great interest in advanced control of batch crystallizers over the past decade.

1.1.1 Significance of batch crystallization

The amount and variety of particulate crystalline products is enormous. According to Christofides et al. (2008), 60 % of the end products in the chemical industry are manufactured as particulate solids with an additional 20 % using powders as ingredients.

Batch crystallization is widely used in the chemical, pharmaceutical, and food industries to separate and purify high value-added chemical substances. The significance of batch crystallization processes can be illustrated by the global market trends of pharmaceutical and semiconductor industries, amongst others. The pharmaceutical and semiconductor industries reported revenues of US$712 billion and US$255 billion in 2007, respectively (PRLog; In-Stat). The global pharmaceutical industry is expected to earn over US$1 trillion in revenues by 2012, whereas the semiconductor industry would surpass US$340 billion in revenues in 2012. These figures clearly indicate the ever-increasing economic value and societal benefits of batch crystallization processes in various high value-added sectors of global markets.

1.1.2 Principles of crystallization

Crystallization products can be formed from a solution, a vapor or a melt. This thesis deals with solution crystallization, which is the most used crystallization process in the chemical industry. The quality of a crystalline material produced in a solution crystallization process is often characterized in terms of crystal size distribution (CSD), purity, crystal shape, and polymorphic state. The driving force of the process is *supersaturation* of the solution. Supersaturation is a key variable in the process that governs crystallization kinetics and therefore largely influences the product quality.

In solution crystallization, the degree of supersaturation is defined as the difference in chemical potential between the solute molecules in the solution and the solid phase (Jones 2002). In most cases, the degree of supersaturation can be approximated by the difference between the solute concentration and the *solubility* of the compound (Mersmann 2001)

$$\Delta C = C(T) - C^*(T), \tag{1.1}$$

where C is the solute concentration; T is the temperature; C^* is the saturation concentration of solute, namely the solubility. Solubility is the equilibrium concentration of the solute in the solvent at the given process conditions. In an *undersaturated solution* the concentration of dissolved materials is lower than the solubility,

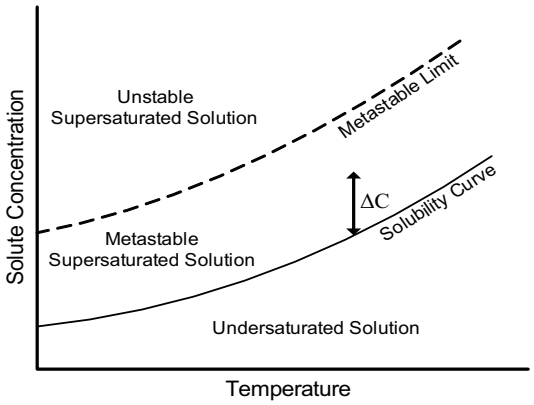

Figure 1.1: The phase diagram.

whereas a *saturated solution* is in equilibrium with excess of the solute present in the solution (Myerson 2002).

A crystallization process can be elucidated by the phase diagram shown in Figure 1.1. The phase diagram provides a schematic representation of the *solubility curve* and the supersaturated zones. The solubility curve depicts the variation of saturation concentration with solution temperature. According to Ostwald (1897), the phase diagram can be divided into three distinct regions (Jones 2002):

1. *undersaturated zone* - the crystals present in the solution will dissolve, making crystallization infeasible;

2. *metastable supersaturated zone* - a supersaturated region that accommodates the growth of crystals in the absence of spontaneous nucleation of the solution;

3. *unstable supersaturated zone* - a region, in which the solution nucleates spontaneously.

It is evident that the supersaturation state is essential for any crystallization process to occur.

A crystallization process is actuated by manipulating the supersaturation generation mechanisms. Supersaturation can be created by lowering the solubility through cooling and addition of antisolvent or by increasing the solute concentration through evaporation of the solvent. Supersaturation governs kinetic phenomena such as nucleation, crystal growth, and agglomeration that in turn determine the product quality and the process productivity. A common practice in batch crystallization is to insert a known amount of crystals with predetermined properties into the crystallizer. The so-called seeding ensures reproducible batch start-ups by suppressing the uncertainties in initial conditions of the process. Hence,

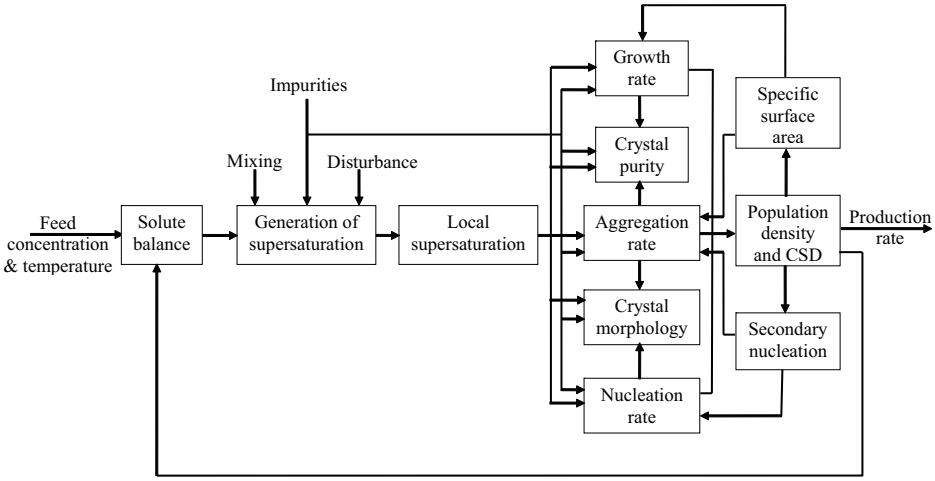

Figure 1.2: The interplay of the kinetic phenomena (Kühberger and Mersmann 1997).

seeding can be regarded as an additional process actuator, which is applied only at the beginning of the batch run.

Figure 1.2 shows the interplay of the different kinetic phenomena. An internal feedback mechanism exists between supersaturation generation and kinetic phenomena through the evolution of crystal population and solute concentration. This feedback mechanism determines the production rate and the quality attributes, e.g. purity, size distribution, and morphology, of the crystals. Therefore, the requirements on the quality of the crystalline product and the process productivity should be fulfilled by controlling the integral effect of the kinetic phenomena. In most cases, the process performance can be monitored by measuring the evolution of crystal population and solute concentration throughout the process.

1.2 State-of-the-art in control of batch crystallizers

1.2.1 Introduction

Due to the fierce economic competition between the companies manufacturing high value-added crystalline products, there is an increasing interest in optimal operation of batch crystallization processes. This is to boost the process productivity as satisfying product quality and batch reproducibility requirements. Batch crystallizers are often operated by tracking predetermined recipes, e.g. temperature, feed flow, and/or heat input profiles, which are largely based on operators'

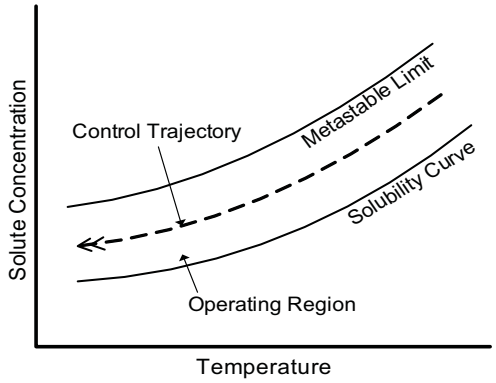

Figure 1.3: The direct design approach (Fujiwara et al. 2005).

experience. However, batch recipes lack the ability to realize optimal operation of the process, while various operational and quality constraints are honored.

With recent advances in measurement and computing technologies (Braatz 2002), numerous control approaches have been proposed for optimal operation of batch crystallizers. These strategies can be broadly categorized into the *direct design approach* and the *model-based control approach*. In the following, a brief overview of the state-of-the-art in advanced control of batch crystallization processes is presented.

1.2.2 The direct design approach

In the vast majority of batch crystallizers, the desired operation window of solute concentration falls in the metastable zone. The most common practice is to experimentally determine an operating policy by trial-and-error. The operating policy should be able to keep the solute concentration within the metastable zone to ensure the production of crystals with acceptable quality attributes. In the advent of process analytical technology, a more effective approach has emerged for feedback control of solute concentration. The principal idea of the so-called direct design approach is depicted in Figure 1.3. The approach aims to follow a predefined concentration-temperature trajectory within the metastable zone. This allows a nearly constant trade-off between the need to suppress excessive nucleation and to avoid overly long batch times (Fujiwara et al. 2005). The direct design approach relies on in-situ solute concentration measurements, which can be obtained by means of spectroscopic instruments. In addition, it requires the thermodynamic knowledge of the crystallizing system.

The direct design approach is a state feedback strategy, which exploits the mathematical description of the solubility curve. In the case of batch cooling crystallization, the temperature setpoint is obtained by solving the algebraic function

of solubility

$$C^*(T) = C - \Delta C \tag{1.2}$$

for T; ΔC is a predefined supersaturation profile within the metastable zone. Note that the predefined setpoint is not an explicit function of time unlike most process control approaches. Therefore, the control trajectory is state-dependent, representing a desired dependency between two states, namely the solute concentration and the temperature; see Figure 1.3. The temperature setpoint is provided to a lower level feedback controller, which applies the calculated setpoint to the crystallizer.

The direct design approach circumvents the need to derive first-principles models and to characterize crystallization kinetics. It also exhibits low sensitivities to most practical disturbances and to variations in the kinetic phenomena (Zhou et al. 2006). Nonetheless, a priori determination of the near-optimal supersaturation profile often requires extensive experimentation.

Several studies on the application of the direct design approach to batch cooling and antisolvent crystallizers have been reported in the literature (Fujiwara et al. 2002; Févotte 2002; Grön et al. 2003; Liotta and Sabesan 2004; Zhou et al. 2006). In these studies, the solute concentration was measured by attenuated total reflection-Fourier transform infrared (ATR-FTIR) spectroscopy. This technique enables accurate measurement of multiple solute concentrations, detection of the metastable limit, and evaluation of impurity concentrations during crystallization (Dunuwila et al. 1994; Dunuwila and Berglund 1997; Wang and Berglund 2000; Lewiner et al. 2001; Togkalidou et al. 2002).

1.2.3 The model-based control approach

In the model-based control approach, a first-principles model constructed from material and energy balances is used as a basis for optimal operation of the batch crystallizer. The operational degrees of freedom of the system are exploited to achieve the desired product properties in accordance with an optimization criterion. The population balance equation (PBE) provides a natural framework for mathematical modeling of batch crystallization processes (Hulbert and Katz 1964). It describes the integral effect of crystallization kinetics on the dynamic evolution of crystal size distribution. The prime difficulty in synthesis of a model-based control approach for industrial batch crystallizers results from the distributed nature of the population balance equation. Finite dimensional approximations of the PBE typically leads to very high-order sets of ordinary differential equations, which may render real-time control of crystallizers computationally impractical. Therefore, in most control-oriented studies the distributed nature of the PBE is approximated by considering only the leading moments of CSD. The so-called moment model consists of a small number of computationally affordable ordinary differential equations that are related to physical properties of interest such as crystal number, length, area, and volume. The moment model cannot describe the complex dynamics of industrial batch crystallizers when the knowledge of full crystal size distribution is required.

The model-based approach to control of batch cooling crystallizers has been extensively investigated in the literature. Implementation of programmed temperature profiles on batch cooling crystallizers dates back to early 1970s. The pioneering work of Mullin and Nyvlt (1971) as well as Jones and Mullin (1974) established that a programmed cooling profile leads to better CSD characteristics in comparison with natural or linear cooling policies. Mayrhofer and Nyvlt (1988) analyzed programmed cooling of batch crystallizers on the basis of a moment model. They devised a theoretical cooling profile with an arbitrary ratio of seeding to spontaneous nucleation that could be simplified to the previously reported expressions. Early on, the optimal control theory was also employed to determine cooling policies. Jones (1974) used the maximum principle to compute a cooling profile that maximized the final size of seed crystals. Chang and Epstein (1982) applied a gradient method to determine optimal temperature profiles for various objective functions expressed in terms of average size, volume or variance of the final CSD.

Over the past decade, dynamic optimization of batch crystallizers has received particular attention due to advances in modeling and optimization tools. Dynamic optimization exploits a process model to systematically push the system to its most optimal operating regime as honoring various operational and product quality considerations. The explicit formulation of constraints in a dynamic optimization problem facilitates optimal process operation realized at the constraints.

Producing a crystalline product with a large mean crystal size and a narrow size distribution is traditionally the prime objective in model-based control of batch crystallizers (Rawlings et al. 1993). Matthews and Rawlings (1998) identified a model for batch cooling crystallization of an organic photochemical heptane system; model parameter uncertainties were minimized by applying different optimal experiment design techniques. Open-loop optimization of the temperature profile was performed to improve filtration properties of the crystallization slurry. Lang et al. (1999) computed the optimal programmed cooling curve of an industrial batch cooling crystallizer by solving a dynamic optimization problem that maximized the final crystal size. The optimal temperature profile led to a drastic increase in the mean crystal size in comparison with the operating policy obtained by the maximum principle optimization and the original operating conditions determined by trial-and-error. Chung et al. (1999) performed a comprehensive study on dynamic optimization of the seed distribution in a batch cooling crystallizer. Certain properties of the crystalline product were optimized over the supersaturation profile and the seed characteristics. It was shown that optimizing over the seed distribution could have a larger effect on the product quality than optimizing over the supersaturation profile. The latter study was extended by Ma et al. (1999) to quantify the impact of parameter and control implementation inaccuracies on the performance of open-loop control policies. In addition, Ma et al. (2002b) investigated the optimal control of batch formation of multidimensional crystals. They showed that a subtle change in the optimal control objective could have a significant impact on the crystal size and shape distributions of the crystalline product. Later on, Nagy and Braatz (2004) demonstrated the high sensitivity of optimal control trajectories to model uncertainties. They presented a new

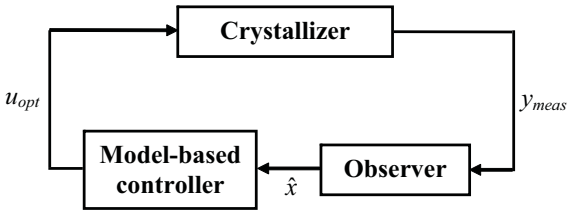

Figure 1.4: The output feedback model-based control approach.

approach for incorporating robustness in the model-based control of batch crystallization processes. Optimal control of batch cooling crystallizers was also studied by Hu et al. (2005c). They proposed a new method for numerical solution of the population balance equation. The system-specific kinetic parameters of the crystallizing system were estimated on the basis of the maximum likelihood method. The identified model was then employed to determine an optimal cooling policy by minimizing the ratio of the mass of the newly nucleated crystals to the seed crystals. Experimental results showed that the optimal temperature profile led to improved operation of the crystallizer in comparison with the natural and linear cooling policies. Nowee et al. (2007) presented a model for a seeded batch cooling crystallization process, in which crystal dissolution took place. The nonlinear process model was utilized to optimize the temperature profile and the initial seed size distribution. Experimental implementation of the off-line optimized profiles resulted in the desired crystal mean size.

Despite the significant efforts to develop model-based control approaches for batch crystallizers, a great deal of the work is limited to open-loop control as discussed above. In this control approach, the information on current states of the system is not used in devising the optimal operating policy. The main shortcomings of the open-loop control approach are its insensitivity to batch-to-batch variations as well as its inability to cope with process uncertainties. In addition, the models used to devise optimal operating policies almost always provide an incomplete description of the process. This is mainly due to the uncertainties associated with the crystallization kinetic models. The model imperfections may degrade the effectiveness of the optimal operating policy.

An effective strategy that alleviates the aforementioned shortcomings is online computation of the optimal operating policy during the batch run. In this approach, an output feedback mechanism is exploited to update the optimal operating policy by using measurements; see Figure 1.4. An observer is required to estimate the states of the system to recursively initialize the dynamic optimizer at regular time intervals. The state estimation in combination with the feedback mechanism essentially accounts for model imperfections as well process uncertainties.

Among the numerous attempts to perform output feedback control of batch crystallizers, the work of Chang and Epstein (1987) can be recognized as a pioneering study. They incorporated a feedback mechanism into the optimal con-

trol scheme presented in their earlier work (Chang and Epstein 1982). The application of the feedback control strategy for a batch crystallizer was then demonstrated by simulation studies. Eaton and Rawlings (1990) investigated feedback control of several constrained nonlinear multivariable chemical processes, including a batch cooling crystallizer, using nonlinear estimation and optimal control strategies. Zhang and Rohani (2003) developed an online control strategy for optimal control of a seeded batch cooling crystallizer. An extended Kalman filter was employed to estimate the unmeasurable state variables and to account for plant-model mismatch as well as process uncertainties. The simulation results showed notable improvements in the product CSD in comparison with that obtained by open-loop implementation of the optimal cooling policy.

Recently, several experimental studies on output feedback control of batch crystallizers have been reported in the literature. Abbas and Romagnoli (2006) presented a model-based control approach comprised of a modeling software, a linear model predictive controller, and a state estimator. At the top layer of the control hierarchy, dynamic optimization was used to determine off-line the optimal mean crystal size, which became the setpoint for the lower layer real-time optimizer. The feedback mechanism was introduced at the latter layer through a state estimator that estimated the mean crystal size based on temperature and conductivity measurements. The control approach was tested on a 75-liter batch cooling crystallizer, where the experimental results showed a rather successful setpoint tracking towards the batch end. Sheikhzadeh et al. (2007) employed an in-situ focused beam reflectance measurement (FBRM) probe in combination with ATR-FTIR spectroscopy to obtain online measurements of crystallization kinetics and solute concentration. The measurements were used in a feedback fashion to update the optimal operating policy at each optimization time interval. They investigated the effect of single- and multi-objective optimal control on properties of the crystals produced in a laboratory-scale semi-batch antisolvent crystallizer. The experimental results demonstrated that the multi-objective optimization led to better size distribution properties of the crystalline product.

To summarize one can say that compared to the direct design approach, a great deal of work has been done on the model-based control of batch crystallizers. The latter studies mostly concern open-loop control of laboratory-scale cooling crystallizers on the basis of a simplified moment model. Thus, the control strategies may not be suitable for control of a wide range of industrial batch crystallizers. In addition, the open-loop implementation of optimal operating policies may deteriorate their effectiveness due to model imperfections and process uncertainties.

1.3 Challenges in control of industrial batch crystallizers

It follows from Section 1.2 that there are yet several challenges in advanced control of industrial batch crystallizers. The difficulties mainly arise from the distributed nature of the nonlinear process models, modeling of the crystallization kinetics,

sensor limitations in accurate measurement of process variables, inherent process uncertainties, and lack of process actuation. These challenges are further elaborated below.

Complexity of process models

Most of the model-based control approaches proposed in the literature exploit a reduced-order moment model to compute the optimal operating policies; see Section 1.2.3. However, the use of moment models encounters a practical barrier in the vast majority of industrial batch crystallizers. A moment model is not capable of describing the integral effect of any combination of crystallization kinetics on the evolution of crystal population. In addition, complex dynamics of industrial batch crystallizers may not be described by a moment model when the knowledge of full crystal size distribution is required, e.g. crystallizers equipped with fines removal and dissolution or product classification systems.

The aforementioned shortcomings of moment models call for the use of full population balance models. However, the complexity of population balance models has certain implications for the computational efficiency of the control approach. In addition, accurate numerical solution of the population balance equation is often challenging. This is due to the convective nature of the PBE, which may lead to numerical diffusion and stability problems, particularly in the event of steep moving fronts and/or sharp discontinuities (Qamar et al. 2006). The resulting numerical inaccuracies are largely detrimental to the descriptive capability of a population balance model. Inadequate description of process dynamics may in turn worsen the effectiveness of state estimation and dynamic optimization to a large extent.

Modeling of the crystallization kinetics

First-principles models provide insights into crystallization processes by enabling systematic simulation and optimization of various kinetic phenomena. Accurate determination of crystallization kinetics is essential in the model-based control approach. The advent of in-situ sensors and the use of multivariate statistics have largely facilitated reliable data collection and analysis for identification of the kinetic models (Braatz 2002). However, modeling of more complex kinetic phenomena, e.g. agglomeration, dendritic growth, polymorphic transitions, etc., yet remains to be a challenge.

Moreover, the parameters of kinetic models are typically determined on the basis of laboratory-scale experiments. It is often impractical to achieve the same localized mixing and supersaturation in an industrial-scale crystallizer due to different heat transfer and mixing characteristics (Bermingham 2003). In addition, the kinetic parameters can be largely sensitive to feed impurities. The inadequacies of the identified kinetic models for industrial-scale crystallizers may severely degrade the effectiveness of a model-based control approach.

Inadequate performance objectives

Optimization of a crystallization process is most effective when an explicit performance objective in terms of practical crystallization objectives is used. For many batch crystallization processes, performance objectives relating the crystal

size and shape distributions to many of the practical objectives such as filterability and product stability are not available (Fujiwara et al. 2005). The use of surrogate performance objectives, see, e.g., (Rawlings et al. 1993; Braatz 2002), is likely to diminish the usefulness of a model-based control approach.

Uncertain initial conditions

Uncertainties in the initial conditions of batch crystallization processes can be detrimental to the reproducibility of batch runs. The initial conditions have an irreversible influence on the process dynamics. In general, the initial conditions can affect the process performance to an extent, which may not be undone easily (Kalbasenka 2009). The reproducibility of batch start-ups can be ensured rather effectively by using seeding heuristics; see, e.g., (Lakerveld 2010) and the references therein. However, experimental optimization of seeding procedures is system-specific and often labor intensive. On the other hand, most practical issues are disregarded in model-based optimization of seeding procedures (Chung et al. 1999). Despite of the numerous attempts to devise optimal seeding procedures, reproducible start-up of batch crystallizers yet remains to be a challenge.

Difficulties in reliable measurement of process variables

Recent measures put into effect by regulatory bodies, e.g., the US Food and Drug Administration (FDA), and advances in the process analytical technology have significantly promoted the use of in-situ measurement techniques, particularly in pharmaceutical crystallization. However, the application of in-situ sensors is mostly investigated at laboratory-scale (Neumann and Kramer 2002; Kadam et al. 2010b). The precision and robustness of the sensors in harsh industrial environments remains obscure. Lack of reliable sensors for in-situ measurement of the critical process variables poses a challenge in output feedback control of industrial batch crystallizers.

Computational complexity

The computational complexity of model simulation and optimization may render output feedback control of industrial batch crystallizers infeasible. The model simulation and optimization tasks should be performed within short intervals between measurement sampling time instants.

Lack of process actuation

The inherent dynamic behavior of batch crystallization processes necessitates the availability of effective actuation mechanisms to realize the intended control objectives in a finite time. The lack of process actuation often poses a great difficulty in control of batch crystallizers (Huesman et al. 2009). The actuation mechanisms of conventional industrial batch crystallizers may not allow us to effectively control the integral effect of crystallization kinetics on crystal characteristics. This in turn obstructs the achievement of desired product quality and process productivity.

1.4 Problem statement

It follows from the previous section that there are several open issues in control of industrial batch crystallizers, which deserve a thorough investigation. This thesis aims to address the inherent challenges of real-time control of existing industrial batch crystallizers by using a nonlinear model-based control approach. The control strategy is intended to serve as a means to transform the art of controlling industrial batch crystallizers into an engineering task. The problem statement is formulated as follows:

- Primary research objective -

Evaluate the opportunities for real-time model-based control to improve product quality and process productivity of industrial batch crystallizers.

The four core elements central to the problem statement are:

i. *Industrial batch crystallizers*: The model-based controller should be applicable to a wide range of existing industrial batch crystallizers. The use of a generic modeling framework is a prerequisite for this requirement. The modeling framework should allow us to simulate diverse crystallization kinetics of any complexity. In addition, it should incorporate the effect of actuation mechanisms commonly exploited in industrial batch crystallizers. These processes are notorious for lack of actuation, which may obstruct the achievement of control objectives. Improving the process controllability through redesign falls beyond the scope of this thesis as the focus is on the control of existing crystallizers. It should be noted that due to various technological and economical limitations, in-situ measurement of all process variables is often not viable in industrial batch crystallizers.

ii. *Improved process operation*: Enhanced control of batch crystallization processes should ensure better crystalline product quality, shorter process times, and increased batch-to-batch uniformity. The reproducibility of batch runs largely depends on the initial states of the system, whose uncertainties need to be minimized. Furthermore, supersaturation control within the metastable zone necessitates a trade-off between the achievement of the desired product quality and the maximization of batch productivity.

iii. *Model-based control approach*: The descriptive capability of the process model as the cornerstone of a model-based controller is of paramount importance. There is often some degree of uncertainty associated with kinetic parameters of crystallization models. In addition, the models cannot describe the effects of most process uncertainties inherent in industrial batch crystallization. Thus, the effectiveness of the control approach in the presence of model imperfections and process uncertainties must be ensured.

iv. *Real-time control*: Real-time implementation of the model-based controller requires the use of computationally efficient model solution techniques as well as optimization strategies. This is to ensure the online computation of optimal operating policies in the short intervals between measurement sampling time instants.

In pursuit of the research objective, the following goals can be identified:

1. Develop a first-principles model that can adequately describe the dynamics of a wide range of industrial batch crystallizers

- **(a)** Explore how the computational burden of a population balance model can be reduced as preserving its descriptive capability.
- **(b)** Investigate the use of in-situ solute concentration measurements for improving the estimation quality of the kinetic parameters and consequently the model validity.

2. Evaluate the effectiveness of state estimation in the presence of plant-model mismatch and process uncertainties

- **(a)** Explore what state estimation technique can best cope with the inherent characteristics of batch crystallization processes in an output feedback model-based control framework.
- **(b)** Investigate how the process uncertainties that degrade the control performance can be effectively suppressed.

3. Demonstrate the real-time viability of the model-based control approach

- **(a)** Explore whether direct optimization strategies can ensure online computation of the optimal control problem.
- **(b)** Investigate how the lack of actuation will hamper the fulfillment of control objectives.

These subgoals allow us to design an output feedback nonlinear model-based controller, which can be exploited for real-time control of a wide range of industrial batch crystallizers.

1.5 Organization of this thesis

This thesis is divided into five main chapters that describe the first-principles modeling of batch crystallization processes, the numerical solution of the population balance equation, the nonlinear state estimation techniques, the output feedback nonlinear model-based control approach, and the experimental results of real-time implementation of the control approach. Figure 1.5 gives an overview of the chapters and their relations.

Chapter 2 presents a first-principles modeling framework for industrial batch crystallizers. Various components of the modeling framework, namely the population balance equation, mass and energy balances, and kinetic expressions are described. Subsequently, a dynamic model for semi-industrial fed-batch evaporative crystallization of ammonium sulphate is developed. The state space representation of system dynamics is derived for two model formulations, namely a population balance model and a moment model.

In addition, Chapter 2 describes the parameter estimation and validation of the population balance model. The focus is on the use of in-situ solute concentration measurements, along with on-line crystal size distribution data, to estimate the system-specific kinetic parameters. A rapid calibration technique that facilitates the use of ATR-FTIR spectroscopy in industrial-scale batch crystallization is presented.

Chapter 3 describes the numerical solution of the population balance equation for crystallization processes undergoing simultaneous nucleation and crystal growth. The numerical solution methods discussed in this thesis are the method of characteristics, the finite volume methods, and the finite element methods. This chapter presents a series of results on the dynamic simulation of various test cases as well as industrial crystallization case studies.

Chapter 4 describes various deterministic and Bayesian state estimation techniques, which are suitable for process monitoring and output feedback control of nonlinear systems. A review of state estimation efforts in the field of crystallization is presented. In addition, several state estimation techniques, namely the extended Luenberger technique, the extended Kalman filtering, the unscented Kalman filtering, the ensemble Kalman filtering, and the moving horizon estimation, are used to develop nonlinear observers for a semi-industrial batch crystallizer. Open-loop performance of the state observers when applied to a plant-simulator is discussed.

Chapter 5 presents the output feedback nonlinear model-based control approach. An optimal control problem pertaining to batch evaporative crystallization is formulated. The control approach is applied to two case studies, namely a single-input single-output semi-industrial crystallizer and a multi-input multi-output industrial crystallizer. The effect of different direct optimization strategies on the optimal operation of batch crystallizers is investigated. In addition, the ability of the output feedback control approach to cope with model imperfections and process uncertainties is examined.

Chapter 6 describes the experimental implementation of the control approach on a $75 - liter$ draft tube crystallizer. This chapter demonstrates the real-time implementation of the control approach when the system dynamics are described by the moment model as well as the population balance model. In addition, the real-time performance of the control approach is compared with that of a model predictive controller.

Chapter 7 summarizes the findings of the thesis and presents some perspectives for future work.

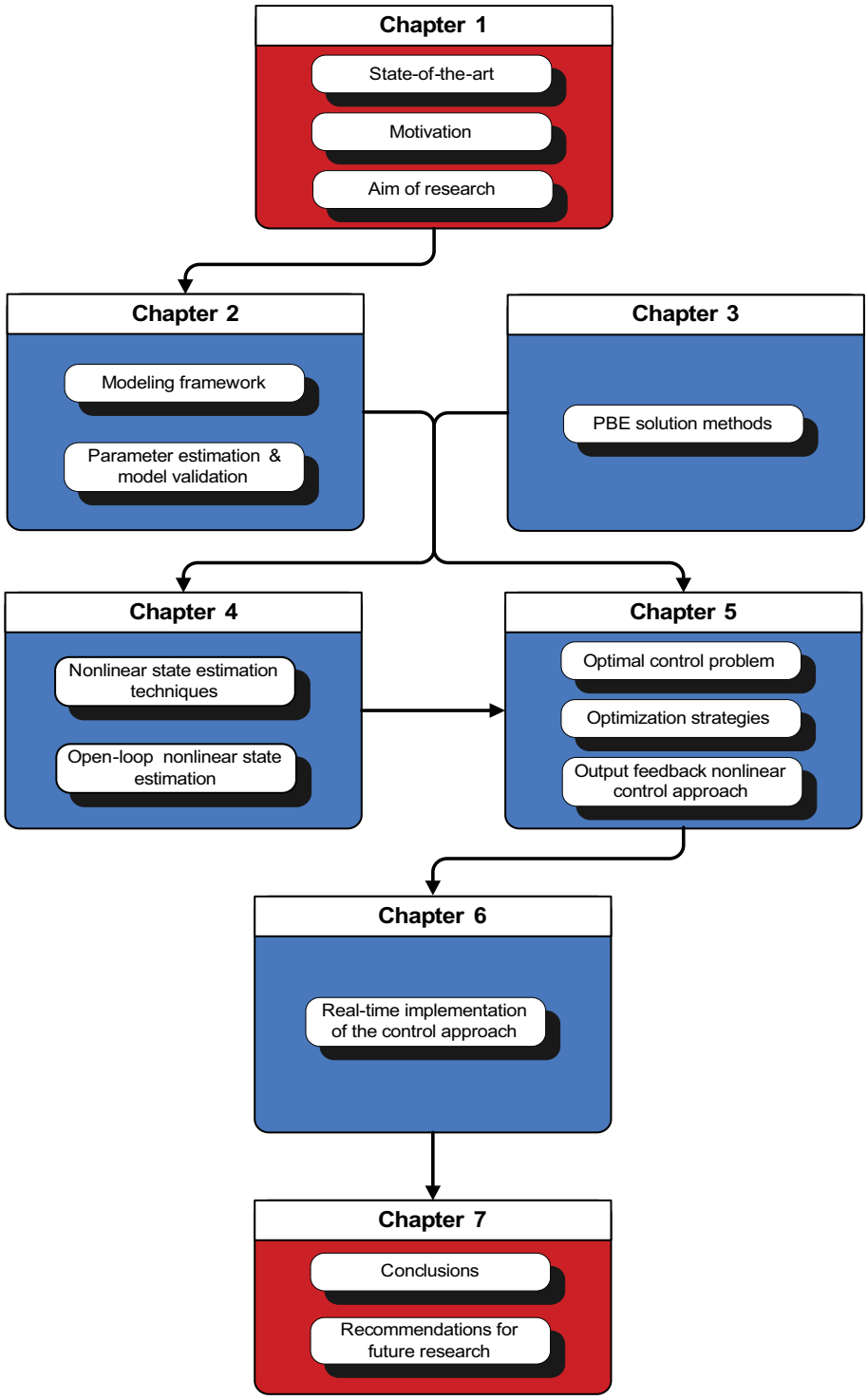

Figure 1.5: Structure of the thesis.

2 CHAPTER

Model Development

Essentially, all models are wrong, but some are useful.

George E.P. Box

The process of first-principles model development for a crystallization system consists of two interrelated steps. First, a general model structure must be established. The model structure should account for the pertinent states of the process. The second step involves the estimation of model parameters from experimental data collected for a specific crystallizing system.

This chapter describes the process of model development for industrial seeded batch crystallizers. Different components of the modeling framework, namely the population balance equation, mass and energy balances, and kinetic expressions for nucleation and crystal growth are presented. When a batch crystallizer is operated within the metastable zone, nucleation and crystal growth are typically the most dominant kinetic phenomena.

The general modeling framework is used to develop a dynamic model for fed-batch evaporative crystallization of ammonium sulphate. The state space representation of system dynamics is derived for two model formulations, namely the population balance model and the moment model. The last section of this chapter concerns the inference of model parameters from experimental data. A rapid online calibration technique is developed to predict solute concentration from infrared spectra collected from a semi-industrial seeded fed-batch crystallizer. The in-situ concentration measurements, along with online crystal size distribution data, are employed to estimate the kinetic parameters of the population balance model. Finally, the model is validated against independent experimental data.

2.1 A general modeling framework

2.1.1 Introduction

A dynamic process model is intended to provide an accurate representation of the behavior of a physical system. This representation, which describes the dynamic relation between inputs and outputs of the system, is the cornerstone of any model-based control approach. Batch crystallization processes are particularly challenging to model. Their system dynamics depend not only on process variables such as concentration and temperature, but are also a function of certain properties of the individual crystals. Therefore, the system dynamics are of distributed nature. The distributed characteristic variables of crystals are characterized by a complex interplay of various phenomena, namely nucleation, crystal growth, agglomeration, breakage, and dissolution.

In general, the model structure and its level of complexity should be tailored according to its intended purpose. In control applications, the model must enable accurate prediction of the process dynamics within the relevant operational envelop. In addition, the model structure should allow us to describe the control objectives that are to be sought (Roffel and Betlem 2006). In this thesis, a *first-principles modeling* approach is adopted to model industrial batch crystallizers. The conservation laws, namely material and energy balances, constitute the basis of first-principles crystallization models, where the crystallization kinetics are often described by empirical expressions. This differs from the *black-box modeling* approach, which builds an input-output relation using experimental data of the system (Ljung 1987). The primary merit of first-principles models lies in preserving the physical insight into the process. Their general structure allows us to describe the dynamics of a wide range of industrial batch crystallizers over a relatively large operational envelop. In addition, the need for extensive experimentation as in the black-box modeling approach is circumvented, though the first-principles approach requires a priori process knowledge.

The complexity of first-principles modeling of crystallization systems mainly arises from the distributed nature of the characteristic variables of crystals. Most model-based control studies exploit a lumped model, which discards the distributed characteristic variables of crystals. Hence, the latter control approaches disregard the infinite-dimensional description of a crystallization process by assuming that the relevant process dynamics for control are of low-dimension. This makes the control approaches simpler and computationally less demanding. However, their performance objectives can be defined merely in terms of combinations of lumped variables, e.g. the mean crystal size, the third moment of the crystal size distribution, etc.

The simplified structure of lumped models, viz *moment models*, usually obstructs their application for control and optimization of industrial batch crystallizers. Certain dynamics of industrial-scale crystallizers such as classification of crystals and complex crystallization kinetics cannot be described by lumped models. In addition, the use of classical performance objectives that are only functions

of lumped variables may lead to conservative and economically inefficient process operation. Thus, distributed first-principles models are essential for effective model-based control of a wide range of industrial batch crystallizers.

The *population balance modeling* approach presents a general framework capable of describing the dynamic distribution of the characteristic variables of crystals, along with the state variables of the continuous phase. The modeling framework consists of mass balances for the liquid phase components, population balance(s) for the solid phase(s), and the energy balance. The population balance of the dispersed phase is connected with the continuous phase component mass balances through crystallization kinetics. In the following, a population balance modeling framework for batch and semi-batch operation of cooling, flash-cooling, and evaporative crystallizers is presented.

2.1.2 Population balance

The properties of crystalline products are distributed over the internal crystal states, e.g. size and shape. Thus, a comprehensive description of the product quality involves a multivariable distribution of the crystal population over various internal states. In control applications, only one internal coordinate system, namely the crystal size, is used to describe the characteristics of a crystalline material (Rawlings et al. 1993; Braatz 2002). This is to avoid the high computational effort of detailed mechanistic models that may be prohibitive for implementation of control approaches.

The population balance equation is a well-established mathematical framework for dynamic modeling of particle size distribution in numerous particulate systems such as polymerization, precipitation, etc. (Ramkrishna 2000). Hulbert and Katz (1964) originally put forward this theory to describe the evolution of crystal identities during a crystallization process. The population balance equation (PBE) provides a deterministic description of the dynamic distribution of crystal size by forming a balance to calculate the number of crystals in a crystallizer. The solution of such a balance equation provides the distribution of the number of crystals across the temporal and spatial domains. The spatial domain may include both internal and external coordinates. The external coordinates typically involve the ordinary rectangular coordinate system, specifying the location of crystals in the crystallizer, whereas the internal coordinates represent the characteristic size of crystals.

In industrial applications, the crystallizer is often assumed to be well-mixed. Thus, the population balance equation can be expressed in terms of the internal coordinates only. In addition, nucleation and crystal growth are normally the most dominant kinetic phenomena when a batch crystallizer is operated within the metastable zone (Fujiwara et al. 2005). The one-dimensional PBE for a crystallization process undergoing nucleation and crystal growth can be written as

(Randolph and Larson 1988)

$$\frac{\partial(V(t)n(L,t))}{\partial t} + V(t)\frac{\partial(G(L,t)n(L,t))}{\partial L} = V(t)B(L,t) + \left(\sum_{k=1}^{N_i}\phi_{V,in,k}(t)n_{in,k}(L,t) - \sum_{l=1}^{N_o}\phi_{V,out,l}(t)h_{cf}(L)n(L,t)\right), \tag{2.1}$$

where $n(L,t)$ is the number density function $(\#/m^4)$; t is the time (s); L is the internal coordinate, viz the crystal characteristic size (m); $G(L,t)$ is the crystal growth rate (m/s); $B(L,t)$ is the nucleation rate $(\#/m^4 s)$; $V(t)$ is the crystallizer volume (m^3); N_i and N_o are the number of inlet and outlet streams, respectively; $\phi_V(t)$ is the volumetric flow rate (m^3/s); $h_{cf}(L)$ is the crystal classification function. An extensive description of the classification function is given in Bermingham (2003). The initial condition of the PBE is

$$n(L,t_0) = n_0(L). \tag{2.2}$$

Equation (2.2) represents either a clear solution with no crystal population or the size distribution of seed crystals. In addition, the boundary condition of the PBE is expressed as

$$n(L_0,t) = 0 \quad if \quad G(L,t) \geq 0, \quad \forall L. \tag{2.3}$$

Equation (2.3) implies that there exists no crystals with size L_0.

A common practice in industrial batch crystallization is to run seeded batches to avoid the occurrence of undesirable phenomena such as primary nucleation and agglomeration. For seeded batch crystallization processes, equation (2.1) can be simplified to the following partial differential equation

$$\frac{\partial(V(t)n(L,t))}{\partial t} + V(t)\frac{\partial(G(L,t)n(L,t))}{\partial L} = \left(\sum_{k=1}^{N_i}\phi_{V,in,k}(t)n_{in,k}(L,t) - \sum_{l=1}^{N_o}\phi_{V,out,l}(t)h_{cf}(L)n(L,t)\right) \tag{2.4}$$

with the left boundary condition

$$n(L_0,t) = \frac{B_0(t)}{G(t)|_{L_0}}, \tag{2.5}$$

where $B_0(t)$ denotes the total nucleation rate of crystals of infinitesimal size $(\#/m^3 s)$.

2.1.3 Mass and energy balances

Equation (2.1) indicates that the evolution of crystal size distribution (CSD) is driven by the rates of crystal growth and nucleation. These phenomena are governed by the change in chemical potential of the solute molecules between the solution and the crystalline phases. The chemical potential difference is expressed

as (Jones 2002)

$$\Delta\mu_c = kT\ln(\frac{C(T)}{C^*(T)}), \tag{2.6}$$

where $\Delta\mu$ is the change in chemical potential; C is the solute concentration $(wt.\%)$; C^* is the saturation concentration $(wt.\%)$; T is the solution temperature (K); k is the Boltzmann constant (J/K). It is common practice to use supersaturation as the driving force for the process. Supersaturation can be defined as

$$\Delta C = C(T) - C^*(T). \tag{2.7}$$

Equation (2.7) implies that supersaturation is the concentration driving force for a crystallization process. It is evident that supersaturation is a function of solute concentration and temperature. Thus, the PBE must be coupled with mass and energy balances to determine the state variables of the continuous phase.

Energy balance

The energy balance can be transformed into an enthalpy balance since the kinetic energy, potential energy, and shaft work are often assumed to be negligible in a crystallizer. This results in

$$\frac{\mathrm{d}H(t)}{\mathrm{d}t} = \sum_{k=1}^{N_i}\phi_{H,in,k}(t) - \sum_{l=1}^{N_o}\phi_{H,out,l}(t) - \phi_{H,V,out}(t) + Q(t) \tag{2.8}$$

with the initial condition

$$H(t_0) = H_0. \tag{2.9}$$

In the energy balance, $H(t)$ is the enthalpy (J); $\phi_H(t)$ and $\phi_{H,V}(t)$ are the enthalpies of solution and vapor streams, respectively (J/s); $Q(t)$ is the net rate of heat addition to the system (J/s).

Mass balance

The liquid phase component mass balance for the solvent is

$$\begin{aligned}\frac{\mathrm{d}m_{L,solvent}(t)}{\mathrm{d}t} &= \sum_{k=1}^{N_i}\phi_{m,L,solvent,in,k}(t) - \sum_{l=1}^{N_o}\phi_{m,L,solvent,out,l}(t)\\ &\quad - \phi_{m,V,solvent,out}(t)\\ &\quad + M_{solvent}\sum_{q=1}^{N_s}\nu_{s,solvent,q}[\phi_{mol,grow,q}(t) + \phi_{mol,nucl,q}(t)]\end{aligned} \tag{2.10}$$

with the initial condition

$$m_{L,solvent}(t_0) = m_{L,solvent,0}. \tag{2.11}$$

In equation (2.10), $m_{L,solvent}(t)$ is the mass of solvent (kg); $\phi_{m,L,solvent}(t)$ and $\phi_{m,V,solvent}(t)$ are the solvent mass flow rates in liquid and vapor phases, respectively (kg/s); $M_{solvent}$ is the solvent molecular weight $(kg/mole)$; $\nu_{s,solvent}$ is the solvent stoichiometric coefficients in the solid phase; N_s is the number of solid

phases; $\phi_{mol,grow}(t)$ and $\phi_{mol,nucl}(t)$ are the molar flows of crystal growth and nucleation $(mole/s)$, respectively.

Assuming that the vapor stream is free of solute and crystalline material, the liquid phase component mass balance for the solute is given by

$$\begin{aligned}\frac{\mathrm{d}m_{L,solute}(t)}{\mathrm{d}t} &= \sum_{k=1}^{N_i}\phi_{m,L,solute,in,k}(t) - \sum_{l=1}^{N_o}\phi_{m,L,solute,out,l}(t) \\ &+ M_{solute}\sum_{q=1}^{N_s}\nu_{s,solute,q}[\phi_{mol,grow,q}(t) + \phi_{mol,nucl,q}(t)]\end{aligned} \tag{2.12}$$

with the initial condition

$$m_{L,solute}(t_0) = m_{L,solute,0}. \tag{2.13}$$

In equation (2.12), $m_{L,solute}(t)$ is the mass of solute (kg); $\phi_{m,L,solute}(t)$ is the solute mass flow rate in the liquid phase (kg/s); M_{solute} is the solute molecular weight $(kg/mole)$; $\nu_{s,solute}$ is the solute stoichiometric coefficients in the solid phase.

The component mass balances and population balance are coupled by the molar flows of crystal growth and nucleation

$$\phi_{mol,grow}(t) = -\frac{k_v\rho_s}{M_{solute}}V(t)\int_{L_0}^{\infty}\frac{\partial(G(L,t)n(L,t))}{\partial L}L^3\mathrm{d}L \tag{2.14}$$

$$\phi_{mol,nucl}(t) = \frac{k_v\rho_s}{M_{solute}}V(t)\int_{L_0}^{\infty}B(L,t)L^3\mathrm{d}L, \tag{2.15}$$

where k_v is the volume shape factor of the crystalline material; ρ_s is the density of the crystalline material (kg/m^3). Expressions for the rates of crystal growth and nucleation follow from the kinetic models.

2.1.4 Crystallization kinetics

Crystallization kinetics relate the dynamic evolution of crystal population to the state variables of the continuous phase. As indicated in Section 2.1.2, only crystal growth and nucleation processes are considered in this thesis. Growth and nucleation merely take place if supersaturation is positive, implying a thermodynamically favorable transition of the solute into the solid phase.

Nucleation

Nucleation involves the formation of a new crystalline phase. The generation of crystals is broadly categorized into *primary nucleation* and *secondary nucleation*; see Figure 2.1. Primary nucleation occurs in the absence of crystalline surfaces. Two primary nucleation mechanisms can be distinguished, namely *homogeneous* and *heterogeneous* nucleation. Homogeneous nucleation takes place spontaneously in a pure solution through the formation of clusters of solute molecules. On the

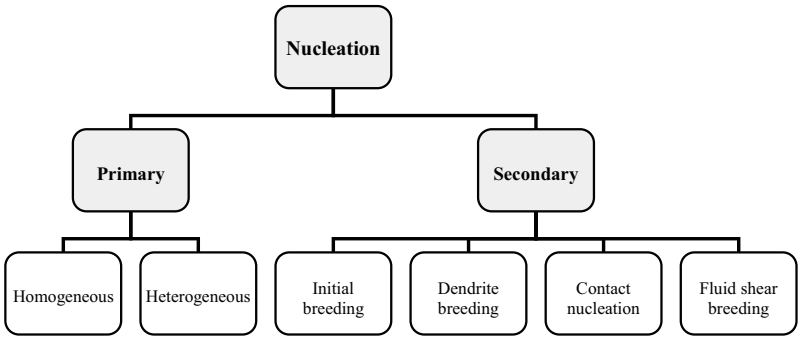

Figure 2.1: Mechanisms of crystal nucleation.

other hand, heterogeneous nucleation is induced by the presence of impurities. Primary nucleation occurs at high levels of supersaturation, typically exceeding the metastable limit. The most common practice in industrial batch crystallization is to circumvent primary nucleation since it is often detrimental to the product quality. This can be done by restraining the supersaturation within the metastable zone. The modeling of primary nucleation is not treated in this thesis.

Secondary nucleation takes place in the presence of crystals at relatively lower levels of supersaturation. Figure 2.1 shows a variety of secondary nucleation mechanisms. *Initial breeding* happens when crystalline dust fragments adhered to the surface of dry seed crystals are washed off upon introduction into a supersaturated solution. Breakage of dendrites from the parent crystals leads to *dendrite breeding*, whereas *fluid shear breeding* occurs due to the breakage of a growing crystal face under hydrodynamic shear forces. On the other hand, *contact nucleation* results from mechanical forces, namely vigorous crystal-crystal, crystal-impeller, and crystal-hardware collisions (Botsaris 1976; van der Heijden and van Rosmalen 1993).

Among the various secondary nucleation mechanisms, contact nucleation generally dominates in industrial solution crystallization (Mersmann et al. 1988). The so-called *attrition* is a two-step process consisting of the generation of attrition fragments and their subsequent growth. The attrition fragments are created mainly due to crystal-crystal and crystal-hardware collisions. The formation of secondary nuclei is dependent on the properties of the crystalline material and the hydrodynamic conditions inside the crystallizer. It has been shown that the mechanical stress applied to crystals results in distortion of the crystal lattice of the attrition fragments (van der Heijden et al. 1994; ÓMeadhra 1995). The lattice strain strongly affects the survival and the outgrowth of these fragments (Gahn and Mersmann 1997).

A great deal of work has been dedicated to empirical modeling of contact nucleation in a variety of crystallizing systems. The empirical secondary nucleation expressions mostly describe contact nucleation as a power-law function of crystal mass and supersaturation. Crystal mass enters the nucleation expression since

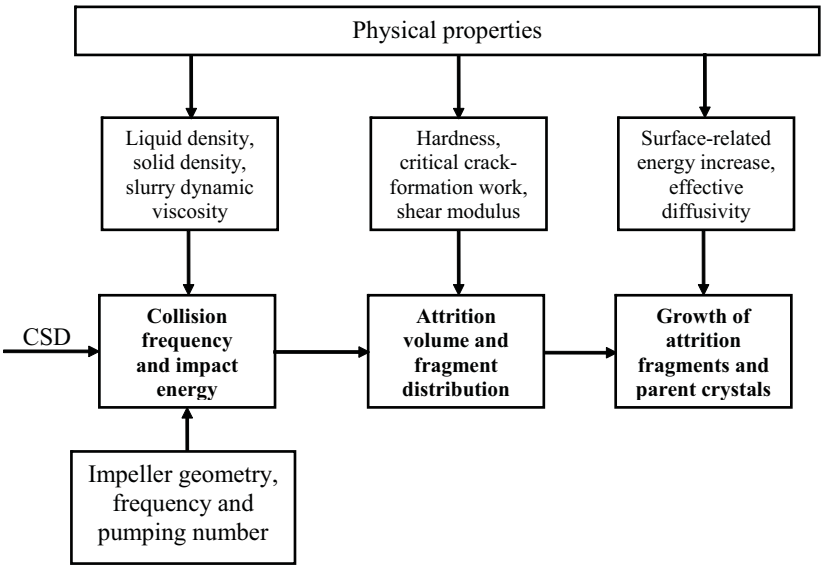

Figure 2.2: The framework of the kinetic model of Gahn and Mersmann (1999a,b) (after Bermingham (2003)).

collisional energy of crystal-crystal and crystal-hardware collisions is assumed to be proportional to the momentum of the collision, i.e. crystal mass multiplied by the square of the velocity of the collision. On the other hand, surface structures of the generated nuclei reestablish themselves by the process of crystal growth, which is correlated with the degree of supersaturation (Matthews 1997). van der Heijden et al. (1994) and ÓMeadhra (1995) present an overview of different empirical secondary nucleation models, specifically addressing issues such as the effect of CSD, supersaturation, and agitation.

More recently, Gahn and Mersmann (1999a,b) have proposed a mechanistic model for secondary nucleation and crystal growth, which provides a more physical basis for attrition modeling. Its number of kinetic parameters is considerably less than that of empirical kinetic models and more importantly the parameters have a physical meaning. As shown in Figure 2.2, the kinetic model of Gahn and Mersmann consists of three sub-models (Neumann 2001):

1. A procedure to determine the total number of crystals colliding per second with the face and edge of the impeller blades as well as the corresponding impact energy per collision (Pohlisch and Mersmann 1988; Ploß and Mersmann 1989).

2. A relation between the impact energy and the attrition volume produced due to a single collision of a crystal corner with a hard, flat surface; the re-

sulting number of attrition fragments and their number density distribution (Gahn and Mersmann 1997).

3. A relation to describe the growth rate of the fragments formed by the attrition process (Gahn and Mersmann 1999b).

Bermingham (2003) investigated the predictive quality of the latter mechanistic kinetic model in comparison with empirical secondary nucleation models. It was shown that the model of Gahn and Mersmann outperforms the considered empirical models. This is due to the lack of descriptive capability of empirical secondary nucleation models for particle mechanics and hydrodynamic effects.

Crystal growth

Once stable nuclei have been formed in a supersaturated solution, they begin to grow into crystals of visible size. The surface of crystals increases when solute molecules are incorporated into the accessible and energetically favorable kinks or steps of the crystal lattice (Mullin 2001).

Crystal growth from a solution primarily consists of two steps, namely diffusion of the solute molecules towards the crystal surface and integration of these growth units into the crystal lattice. The diffusion step entails mass transfer of the solute molecules from bulk through a stagnant layer around the crystal surface. This is followed by surface diffusion, spatial orientation, and the subsequent surface integration reaction that constitute the integration step. The individual steps of the crystal growth process are often described in terms of power-law functions of supersaturation. A thorough review of two-step crystal growth models is given in Garside (1984).

Depending on the rate coefficients of diffusive transport and surface integration as well as the supersaturation level, the crystal growth process can be diffusion-controlled, surface integration-controlled or a combination of both. In crystallization of very well soluble compounds, the surface integration is typically not rate limiting at a given supersaturation level. Hence, the crystal growth rate is mostly governed by diffusion through the stagnant layer around the crystal. For poorly soluble compounds, on the other hand, the surface integration reaction is often considerably slower than diffusion of the solute molecules towards the crystal surface (Menon 2006). Both crystal growth steps often play a dominant role in most crystallizing systems.

The growth rate of individual crystals can be affected by additional factors such as lattice stress, crystal size, and fluid dynamics. The prominent theories that describe the effect of these factors on crystal growth are *growth rate dispersion* and *size-dependent growth*. In the latter mechanism, crystals of different sizes grow at different rates, whereas growth rate dispersion is a phenomenon in which crystals of the same size have different growth rates under identical supersaturation level and hydrodynamic conditions. Extensive descriptions of growth rate dispersion and size-dependent growth mechanisms can be found in Liang et al. (1987); Zumstein and Rousseau (1987); Ristić et al. (1990); ÓMeadhra (1995); Menon (2006).

2.2 Modeling of a fed-batch evaporative crystallizer

2.2.1 Process description

This section describes the model development for seeded fed-batch evaporative crystallization of an ammonium sulphate-water system, which is considered in the remainder of this thesis. The crystallization takes place in the $75-liter$ draft tube crystallizer shown in Figure 2.3. The piping and instrumentation diagram of the semi-industrial crystallizer is given in Appendix A. The crystallizer can be considered as a single well-mixed compartment with one inlet and two outlet streams. The evaporative crystallization is carried out isothermally at $50\ ^{\circ}C$. The fed-batch operation is exercised to compensate for losses in crystallization volume due to the evaporation of solvent, i.e. water, and the slurry sampling. The crystallizer is continuously fed throughout a batch run with a crystal-free feed stream containing saturated ammonium sulphate solution. The outlet flows from the crystallizer include an unclassified product removal stream as well as a vapor stream, which is free from crystal and solute. A detailed description of the semi-industrial crystallizer can be found in Westhoff (2002).

To ensure the reproducibility of batch runs and the achievement of desired product specifications, seeding is carried out. Ground seeds are prepared by milling and sieving of the commercial product crystals of ammonium sulphate (DSM, The Netherlands) to collect $0.6\ kg$ of the $90-125\ \mu m$ sieve fraction. Prior to insertion into the crystallizer, the seed crystals are aged for one hour in a saturated

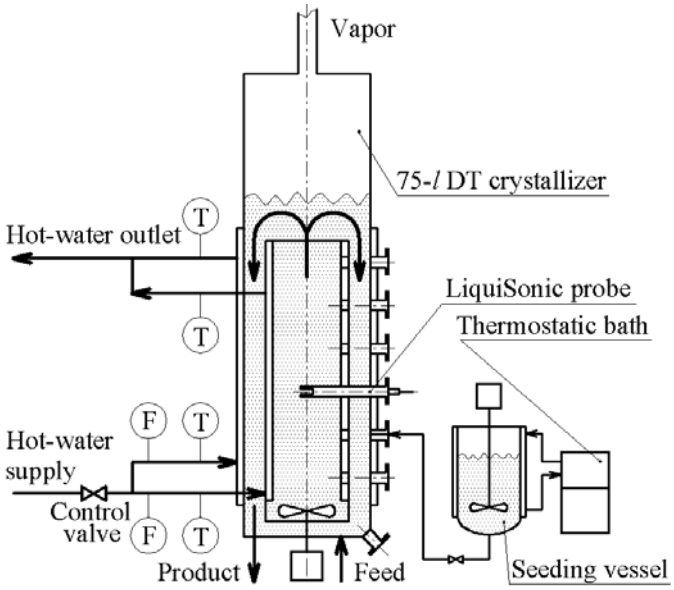

Figure 2.3: The $75-liter$ draft tube crystallizer.

solution of ammonium sulphate at $50\,°C$ (Kalbasenka et al. 2007). A concentration measuring probe is utilized to detect the predetermined supersaturation, at which the seeds are introduced to the vessel.

2.2.2 Measurement equipment

In most crystallization applications, measurements of crystal size distribution and solute concentration, along with temperature, are essential. Contrary to temperature measurements, several challenges exist in reliable measurement of the evolution of CSD and solute concentration during a batch crystallization process.

An overview of the existing techniques

The crystal size distribution can be measured either offline, online or in-situ. Offline monitoring of the CSD largely relies on good sampling that is often difficult to achieve. In addition, the samples may not adequately describe the system dynamics since they are subject to change while being transferred to the offline measuring instrument (Yu et al. 2007). The sampling deficiencies are alleviated in online and in-situ CSD measurement techniques. One of the most commonly used online techniques is laser diffraction, which is based on forward light scattering. In this technique, the particles are illuminated by a beam of visible light that leads to a diffraction pattern. The diffraction pattern is inverted to reconstruct the size distribution using mathematical algorithms. The use of the laser diffraction technique is limited to low solid concentrations, i.e. $1.5\ vol.\%$ (Neumann and Kramer 2002).

In-situ CSD measurements can be obtained by ultrasound extinction and laser back scattering techniques. The ultrasound extinction technique measures the attenuation of ultrasound while passing through the slurry. The main merit of this technique lies in its ability to measure the CSD in high slurry concentrations, i.e. $40\ vol.\%$. However, it is insensitive to small fractions of solid (Neumann and Kramer 2002). In addition, thermal and viscous losses in the crystallizing system may deteriorate the CSD measurements (Dukhin et al. 1996). The laser back scattering technique measures the back-diffraction characteristics of the suspension, taking solvent and solute properties, e.g., the refractive index and the morphology, into account. This technique gives chord length distribution, from which the crystal size distribution is calculated using statistical models. The restoration of CSD is often complicated as it requires accurate information on the optical properties and the shape of crystals (Barthe and Rousseau 2006).

The concentration monitoring techniques are based on the measurement of a wide range of solution properties such as the refractive index (Helt and Larson 1977), the conductivity (Hlozny et al. 1992), the density of the liquid phase (Gutwald and Mersmann 1990), the absorbance of the electromagnetic light (Wang and Berglund 2000; Doki et al. 2001), etc. The measurement of the refractive index can be performed by a differential refractometer, which consists of cells for the sample and for a reference material. The refractometer measures the light deflection resulting from the differences between the refractive indices of the reference material and the sample. These measurements require strict regulation of conditions

in the crystallizer that may become impractical in the presence of crystals (Helt and Larson 1977).

The measurement of conductivity as a means to determine concentration is restricted to electrolyte solutions (Hlozny et al. 1992). Density measurements are widely used at laboratory-scale to monitor concentration. However, the use of this technique in industrial-scale crystallization is limited. This is due to its sensitivity to unknown impurities and temperature changes as well as the need for prior solid-liquid separation (Gutwald and Mersmann 1990).

Most of the aforementioned shortcomings are effectively addressed by using spectroscopic techniques for measuring concentration. These techniques can be utilized in-situ, alleviating the need for sampling (Fujiwara et al. 2002). Attenuated total reflectance Fourier transform infrared (ATR-FTIR) is the most commonly used spectroscopic technique in crystallization applications (Dunuwila and Berglund 1997; Togkalidou et al. 2001; Hojjati and Rohani 2006; Borissova et al. 2009). The ATR-FTIR spectroscopy relies on the mid-infrared region of the electromagnetic spectrum, i.e. $2.5\ \mu m$ to $25\ \mu m$. The spectrum is a characteristic of the vibrational structure of the material (Dunuwila and Berglund 1997). The in-situ instrument typically consists of an ATR probe connected to an interferometer with a fiber optic guide. The probe head is made of an internal reflection element that is in intimate contact with the slurry. The effective contact between the probe head and the slurry is limited to the liquid phase as the penetration depth of radiations in the solution is in the order of few microns (Dunuwila et al. 1994).

Data acquisition from the $75-liter$ crystallizer

The CSD measurements are performed online by a laser diffraction instrument (HELOS-Vario, Sympatec, Germany). To facilitate the online sampling, a small product stream is withdrawn from the crystallizer at regular time intervals, viz $100\ s$. The product stream is diluted with a saturated ammonium sulphate solution to obtain a crystal concentration of less than $1.5\ vol.\%$. Dilution is essential for ensuring the adequate accuracy of CSD measurements by avoiding effects of multiple scattering. The diluted sample stream is pumped through the measurement cell of the HELOS instrument for $20\ s$. The actual measurement has a time resolution of $100\ ms$ and lasts $10.3\ s$. Prior to each CSD measurement, a background measurement is taken from the dilution stream, i.e. the saturated ammonium sulphate solution. The measurement principle and the automatic dilution procedure are described in more detail in Neumann (2001); Kalbasenka (2009).

The HELOS instrument gives a normalized cumulative volume density distribution $\bar{Q}_3$ defined as

$$\bar{Q}_3(n) = \sum_{j=1}^{m} \Delta\bar{Q}_3(j) = 100\% \quad \Delta\bar{Q}_3(j) = \bar{Q}_3(j+1) - \bar{Q}_3(j), \tag{2.16}$$

where m is the number of size classes, viz $m = 31$. The volume density distribution can be computed from the CSD measurements by

$$q_3(j) = 0.01\frac{\Delta\bar{Q}_3(j)(1-\varepsilon)}{\Delta L(j)}, \tag{2.17}$$

where $q_3(j)$ is the volume density distribution of crystals in the size class j $(1/m)$; $\Delta L(j)$ is the difference between the adjacent grid points, i.e. $\Delta L(j) = L(j+1) - L(j)$; ε is the liquid fraction of the slurry in the crystallizer that is inferred from density measurements of the product slurry, i.e. ρ_p (kg/m^3),

$$\varepsilon = 1 - \frac{\rho_p - \rho_l}{\rho_s - \rho_l}. \tag{2.18}$$

To calculate the moments of CSD, the volume density distribution is converted into the number density distribution

$$n(j) = \frac{q_3(j)}{k_v L_m^3(j)}, \tag{2.19}$$

where $L_m(j)$ is the arithmetic mean of each size class. Subsequently, the moments of CSD are computed as

$$\mu_i = \sum_{j=1}^{m} n(j) L_m^i(j) \Delta L(j) \qquad i = 0, 1, \cdots, 4. \tag{2.20}$$

The relative standard deviations in the moments of the measured crystal size distributions are estimated by fitting a linear relationship and calculating the average standard deviation of all data points. This approach is a valid approximation of measurement errors since the time intervals between any two successive data points are in the order of two minutes, whereas the characteristic time of the process dynamics is in the order of hours (Bermingham 2003).

In addition to the HELOS instrument, the semi-industrial crystallizer is equipped with an *ultrasonic analyzer* (Liquisonic 20, SensoTech, Germany). Kalbasenka (2009) verified the suitability of the ultrasonic analyzer for measuring concentration of ammonium sulphate. He demonstrated that the analyzer can be used to detect the point of primary nucleation or seed insertion into the crystallizer. However, it is incapable of measuring the solute concentration in the presence of crystals.

An ATR-FTIR probe (Matrix MF, Bruker Optics, Germany) is utilized in one batch run to measure the evolution of solute concentration throughout the crystallization process. The use of the ATR-FTIR probe requires laborious calibration work to develop a partial least squares (PLS) model, which accurately quantifies the concentration of ammonium sulphate from the collected infrared spectra. It is demonstrated in Kadam et al. (2010a) that a PLS model developed at laboratory-scale cannot adequately predict the solute concentration profile in the semi-industrial crystallizer. The PLS model led to a concentration profile that deviated by almost 16 % from the reference concentration profile determined by the ultrasonic analyzer till the seeding point. Figure 2.4 shows the infrared spectra of ammonium sulphate collected from a laboratory-scale and the semi-industrial crystallizer under identical process conditions. The spectra are collected over the absorbance region $4000 - 400\, cm^{-1}$ with resolution of $8\, cm^{-1}$; each spectrum consists of 16 co-added scans. As can be seen, both spectra have the same peaks, sug-

gesting that the inadequacy of the PLS model could not be due to solution impurities in the semi-industrial crystallizer. The broad absorbance region at $3500 - 2700$ cm^{-1} comprises an O-H stretch absorption at $3500 - 3000$ cm^{-1}, along with an overlapping band for the N-H stretch at $3300 - 2700$ cm^{-1}; the shoulders on the absorption band are due to solute-solvent interactions. The band at 1640 cm^{-1} results from water bending, whereas bands at 1450 cm^{-1} and 1000 cm^{-1} are due to N-H bending and sulphate, respectively.

Figure 2.4 suggests that the spectra exhibit differences in their intensities. The differences can be attributed to thermal and mechanical stresses in the fiber optic guide of the ATR-FTIR probe. It is speculated that thermal stresses lead to expansion or contraction of the fiber optic guide, altering its characteristic absorption. On the other hand, mechanical stresses result from the differences in curvature of the fiber optic guide. The absorption of radiations inside the fiber rises with an increase in the curvature of the fiber optic guide. These deficiencies indicate that a PLS model developed on the basis of laboratory experiments is unlikely to be applicable for concentration monitoring in an industrial crystallizer.

In this thesis, a rapid online calibration technique that avoids extensive laboratory experimentation to develop a PLS model is devised. This technique relies on relatively few spectra, alleviating the need for data preprocessing and validation of the PLS model using an independent data set. Therefore, it substantially reduces the calibration time.

The online calibration is performed with the aid of the ultrasonic analyzer. The solute concentration is measured simultaneously by the ultrasonic analyzer and the ATR-FTIR probe in the initial phase of the batch run prior to seed insertion.

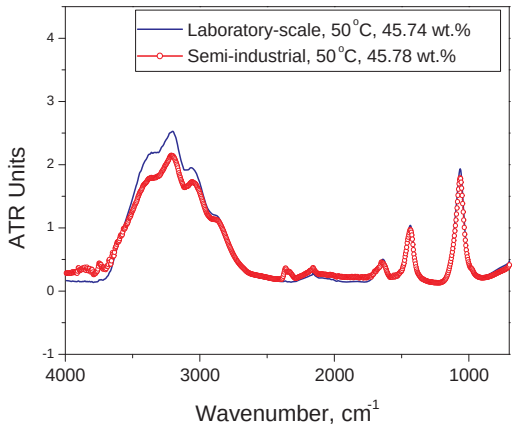

Figure 2.4: The infrared spectra of ammonium sulphate collected from laboratory-scale and semi-industrial crystallizers.

A PLS model is developed on the basis of the spectra collected by the ATR-FTIR probe and the solute concentration measurements of the ultrasonic analyzer. The PLS model is then validated online by comparing its predictions with solute concentration measurements of the ultrasonic analyzer till the seeding point. The online calibration results are presented in Section 2.3.2.

2.2.3 The population balance model

Crystallization of a well-soluble compound such as ammonium sulphate is dominated by secondary nucleation, in particular contact nucleation, and crystal growth (Mersmann et al. 1988). To restrict the model complexity, the following simplifying assumptions are made:

- constant feed temperature;
- a crystal-free saturated feed stream;
- constant crystallization volume;
- negligible heat of crystallization and heat losses to the environment;
- negligible energy input via the mechanical action of the impeller;
- a pure single-component solid phase;
- solute- and crystal-free vapor stream;
- non-classified product removal;
- constant material properties during the isothermal operation;
- negligible primary nucleation, agglomeration, and breakage;
- formation of nuclei of infinitesimal size;
- size-independent growth of crystals.

Population balance equation

Under the aforementioned assumptions, the dynamic evolution of CSD in a well-mixed compartment with one inlet stream and two outlet streams, namely the product and vapor streams, is represented by

$$\frac{\partial n(L,t)}{\partial t} = -G(t)\frac{\partial n(L,t)}{\partial L} - \frac{\phi_{V,product}}{V}n(L,t) \tag{2.21}$$

with the left boundary condition

$$n(L_0,t) = \frac{B_0(t)}{G(t)}. \tag{2.22}$$

$\phi_{V,product}$ is the volumetric flow rate of the product stream (m^3/s).

In model-based control applications, empirical power-law functions are the most commonly used kinetic relationships to model the total nucleation rate and the size-independent crystal growth rate (Braatz and Hasebe 2002). The expressions used to describe the latter phenomena in crystallization of ammonium sulphate are chosen as (Daudey et al. 1990)

$$B_0(t) = k_b \mu_3 S^b \tag{2.23}$$

$$G(t) = k_g S^g, \tag{2.24}$$

where k_b is the nucleation rate constant $(\#/m^4)$; b is the nucleation rate exponent; k_g is the crystal growth rate constant (m/s); g is the crystal growth rate exponent; $S = C - C^*$ is the degree of supersaturation; C is the solute concentration $(kg_{solute}/kg_{solution})$; C^* is the saturation concentration at the given operating temperature; μ_i is the i^{th} moment of crystal size distribution defined as

$$\mu_i = \int_{L_0}^{\infty} n(L,t) L^i \mathrm{d}L \qquad i = 0, 1, \cdots, 4. \tag{2.25}$$

The kinetic parameters in equations (2.23) and (2.24) will be estimated using data of batch crystallization experiments.

Crystal mass balance equation

The mass balance for the solid phase results from the difference between the crystal production term and the crystal mass in the product stream

$$V\rho_s \frac{\mathrm{d}(1-\varepsilon)}{\mathrm{d}t} = -\phi_{V,product}(1-\varepsilon)\rho_s + \phi_{m,grow}, \tag{2.26}$$

where ε is the liquid fraction; $\phi_{m,grow}$ is the crystal production term due to crystal growth

$$\phi_{m,grow} = 3\rho_s k_v V G \mu_2. \tag{2.27}$$

Hence, the evolution of liquid fraction in the crystallizer becomes

$$\frac{\mathrm{d}\varepsilon}{\mathrm{d}t} = \frac{\phi_{V,product}}{V}(1-\varepsilon) - 3k_v G\mu_2. \tag{2.28}$$

Overall mass balance equation

The overall mass balance is formulated as

$$V\frac{\mathrm{d}\big(\varepsilon\rho_L + (1-\varepsilon)\rho_s\big)}{\mathrm{d}t} = \phi_{V,feed}\rho_L - \phi_{V,product}(\varepsilon\rho_L + (1-\varepsilon)\rho_s) - \phi_{m,vapor}, \tag{2.29}$$

where ρ_L is the liquid density (kg/m^3); $\phi_{V,feed}$ is the volumetric flow rate of the feed stream (m^3/s); $\phi_{m,vapor}$ is the mass flow rate of the vapor stream (kg/s).

Energy balance equation

Under the aforementioned assumptions, the enthalpy balance for a fed-batch evaporative crystallizer is expressed as

$$V\frac{\mathrm{d}\big(\varepsilon\rho_L h_L+(1-\varepsilon)\rho_s h_s\big)}{\mathrm{d}t}=\phi_{V,feed}\rho_L h_L-\phi_{V,product}(\varepsilon\rho_L h_L+(1-\varepsilon)\rho_s h_s)-\phi_{m,vapor}h_V+Q, \tag{2.30}$$

where h_L, h_s, and h_V are the specific enthalpy of liquid, solid, and vapor phases, respectively (J/kg).

Solute mass balance equation

The mass balance for the crystallizing solute in the liquid and in the solid phases is

$$V\frac{\mathrm{d}\big(\varepsilon\rho_L C+(1-\varepsilon)\rho_s\big)}{\mathrm{d}t}=\phi_{V,feed}\rho_L C^*-\phi_{V,product}(\varepsilon\rho_L C+(1-\varepsilon)\rho_s). \tag{2.31}$$

By resolving equation (2.31) for $\mathrm{d}C/\mathrm{d}t$, the following expression for the evolution of the solute concentration during the batch run is obtained

$$\frac{\mathrm{d}C}{\mathrm{d}t}=\frac{1}{V\varepsilon\rho_L}\left(V(\rho_s-\rho_L C)\frac{\mathrm{d}\varepsilon}{\mathrm{d}t}+\phi_{V,feed}\rho_L C^*-\phi_{V,product}\big(\varepsilon\rho_L C+(1-\varepsilon)\rho_s\big)\right). \tag{2.32}$$

Equation (2.32) can be further simplified by substituting equation (2.28) and solving the resulting equation for $\phi_{V,feed}$ and $\phi_{m,vapor}$ using the overall mass balance and energy balance equations. Hence, the solute concentration balance becomes

$$\frac{\mathrm{d}C}{\mathrm{d}t}=\frac{\phi_{V,product}(C^*-C)/V+3k_v G\mu_2(k_1+C)}{1-k_v\mu_3}+\frac{k_2 Q}{1-k_v\mu_3} \tag{2.33}$$

with the initial condition

$$C(t_0)=C_0. \tag{2.34}$$

The constant coefficients k_1 and k_2 in equation (2.33) are defined as

$$k_1=\frac{h_V C^*}{h_V-h_L}\left(\frac{\rho_s}{\rho_L}-1+\frac{\rho_L h_L-\rho_s h_s}{\rho_L h_V}\right)-\frac{\rho_s}{\rho_L} \tag{2.35}$$

$$k_2=\frac{C^*}{V\rho_L(h_V-h_L)}. \tag{2.36}$$

It follows from the above analysis that equations (2.21-2.25) and (2.33-2.36) provide a complete description of the dynamics of the semi-industrial crystallizer under study. The model parameters and the physical properties of the ammonium sulphate-water crystallizing system are listed in Table 2.1.

Table 2.1: Model parameters and physical properties of the ammonium sulphate-water crystallizing system.

Parameter[a]	Value
C^*, $kg_{solute}/kg_{solution}$	0.46
h_L, kJ/kg	69.86
h_s, kJ/kg	60.75
h_V, kJ/kg	2.59×10^3
k_v	0.43
V, m^3	7.50×10^{-2}
$\phi_{V,product}$, m^3/s	1.73×10^{-6}
ρ_L, kg/m^3	1248.93
ρ_s, kg/m^3	1767.35

[a]The physical properties are calculated at $50\ ^\circ C$.

2.2.4 The moment model

The *method of moments* is utilized as a model reduction technique to obtain the analytical solution of equation (2.21). This method allows us to reduce the PBE to a set of nonlinear ordinary differential equations. However, the resulting moment model has several shortcomings. The CSD cannot be uniquely reconstructed from a finite number of moments since the inverse problem is ill-conditioned (Randolph and Larson 1988). In addition, the use of size-dependent functions prohibits the closure of moment equations. Thus, the moment model cannot adequately describe the dynamics of most crystallization systems with fines dissolver, classifiers, or size-dependent crystal growth and dissolution kinetics.

The reduction of the PBE to a closed set of ordinary differential equations (ODEs) enables us to efficiently solve the crystallization model to a prespecified accuracy. This makes the use of the moment model particularly suitable for control applications. In addition, the four leading moments of CSD have physical significations:

$$\mu_0 = \texttt{total crystal number per unit volume}$$
$$\mu_1 = \texttt{total crystal length per unit volume}$$
$$\mu_2 \propto \texttt{total crystal surface area per unit volume}$$
$$\mu_3 \propto \texttt{total crystal volume per unit volume}.$$

The mean crystal size can be defined as the ratio of μ_4 to μ_3.

The method of moments is a special case of the method of weighted residuals in which the weight functions are defined as (Ramkrishna 2000)

$$\omega(L) = L^{i-1}. \tag{2.37}$$

The moment equations are derived by multiplying the PBE

$$\frac{\partial n(L,t)}{\partial t} = B_0(t)\delta(L-L_0) - G(t)\frac{\partial n(L,t)}{\partial L} - \frac{\phi_{V,product}}{V}n(L,t) \tag{2.38}$$

by L^i and integrating over all crystal sizes

$$\begin{aligned}\frac{\partial}{\partial t}\int_{L_0}^{\infty} n(L,t)L^i \mathrm{d}L = \int_{L_0}^{\infty} B_0(t)\delta(L-L_0)L^i \mathrm{d}L - \\ G(t)\int_{L_0}^{\infty}\frac{\partial n(L,t)}{\partial L}L^i \mathrm{d}L - \frac{\phi_{V,product}}{V}\int_{L_0}^{\infty} n(L,t)L^i \mathrm{d}L.\end{aligned} \tag{2.39}$$

In equation (2.38), the nucleation of crystals of infinitesimal size is represented as a point source term, where $\delta(L-L_0)$ is a Dirac delta function. Performing integration by parts on the second term on the right hand side of equation (2.39) gives

$$\begin{aligned}-G(t)\int_{L_0}^{\infty}\frac{\partial n(L,t)}{\partial L}L^i \mathrm{d}L = -G(t)L^i n(L,t)|_{L_0}^{\infty} + \\ iG(t)\int_{L_0}^{\infty} n(L,t)L^{i-1}\mathrm{d}L.\end{aligned} \tag{2.40}$$

When $n(L_0,t)$ is finite and the distribution contains no crystals of infinite size, the first term on the right hand side of equation (2.40) vanishes. Substituting equation (2.40) into equation (2.39) and letting $L_0 \longrightarrow 0$ results in

$$\begin{aligned}\frac{\mathrm{d}}{\mathrm{d}t}\int_{L_0}^{\infty} n(L,t)L^i \mathrm{d}L = B_0(t)0^i + iG(t)\int_{L_0}^{\infty} n(L,t)L^{i-1}\mathrm{d}L - \\ \frac{\phi_{V,product}}{V}\int_{L_0}^{\infty} n(L,t)L^i \mathrm{d}L.\end{aligned} \tag{2.41}$$

Given that the i^{th} moment of CSD is expressed as in equation (2.25), the set of ODEs describing the evolution of the five leading moments of CSD in time becomes

$$\frac{\mathrm{d}\mu_i}{\mathrm{d}t} = 0^i B_0(t) + iG(t)\mu_{i-1} - \frac{\mu_i \phi_{V,product}}{V} \qquad i = 0,\cdots,4 \tag{2.42}$$

with the initial conditions

$$\mu_i(t_0) = \mu_{i,0}. \tag{2.43}$$

To simulate the dynamics of the crystallizer, equation (2.43) should be coupled with the solute concentration balance and the kinetic expressions introduced in Section 2.2.3. The kinetic parameters of the moment model are estimated by Kalbasenka (2009).

2.2.5 Model summary

The input-output diagram of the $75-liter$ draft tube crystallizer under study is depicted in Figure 2.5. The heat input serves as the primary means of control in evaporative batch crystallization. The heat input governs the rate of supersaturation generation, which in turn influences crystal growth and nucleation. A thorough seeding procedure is applied in batch runs to minimize secondary nucleation and consequently narrow the operational envelop. Kalbasenka et al. (2007) showed that the reproducibility of batch runs can be improved by optimizing the initial conditions, namely the size, mass, and quality of seeds as well as the initial supersaturation. Optimal seeding minimizes secondary nucleation by suppressing excessive supersaturation in a batch run. This leads to an operational envelop, in which the crystal growth mainly dictates the process dynamics. In this operational envelop, crystallization kinetics are primarily governed by the heat input into the crystallizer (Kalbasenka et al. 2005).

The crystal size distribution measurements comprise the process outputs. It should be noted that the evolution of solute concentration is measured during one batch run only. In the following, the state space representation of the population balance model and the moment model are presented.

The population balance model

Chapter 3 gives a comprehensive analysis of the solution methods commonly used to solve the population balance equation. It is shown that the high order finite volume methods with flux limiting functions are best suited for solution of the PBE in online control applications. By adopting this numerical technique to solve equation (2.21), the dynamics of the semi-industrial crystallizer can be represented by a set of nonlinear differential algebraic equations

$$\begin{aligned} \dot{x} &= f(t,x,z,y,u,\theta) \qquad x(t_0) = x_0 \\ 0 &= g(t,x,z,y,u,\theta) \\ y &= h(t,x,z,y,u,\theta), \end{aligned} \tag{2.44}$$

where t is the time; $x(t) \in R^{n_x}$ is the state vector comprised of values of the crystal population in each crystal cell and the solute concentration

$$x(t) = [n(L,t) \quad C(t)]^T; \tag{2.45}$$

$z(t) \in R^7$ is the vector of algebraic variables

$$z(t) = [\mu_0(t) \quad \mu_1(t) \quad \mu_2(t) \quad \mu_3(t) \quad \mu_4(t) \quad B_0(t) \quad G(t)]^T; \tag{2.46}$$

Figure 2.5: The input-output diagram of the $75-liter$ draft tube crystallizer.

$y(t) \in R^5$ is the vector of measured variables

$$y(t) = [\mu_0(t) \quad \mu_1(t) \quad \mu_2(t) \quad \mu_3(t) \quad \mu_4(t)]^T; \tag{2.47}$$

$u(t) \in U \subset R$ is the vector of process inputs

$$u(t) = [Q(t)]; \tag{2.48}$$

$\theta \in \Theta \subset R^4$ is the vector of kinetic parameters

$$\theta = [k_b \quad b \quad k_g \quad g]^T; \tag{2.49}$$

$f : R^{n_x} \times R^7 \times R^{n_y} \times U \times \Theta \rightarrow R^{n_x}$ is the vector function of the dynamic state equations; $g : R^{n_x} \times R^7 \times R^{n_y} \times U \times \Theta \rightarrow R^7$ is the vector function of the algebraic equations; $h : R^{n_x} \times R^7 \times R^{n_y} \times U \times \Theta \rightarrow R^{n_y}$ is the vector function of the measurement equations; x_0 represents the initial states of the system that are governed by the seed distribution and the initial solute concentration. It is assumed that the seed crystals have a log-normal distribution

$$n(L,0) = \left(\frac{1-\varepsilon}{k_v L^3}\right) \frac{1}{\ln(\sigma_g)\sqrt{2\pi}L} \exp\left(-\frac{\left(\ln\left(\frac{L}{L_0}\right)\right)^2}{2(\ln(\sigma_g))^2}\right), \tag{2.50}$$

where L_0 is the mean of the distribution (m); σ_g is the geometric standard deviation of the distribution. It is self-evident that the dimension of the state vector depends on the number of crystal cells used to discretize the crystal size distribution over L.

The moment model

The moment model presented in Section 2.2.4 can be recast as a smooth affine control system

$$\begin{aligned} \dot{x} &= \mathcal{F}(x) + \mathcal{G}(x)u \\ y_i &= \mathcal{H}_i(x) \qquad i = 1, 2, \ldots, 5, \end{aligned} \tag{2.51}$$

where the system states $x(t) = [\mu_0(t) \;\; \mu_1(t) \;\; \mu_2(t) \;\; \mu_3(t) \;\; \mu_4(t) \;\; C(t)]^T$ constitute the local coordinates for a smooth manifold M, viz the state space manifold; $u(t) = [Q(t)] \in U \subset \mathbb{R}$ is the input to the system; $\mathcal{F}$ and $\mathcal{G}$ are smooth vector fields on M; $\mathcal{H}$ is the smooth output map of the system. The vector fields of the smooth affine control system are defined as

$$\mathcal{F} = \begin{bmatrix} k_b\mu_3(C-C^*)^b - \frac{\mu_0\phi_{V,product}}{V} \\ k_g(C-C^*)^g\mu_0 - \frac{\mu_1\phi_{V,product}}{V} \\ 2k_g(C-C^*)^g\mu_1 - \frac{\mu_2\phi_{V,product}}{V} \\ 3k_g(C-C^*)^g\mu_2 - \frac{\mu_3\phi_{V,product}}{V} \\ 4k_g(C-C^*)^g\mu_3 - \frac{\mu_4\phi_{V,product}}{V} \\ \frac{\frac{\phi_{V,product}(C^*-C)}{V} + 3k_v k_g(C-C^*)^g\mu_2(k_1+C)}{1-K_v\mu_3} \end{bmatrix}, \quad \mathcal{G} = \begin{bmatrix} 0 \\ 0 \\ 0 \\ 0 \\ 0 \\ \frac{k_2}{1-K_v\mu_3} \end{bmatrix}, \tag{2.52}$$

$$and \quad \mathcal{H} = \begin{bmatrix} \mu_0 \\ \mu_1 \\ \mu_2 \\ \mu_3 \\ \mu_4 \end{bmatrix}.$$

Note that the smooth output map of the system, i.e. $\mathcal{H} : \mathbb{R}^6 \rightarrow \mathbb{R}^5$, only consists of the five leading moments of CSD.

2.3 Parameter estimation and model validation

Section 2.2 presented a general model structure for fed-batch evaporative crystallization of an ammonium sulphate-water system. The inference of model parameters from experimental data comprises the second step in the process of model development. The parameters of interest are the kinetic parameters that define the nucleation and crystal growth phenomena. These kinetic processes govern the evolution of CSD during a batch run. Therefore, the descriptive capability of the crystallization model largely relies on accurate determination of the kinetic parameters when the model structure is adequate.

2.3.1 Formulation of the parameter estimation problem

Optimization-based approaches are commonly used for parameter estimation of batch crystallization systems (Palwe et al. 1985; Dash and Rohani 1993; Miller and Rawlings 1994; Qiu and Rasmuson 1994; Livk et al. 1995; Matthews and Rawlings 1998; Hu et al. 2005c; Nowee et al. 2007). In an optimization-based approach, the model equations are solved to compute an objective function that calculates the difference between the model predictions and the corresponding measurement data. The objective function is minimized by nonlinear optimization algorithms. The optimization-based approaches allow us to exploit statistical tools to assess the quality of parameter estimates.

In this thesis, a nonlinear weighted least squares optimization problem is formulated to estimate the parameters of the population balance model. The optimization problem is as follows

$$\begin{aligned} \hat{\theta} := \arg \min_{\theta} \quad & \sum_{i=1}^{N_m} \sum_{j=1}^{N_v} w_i (\tilde{y}_{ij} - y_{ij})^2 \\ \text{subject to:} \quad & \\ & \dot{x} = f(t, x, z, y, u, \theta) \qquad x(t_0) = x_0 \\ & 0 = g(t, x, z, y, u, \theta) \\ & y = h(t, x, z, y, u, \theta), \end{aligned} \tag{2.53}$$

where a variable subscripted by ij represents the j^{th} value of the i^{th} variable; $\tilde{y}$

denotes the measured variables

$$\tilde{y} = y(\theta) + \mathsf{e}; \tag{2.54}$$

e is the white measurement error; N_m is the number of measured variables; N_v is the number of measurements of each variable; w_i is a nonnegative weight factor to account for differences in measurement errors. The nonlinear programing problem stated in equation (2.53) is solved in MATLAB using the nonlinear curve fitting function `lsqnonlin`.

Using a statistical approach, the weighted least squares estimator also provides a means to characterize the uncertainty of the estimated parameters by specifying the asymptotic probability density function of the estimator. Under mild regulatory conditions and including conditions on the information content of the considered data sets, i.e. the correctness of the model structure, the parameter estimates converge to a normal distribution

$$\sqrt{N}(\hat{\theta}^N - \theta_0) \rightarrow \mathcal{N}(0, \mathsf{P}) \quad \text{if} \quad N \rightarrow \infty, \tag{2.55}$$

where $\mathcal{N}$ represents a normal distribution; θ_0 is the vector of true system parameters; P is the asymptotic parameter covariance matrix determined by

$$\mathsf{P} = \mathsf{W_e}\mathbb{E}\big[\big(\frac{\partial y(\theta)}{\partial \theta}\big)\big(\frac{\partial y(\theta)}{\partial \theta}\big)^T\big]^{-1}_{\theta=\theta_0}\mathsf{W_e}, \tag{2.56}$$

where $\mathsf{W_e}$ is the covariance matrix of the measurement noise, i.e. $\mathsf{W_e} = \mathbb{E}[\mathsf{e}\mathsf{e}^T]$ (Söderström and Stoica 1989).

An approximation of the parameter covariance matrix can be obtained by linearizing the model equations in the vicinity of the estimated parameters $\hat{\theta}$

$$y_{ij}(\theta) \approx y_{ij}(\hat{\theta}) + \Gamma_{ij}(\theta - \hat{\theta}), \tag{2.57}$$

where

$$\Gamma_{ij} = \frac{\partial y_{ij}}{\partial \theta}|_{\theta=\hat{\theta}} \tag{2.58}$$

is a $1 \times N_p$ vector; N_p denotes the number of parameters. The linearized model is exploited to approximate the parameter uncertainty regions, which surround the point estimates $\hat{\theta}$. In practice, the prior information on parameter uncertainty is often neglected. Hence, the uncertainty regions can be expressed in terms of the approximated covariance matrix V_θ defined as (Bard 1974)

$$\mathsf{V}_\theta = \left(\sum_{i=1}^{N_m}\sum_{j=1}^{N_v}\sigma_i^{-2}\Gamma_{ij}^T\Gamma_{ij}\right)^{-1}, \tag{2.59}$$

where σ_i^{-2} is the inverse of the variance of the measurement errors.

The boundaries of the parameter uncertainty region correspond to contours of constant probability density. When projected into the parameter space, each contour is ellipsoidal in shape with a volume that relates to some fraction of the total

probability expressed by the posterior distribution. In the considered situation, the value of

$$(\theta - \hat{\theta})^T \mathsf{V}_\theta^{-1} (\theta - \hat{\theta}) \tag{2.60}$$

has a χ_p^2-distribution with N_p degrees of freedom (Seber and Wild 1989). Hence, the estimated parameters lie in an ellipsoidal region with a probability greater than α, i.e.

$$\hat{\theta} \in \{\theta | (\theta - \hat{\theta})^T \mathsf{V}_\theta^{-1} (\theta - \hat{\theta}) \leq \chi_p^2(\alpha)\}. \tag{2.61}$$

The linear $95\ \%$ confidence intervals given in the remainder of this section are determined by

$$\theta_i \approx \hat{\theta}_i \pm \sqrt{\chi_p^2(\alpha) \mathsf{V}_\theta(i,i)}, \tag{2.62}$$

where $\alpha = 0.025$. Equation (2.62) provides the dimensions of a hyperbox in the parameter space that circumscribes the ellipsoidal confidence region (Fedorov 1972).

2.3.2 Parameter estimation of the population balance model

The adequacy of the population balance model presented in Section 2.2.3 is examined on the basis of several seeded fed-batch evaporative experiments. The process model equipped with the estimated parameters should be capable of describing the dynamics of seeded batch runs taking place in the $75 - liter$ draft tube crystallizer. As discussed in Section 2.2.1, seeding allows us to ensure the reproducibility of batch runs.

The unknown kinetic parameters of the model are estimated using historical data of batch run DT_c88. The experimental settings are given in Table 2.2. Figure 2.6 shows the heat input profile applied to the semi-industrial crystallizer. As can be seen, the heat input is varied between $4.5\ kW$ and $13\ kW$ during the batch run to more profoundly excite the system dynamics.

In addition to the evolution of CSD, solute concentration is measured throughout the batch run by means of the ATR-FTIR probe. The online calibration method introduced in Section 2.2.2 is used to develop a PLS model. Figure 2.7 shows the solute concentration profiles measured by the ATR-FTIR probe and the ultrasonic analyzer during batch run DT_c88. It is observed that the predictions of the PLS model and the solute concentration measurements of the ultrasonic analyzer are in good agreement till the seeding point. As expected, the ultrasonic analyzer

Table 2.2: Description of the seeded fed-batch evaporative crystallization experiments.

Experiment	Operating conditions				Seeding conditions	
	Temperature, $^\circ C$	Pressure, $mbar$	Impeller frequency, rpm	Heat input, kW	Seed aging time, min	Initial supersaturation
DT_c31	50	100	450	9.0	57	0.01627
DT_c88	50	100	450	Figure 2.6	59	0.01443

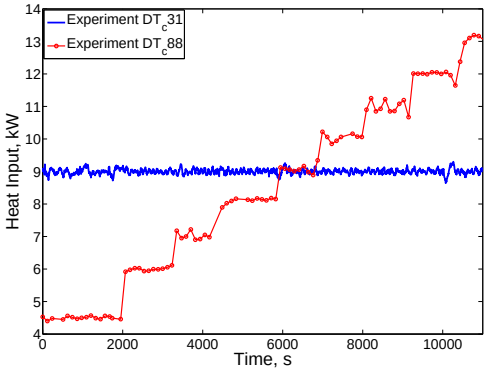

Figure 2.6: Heat input profiles.

fails to monitor the solute concentration after seeding due to the presence of crystals. On the contrary, the ATR-FTIR probe allows us to measure the solute concentration till the end of the batch run when it stabilizes close to the saturation concentration. The peaks in the temperature profile and consequently in the saturation concentration are due to the step-wise increase in the heat input. Although the predictions of the PLS model could not be examined by independent measurements, it is evident that the online calibration technique is an attractive alternative for calibration at laboratory-scale. A more thorough discussion on the results of the online calibration technique can be found in Kadam et al. (2010a).

The kinetic parameters to be estimated include the nucleation rate constant k_b,

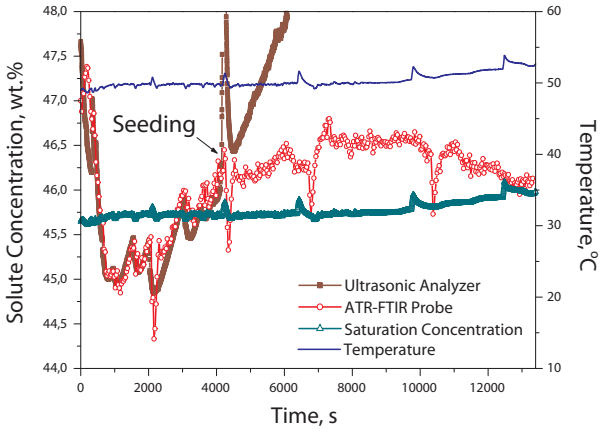

Figure 2.7: Online calibration of the ATR-FTIR probe during experiment DT_c88.

Table 2.3: Initial conditions of the seeded fed-batch evaporative crystallization experiments.

Experiment	Solute concentration, $wt.\%$	Estimated parameters of log-normal distribution	
		L_0, μm	σ_g
DT_c31	45.71	327.6	1.47
DT_c88	46.20	395.7	1.58

the crystal growth rate constant k_g, and the crystal growth rate exponent g; the nucleation rate exponent b is assumed to be 1.0. The solute concentration as well as the calculated second, third, and forth moments of the CSD measurements are used to estimate the kinetic parameters. The moments of CSD are calculated on the basis of the volume density distribution and the slurry density measurements as discussed in Section 2.2.2. The zeroth and the first moments of CSD are not incorporated in the parameter estimation problem due to their large inaccuracies. The laser diffraction instrument has a low sensitivity to the smallest crystals that are small in volume but large in numbers. Therefore, the measured zeroth moment of CSD, which corresponds to the number of crystals present in the sample, is to a great extent unreliable. In addition, the calculation of the moments of CSD from the measured volume density distributions relies on accurate determination of the liquid fraction, i.e. equation (2.17). Small inaccuracies in liquid fraction lead to large errors in the calculated number density distributions that are more pronounced in the lower moments of CSD.

The initial conditions of the population balance equation are obtained by fitting the log-normal distribution

$$v(L) = \frac{1}{\ln(\sigma_g)\sqrt{2\pi}L} \exp\left(- \frac{\left(\ln\left(\frac{L}{L_0}\right)\right)^2}{2(\ln(\sigma_g))^2} \right) \tag{2.63}$$

to the first volume density distribution measurement. The fit parameters L_0 and σ_g represent the mean and the spread of the initial volume density distribution, respectively. The estimated fit parameters are listed in Table 2.3. Figure 2.8 depicts the simulated and the measured initial volume density distributions. It is observed that there is good agreement between the two distributions.

The values of the estimated kinetic parameters of the population balance model and their associated 95% confidence intervals are given in Table 2.4. The estimated

Table 2.4: Estimated kinetic parameters of the population balance model (95% confidence intervals).

Parameter	Estimated value	Relative error, $\%$
g	$(9.11 \pm 0.27) \times 10^{-1}$	2.96
k_b, $\#/m^3 s$	$(1.13 \pm 0.19) \times 10^{8}$	16.81
k_g, m/s	$(4.37 \pm 0.08) \times 10^{-6}$	1.83

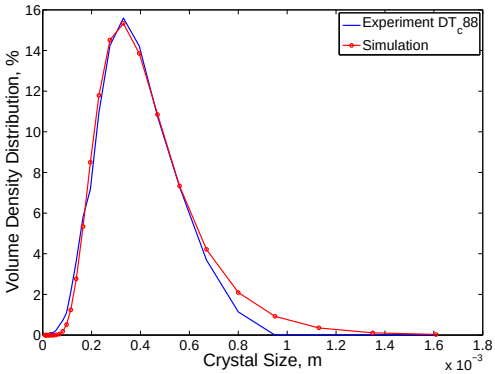

Figure 2.8: A comparison of simulated and measured initial volume density distributions in experiment DT_c88.

kinetic parameters are lower in value compared to those reported by Kalbasenka (2009) for the moment model. The evolution of simulated and measured crystal size distributions in the course of batch run DT_c88 is depicted in Figure 2.9. As can be seen, the fit achieved between the simulated and the measured volume density distributions is acceptable. Figure 2.10 shows the simulated and the measured solute concentration profiles throughout the batch run. The maximum deviation of the simulated solute concentration profile with respect to the measurements is approximately $1.7\,\%$. The higher values of the measured solute concentration profile can be attributed to partial dissolution of seeds.

The population balance model equipped with the estimated kinetic parameters is validated by simulation of batch run DT_c31. The model is initialized with a size distribution obtained by fitting the first CSD measurement to the log-normal distribution given in equation (2.63). The initial conditions of the batch run are listed

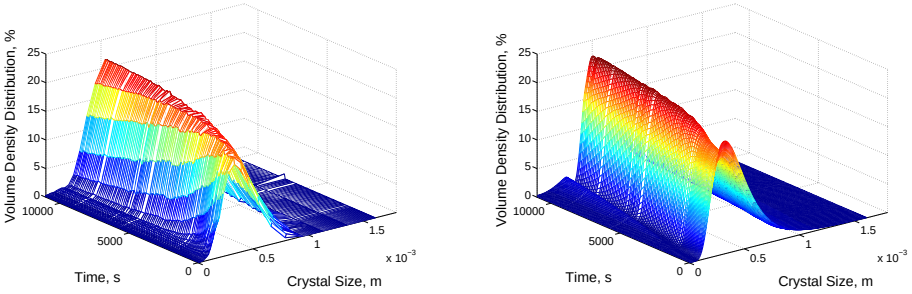

(a) Measured (b) Simulated

Figure 2.9: A comparison of simulated and measured crystal size distributions in experiment DT_c88.

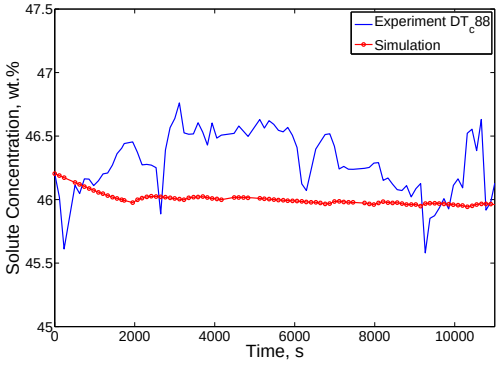

Figure 2.10: A comparison of simulated and measured solute concentration profiles in experiment DT_c88.

in Table 2.3. Figure 2.11 depicts the evolution of simulated and measured crystal size distributions throughout the batch run. As can be seen in Figure 2.11(a), the first few CSD measurements have bimodal distributions. This is due to plugging in the product line of the semi-industrial crystallizer. By rinsing the product line, the crystals are transferred to the laser diffraction instrument and consequently result in bimodal measurements. Apart from the first few measurements, the simulated and the measured volume density distributions are in good agreement.

The descriptive capability of the population balance model is better illustrated in Figure 2.12, which shows the evolution of simulated and measured mean crystal size during batch run DT_c31. The first few bimodal crystal size distributions are not considered. Figure 2.12 displays two simulated mean crystal size profiles. In simulation case 1, the model is equipped with the kinetic parameters estimated using the crystal size distribution and the solute concentration measurements. On

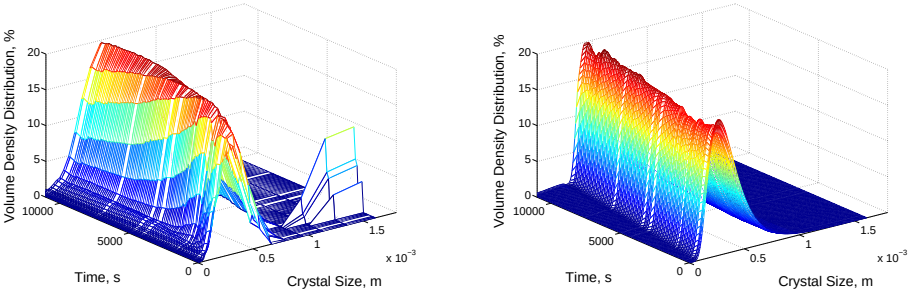

(a) Measured (b) Simulated

Figure 2.11: A comparison of simulated and measured crystal size distributions in experiment DT_c31.

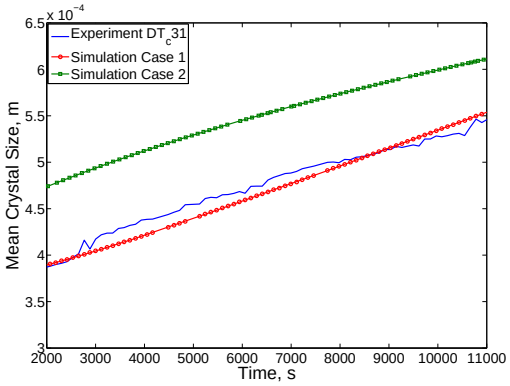

Figure 2.12: A comparison of simulated and measured mean crystal size profiles in experiment DT_c31.

the other hand, the model parameters in simulation case 2 are estimated only on the basis of the CSD measurements. As can be seen, the mean crystal size profile in simulation case 2 deviates significantly from the measured profile. This is due to overestimation of the crystal growth rate constant when the solute concentration measurements are not incorporated into the parameter estimation problem. Figure 2.12 suggests that the population balance model in simulation case 1 is able to satisfactorily predict the measured mean crystal size profile. Towards the end of the batch run, the model overpredicts the mean crystal size. The discrepancy is attributed to improper mixing in the vessel. When the batch crystal volume content increases as crystals grow larger, the impeller may not be able to keep the crystals in suspension. This leads to inaccuracies in the measured crystal size distributions.

2.4 Summary

The dynamics of batch crystallization processes depend not only on process variables such as concentration and temperature, but are also a function of certain qualities of the individual crystals. In this chapter, a general first-principles modeling framework has been developed for batch crystallization processes. The so-called population balance modeling approach consists of material and energy balances, describing the dynamic distribution of the characteristic variables of crystals, along with state variables of the continuous phase. The modeling approach preserves the physical insight into the process and is able to represent the dynamics of a wide range of industrial batch crystallizers over a relatively large operational envelop.

The first-principles modeling framework has been used to develop a dynamic model for fed-batch evaporative crystallization of ammonium sulphate in a semi-industrial crystallizer, which is considered in the remainder of this thesis. The

state space representation of the system dynamics has been derived for two model formulations, namely the population balance model and the moment model. The method of moments allows us to reduce the population balance equation to a set of closed ordinary differential equations when the crystallization kinetics are described by empirical power-law functions.

The adequacy of the population balance model for accurately describing the system dynamics has been examined on the basis of several seeded fed-batch experiments performed in a semi-industrial crystallizer. The applicability of ATR-FTIR spectroscopy for in-situ concentration monitoring of the aqueous ammonium sulphate solution has been demonstrated. A rapid online calibration technique that circumvents the need for extensive laboratory experimentation to develop a PLS model has been devised. The technique substantially reduces the calibration time since it does not require data preprocessing and an independent data set to validate the PLS model. The model validation results suggest that the use of in-situ solute concentration measurements, along with on-line crystal size distribution measurements, leads to improved estimation of the kinetic parameters.

3 CHAPTER

Numerical Solution of the Population Balance Equation

Physics is mathematical not because we know so much about the physical world, but because we know so little; it is only its mathematical properties that we can discover.

Bertrand Russell

The occurrence of steep moving fronts and / or sharp discontinuities in simulation of batch crystallization processes often complicates numerical solution of the population balance equation. This chapter gives a comprehensive analysis of the most widely used population balance solution methods, namely the method of characteristics, the finite volume methods, and the finite element methods. The solution methods are examined in terms of the performance requirements essential for online control applications. Dynamic simulation of various test cases as well as industrial crystallization processes undergoing simultaneous nucleation and crystal growth is investigated. Numerical simulations of the real crystallization processes considered in this chapter provide realistic scenarios to identify the advantages and pitfalls of a particular solution method.[1]

3.1 Introduction

The modeling framework presented in Chapter 2 consists of a set of coupled, nonlinear integro-differential equations. The cornerstone of the modeling framework is the population balance equation that describes the evolution of CSD in relation to states of the continuous phase. The PBE is a hyperbolic partial differential equation due to the convection term $\frac{\partial(G(L,t)n(L,t))}{\partial L}$. The convective nature of the PBE

[1]This chapter has been published as: A. Mesbah, H.J.M. Kramer, A.E.M. Huesman, and P.M.J. Van den Hof. A control oriented study on the numerical solution of the population balance equation for crystallization processes. *Chemical Engineering Science*, 64:4262−4277, 2009.

may lead to numerical diffusion and stability problems, particularly in the event of steep moving fronts and / or sharp discontinuities.

The oldest and most widely used method to solve the PBE is the method of moments (Hulbert and Katz 1964; Randolph and Larson 1988). In this technique, the PBE is transformed into a set of ordinary differential equations that describe the evolution of the moments of crystal size distribution; see Section 2.2.4. However, the moment equations cannot reconstruct the full crystal size distribution. In addition, the PBE formulation in most industrial crystallization processes cannot be reduced to the moment equations. This necessitates recourse to numerical solution methods of the population balance equation.

Accurate numerical solution of the PBE is often challenging. Common problems associated with the numerical solution of equation (2.4) for seeded batch crystallization processes include numerical diffusion and instability. The former problem usually stems from incompatibility between the initial condition and the boundary condition of the PBE. The number density distribution of seeds is unlikely to be the same as that of the formed nuclei. In case that their values match, the first derivative of the distribution may not be identical. This can lead to sharp discontinuities that are rapidly broadened by numerical diffusion (Mahoney and Ramkrishna 2002). The occurrence of steep moving fronts, which is a prime source of numerical instability, is the other frequently encountered difficulty in solving equation (2.4). This problem mainly arises from the convective nature of crystal growth dominated processes.

The above mentioned complexities related to numerical solution of the PBE have awakened the attention in many researchers to develop specialized algorithms. These techniques can be broadly classified into four categories, namely the finite difference methods, the discretization techniques, the method of weighted residuals, and the Monte Carlo methods.

Finite difference methods are the most frequently used general approach for solving partial differential equations. However, these schemes may not adequately cope with the hyperbolic nature of the PBE. Finite difference methods often lead to the broadening of sharp discontinuities due to numerical diffusion (Mahoney and Ramkrishna 2002). Furthermore, they ensure number and mass conservation of the crystal population only in the limit of infinite resolution (Patankar 1980). These drawbacks, along with the inherent complexity of choosing stable integration schemes, make the use of the finite difference methods less appealing. Performance analysis of several finite difference methods for crystallization processes undergoing nucleation and crystal growth can be found in Muhr et al. (1996) and Wojcik and Jones (1998). Bennett and Rohani (2001) have applied a combined Lax-Wendroff / Crank-Nicholson method to solve the PBE. The latter method exhibits rather promising results that are free from numerical instabilities.

Discretization techniques comprise a wide variety of numerical methods including discretized population balances and finite volume methods. In the discretized population balance equations (Baterham et al. 1981; Hounslow et al. 1988), the independent variable, viz the spatial domain, is divided into a finite number of intervals. The mean-value theorem is employed to convert the continuous PBE

into a series of discrete equations, which are expressed in terms of either the number of crystals, i.e. the M-I approach, or the average crystal population density in each interval, i.e. the M-II approach. Subsequently, the resulting set of stiff, nonlinear differential algebraic equations is integrated numerically. The discretized population balance equations have been extensively exploited in the literature to simulate and optimize various crystallization processes (Marchal et al. 1990; David et al. 1991; Litster et al. 1995; Matthews and Rawlings 1998; David et al. 2003). This technique allows accurate determination of the desired characteristics of the distribution, though construction of the entire distribution is usually subject to severe errors. In addition, the discretized population balance equations often exhibit either oscillatory behavior, resulting in negative number densities, or suffer from numerical diffusion at discontinuous moving fronts. The latter problem emerges when the discretized version of a partial differential equation corresponds to a different original equation, one with an added diffusion term (Lapidus and Pinder 1982). As will be explained later, Kumar and Ramkrishna (1997) proposed a modified formulation of the discretized population balance equations, the so-called method of characteristics (MOC), to alleviate the shortcomings of this technique. The method of characteristics has received a great deal of attention in various crystallization modeling and optimization applications (Lim et al. 2002; Hu et al. 2005a; Qamar and Warnecke 2007). This is due to its capability to capture sharp fronts using moving size intervals. Paengjuntuek et al. (2008) used the MOC formulation proposed by Hu et al. (2005b) for batch-to-batch optimization and nonlinear control of seeded crystallization processes.

The discretization techniques also involve another category of numerical schemes known as the finite volume methods (FVMs). These methods were originally applied in the field of fluid dynamics since their formulation enables us to cope with the convective nature of hyperbolic partial differential equations (Versteeg and Malalasekera 1995). Lately, FVMs have become increasingly popular for numerical solution of the PBE in crystallization processes (Gerstlauer et al. 2001; Ma et al. 2002a; Gunawan et al. 2004; Qamar et al. 2006). As will be shown, the high order finite volume methods in combination with a flux limiting function ensure accurate solution of the PBE. The so-called high resolution schemes are able to resolve sharp discontinuities as suppressing numerical oscillations.

Another class of methods widely used to solve the PBE is the method of weighted residuals, which is a general technique for solving partial differential equations. The methods associated with this technique retrieve the full distribution by approximating the solution with a series of basis functions. The coefficients of the basis functions are specified such that their sum satisfies the PBE. The formulation of these methods is largely determined by the choice of the basis functions, viz global and local functions. The use of the global basis functions is limited to problems in which the shape of the resulting distribution is known a priori. This is due to the inability of global functions to accommodate sharp changes and discontinuities of an arbitrarily-shaped distribution (Rigopoulos and Jones 2003). The generality and flexibility of the method of weighted residuals is restored by adopting local basis functions. The latter formulation results in the so-called finite element methods (FEMs) that are capable of describing highly irregular distribu-

tions. There is a vast number of studies in which the finite element methods are used to solve the PBE in crystallization processes (Gelbard and Seinfeld 1978; Nicmanis and Hounslow 1998; Mahoney and Ramkrishna 2002; Alexopoulos et al. 2004). The main merits of the FEMs are accurate reconstruction of the crystal size distribution and their flexibility to cope with any possible formulation of the PBE (Rigopoulos and Jones 2003). Nonetheless, the finite element methods are difficult to implement and computationally expensive. More importantly, they cannot effectively deal with discontinuous distributions and steep moving fronts.

In addition to the above discussed deterministic methods, the PBE can be solved by the probabilistic Monte Carlo method (Maisels et al. 1999; Song and Qiu 1999; Meimaroglou et al. 2006). In this approach, the histories of individual crystals, each exhibiting random behavior in accordance with a probabilistic function, are tracked by means of the Markov conditional probability. The Monte Carlo methods are more suitable for multivariate problems, where the aforementioned numerical techniques usually become less efficient (Rigopoulos and Jones 2003).

Demands on the solution method of the PBE generally differ with the nature of the application and the crystallization processes under consideration. In this thesis, the PBE solution methods that are expected to best suit online process control applications are investigated. The solution methods should be well capable of dealing with steep moving fronts and discontinuities that are commonly encountered in batch crystallization processes. In addition, the computational burden of model solution is of paramount importance since control actions need to be computed in real-time. It is worth mentioning that the closed-loop implementation of a model-based control approach permits tolerance of reduced accuracy through estimation of the system states.

In the following, the method of characteristics, the finite volume methods, and the finite element methods are analyzed. The method of characteristics and the finite volume methods are known to be capable of dealing with numerical diffusion as well as instability problems on a coarse grid mesh. This makes them particularly amenable to online control applications due to improved computational efficiency. The finite element methods, on the other hand, allow exact prediction of the entire distribution, which is essential when the control of a full crystal size distribution is sought. The numerical techniques are examined in terms of their numerical accuracy, computational efficiency, and implementation-related issues for crystallization processes undergoing simultaneous nucleation and crystal growth. Depending on the choice of the dynamic optimization strategy adopted in an online control approach, the computational efficiency of dynamic simulations may serve as an indication of the computational burden required for dynamic optimization of the crystallization process.

What distinguishes the analysis of PBE solution methods presented in this thesis with extensive reviews in the literature, e.g., (Ramkrishna 1985; Costa et al. 2007), is the diversity and comprehensiveness of the case studies by which the solution methods are examined. The numerical techniques are assessed not only on the basis of the test problems commonly used in the literature, but are also applied for simulation of semi-industrial batch and industrial continuous crystal-

lization case studies with varying supersaturation profiles. Dynamic simulation of real crystallization processes is further complicated by the nonlinear dependence of crystallization phenomena on state variables of the continuous phase, i.e. temperature and solute concentration. Therefore, the presented case studies allow us to better identify the advantages and pitfalls of a particular PBE solution method.

3.2 Method of characteristics

Kumar and Ramkrishna (1997) proposed a numerical technique that substantially enhances the accuracy of the discretized population balance equations. In this method, the convection term in equation (2.1) is eliminated through differentiating $\frac{\partial(G(L,t)n(L,t))}{\partial L}$ by parts

$$\frac{\partial n(L,t)}{\partial t} + n(L,t)\frac{\partial G(L,t)}{\partial L} + G(L,t)\frac{\partial n(L,t)}{\partial L} = B(L,t) + Q(L,t,n), \tag{3.1}$$

where $Q(L,t,n)$ represents crystals entering or leaving the crystallizer $(\#/m^4 s)$. The crystal growth rate is expressed as

$$\frac{\mathrm{d}L}{\mathrm{d}t} = G(L,t). \tag{3.2}$$

Substituting equation (3.2) and a total derivative of the number density

$$\frac{\mathrm{d}n(L,t)}{\mathrm{d}t} = \frac{\partial n(L,t)}{\partial t} + \frac{\partial n(L,t)}{\partial L}\frac{\mathrm{d}L}{\mathrm{d}t} \tag{3.3}$$

in equation (3.1) leads to

$$\frac{\mathrm{d}n(L,t)}{\mathrm{d}t} = -n(L,t)\frac{\mathrm{d}G(L,t)}{\mathrm{d}L} + B(L,t) + Q(L,t,n). \tag{3.4}$$

Equation (3.4) describes the evolution of crystal number density, whereas equation (3.2) governs the movement of crystal cells.

The mathematical procedure of transforming equation (2.1) to equations (3.2) and (3.4) and solving the latter for a solution is known as the method of characteristics. This formulation implies that there exists unique characteristic curves along which information propagates. When the number density information moves along these pathlines, the convection term in the PBE disappears. This results in a significant improvement in the solution accuracy since the convection term is the prime source of numerical diffusion and instability.

Nonetheless, the presence of crystal nucleation poses a difficulty in the method of characteristics. As the crystal cells move with the growth of crystals, i.e. equation (3.2), a situation arises that some or all of the nuclei become smaller than the smallest crystal size. Thus, the nucleation term is no longer represented accurately since the newly formed crystals cannot be placed in the first cell. To overcome this

problem, a new cell of nuclei with zero crystal population should be added at regular time intervals. However, this leads to a rapid increase in the number of cells and consequently the number of differential equations, making the method computationally too expensive.

The main feature of the MOC formulation proposed by Kumar and Ramkrishna (1997) comes into play when the computational efficiency is to be restored. In their approach, crystal cells are added at the smallest size to account for the crystal nucleation, whereas they are collapsed elsewhere to preserve the coarseness of the grid mesh. For any three size classes located such that $L_{i+1}/L_{i-1} < r_{critical}$, the i^{th} class is collapsed and its population is assigned to the adjacent size classes while two arbitrary properties of the crystal size distribution are preserved. The crystal population fraction assigned to the $(i+1)^{th}$ and $(i-1)^{th}$ size classes should satisfy

$$\eta_{i+1} = \frac{L_i^{\zeta} L_{i-1}^{\nu} - L_{i-1}^{\nu} L_{i-1}^{\zeta}}{L_{i+1}^{\zeta} L_{i-1}^{\nu} - L_{i+1}^{\nu} L_{i-1}^{\zeta}} \tag{3.5}$$

$$\eta_{i-1} = \frac{L_i^{\zeta} L_{i+1}^{\nu} - L_{i-1}^{\nu} L_{i+1}^{\zeta}}{L_{i+1}^{\nu} L_{i-1}^{\zeta} - L_{i+1}^{\zeta} L_{i-1}^{\nu}}. \tag{3.6}$$

The integer constants ζ and ν should be chosen such that the desired properties of the CSD are conserved.

It is evident that the primary merit of this technique is efficient calculation of the desired properties of the crystal population, rather than approximating the continuous crystal size distribution on a suitably fine grid mesh. In addition, the MOC enables adapting geometric discretization schemes, which allow us to tune coarseness of the grid mesh. However, there are some limitations in the method of characteristics that may restrict its use for online control applications. The main difficulty is the trade-off between the choice of the time step at which new crystal cells are added and the computational burden. Accurate preservation of the number of newly born crystals necessitates short time steps, whereas a relatively small number of cells is desirable to ensure computational efficiency.

3.3 Finite volume methods

The finite volume methods involve discretization of the spatial variable domain and the use of piecewise functions to approximate derivatives with respect to the spatial variable. The resulting set of ODEs, one for each grid point, is integrated over time along lines parallel to the time axis in the time-space domain.

The family of the finite volume methods consists of a variety of numerical schemes that differ in grid discretization and / or in functions used to approximate the spatial derivatives. In these methods, the hyperbolic PBE reduces to a semi-discrete equation per grid point. In the case of $Q(L,t,n) = 0$, i.e. no inlet and

outlet streams, the semi-discrete equation is cast as

$$\frac{\partial n_i}{\partial t} + \frac{1}{\Delta L}([(Gn)_{L_i^+} - \mathbf{B}_{L_i^+}] - [(Gn)_{L_i^-} - \mathbf{B}_{L_i^-}]) = 0, \tag{3.7}$$

where $\mathbf{B}(L,t) = \int_0^L B(\xi,t)d\xi$. Note that n_i is a representative value for the crystal population in the cell i confined to $(L_{i-\frac{1}{2}}, L_{i+\frac{1}{2}})$; see the cell centered grid mesh depicted in Figure 3.1. Hence, in the finite volume methods the computations are merely done on the cell boundaries.

Calculation of equation (3.7) for each grid point requires values of the crystal growth and nucleation rates as well as the number density on the cell boundaries. Though the crystal growth and nucleation rates can be directly obtained form kinetic expressions, estimation of the number density on the cell boundaries poses a difficulty. The approach by which the cell-face fluxes, i.e. $(Gn)_{L_i^+}$, are approximated determines the accuracy of a finite volume method. The simplest interpolation formula to approximate the number density on each cell boundary is the upwind interpolation scheme. This formulation is equivalent to using a first order backward or forward difference approximation for the partial derivatives depending on the flow direction, i.e. crystal growth or dissolution. In the case of positive convection term, namely crystal growth, the first order interpolation scheme leads to

$$\frac{\partial n_i}{\partial t} + \frac{1}{\Delta L}([n_i G_{L_i^+} - \mathbf{B}_{L_i^+}] - [n_{i-1} G_{L_i^-} - \mathbf{B}_{L_i^-}]) = 0 \qquad G(L) > 0. \tag{3.8}$$

When nucleation only occurs at infinitesimally small crystal sizes, the flux across the inflow boundary, i.e. L_{1^-}, need not be approximated since $n_{1^-} = n_{in} = \frac{B_0}{G|_{L_0}}$.

The first order upwind finite volume method does not exhibit instability. It does however suffer from numerical diffusion unless a fine grid mesh is used. In order to circumvent the diffusion problem, higher order linear or quadratic interpolation schemes such as the piecewise polynomial interpolation formula (Qamar

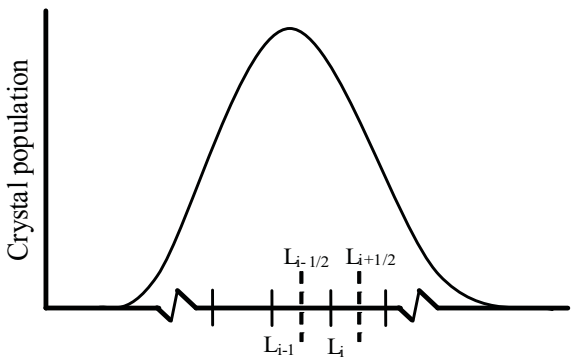

Figure 3.1: A cell centered grid mesh.

Table 3.1: The formulation of the high order finite volume method with different flux limiting functions ($G(L) > 0$).

Koren (1993)($\kappa = \frac{1}{3}$)
$\left((Gn)_{1/2}-\mathbf{B}_{1/2}\right)=G_{1/2}n_{in}-\mathbf{B}_{1/2}$
$\left((Gn)_{3/2}-\mathbf{B}_{3/2}\right)=\frac{1}{2}\left((G_{3/2}n_1-\mathbf{B}_{3/2})+(G_{3/2}n_2-\mathbf{B}_{3/2})\right)$
$\left((Gn)_{L_i^+}-\mathbf{B}_{L_i^+}\right)=\left((G_{L_i^+}n_i-\mathbf{B}_i)+\frac{1}{2}\phi(r_i^+)\left[(G_{L_i^+}n_i-\mathbf{B}_i)-(G_{L_i^+}n_{i-1}-\mathbf{B}_{i-1})\right]\right) \quad i=1,\ldots,N-1$
$\left((Gn)_{N+1/2}-\mathbf{B}_{N+1/2}\right)=\left((G_{N+1/2}n_N-\mathbf{B}_N)+\frac{1}{2}\left[(G_{N+1/2}n_N-\mathbf{B}_N)-(G_{N+1/2}n_{N-1}-\mathbf{B}_{N-1})\right]\right)$
$r_i^+=\frac{(G_{L_i^+}n_{i+1}-\mathbf{B}_{i+1})-(G_{L_i^+}n_i-\mathbf{B}_i)+\varepsilon}{(G_{L_i^+}n_i-\mathbf{B}_i)-(G_{L_i^+}n_{i-1}-\mathbf{B}_{i-1})+\varepsilon}$
$\phi(r_i^+)=max\left(0,min\left(2r_i^+,min\left(\frac{1}{3}+\frac{2}{3}r_i^+,2\right)\right)\right)$
van Leer (1985) ($\kappa = -1$)
$\left((Gn)_{1/2}-\mathbf{B}_{1/2}\right)=G_{1/2}n_{in}-\mathbf{B}_{1/2}$
$\left((Gn)_{3/2}-\mathbf{B}_{3/2}\right)=\frac{1}{2}\left((G_{3/2}n_1-\mathbf{B}_{3/2})+(G_{3/2}n_2-\mathbf{B}_{3/2})\right)$
$\left((Gn)_{L_i^+}-\mathbf{B}_{L_i^+}\right)=\left((G_{L_i^+}n_i-\mathbf{B}_i)+\frac{1}{2}\phi(r_i^+)\left[(G_{L_i^+}n_{i+1}-\mathbf{B}_{i+1})-(G_{L_i^+}n_i-\mathbf{B}_i)\right]\right) \quad i=1,\ldots,N$
$r_i^+=\frac{(G_{L_i^+}n_i-\mathbf{B}_i)-(G_{L_i^+}n_{i-1}-\mathbf{B}_{i-1})+\varepsilon}{(G_{L_i^+}n_{i+1}-\mathbf{B}_{i+1})-(G_{L_i^+}n_i-\mathbf{B}_i)+\varepsilon}$
$\phi(r_i^+)=\frac{\lvert r_i^+\rvert+r_i^+}{1+\lvert r_i^+\rvert}$

et al. 2006)

$$(Gn)_{L_i^+} = G_{L_i^+}\left(n_i + \frac{1+\kappa}{4}(n_{i+1}-n_i) + \frac{1-\kappa}{4}(n_i-n_{i-1})\right) \qquad \kappa \in [-1,1] \tag{3.9}$$

are used. Equation (3.9) results in a weighted blend between the central scheme and the fully one-sided scheme for different values of κ.

In spite of the fact that the higher order interpolation schemes suppress numerical diffusion to a large extent, they often lead to numerical oscillations (Ferziger and Peric 1996). The oscillatory behavior results in negative solutions, which are physically meaningless. This problem can be rather easily tackled by limiting the flux across the cell boundaries with the aid of flux limiting functions. The latter functions ensure monotonicity and consequently prevent the occurrence of negative solutions. The formulation of the high order finite volume method with two of the most widely used flux limiting functions is given in Table 3.1; r_i^+ and $\phi(r_i^+)$

denote the so-called upwind ratio of two consecutive solution gradients and the flux limiting function, respectively. These schemes provide second order accuracy in smooth regions and first order accuracy in the vicinity of discontinuities (Qamar and Warnecke 2007). Note that the flux limiting functions cannot be applied to the left and right boundaries. Therefore, the first order upwind formulation should be used in the boundary cells. A thorough analysis of various flux limiting functions can be found in LeVeque (2002).

3.4 Finite element methods

The population balance equation can be solved in its continuous form by the finite element methods. These techniques approximate the solution by means of piecewise low-order polynomials. This makes the FEMs capable of describing highly irregular solutions (Rigopoulos and Jones 2003). Rawlings et al. (1993) indicated that the finite element methods normally have modest computational burden, which facilitates their use in online control applications. The solution procedure pertaining to the FEMs can be generally summarized in the following steps:

1. The spatial domain is first divided into ne elements. The discretization scheme needs to be selected carefully since it largely influences the accuracy and computational efficiency of the solution. In general, the discretization scheme should be tailored to the needs of the problem under consideration to achieve the best performance. For simultaneous nucleation and crystal growth processes, geometric discretization schemes are often suited best (Kumar and Ramkrishna 1997). They provide a refined grid mesh at smaller size ranges to capture nucleation, while covering a broad range of size that is essential for large and size-dependent crystal growth rates.

2. The continuous number density function $n(L,t)$ should then be approximated by a basis function. There is a variety of choices for the basis function. The majority of FEM applications are favored to the higher order basis functions such as cubic splines (Gelbard and Seinfeld 1978; Eyre et al. 1988), wavelets (Chen et al. 1996; Liu and Cameron 2003), Chebyshev polynomials (Sandu and Borden 2003), and high order Lagrangian polynomials (Nicmanis and Hounslow 1998; Alexopoulos et al. 2004; Roussos et al. 2005). Nonetheless, Mahoney and Ramkrishna (2002) and Rigopoulos and Jones (2003) used linear basis functions to solve the dynamic PBE. The FEM formulation using linear basis functions is free from structural complexities inherent in the higher order functions and therefore is easier to implement. However, fairly accurate results can only be obtained at the cost of large number of nodal points. The first order basis functions typically accommodate a much finer grid mesh in the same amount of computation time required by the higher order basis functions. The latter functions entail many more evaluations and interpolations for a given number of nodal points.

3. Next step is to formulate the weighted residual expressions. According to the formulation proposed by Finlayson (1980), the weighted residual expressions are obtained by multiplying the PBE

$$F(L,t) = \frac{\partial n(L,t)}{\partial t} + \frac{\partial (G(L,t)n(L,t))}{\partial L} - B(L,t) - Q(L,t,n) = 0 \quad (3.10)$$

by a weight function. This results in the following weighted residual expression for each element

$$\int_{\Omega_e} \omega(L) F(L,t) = 0, \quad (3.11)$$

which suggests that equation (3.10) only holds when the function $F(L,t)$ is orthogonal to the weight function $\omega(L)$. Common choices of the weight function include Dirac delta functions, i.e. $\omega(L) = \delta(L - L_i)$, resulting in collocation on finite element methods (Gelbard and Seinfeld 1978; Alexopoulos et al. 2004; Rigopoulos and Jones 2003), and the basis functions themselves, leading to Galerkin's techniques (Chen et al. 1996; Mahoney and Ramkrishna 2002; Roussos et al. 2005). In the collocation methods, equation (3.11) is evaluated on the nodal points, whereas it should be integrated over each element in the Galerkin's methods. This implies that the Galerkin's techniques are computationally more expensive. A comparative analysis of various integration formulas used to solve the Galerkin's methods can be found in Roussos et al. (2005).

4. The resulting set of stiff, nonlinear differential algebraic equations should be integrated in time.

When nucleation only occurs at infinitesimally small crystal sizes, handling of the nucleation term in the FEM formulation requires special care. Since nucleation is implemented as a point source on the first nodal point, the common continuous non-singular basis functions cannot resolve the pulse-like nucleation term. Hence, it is assumed that nucleation spreads over a specified size range (Rigopoulos and Jones 2003; Alexopoulos and Kiparissides 2005). However, this approach may severely suffer from numerical problems as the number density at size zero possesses two values corresponding to the initial distribution and the nucleation rate. The incompatibility between the initial condition, i.e. the initial distribution, and the boundary condition, i.e. the nucleation rate, gives rise to moving discontinuities. This problem can be rather effectively dealt with by discontinuous finite element methods (Mahoney and Ramkrishna 2002).

Another numerical problem that is commonly encountered in the finite element methods arises from the convective nature of the PBE. The basis functions are evaluated on interior points of each element. As a result, information flows to the nodal points from both ends of the element. However, this mechanism is not entirely valid for numerical solution of the PBE since crystals only grow in one direction, from smaller to larger sizes. Numerical instability problems that arise from this shortcoming can be alleviated by adopting a geometric grid discretization scheme and tuning its resolution. Another common practice is to include

an artificial diffusion term to dampen the oscillations that appear in distributions with steep moving fronts (Alexopoulos et al. 2004; Roussos et al. 2005).

In this thesis, the orthogonal collocation on finite elements (OCFE) and the Galerkin's finite element method (GFEM) are studied. The continuous number density function over each element is approximated by

$$n_e(L,t) = \sum_{j=1}^{n_p} n_j^e(t)\varphi_j^e(L), \tag{3.12}$$

where n_p and $\varphi_j^e(L)$ denote the number of nodal points and the basis functions, respectively. In order to investigate the effect of basis functions on the performance of either of the finite element methods, the high order Lagrangian interpolation polynomial

$$\varphi_j^e(L) = \prod_{j=1, j\neq i}^{n_p+1} \frac{(L - L_j^e)}{(L_i^e - L_j^e)} \tag{3.13}$$

as well as the linear basis function (Rigopoulos and Jones 2003)

$$\varphi(L)_{[j-1,j]} = \left(\frac{L - L_{j-1}}{L_j - L_{j-1}}, \frac{L_j - L}{L_j - L_{j-1}} \right) \tag{3.14}$$

are used to approximate the number density function. In the latter formulation, the number density over an element is expressed as

$$n(L,t)_{[j-1,j]} = n(L_{j-1},t)\frac{L - L_{j-1}}{L_j - L_{j-1}} + n(L_j,t)\frac{L_j - L}{L_j - L_{j-1}}. \tag{3.15}$$

3.5 Test cases

The method of characteristics, the finite volume methods, and the finite element methods are exploited to simulate various crystallization processes undergoing simultaneous nucleation and crystal growth. The following characteristics of the solution methods are studied:

- cell elimination in the method of characteristics;
- the choice of interpolation formulas in the finite volume methods;
- the choice of basis functions and weight functions in the finite element methods.

The PBE solution methods are utilized to simulate four test cases for which analytical solutions are available; the supersaturation level is constant in the considered test cases. In addition to investigating the implementation-related issues, the performance of the solution methods is assessed with respect to their numerical accuracy and computational efficiency. The accuracy of the numerical techniques is expressed in terms of the errors in the zeroth and the third moments of

the number density distribution obtained at the end of the process

$$\mu_i\textbf{Error} = |(\mu_i)_{analytical} - (\mu_i)_{numerical}| \qquad i = 0, 3. \tag{3.16}$$

All the test cases presented in this section are implemented in MATLAB (version 7.5.0.342), where the initial value problems are solved using the Euler integration method. The reported CPU times correspond to the Microsoft Windows XP (Professional) operating system running on a Genuine Intel(R) T2050 @1.60GHz processor with 1 GB RAM.

3.5.1 Test case 1: size-independent growth of an existing distribution

The first test case concerns size-independent growth of a complex initial distribution. Though in practice initial crystal size distributions are typically Gaussian, under certain circumstances, e.g., burst of infinitesimally crystals after insertion of seeds to a supersaturated solution, they may exhibit sharp discontinuities. This test case allows us to investigate how effectively the PBE solution methods can deal with discontinuous number density distributions.

The initial number density, distributed over an equidistant grid mesh from $L_{min} = 0\ \mu m$ to $L_{max} = 100\ \mu m$, is defined as

$$n(L,0) = \begin{cases} 0.0 & \text{if} \quad L \leq 2.0 \\ 10^9 & \text{if} \quad 2.0 < L \leq 10.0 \\ 0.0 & \text{if} \quad 10.0 < L \leq 18.0 \\ 10^9 \cos^2(\pi(L-26)/64) & \text{if} \quad 18.0 < L \leq 34.0 \\ 0.0 & \text{if} \quad 34.0 < L \leq 42.0 \\ 10^9\big(1-(L-50)^2/64)\big)^{0.5} & \text{if} \quad 42.0 < L \leq 58.0 \\ 0.0 & \text{if} \quad 58.0 < L \leq 66.0 \\ 10^9 \exp(-(L-70)^2/\Delta L^2) & \text{if} \quad 66.0 < L \leq 74.0 \\ 0.0 & \text{if} \quad L > 74.0, \end{cases} \tag{3.17}$$

where $\Delta L = \frac{L_{max}-L_{min}}{N-1}$; N denotes the number of grid points. The analytical

Table 3.2: Errors and computation times of test case 1 ($t_{end} = 60\ s$ and $dt = 0.1\ s$).

	Ngrids	**CPU Time**, s	μ_0**Error**, %	μ_3**Error**, %
MOC	100	0.21	0.12	0.15
First Order FVM	100	0.16	3.70	0.50
High Order FVM: van Leer	100	0.16	1.72	0.26
High Order FVM: Koren	100	0.18	1.72	0.22
OCFE: Linear B.F.	100	0.24	3.95	0.90
OCFE: Lagrange B.F.	75	0.40	5.28	2.63

solution of this test case is

$$n(L,t) = n_0(L - Gt). \tag{3.18}$$

Equation (3.18) implies that the initial distribution is shifted for a distance of Gt; G is assumed to be $0.1\ \mu m/s$.

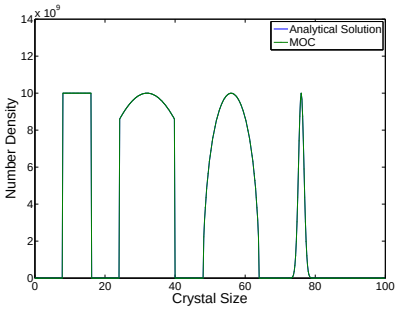

(a) Method of characteristics

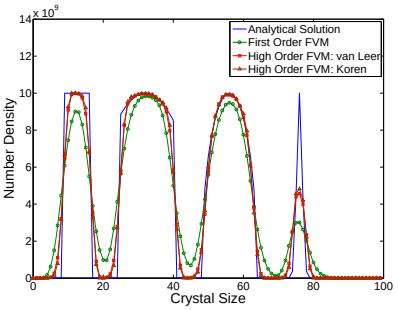

(b) Finite volume methods

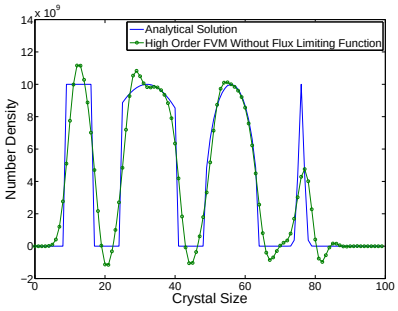

(c) High order finite volume method (without flux limiting function)

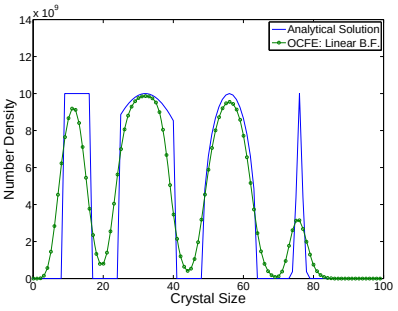

(d) Orthogonal collocation on finite elements (linear basis function)

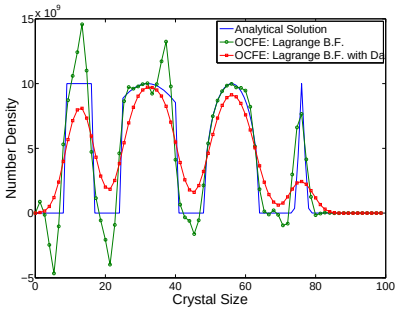

(e) Orthogonal collocation on finite elements (Lagrange basis function)

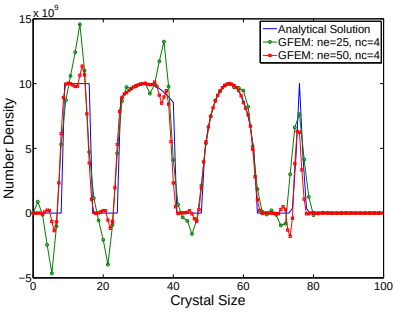

(f) Galerkin's finite element method (Lagrange basis function)

Figure 3.2: A comparison of analytical and numerical simulation results of test case 1.

Figure 3.2 displays the simulation results of various solution methods after integration time of $60\ s$. The errors and computation times corresponding to integration time step, i.e. dt, of $0.1\ s$ are listed in Table 3.2. Clearly, the method of characteristics provides the most accurate numerical results. On the contrary, simulation results of the first order upwind finite volume method exhibit fairly large numerical diffusion. This problem is alleviated to a large extent in the high

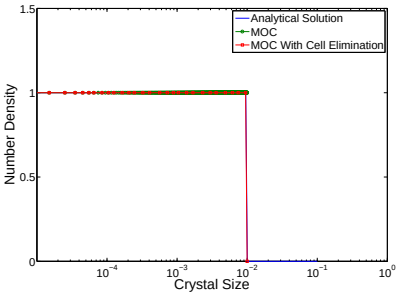

(a) Method of characteristics

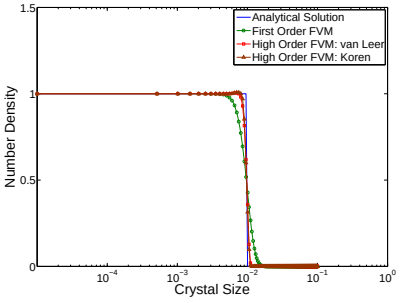

(b) Finite volume methods

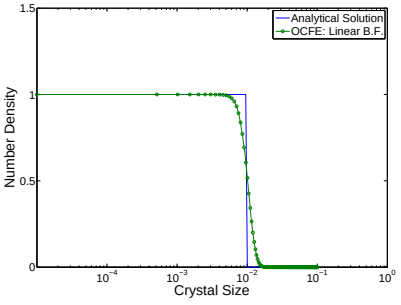

(c) Orthogonal collocation on finite elements (linear basis function)

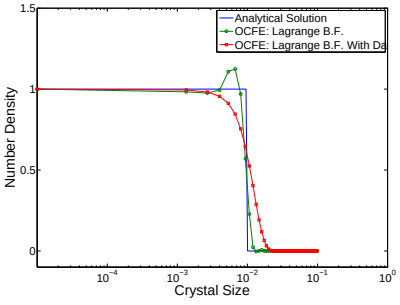

(d) Orthogonal collocation on finite elements (Lagrange basis function)

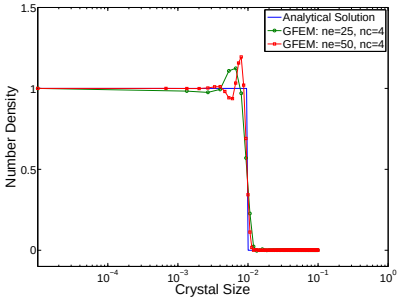

(e) Galerkin's finite element method (Lagrange basis function)

Figure 3.3: A comparison of analytical and numerical simulation results of test case 2.

order finite volume methods combined with flux limiting functions. It is essential to use a flux limiting function in the high order finite volume methods to suppress their inherent oscillatory behavior resulting in negative solutions; see Figure 3.2(c). The choice of the flux limiting function, namely van Leer (1985) and Koren (1993), barely affects the accuracy and computational efficiency of the high order finite volume methods.

The simulation results of the orthogonal collocation and the Galerkin's finite element methods are prone to higher inaccuracies. The numerical accuracy of the orthogonal collocation method with the linear basis function is comparable to that of the first order upwind finite volume method. This results from the formulation of the orthogonal collocation method that consists of collocation on linear elements with an upwind propagation of crystal growth to ensure the stability of the scheme. On the other hand, the orthogonal collocation and the Galerkin's methods with the Lagrange basis function, which do no exploit this stability condition, display oscillatory behavior. This problem can be overcome to a certain extent either by employing the so-called artificial diffusion term, i.e. Da, or increasing the number of elements as shown in Figure 3.2(e) and Figure 3.2(f); ne represents the number of finite elements, whereas nc is the number of collocation points. Even though increasing the number of elements slightly improves the numerical accuracy, the Galerkin's method fails to fully suppress the oscillations with reasonable number of elements. In addition, Table 3.2 indicates that the finite element methods are computationally more expensive than the high order finite volume methods with flux limiting functions.

3.5.2 Test case 2: nucleation and size-independent growth from a clear solution

This test case involves simultaneous nucleation and size-independent crystal growth from a clear solution, i.e. unseeded batch crystallization. Under this scenario, the population balance equation simplifies to (Hounslow et al. 1988)

$$n(L,t) = \frac{B_0}{G} u\big(t - \frac{L}{G}\big), \tag{3.19}$$

where u is the unit step function. It follows that the number density in the i^{th} interval is

$$n_i = \begin{cases} \frac{\Delta L_i B_0}{G} & L_{i+1} \leq tG \\ \frac{B_0(tG - L_i)}{G} & L_{i+1} \geq tG > L_i \\ 0 & L_i > tG. \end{cases} \tag{3.20}$$

Clearly, this problem exhibits severe numerical instabilities since the solution is a discontinuity that moves with time. B_0 and G are both taken as 1.0.

The simulation results of this test case are depicted in Figure 3.3. Yet again the method of characteristics gives the best numerical accuracy. However, this is obtained at the cost of a much higher computational burden in comparison with the other PBE solution methods; see Table 3.3. An effective way to restore the computational efficiency of the MOC without jeopardizing its accuracy is to collapse

Table 3.3: Errors and computation times of test case 2 ($t_{end} = 0.01\ s$ and $dt = 10^{-5}\ s$).

	Ngrids	**CPU Time**, s	μ_0**Error**, %	μ_3**Error**, %
MOC	1000	69.62	0.07	0.13
MOC: Cell elimination	28	0.61	0.10	0.41
First Order FVM	100	0.89	4.19	46.74
	200	2.15	1.69	29.26
High Order FVM: van Leer	100	0.88	1.19	3.75
	200	2.22	0.69	0.51
High Order FVM: Koren	100	0.90	1.19	3.66
	200	2.15	0.69	0.55
OCFE: Linear B.F.	100	0.97	8.71	49.05
	200	2.22	4.21	31.93
OCFE: Lagrange B.F.	75	1.30	9.11	37.49
GFEM: Lagrange B.F.	150	2.83	3.04	26.33

the redundant cells. Their population should then be assigned to the adjacent cells such that any two desired properties of the distribution are conserved. This strategy drastically reduces the computational burden as preserving the numerical accuracy of the solution fairly well.

Figure 3.3(b) suggests that the first order upwind as well as the high order finite volume methods with flux limiting functions lead to stable results. However, the solution accuracy at the steep moving front is impaired due to numerical diffusion. This effect can be partially mitigated, particularly for the first order upwind FVM, by the use of a finer grid mesh; see Table 3.3. The numerical accuracy of the orthogonal collocation method with the linear basis function can also be improved by increasing the number of elements, clearly at the expense of a higher computational burden. On the other hand, the orthogonal collocation and the Galerkin's methods with the Lagrange basis function are not numerically stable. Like the previous test case, the stability of the finite element methods can be restored either by introducing the artificial diffusion term or increasing the number of elements. Table 3.3 indicates that the finite element methods are considerably less accurate than the other PBE solution methods.

3.5.3 Test case 3: nucleation and size-independent growth of an existing distribution

The third test case consists of nucleation of infinitesimal crystals and size-independent crystal growth. The square step initial number density distribution is

$$n(L,0) = \begin{cases} 100 & 0.4 \leq L \leq 0.6 \\ 0.01 & \text{elsewhere,} \end{cases} \tag{3.21}$$

Table 3.4: Errors and computation times of test case 3 ($t_{end} = 0.6\ s$ and $dt = 10^{-3}\ s$).

	Ngrids	**CPU Time**, s	μ_0**Error**, %	μ_3**Error**, %
MOC	200	1.14	0.01	0.82
First Order FVM	200	0.72	2.34	6.13
High Order FVM: van Leer	200	0.75	1.63	1.15
High Order FVM: Koren	200	0.75	1.54	1.41
OCFE: Linear B.F.	200	0.76	2.95	9.67
OCFE: Lagrange B.F.	150	1.11	3.28	14.43

where the crystal size range is $0 \leq L \leq 2.0$. Assuming that the nucleation term has the following dependence on time

$$B_0(t) = 100 + 10^6 \exp(-10^4 (t - 0.215)^2), \tag{3.22}$$

the analytical solution of this test case is expressed as (Lim et al. 2002)

$$n(L,t) = \begin{cases} 100 + 10^6 \exp(-10^4((Gt - L) - 0.2)^2) & 0.0 \leq L \leq Gt \\ 100 & 0.4 \leq L - Gt \leq 0.6 \\ 0.01 & \text{elsewhere.} \end{cases} \tag{3.23}$$

Equation (3.23) implies that the solution is comprised of a discontinuous shock and a narrow wave originated from the seed distribution and the nucleation, respectively. G is assumed to be 1.0.

The simulation results are shown in Figure 3.4. As expected, the MOC can effectively cope with the discontinuities, whereas the first order upwind FVM and the orthogonal collocation method with the linear basis function suffer from numerical diffusion. The high order finite volume methods with flux limiting functions resolve the discontinuous distributions fairly well; see Table 3.4. On the other hand, the orthogonal collocation and the Galerkin's methods with the Lagrange basis function are prone to severe numerical oscillations, leading to negative number densities. Qamar et al. (2006) reported that PARSIVAL, which is a commercial package using the hp-Galerkin's finite element method as its core scheme (Wulkow et al. 2001), gives highly oscillatory solutions for this test case.

3.5.4 Test case 4: exponential nucleation and size-independent growth of an existing distribution

This test case involves a process with exponential nucleation

$$B(L) = \frac{B_0}{L_{0,n}} \exp(-\frac{L}{L_{0,n}}) \tag{3.24}$$

and size-independent crystal growth, i.e. $G = G_0$. The process starts with an existing crystal population of the form

$$n_0(L) = \frac{N_0}{L_0} \exp(-\frac{L}{L_0}). \tag{3.25}$$

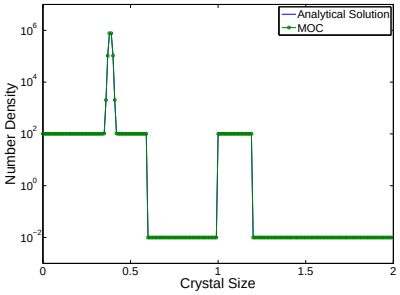

(a) Method of characteristics

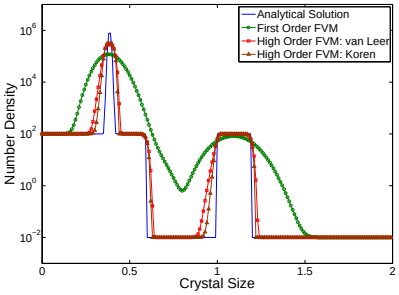

(b) Finite volume methods

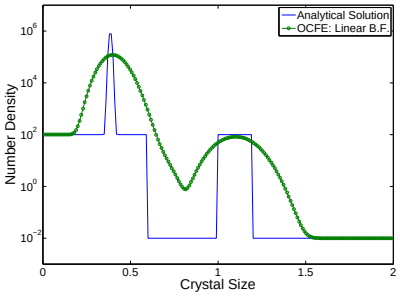

(c) Orthogonal collocation on finite elements (linear basis function)

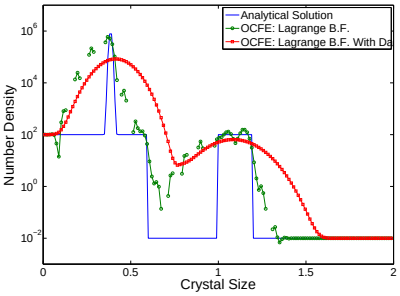

(d) Orthogonal collocation on finite elements (Lagrange basis function)

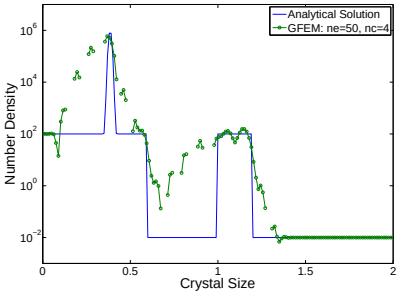

(e) Galerkin's finite element method (Lagrange basis function)

Figure 3.4: A comparison of analytical and numerical simulation results of test case 3.

Table 3.5: Parameters of test case 4.

Variable	B_0	G_0	N_0	L_0	$L_{0,n}$
Value	10^5	1	10	0.01	0.001

According to Kumar and Ramkrishna (1997), the analytical solution of this test case is expressed as

$$\begin{aligned} n(t,L) &= n_0(L-Gt) + \tfrac{B_0}{G_0}[\exp(-\tfrac{L_{low}}{L_{0,n}}) - \exp(-\tfrac{L}{L_{0,n}})] \\ L_{low} &= \max(L_0, L - G_0 t), \end{aligned} \tag{3.26}$$

where the parameters are listed in Table 3.5. This process is more complex than the previous test case in that the new crystals are born in all size classes, rather than only the first one.

To solve the PBE, the spatial domain is partitioned using the geometric discretization scheme

$$L_{1/2} = L_{min}, \quad L_{i+1/2} = L_{min} + 2^{(i-N)/q}(L_{max} - L_{min}), \quad i = 1, ..., N \tag{3.27}$$

where N and q are chosen to be 100 and 7, respectively. The geometric discretization scheme enables us to better simulate the initial part of the number density distribution with sufficient number of cells. In addition, it avoids a very fine grid mesh that may be detrimental to computational efficiency of the solution method.

The numerical results are compared with the analytical solution in Figure 3.5. Despite of the fact that the simulation results of the MOC are in excellent agreement with the analytical solution, this approach is significantly more computation intensive than other methods. This is due to the inclusion of a crystal cell at each integration time step to account for the newly created crystals. As a result, the number of cells increases from 100 to 1100 when $t_{end} = 10^{-2}$ s and $dt = 10^{-5}$ s. The redundant cells are therefore eliminated as preserving the two desired moments of the number density distribution. Table 3.6 suggests that in spite of the significant improvement in the computational efficiency, the accuracy of the numerical results remains almost intact. Similar to the previous test cases, the high order FVMs with flux limiting functions exhibit superior performance to the first

Table 3.6: Errors and computation times of test case 4 ($t_{end} = 10^{-2}$ s and $dt = 10^{-5}$ s).

	Ngrids	**CPU Time**, s	μ_0**Error**, %	μ_3**Error**, %
MOC	1100	35.18	1.20	0.46
MOC: Cell elimination	49	1.85	1.22	0.48
First Order FVM	100	0.93	11.39	19.02
High Order FVM: van Leer	100	1.08	3.69	3.37
High Order FVM: Koren	100	1.06	3.69	3.59
OCFE: Linear B.F.	200	2.30	5.10	17.92

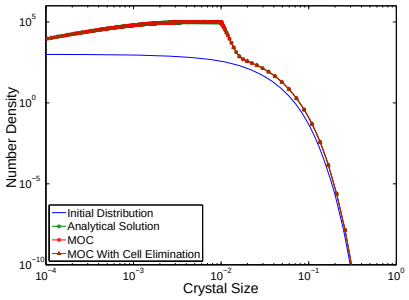

(a) Method of characteristics

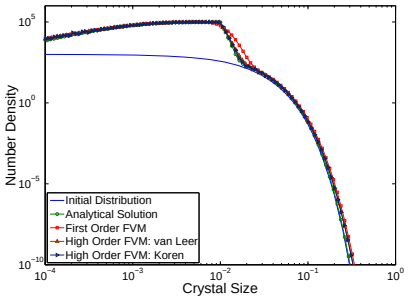

(b) Finite volume methods

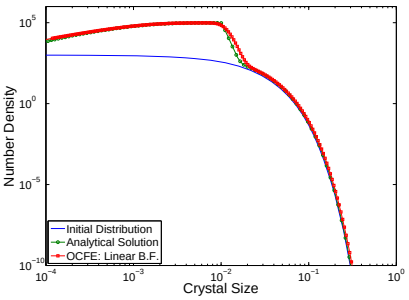

(c) Orthogonal collocation on finite elements (linear basis function)

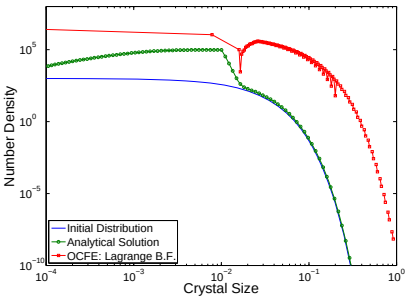

(d) Orthogonal collocation on finite elements (Lagrange basis function)

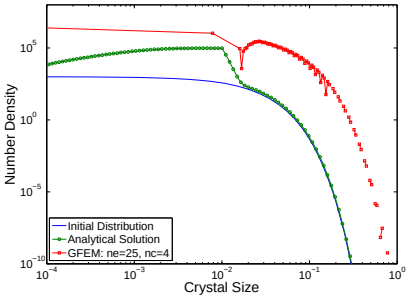

(e) Galerkin's finite element method (Lagrange basis function)

Figure 3.5: A comparison of analytical and numerical simulation results of test case 4.

order upwind FVM and the collocation method with the linear basis function. The finite element methods with the Lagrange basis function yet again fail to describe the steep moving front; see Figure 3.5(d) and Figure 3.5(e).

Table 3.7: Parameters of the seed distribution and the power-law kinetic expressions in the semi-industrial crystallization case study.

Parameter	Value
b	1.0
g	1.0
k_b, $\#/m^3 s$	7.65×10^9
k_g, m/s	7.50×10^{-5}
L_0, m	310.3×10^{-6}
ε	0.962
σ_g	1.51

3.5.5 A semi-industrial fed-batch crystallizer

The PBE solution methods are exploited for dynamic simulation of the seeded fed-batch evaporative crystallizer presented in Section 2.2.1. In general, the nonlinear dependence of nucleation and crystal growth rates on the states of the continuous phase, e.g., solute concentration, further complicates numerical solution of the PBE in real crystallization processes. The PBE describing the dynamics of the semi-industrial crystallizer under study is solved by the method of characteristics, the finite volume methods, and the finite element methods. Three variants of the MOC formulation are considered:

- case 1, without crystal cell elimination;
- case 2, in which only the last crystal cell is eliminated;
- case 3, where the cells for which $L_{i+1}/L_{i-1} < r_{critical} = 1.05$ are eliminated.

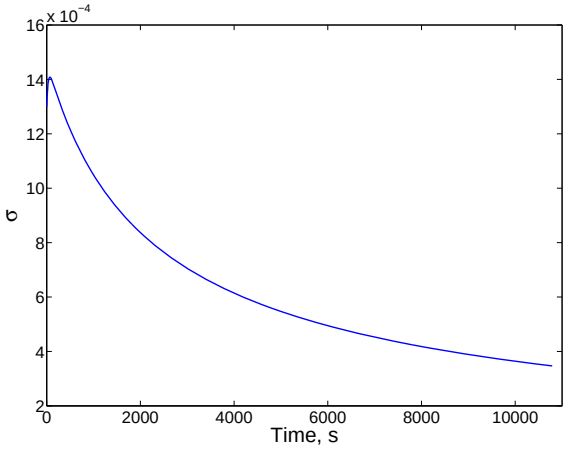

Figure 3.6: The evolution of relative supersaturation throughout the batch run.

Table 3.8: Errors and computation times of the method of characteristics used for dynamic simulation of the semi-industrial crystallizer ($t_{end} = 10800\ s$ and $dt = 10\ s$).

	Case 1	**Case 2**	**Case 3**
Ngrids	2280	1200	270
CPU Time, s	167.6	58.3	34.0
μ_0**Error**, %	0.21	0.21	1.10
μ_1**Error**, %	0.14	0.14	0.65
μ_2**Error**, %	0.14	0.16	0.13
μ_3**Error**, %	0.21	0.27	0.38
μ_4**Error**, %	0.30	0.46	0.80
L_{mean}**Error**, %	0.09	0.20	0.42

The numerical accuracy of the solution methods is assessed in comparison with the moment model. The method of moments provides the analytical solution of the PBE for the given power-law kinetic expressions; see Section 2.2.4. The batch process is initiated by seeding. It is assumed that the seeds have a log-normal distribution, i.e. equation (2.50), which is discretized using an equidistant grid mesh with 1200 crystal cells. The parameters of the seed distribution and the kinetic expressions are given in Table 3.7.

Figure 3.6 shows the evolution of relative supersaturation throughout a batch run of 10800 s. The crystal size distributions corresponding to different time instants during the batch run are displayed in Figure 3.7. It is observed that the MOC leads to simulation results that are free from numerical diffusion. Table 3.8 indicates that the cell elimination drastically reduces the computational burden of the MOC. The accuracy of the numerical results is preserved fairly well when the last crystal cell is eliminated, i.e. case 2. The loss of accuracy in case 3 is more pronounced, particularly in the zeroth and the first moments of the CSD. This suggests that $r_{critical}$ should be chosen carefully in case 3 since large values of $r_{critical}$ will substantially worsen the numerical accuracy.

Table 3.9: Errors and computation times of the finite volume methods used for dynamic simulation of the semi-industrial crystallizer ($t_{end} = 10800\ s$ and $dt = 10\ s$).

	First Order FVM	**High Order FVM**: van Leer	**High Order FVM**: Koren
CPU Time, s	24.6	24.8	24.9
μ_0**Error**, %	0.44	0.11	0.11
μ_1**Error**, %	0.86	0.33	0.31
μ_2**Error**, %	0.55	0.39	0.37
μ_3**Error**, %	1.84	0.29	0.26
μ_4**Error**, %	3.62	0.34	0.30
L_{mean}**Error**, %	1.75	0.05	0.04

The simulation results of the first order upwind and the high order finite volume method with the van Leer flux limiting function are depicted in Figure 3.7(b) and Figure 3.7(c), respectively. As expected, the first order upwind finite volume method results in numerical diffusion, whereas the high order finite volume method with the flux limiting function exhibits this problem to a considerably less extent. Table 3.9 suggests that the numerical accuracy of the high order FVMs is

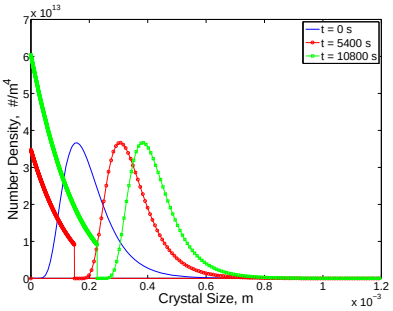

(a) Method of characteristics (case 2)

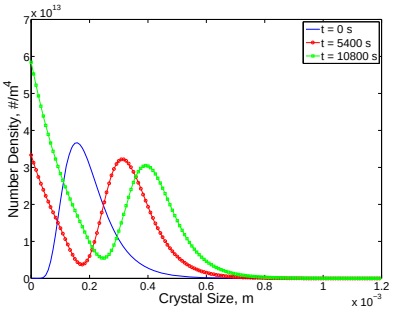

(b) First order FVM

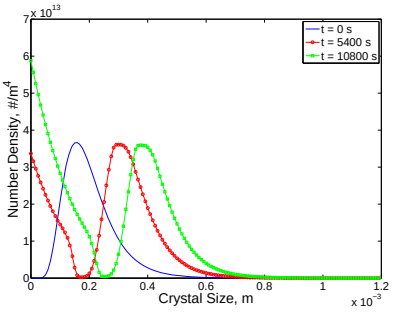

(c) High order FVM: van Leer

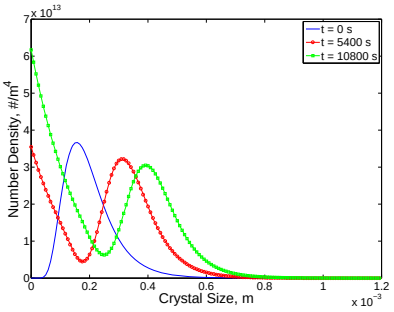

(d) Orthogonal collocation on finite elements (linear basis function)

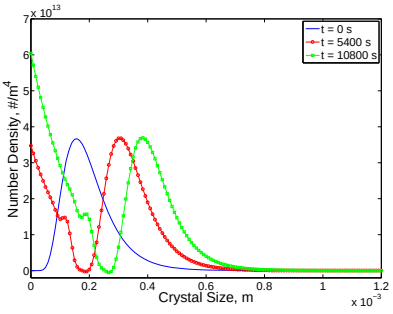

(e) Orthogonal collocation on finite elements (Lagrange basis function)

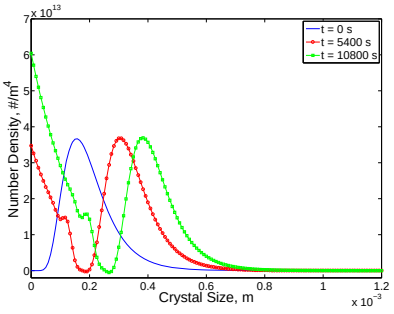

(f) Galerkin's finite element method (Lagrange basis function)

Figure 3.7: Crystal size distributions at different time instants during the batch run.

Table 3.10: Errors and computation times of the finite element methods used for dynamic simulation of the semi-industrial crystallizer ($t_{end} = 10800\ s$ and $dt = 10\ s$).

	OCFE: Linear B.F. (ne=1200)	**OCFE**: Lagrange B.F. (ne=400,nc=4)	**GFEM**: Lagrange B.F. (ne=400,nc=4)
CPU Time, s	24.7	58.3	58.5
μ_0**Error**, %	4.13	1.66	1.65
μ_1**Error**, %	1.15	0.17	0.17
μ_2**Error**, %	1.01	0.16	0.17
μ_3**Error**, %	1.86	0.26	0.26
μ_4**Error**, %	3.39	0.39	0.38
L_{mean}**Error**, %	1.51	0.13	0.13

significantly better than that of the first order upwind FVM, particularly in the higher moments. Note that the different variants of the FVMs have almost the same computational efficiency; see Table 3.9. In addition, the numerical accuracy of the high order finite volume methods with flux limiting functions is comparable to that of the method of characteristics when the redundant crystal cells are eliminated. However, the high order FVMs outperform the MOC in terms of computational efficiency. The lower computational burden of the high order FVMs can be attributed to their Jacobian matrix that consists of $Ngrids \times Ngrids$ entries; $Ngrids$ denotes the number of grid points. The method of characteristics has a $2Ngrids \times 2Ngrids$ Jacobian matrix since the PBE translates to two ordinary differential equations for each grid point; see equations (3.2) and (3.4). This makes the MOC computationally more expensive.

Figure 3.7(d) indicates that the orthogonal collocation method with the linear basis function suffers from the numerical diffusion problem. On the other hand, Figure 3.7(e) and Figure 3.7(f) suggest that the simulation results obtained by the orthogonal collocation and the Galerkin's finite element methods with the

Table 3.11: Model parameters in the industrial crystallization case study.

Parameter	**Value**
g	0.676
$k_b, \#/m^3 s$	5.95×10^9
$k_g, m/s$	1.5×10^{-6}
L_f, m	80.0×10^{-6}
L_0, m	234.1×10^{-6}
L_{SN}, m	650.0×10^{-6}
R	1.125
ε	0.926
σ_g	1.54
τ, s	4400
τ_f, s	645

Lagrange basis function are almost free from numerical diffusion. However, the latter methods lead to oscillatory behavior. This can be alleviated to a large extent by increasing the number of elements at the expense of a higher computational burden. Table 3.10 indicates that the FEMs using the Lagrange basis function are computationally less efficient than the orthogonal collocation method with the linear basis function.

3.5.6 An industrial continuous crystallizer

The solution methods are applied to simulate continuous evaporative crystallization of an ammonium sulphate-water system in a 1100-liter draft tube baffle crystallizer (Bermingham 2003). For the continuous well-mixed crystallizer equipped with a fines removal system, the general population balance equation given in equation (2.1) can be rewritten as

$$\frac{\partial n(L,t)}{\partial t} + \frac{\partial (G(L,t)n(L,t))}{\partial L} = -\frac{n(L,t)}{\tau} - h_{cf}(L)\frac{n(L,t)}{\tau_f}. \tag{3.28}$$

It is assumed that the inlet flow to the crystallizer is crystal free. In equation (3.28), τ and τ_f are the mean residence times of the dispersed phase in the crystallizer and in the fines removal system, respectively (s); $h_{cf}(L)$ is the crystal classification function. The boundary condition of the PBE is expressed by equation (2.5).

Like the previous case study, a time-varying supersaturation profile computed from the solute concentration balance governs the nucleation and crystal growth rates. The crystal growth is described by the power-law relation given in equation (2.24). The empirical expression (Ottens et al. 1972)

$$B_0 = k_b \int_{L_{SN}}^{\infty} n(L,t)L^3 dL \tag{3.29}$$

is used to model secondary nucleation. The process is initiated by seeding with crystals having a log-normal distribution; see equation (2.50).

To obtain the analytical solution of equation (3.28) for the steady state condition, the crystal classification in the fines removal system is described by an ideal

Table 3.12: Errors and computation times of the solution methods used for dynamic simulation of the industrial crystallizer ($t_{end} = 129600s$ and $dt = 10s$).

	Ngrids	**CPU Time**, s	μ_0**Error**, %	μ_3**Error**, %
MOC	229	3501.12	0.07	0.24
High Order FVM: Koren	100	700.65	0.17	0.38
OCFE: Lagrange B.F.	120	769.32	1.27	2.74
GFEM: Lagrange B.F.	120	787.11	1.26	2.73

function

$$h_{cf}(L) = \begin{cases} 1 & \texttt{if} \quad L < L_f \\ 0 & \texttt{if} \quad L \geq L_f. \end{cases} \tag{3.30}$$

According to Randolph and Larson (1988), under this assumption the number density at the steady state is

$$n(L) = \begin{cases} n(0)\exp\left(-\frac{RL}{G_{ss}\tau}\right) & \texttt{if} \quad L < L_f \\ n(0)\exp\left(-\frac{(R-1)L_f}{G_{ss}\tau}\right)\exp\left(-\frac{L}{G_{ss}\tau}\right) & \texttt{if} \quad L \geq L_f, \end{cases} \tag{3.31}$$

where $R-1$ indicates the ratio between the product flow rate and the fines removal flow rate; G_{ss} is the crystal growth rate at the steady state (m/s). The model parameters are listed in Table 3.11.

Figure 3.8 shows the natural logarithm of the predicted number density distribution at the steady state. As can be seen, the method of characteristics and the high order finite volume method with the Koren flux limiting function are able to describe the sharp discontinuity of the classification function fairly well. However, the MOC is computationally more expensive; see Table 3.12. This results from the addition of a crystal cell at every time step. For a large process time of

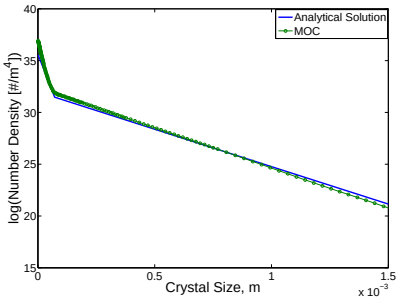

(a) Method of characteristics

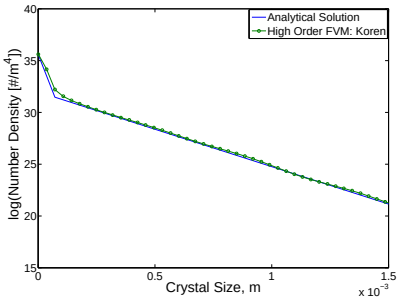

(b) High order FVM: Koren

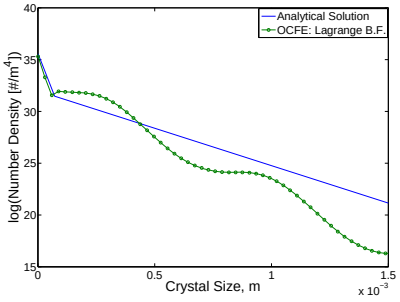

(c) Orthogonal collocation on finite elements (Lagrange basis function)

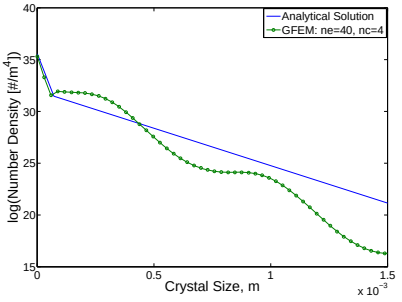

(d) Galerkin's finite element method (Lagrange basis function)

Figure 3.8: The natural logarithm of the crystal size distribution obtained at the steady state of the continuous crystallizer.

$129600s$, a substantially great number of cells is required to describe nucleation. In spite of the fact that the elimination of the redundant cells restores the computational efficiency to a very large extent, the method of characteristics is the least efficient solution method applied to this case study.

Figure 3.8(c) and Figure 3.8(d) suggest that the finite element methods, viz the orthogonal collocation method and the Galerkin's technique using the Lagrangian basis function, are incapable of dealing with the sharp discontinuity of the classification function. Despite of the fact that their computational efficiency is comparable to that of the high order finite volume method, their numerical predictions are much less accurate.

3.6 Summary

Requirements on the solution method of the population balance equation greatly depend on the nature of the application as well as the crystallization process under consideration. This implies that universal guidelines for selection of the solution method may be inadequate. Nonetheless, this chapter has been intended to provide an overview of the most widely used PBE solution methods, which can be best applied for online control of crystallization processes.

The occurrence of steep moving fronts and / or sharp discontinuities often complicates numerical solution of the population balance equation in batch crystallization processes. The numerical difficulties typically arise from the convective nature of the partial differential equation and the incompatibility between its boundary and initial conditions. In this chapter, several numerical solution methods belonging to the family of discretization techniques and the finite element methods have been used to simulate the dynamic behavior of various crystallization test cases undergoing nucleation and crystal growth.

The simulation results suggest that the method of characteristics gives the most accurate numerical predictions, while the high computational burden limits its use for real crystallization processes. It is observed that the finite element methods may severely suffer from numerical problems. This shortcoming, in addition to their complex implementation and low computational efficiency, makes the finite element methods inadequate for online control applications.

The study reveals that the high order finite volume methods with a flux limiting function are well capable of describing sharp discontinuities and steep moving fronts. The high order finite volume methods have a relatively low computational burden as benefiting from ease of implementation in comparison with the other solution methods considered in this work. These features render the high order finite volume methods with a flux limiting function best suited for solution of the population balance equation in online control applications.

4 CHAPTER

Nonlinear State Estimation

One of the most insidious and nefarious properties of scientific models is their tendency to take over, and sometimes supplant, reality.

Erwin Chargaff

Model-based control and performance monitoring of industrial batch crystallization processes require the knowledge of state variables of the system. Despite the advent of process analytical technology in recent years, online measurement of all process variables is not often viable due to various technological and economical limitations. State observers that combine information from two sources, viz a process model and available online measurements, can be used to estimate the states of a batch crystallization process in real time. State estimation is essential for the output feedback structure of the nonlinear model-based control approach to be described in Chapter 5. It allows us to cope with model imperfections and process uncertainties such as measurement errors and uncertain initial conditions.

This chapter presents an overview of several state estimation techniques, namely the extended Luenberger technique, the extended Kalman filtering, the unscented Kalman filtering, the ensemble Kalman filtering belonging to the broader class of Monte Carlo filters, and the moving horizon estimation technique. These deterministic and Bayesian state estimation techniques are exploited to design nonlinear observers for seeded fed-batch evaporative crystallization of an ammonium sulphate-water system. In addition to the observability of the semi-industrial crystallizer under study, the open-loop performance of the nonlinear observers is evaluated in terms of the accuracy of the estimated state variables. The adequacy of the observers for output feedback control of the batch crystallizer is discussed in Chapter 5.

4.1 Introduction

A wide variety of approaches for state estimation of nonlinear dynamic systems have been proposed in the literature. The nonlinear state observers commonly used in (bio)chemical process applications can be categorized into exponential and asymptotic estimation techniques (Bastin and Dochain 1990). The former class of observers assume a perfect knowledge of the model structure including the process kinetics, whereas the asymptotic observers merely rely on conservation laws without requiring the knowledge of process kinetics. Thus, the great deal of uncertainty associated with the kinetic parameters is eliminated in the asymptotic observers. However, this is achieved at the expense of a convergence rate that is fully governed by the process conditions, whereas the adjustable rate of convergence of the exponential observers is determined by tuning parameters (Dochain 2003). To overcome the shortcomings of these estimation techniques, several hybrid observers have recently been proposed. These observers evolve between an exponential and an asymptotic observer in accordance with the quality of the kinetic model (Bogaerts 1999; Lemesle and Gouze 2001; Hulhoven et al. 2006). A more common approach is however the use of the so-called adaptive exponential observers that combine the state observation with the estimation of poorly known parameters (Soroush 1998; Perrier et al. 2000; Oliveira et al. 2002; Dochain 2003; Chen et al. 2005; Bakir et al. 2006; Nagy et al. 2007).

As shown in Figure 4.1, the nonlinear exponential observers can be broadly classified into two categories, namely the techniques developed under a deterministic framework and those developed under the Bayesian framework. The extension of the Luenberger observer (Luenberger 1964), which was originally developed for linear systems, is a deterministic state estimator that neglects any noise acting on the system (Zeitz 1987). On the other hand, the nonlinear observers developed under the Bayesian framework are formulated in a probabilistic setting. The so-called stochastic observers aim to construct the probability density function (pdf) of states, given that the process model and measurements are potentially subject to random disturbances.

The most widely used variant of the nonlinear stochastic observers is the extended Kalman filter (EKF). In the EKF, which involves linearization of the system model, the state as well as the process and measurement noise pdfs are assumed to be Gaussian. Hence, the EKF may not be used when the system is highly nonlinear or the state pdfs are non-Gaussian. In addition, the EKF requires the calculation of the Jacobian matrices, making its application impractical for nondifferentiable systems. To alleviate the drawbacks of the EKF, derivative free stochastic observers, namely the unscented Kalman filter (UKF) (Julier and Uhlmann 2004) and Monte Carlo filters (Gordon et al. 1993) have been developed. While the state pdfs are yet assumed to be Gaussian, the UKF avoids linearization of the system model through an unscented transformation. As a result, the UKF circumvents the need for computing the Jacobian matrices. On the other hand, the Monte Carlo filters have found widespread use owing to the ever increasing computing power. These filters are capable of dealing with nonlinear state estimation problems with multimodal and non-Gaussian pdfs (Arulampalam et al. 2002). As reported in Daum

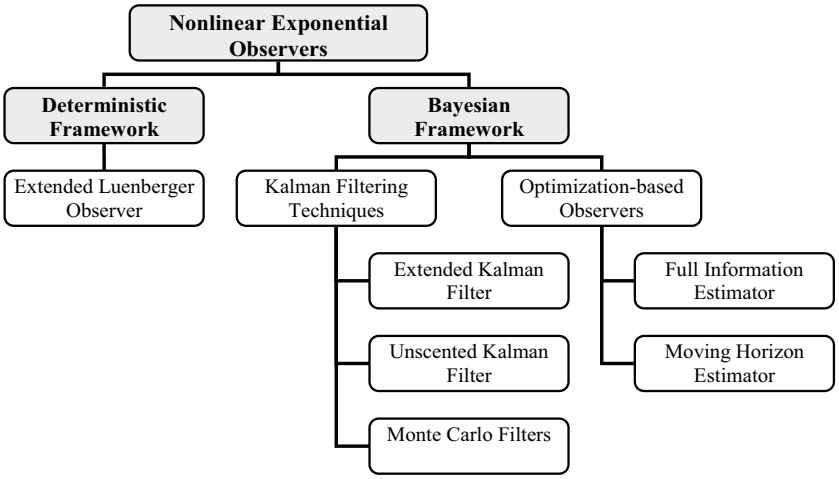

Figure 4.1: A classification of nonlinear exponential observers.

(2005), there is a large variety of Monte Carlo filters that use Monte Carlo simulation techniques to implement the recursive Bayesian estimation framework. The Gaussian assumption is avoided by approximating the continuous state pdfs using randomly generated points. The merit of Monte Carlo filters lies in their ability to handle nonlinear process dynamics without making any assumptions neither on the nature of dynamics nor on the shape or any other characteristics of pdfs.

In addition to stochastic observers, the estimation techniques developed under the Bayesian framework include optimization-based estimators. It is well-known that (bio)chemical processes are often subject to constraints due to various operational and economical considerations. Optimization-based state estimation, which enables the explicit inclusion of constraints into the nonlinear estimation problem, has become an active research area in recent years (Tenny and Rawlings 2002; Gatzke and Doyle 2002; Rao et al. 2003; Haseltine and Rawlings 2005; Qu and Hahn 2008; Schei 2008). A historical review on the developments of this approach is given in Rao and Rawlings (2002). In contrast to stochastic observers, these estimators utilize the measurements obtained over a certain time horizon to correct for the observation error. The nonlinear optimization-based estimation techniques can be classified as full information or moving horizon estimators (Rawlings and Bakshi 2006). The estimation horizon of the full information estimators grows as new measurements become available, whereas in the moving horizon estimators the optimization is performed over a finite time horizon to avoid excessively large computational burdens. In general, the optimization-based observers do not need any assumptions neither on the state pdfs nor on the noise sequences acting on the system.

Another class of nonlinear state estimation techniques known as the high gain observers has also received substantial attention in the literature (Krener and Re-

spondek 1985; Gauthier and Kupka 1992; Ciccarella et al. 1993; Deza et al. 1993; Bakir et al. 2006; Biagiola and Solsona 2006). The high gain observers are based on the notion of linearization through coordinate transformation (Soroush 1998). These observers tend to have similar characteristics as the extended Luenberger observer and the extended Kalman filter (Dochain 2003).

4.2 Nonlinear state estimation techniques

In the following, the algorithms of the nonlinear state estimation techniques considered in this thesis are briefly presented. The class of nonlinear systems of interest is formulated in a discrete-time state space form

$$\begin{aligned} x_k &= f(x_{k-1}, u_{k-1}, w_{k-1}) \\ y_k &= h(x_k, u_k, v_k), \end{aligned} \tag{4.1}$$

where x_k is the vector of state variables, whose initial values are random variables with a given pdf; u_k is the vector of measured process inputs, which are assumed to be constant over the time interval $[t_{k-1}, t_k]$; y_k is the vector of output measurements; $f(x_{k-1}, u_{k-1}, w_{k-1})$ is the nonlinear process model that is generally the solution of a system of differential algebraic equations (DAEs) over the time interval $[t_{k-1}, t_k]$; $h(x_k, u_k, v_k)$ is a possibly nonlinear measurement model; w_k is the vector of process noise with $\mathbb{E}[w_k] = 0$ and $\mathbb{E}[w_k w_k^T] = Q_k$; v_k is the vector of measurement noise with $\mathbb{E}[v_k] = 0$ and $\mathbb{E}[v_k v_k^T] = R_k$. Given a process model and a sequence of noisy measurements, the observer aims to estimate the state vector.

4.2.1 Extended Luenberger observer

Zeitz (1987) was the first to introduce the extended Luenberger observer (ELO) based on the work of Krener and Isidori (1983) on nonlinear observers. For a deterministic system, i.e. $w = 0$ and $v = 0$, a Luenberger-type observer can be established as

$$\hat{x}_{k+1} = f(\hat{x}_k, u_k) + K_k(y_k - h(\hat{x}_k)), \tag{4.2}$$

where $\hat{x}_k$ is an estimate of the state vector and K_k is the observer gain, which determines the convergence properties of the state estimator. Equation (4.2) shows that the observer equation consists of two parts, namely a copy of the process model and a correction term that is the difference between the estimated and measured output variables multiplied by the gain matrix.

The goal of the ELO is to provide an estimate of the state vector such that the observation error

$$e_{k+1} := x_{k+1} - \hat{x}_{k+1} = f(\hat{x}_k + e_k, u_k) - f(\hat{x}_k, u_k) - K_k(h(\hat{x}_k + e_k) - h(\hat{x}_k)) \tag{4.3}$$

is minimal. For nonlinear systems a condition, under which the error converges to zero, cannot be readily deduced from the error dynamics. This implies that the observer gain should be determined on the basis of a linearized version of the

original process model. Thus, linearizing the nonlinear model around $\hat{x}_k$ yields (Dochain 2003)

$$e_{k+1} = (A_k - K_k C_k)e_k, \tag{4.4}$$

where $A_k = [\frac{\partial f(x_k,u_k)}{\partial x}]_{x_k=\hat{x}_k}$ and $C_k = [\frac{\partial h(x_k,u_k)}{\partial x}]_{x_k=\hat{x}_k}$ are linear approximations of the nonlinear process dynamics, i.e. equation (4.1), around the estimated state vector $\hat{x}_k$. The choice of the time-varying observer gain K_k relies on local stability properties of the state estimator. The gain should be chosen such that the linearized error dynamics are asymptotically stable.

Generally, the estimation accuracy of the ELO largely depends on how well the linearized model represents the nonlinear system dynamics. In addition, initialization of the observer is crucial since accurate linearization of process and measurement functions around $\hat{x}_k$ requires that the observer is initialized sufficiently close to the true states. A few studies on successful application of the ELO for closed-loop control of batch crystallization processes have been reported in the literature (Shi et al. 2005; Landlust et al. 2008). The applied observers are mostly high gain extended Luenberger observers (Ciccarella et al. 1993). The structure of the gain matrix is defined on the basis of physical insights into the process, while its tuning parameters are obtained by running open-loop simulations and evaluating the evolution of the states.

4.2.2 Extended Kalman filter

The Kalman filter calculates minimum variance estimates of the state vector in an optimal probabilistic setting (Kalman and Bucy 1961). This notion can be extended to systems with nonlinear dynamics, whose models are differentiable. The EKF applies the optimal Kalman theory to a linear approximation of the nonlinear system. The mean and the covariance of state pdfs are propagated through a linear approximation of the process model obtained around the operating point at each time instant using a Taylor series expansion. The EKF requires that the initial state variables x_0 and the noise sequences acting on the system, i.e. w and v, to be random variables with Gaussian distributions. These pdfs are however no longer Gaussian when undergoing nonlinear transformations. Thus, the EKF presents a suboptimal solution to the state estimation problem of nonlinear systems since it assumes that the random variables still retain their Gaussian pdfs after the transformation.

The EKF has a recursive algorithm consisting of two parts, namely the prediction stage and the measurement correction stage. In the former stage, the a priori state estimates $\hat{x}_{k+1|k}$ and the associated covariance matrix $P_{k+1|k}$ are determined by propagating the mean $\hat{x}_{k|k}$ and the covariance $P_{k|k}$ of state pdfs at the preceding time step through the nonlinear process model and its first order linearization, respectively, leading to

$$\begin{aligned} \hat{x}_{k+1|k} &= f(\hat{x}_{k|k}, u_k, w_k) \\ P_{k+1|k} &= F_k P_{k|k} F_k^T + W_k Q_k W_k^T, \end{aligned} \tag{4.5}$$

where $F_k = [\frac{\partial f(x_k,u_k,w_k)}{\partial x}]_{x_k=\hat{x}_{k|k}}$ and $W_k = [\frac{\partial f(x_k,u_k,w_k)}{\partial w}]_{x_k=\hat{x}_{k|k}}$. Subsequently, in the measurement correction stage the a posteriori state estimates $\hat{x}_{k+1|k+1}$ and the a posteriori error $P_{k+1|k+1}$ are calculated using current measurements y_k

$$\begin{aligned} \hat{x}_{k+1|k+1} &= \hat{x}_{k+1|k} + K_k(y_k - h(\hat{x}_{k+1|k}, u_k, v_k)) \\ P_{k+1|k+1} &= (I - K_k H_k) P_{k+1|k}. \end{aligned} \tag{4.6}$$

In equation (4.6), K_k is the Kalman filter gain given by

$$K_k = P_{k+1|k} H_k^T (H_k P_{k+1|k} H_k^T + V_k R_k V_k^T)^{-1}, \tag{4.7}$$

where $H_k = [\frac{\partial h(x_k,u_k,v_k)}{\partial x}]_{x_k=\hat{x}_{k+1|k}}$ and $V_k = [\frac{\partial h(x_k,u_k,v_k)}{\partial v}]_{x_k=\hat{x}_{k+1|k}}$.

Among the various nonlinear observers, the EKF is the most widely used state estimation technique in diverse process control applications due to its relatively easy implementation and limited computational burden; e.g. see Soroush (1998), Dochain (2003), and the references therein. The EKF however suffers from several practical shortcomings, namely its inapplicability to highly nonlinear, nondifferentiable systems, difficult tuning, and inability to systematically incorporate state constraints. A critical evaluation of the extended Kalman filter is given in Wilson et al. (1998), where the authors have raised their serious doubts on the usefulness of the EKF in industrial applications. Nonetheless, due to its low computational burden, the EKF has been extensively utilized for model-based control of various processes (Lee and Ricker 1994; Biagiola and Figueroa 2004; Srinivasarao et al. 2006), including batch crystallization processes (Xie et al. 2002; Nagy and Braatz 2003; Zhang and Rohani 2003; Landlust et al. 2008). These studies indicate that successful implementation of the EKF in a nonlinear model predictive control scheme largely relies on the accuracy of model approximations as well as the initial estimate of the state vector.

4.2.3 Unscented Kalman filter

The unscented Kalman filter is primarily developed to alleviate the main deficiency of the EKF, namely linear approximation of the nonlinearities, by applying the unscented transformation to the Kalman estimation notion. The UKF approximates the Gaussian pdf of the states by a number of deterministically chosen points such that their mean and covariance match those of the distribution (Julier and Uhlmann 1997, 2004). The so-called sigma points are propagated through the nonlinear system model to compute estimations of the expectations and covariances of the state estimates. Clearly, this is in contrast to the EKF that propagates only a single point through a linearized version of the original system model and calculates the covariance matrix analytically.

The filter algorithm is defined on the basis of the same steps as in the EKF. A set of $2n + 1$ symmetric sigma points, where n denotes the dimension of the state vector, is generated around the means of the set with a distance of the square root of the covariances. Once the sigma points are chosen, they are propagated through the nonlinear model equations to calculate the mean and covariance of

the state vector from the transformed set of points

$$\begin{aligned}
\chi^i_{k+1} &= f(\chi^i_k, u_k, w_k) \\
\hat{x}_{k+1|k} &= \sum_{i=1}^{2n+1} \alpha_i \chi^i_{k+1} \\
P_{k+1|k} &= \sum_{i=1}^{2n+1} \alpha_i [\chi^i_{k+1} - \hat{x}_{k+1|k}][\chi^i_{k+1} - \hat{x}_{k+1|k}]^T + Q_k,
\end{aligned} \tag{4.8}$$

where α_i denote the weighting coefficients (Qu and Hahn 2008). It is evident that the prediction stage differs from the EKF in that the nonlinear process model is not linearized. Instead, the UKF propagates a cluster of points, centered around the current state estimates, to more accurately approximate the mean and the covariance of the state pdfs. The state vector and its associated covariance are then updated using measurements y_k

$$\begin{aligned}
\gamma^i_{k+1} &= h(\chi^i_k, u_k, v_k) \\
\hat{y}_{k+1|k} &= \sum_{i=1}^{2n+1} \alpha_i \gamma^i_{k+1} \\
P_{yy,k+1|k} &= \sum_{i=1}^{2n+1} \alpha_i [\gamma^i_{k+1} - \hat{y}_{k+1|k}][\gamma^i_{k+1} - \hat{y}_{k+1|k}]^T + R_k \\
P_{xy,k+1|k} &= \sum_{i=1}^{2n+1} \alpha_i [\chi^i_{k+1} - \hat{x}_{k+1|k}][\gamma^i_{k+1} - \hat{y}_{k+1|k}]^T \\
K_k &= P_{xy,k+1|k} P^{-1}_{yy,k+1|k} \\
\hat{x}_{k+1|k+1} &= \hat{x}_{k+1|k} + K_k(y_k - \hat{y}_{k+1|k}) \\
P_{k+1|k+1} &= P_{k+1|k} - K_k P_{yy,k+1|k} K^T_k.
\end{aligned} \tag{4.9}$$

In addition to its easy implementation, the unscented Kalman filter provides at least second order accuracy for the mean value and covariance approximations, while the EKF is only accurate up to the first order moment of the pdfs (Julier and Uhlmann 1997). The computational efficiency of the UKF is comparable to that of the EKF; generally being in the order of $O(n^3)$ operations, provided that the

dimension of the state vector is large compared to the number of measurements, i.e. the dimension of y_k. Some variants of the UKF such as the square root unscented Kalman filter (van der Merwe and Wan 2001) can be implemented using $O(n^2)$ operations. Hao et al. (2007) presented a comparative analysis of several computationally efficient types of the UKF obtained for systems exhibiting certain characteristics, e.g. linear measurement function, additive type noise, etc.

Several studies on open-loop implementation of the UKF in process control applications have been reported (Romanenko and Castro 2004; Romanenko et al. 2004; Qu and Hahn 2008; Schei 2008; Kandepu et al. 2008). However, the UKF has rarely been applied to crystallization processes. Mangold et al. (2009) employed a square root unscented Kalman filter to estimate the particle size distribution of barium sulphate in a semi-batch precipitator. A population balance model was used to describe the process dynamics. Despite the promising state estimation results, closed-loop implementation of the UKF remained to be investigated. More recently, Hermanto et al. (2009) designed an UKF for nonlinear model predictive control of polymorphic transformation of L-Glutamic acid crystals. The simulation results indicate that the UKF provides adequate state estimates that lead to a good overall closed-loop control performance.

4.2.4 Ensemble Kalman filter

Contrary to the UKF, the ensemble Kalman filter (EnKF) constitutes a class of derivative free nonlinear filters that can cope with multimodal and non-Gaussian distributions (Evensen 1997; Burgers et al. 1998). The underlying notion of the EnKF is to represent the state pdfs by a large ensemble of randomly chosen states in order to describe all statistical properties of the system variables. Integrating the ensemble members forward in time according to the stochastic system dynamics allows us to compute the error statistics. This is in contrast to the EKF, in which the error statistics are calculated by means of the approximate error covariance equation.

In the prediction stage of the filter algorithm, a set of sample points, i.e. $\hat{x}^i_{k|k}$, that describes the statistics of the state pdfs is generated by means of a Monte Carlo sampling technique. The sample points are propagated through the nonlinear system in order to compute a cloud of transformed sample points

$$\hat{x}^i_{k+1|k} = f(\hat{x}^i_{k|k}, u_k, w_k). \tag{4.10}$$

These points are then used to estimate the sample mean and error covariances

$$\bar{x}_{k+1|k} = \frac{1}{N}\sum_{i=1}^{N} \hat{x}^i_{k+1|k}$$

$$\bar{y}_{k+1|k} = \frac{1}{N}\sum_{i=1}^{N} h(\hat{x}^i_{k+1|k}, u_k, v_k)$$

$$
\begin{aligned}
E_{x_{k+1|k}} &= [\hat{x}^1_{k+1|k} - \bar{x}_{k+1|k} \quad \cdots \quad \hat{x}^N_{k+1|k} - \bar{x}_{k+1|k}] \\
E_{y_{k+1|k}} &= [\hat{y}^1_{k+1|k} - \bar{y}_{k+1|k} \quad \cdots \quad \hat{y}^N_{k+1|k} - \bar{y}_{k+1|k}] \\
P_{xy,k+1|k} &= \frac{1}{N-1} E_{x_{k+1|k}} E^T_{y_{k+1|k}} \\
P_{yy,k+1|k} &= \frac{1}{N-1} E_{y_{k+1|k}} E^T_{y_{k+1|k}} + R_k
\end{aligned}
\tag{4.11}
$$

where N is the number of ensemble members. It is evident from equation (4.11) that the prediction error covariance matrices are defined around the ensemble mean. This implies that the ensemble mean provides the best prediction estimate of the state variable and the spread of ensemble members around the mean is a natural definition of the error of the ensemble mean. Finally, the EnKF performs an ensemble of parallel data assimilation steps to obtain the state estimates

$$
\begin{aligned}
K_k &= P_{xy,k+1|k} P^{-1}_{yy,k+1|k} \\
\hat{x}^i_{k+1|k+1} &= \hat{x}^i_{k+1|k} + K_k(y_k - h(\hat{x}^i_{k+1|k}, u_k, v_k)) \\
\bar{x}_{k+1|k+1} &= \frac{1}{N} \sum_{i=1}^{N} \hat{x}^i_{k+1|k+1}.
\end{aligned}
\tag{4.12}
$$

The process and measurement noise vectors may have arbitrary, but known distributions.

The computational cost of the EnKF is in the order of $O(pNn)$ operations, where p is the number of outputs of the system, N is the ensemble size, and n is the dimension of the state vector (Gillijns et al. 2006). Thus, if $N << n$, the computational burden of evaluating the approximate covariances in the EnKF will be less than that required by the EKF. When N is large, the EnKF will however become computationally too expensive since the model needs to be simulated N times.

The EnKF has been successfully used in several applications such as meteorology (Houtekamer and Mitchell 2005), oceanography (Rozier et al. 2007), and reservoir engineering (Jansen et al. 2008). In these applications, the nonlinear models are of extremely high order, the initial states are highly uncertain, and a large number of measurements are usually available. The EnKF is particularly advantageous when dealing with such large size problems since a number of ensembles of about 50 to 100 is often sufficient to describe the dynamics of systems with thousands of states. Nonetheless, the use of the EnKF in process applications has received little attention. Gillijns et al. (2006) applied the EnKF to estimate the states of a compressible fluid flow in a one-dimensional channel. They showed that the ensemble Kalman filter provides fairly accurate state estimations once a

threshold ensemble size is reached. Prakash et al. (2008) presented a constrained recursive formulation of the EnKF, which systematically deals with bounds on the states. The effectiveness of the proposed algorithm is demonstrated by its application to a simulated gas-phase reactor. The performance evaluation of the EnKF in the latter studies is merely based on open-loop simulations. The closed-loop performance of the ensemble Kalman filter in process applications, e.g. crystallization processes, has not been explored thus far.

4.2.5 Moving horizon estimator

What distinguishes the moving horizon estimator (MHE) from other estimation techniques is its ability to incorporate constraints into the estimation problem. The MHE is an optimization-based estimator, wherein the state estimates are obtained by solving a minimization problem, e.g. the sum of squared errors, while fulfilling the nonlinear model equations and predefined constraints (Robertson et al. 1996). In optimization-based estimators, the objective function is intended to indicate the accuracy of model predictions with respect to process outputs obtained over a certain time interval. In contrast to the classical state estimators, which utilize the most recent measurements to update the model predictions, the MHE uses measurements gathered over a predetermined time horizon for the observer correction. The latter characteristic of optimization-based estimators typically makes them computationally more expensive than stochastic observers.

The moving horizon estimation problem can be stated in its most general form as the solution of the following optimization problem (Rao and Rawlings 2002)

$$\min_{x_{T-P},\{w_k\}_{k=T-P}^{T-1}} \quad \sum_{k=T-P}^{T-1} ||v_k||^2_{R^{-1}} + ||w_k||^2_{Q^{-1}} + Z_{T-P}(x_{T-P}) \tag{4.13}$$

$$\text{subject to :} \quad \text{equation (4.1)}$$
$$x_k \in X, w_k \in W, v_k \in V,$$

where the sets X, W, and V can be constrained; P is the horizon size. In order to ensure the feasibility of the optimization problem, measurement noise constraints are often avoided. Equation (4.13) implies that the last P measurements are explicitly used to solve the optimal estimation problem over the time horizon $T - P \leq k \leq T - 1$. The remaining process measurements are accounted for by the function $Z_{T-P}(x_{T-P})$, the so-called arrival cost term, which summarizes the effect of prior measurement information on the state estimates obtained at time instant $T - P$. The arrival cost term facilitates the transformation of an infinite-dimensional optimization problem into one of finite dimension. Exact algebraic expressions for the arrival cost term only exist for unconstrained linear systems with Gaussian pdfs. Under these conditions, the moving horizon estimator reduces to the Kalman filter (Robertson et al. 1996). In the case of constrained nonlinear systems, the arrival cost term should be approximated, e.g. by a first order Taylor series approximation of the model around the estimated trajectory

as in the EKF or by evaluating sigma points as in the UKF. The approximation allows us to compute the error covariance of the estimated states at time instant $T - P$. Adequate approximation of the arrival cost term is crucial to guaranteeing stability and performance of the MHE.

The moving horizon estimator has received considerable attention in model-based process control applications due to the duality between constrained estimation and control, e.g. see (Tenny and Rawlings 2002; Leskens et al. 2005; Schei 2008). A few applications of optimization-based estimators in crystallization processes have also been reported in the literature. Mangold et al. (2009) applied the moving horizon estimation technique to a population balance model in order to estimate the evolution of particle size distribution in semi-batch precipitation of barium sulphate. The performance of the MHE was evaluated against a square root unscented Kalman filter based on several open-loop simulations. The results suggest that the MHE is slightly more robust to large uncertainties in initial conditions of the estimator, whereas the unscented Kalman filter outperforms the optimization-based estimator when the measurement data is noisy. Recently, Nagy (2009) presented a nonlinear model predictive control scheme to robustly design the shape of crystal size distribution in batch crystallization processes. In order to facilitate real-time implementation of the model-based control framework, a moving horizon estimator is utilized to estimate the crystal conversion shape parameter using online chord length distribution measurements. The simulation and experimental results indicate adequate estimation of the latter parameter by the optimization-based estimator.

4.3 Design of nonlinear observers for a semi-industrial batch crystallizer

The state estimation techniques are used to design nonlinear observers for fed-batch evaporative crystallization of ammonium sulphate in the semi-industrial crystallizer described in Section 2.2.1. The observability of the nonlinear system is examined to ensure that the unmeasurable process variable, namely the solute concentration, can be estimated from online crystal size distribution measurements. In addition, the performance of the nonlinear observers is evaluated in terms of their open-loop state estimation accuracy.

4.3.1 Observability analysis

For a nonlinear system, the observability problem consists of investigating whether there exists relations binding the state variables to the inputs, outputs, and their time derivatives. The relations should locally define the states uniquely in terms of the measurable outputs. If no such relations exist, the initial states of the system cannot be deduced from observing its input-output behavior.

According to Nijmeijer and van der Schaft (1990), the observation space $\mathbf{O}$ of a smooth affine control system, i.e. equation (2.51), is the linear space (over $\mathbb{R}$) of

functions on the smooth manifold M containing $\mathcal{H}_1, \cdots, \mathcal{H}_5$ as well as all repeated Lie derivatives

$$L_{z_1} L_{z_2} \cdots L_{z_k} \mathcal{H}_j \qquad j = 1, \cdots, 5, \quad k = 1, 2, \cdots \tag{4.14}$$

with z_i, $i \in k$ in the set $\{\mathcal{F}, \mathcal{G}\}$. The observation space $\mathbf{O}$ is used to define the observability codistribution $\mathbf{O}_c$ as

$$\begin{aligned} \mathbf{O_c} = span\{&d\mathcal{H}_1(x_0), \ldots, d\mathcal{H}_p(x_0), dL_{z_1} L_{z_2} \ldots L_{z_k} \mathcal{H}_j(x_0)\} \\ &j = 1, \cdots, 5, \quad k = 1, 2, \ldots \ . \end{aligned} \tag{4.15}$$

It can be stated that the moment model presented in Section 2.2.4 is locally observable at x_0 if

$$\dim(\mathbf{O}_c(x_0)) = 6. \tag{4.16}$$

Note that $\dim M = 6$ in the moment model. The observability codistribution for the system under study is defined as

$$\mathbf{O_c} = \begin{pmatrix} 1 & 0 & 0 & 0 & 0 & 0 \\ 0 & 1 & 0 & 0 & 0 & 0 \\ 0 & 0 & 1 & 0 & 0 & 0 \\ 0 & 0 & 0 & 1 & 0 & 0 \\ 0 & 0 & 0 & 0 & 1 & 0 \\ -\frac{\phi_{V,product}}{V} & 0 & 0 & k_b(C - C^*)^b & 0 & k_b \mu_3 b (C - C^*)^{b-1} \end{pmatrix}. \tag{4.17}$$

It is evident that the codistribution has a full rank of 6 when $(C - C^*)$ is not zero. Hence, the system is locally observable as long as supersaturation is being generated.

4.3.2 Open-loop performance analysis

In this section, the state estimation accuracy of the nonlinear observers is evaluated in an open-loop framework. Figure 4.2 depicts the open-loop arrangement of the nonlinear observer and the plant simulator, to which a predetermined heat input profile is applied. The plant simulator simulates the dynamic behavior of the semi-industrial crystallizer using the moment model, which is identical to that incorporated in the observer. The outputs of the plant simulator, viz the first five leading moments of CSD, are first corrupted by random noise sequences having normal distributions and subsequently fed to the observer every $100\ s$.

The nonlinear observers are implemented in MATLAB. Due to its unconditional numerical stability, the implicit Euler scheme is used in the stochastic observers to discretize the continuous model equations. The MATLAB toolbox OptCon (Nagy et al. 2004) is utilized to implement the moving horizon estimator, where the differential algebraic equations are solved by the DASPK solver (Brown et al. 1994).

The stochastic filters are tuned such that more weight is attached to the process model since the measurement noise is rather large. On the other hand, the tuning

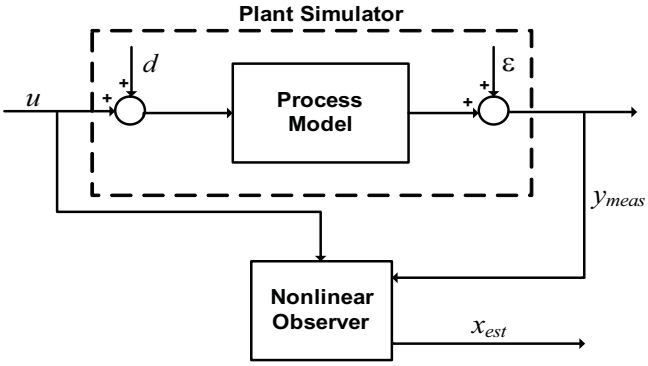

Figure 4.2: The open-loop simulation framework used to evaluate the state estimation accuracy of the nonlinear observers.

parameters of the extended Luenberger observer are determined on the basis of an off-line optimization problem (Kalbasenka et al. 2006). To have a fair performance evaluation, the magnitude of noise sequences applied to the system is kept the same for different observers. The state estimation errors are expressed in terms of the normalized root mean squared error (NRMSE)

$$\mathrm{NRMSE} = \sqrt{\mathbb{E}\Big[\Big(\frac{x(t) - \hat{x}(t)}{x(t)}\Big)^2\Big]}, \tag{4.18}$$

where $x(t)$ denotes the true system states obtained from the plant simulator. The expected values of the relative estimation errors are estimated based on 50 simulation runs.

The open-loop state estimation errors of the nonlinear observers are depicted in Figure 4.3. The plots show the evolution of estimation errors of the five leading moments of CSD along a batch run of $10800\ s$. As can be seen, the estimation errors are zero at the beginning of the batch run since the observers and the plant simulator have identical initial conditions. However, the nonlinear observers give erroneous state estimates in the subsequent sampling time instants due to the stochastic measurement noise.

Figure 4.3 suggests that the estimations made by the ELO and the MHE in the presence of stochastic measurement noise are of somewhat worse quality than those provided by the Kalman filters. This results from the deterministic estimation framework of the ELO and the elimination of the arrival cost term in the MHE. The arrival cost term is not well-defined for batch systems due to large variations of the state variables throughout the batch run. The omission of the arrival cost term reduces the Bayesian framework of the MHE to a deterministic optimization-based estimation technique. The integration of measurements over the estimation horizon in the MHE yet averages out the measurement noise to some degree. Figure 4.3 clearly indicates that the stochastic filters provide fairly accurate state estimates owing to their Bayesian estimation framework.

To further improve the estimation quality of the EKF and the UKF, a tuning method that particularly suits batch processes is adopted (Valappil and Georgakis 2000). In this approach, the information on model uncertainties is used to systematically calculate the process noise covariance matrix. The model uncertainties are specified on the basis of the parameter covariance matrix V_θ obtained during the model development. The time-varying process noise covariance matrix is calculated as

$$Q(t) = \left(\frac{\partial \mathcal{F}}{\partial \theta}\right)_{x(t),u(t),\theta} V_\theta \left(\frac{\partial \mathcal{F}}{\partial \theta}\right)^T_{x(t),u(t),\theta}, \tag{4.19}$$

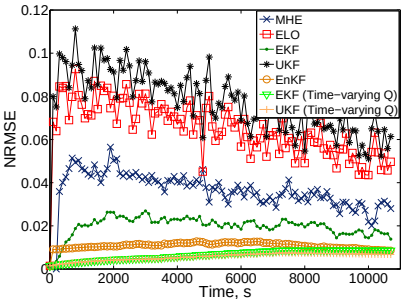

(a) 0^{th} moment

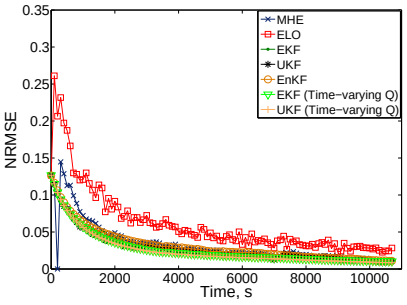

(b) 1^{st} moment

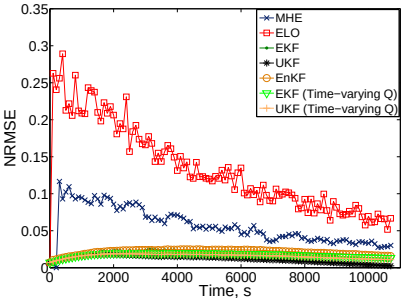

(c) 2^{nd} moment

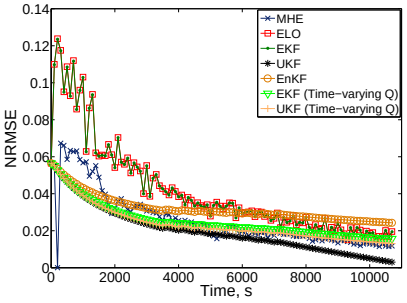

(d) 3^{rd} moment

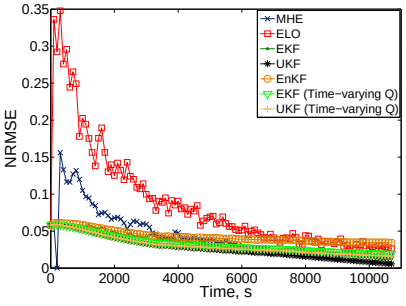

(e) 4^{th} moment

Figure 4.3: Open-loop state estimation errors.

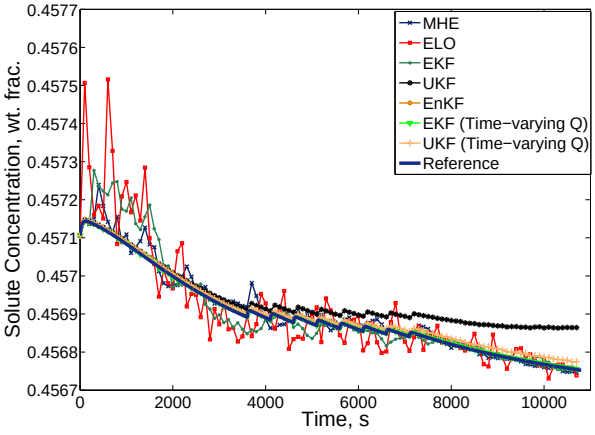

Figure 4.4: A comparison of the estimated solute concentration profiles and the reference profile.

where the sensitivity matrix $\frac{\partial \mathcal{F}}{\partial \theta}$ is determined online. It is evident that the non-diagonal process noise covariance matrix is dependent on the current state of the dynamic system. Figure 4.3 suggests that the latter tuning approach leads to a considerable improvement in the estimation quality of the EKF and the UKF. This is better illustrated in Figure 4.4, which depicts the estimated and the reference solute concentration profiles. As can be seen, the EKF and the UKF with time-varying process noise covariance matrix result in solute concentration estimates

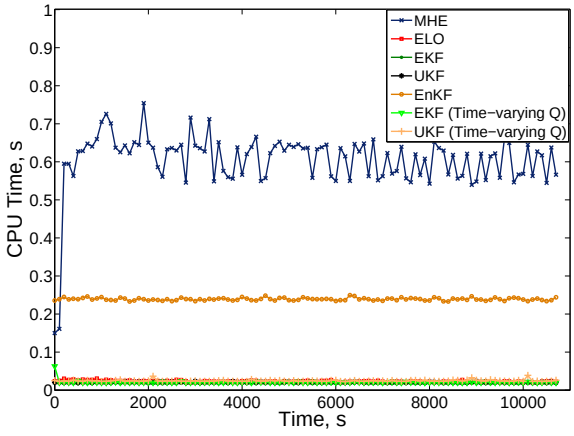

Figure 4.5: CPU times of the nonlinear observers at different sampling time instants throughout a batch run of $10800\ s$.

that are closer to the reference solute concentration profile.

The CPU times of the observers at different sampling time instants along a batch run of $10800\ s$ are shown in Figure 4.5. As expected, the ELO, the EKF, and the UKF have a comparable computational burden, being considerably less than that of the EnKF and the MHE. It is evident that the additional computational burden required for online calculation of the time-varying process noise covariance matrix in the EKF and the UKF is small. Figure 4.5 indicates that the computational efficiency of the nonlinear observers permits their online application as their CPU times along the batch run are well below the measurement sampling time interval, viz $100\ s$.

4.4 Summary

The output feedback structure of the nonlinear model-based control approach to be described in Chapter 5 necessitates the use of a nonlinear state estimator. The detrimental effects of model imperfections and process uncertainties can be compensated for to some degree by state estimation. In addition, state observers allow us to estimate the unmeasurable process variables. In this chapter, several state estimation techniques have been applied to design nonlinear observers for the semi-industrial batch crystallizer under study. The process dynamics are described by a computationally affordable reduced-order moment model. The observability analysis of the nonlinear system verifies that the unmeasurable process variable, namely the solute concentration, can be estimated from the online crystal size distribution measurements.

The state estimation accuracy of the nonlinear observers has been examined using an open-loop simulation framework, in which a predetermined operating policy is applied to a plant simulator. The results indicate that the ELO and the MHE cannot adequately suppress the stochastic measurement noise. This is due to the deterministic framework of the ELO and the elimination of the arrival cost term in the MHE. On the other hand, the stochastic observers provide accurate state estimations owing to their Bayesian estimation framework.

The estimation quality of the EKF and the UKF has been further improved by adopting a time-varying process noise covariance matrix, which is dependent on the current state of the dynamic system. This approach is particularly suitable for batch systems as the system states and consequently the process noise covariance matrix vary largely throughout the batch run. The simulation results suggest that the time-varying process noise covariance matrix allows the EKF and the UKF to provide significantly more accurate estimates of the unmeasurable process variable. It is demonstrated that the computational efficiency of the nonlinear observers enables their application for online control of the semi-industrial crystallizer under study.

5 CHAPTER

Nonlinear Model-based Control

The best way to predict the future is to invent it.

Alan C. Kay

This chapter presents an output feedback nonlinear model-based control approach for optimal operation of industrial batch crystallizers. The control approach allows us to explore the opportunities for online dynamic optimization of crystallizers whose dynamics are described by full population balance models. It also enables us to investigate the detrimental effects of model imperfections and process uncertainties on optimal operation of batch crystallization processes.

The population balance modeling framework presented in Chapter 2 is employed as the cornerstone of the control approach. The modeling framework allows us to apply the control approach to a wide range of industrial batch crystallizers. In addition, it facilitates the use of performance objectives expressed in terms of crystal size distribution.

The core component of the nonlinear model-based control approach is a dynamic optimizer. The dynamic optimizer is implemented in a receding horizon mode, where a nonlinear observer is exploited to estimate the system states. The output feedback structure of the control approach is to preserve the effectiveness of optimal operating policies in the presence of plant-model mismatch and process uncertainties.

The control approach is applied to two simulation case studies, namely a single-input single-output semi-industrial crystallizer and a multi-input multi-output industrial crystallizer. Various direct optimization strategies, viz single shooting, multiple shooting, and simultaneous strategies, are utilized to examine the real-time feasibility of optimal operation of crystallizers. In addition, the performance of different nonlinear estimation techniques is investigated to ensure the adequacy of the control approach in coping with model imperfections and process uncertainties.

5.1 Introduction

Despite the widespread application of batch crystallizers, their advanced control yet poses a significant number of challenges. The difficulties mainly arise from the nonlinear process dynamics described by distributed models, uncertainties of kinetic expressions, non-ideal mixing, sensor limitations in accurate measurement of process variables, inherent process uncertainties, and lack of process actuation (Braatz 2002; Huesman et al. 2009). Nonetheless, advanced control of batch crystallizers is essential for effectively responding to the dynamic market demands of crystalline products. This is to realize the stringent product specifications of the consumer-driven market as enhancing the process productivity.

Numerous strategies have been proposed for advanced control of batch crystallization processes. These strategies can be broadly categorized into the *model-based control approach* (Matthews and Rawlings 1998; Ma et al. 2002b; Nagy and Braatz 2004; Hu et al. 2005c; Sarkar et al. 2006; Nowee et al. 2007; Sheikhzadeh et al. 2008) and the *direct design approach* (Fujiwara et al. 2005; Zhou et al. 2006; Nagy et al. 2008). In the former approach, a process model is used to optimally exploit the degrees of freedom of the system to achieve the desired product properties in accordance with a performance objective. A desirable product typically consists in crystals with a large mean size and a narrow size distribution (Rawlings et al. 1993). In recent years, the advent of process analytical technology has led to the emergence of the direct design approach. This approach aims to control the system within the metastable zone bounded by the solubility curve and the metastable limit. In the direct design approach, a supersaturation profile is determined experimentally with the aid of different process analytical techniques. Subsequently, the setpoint profile is tracked in the phase diagram by means of a supersaturation controller, which relies on in-situ measurement of process state variables. Although the direct design approach circumvents the need for derivation of first-principles models and accurate determination of crystallization kinetics, it only ensures near-optimal operation of the process. A more detailed discussion on the aforementioned control approaches can be found in Section 1.2.

It is self-evident that the cornerstone of any model-based control strategy is its dynamic process model, describing the relation between the relevant inputs and outputs of the system. As discussed in Chapter 2, the population balance equation provides a natural framework for mathematical modeling of the evolution of crystal size distribution in crystallization processes. The prime difficulty in the synthesis of feedback model-based controllers for these processes arises from the distributed nature of the population balance modeling framework. Finite dimensional approximations of the population balance equation typically lead to high order sets of ordinary differential equations. This often makes real-time implementation of model-based controllers computationally prohibitive.

Over the past decade, several studies have been carried out to synthesize low-order feedback controllers that can be implemented in real-time (Lang et al. 1999; Zhang and Rohani 2003; Shi et al. 2005; Landlust et al. 2008; Kalbasenka 2009). The model-based controllers mostly utilize a computationally affordable nonlinear moment model for online repetitive optimization of certain characteristics of

crystal size distribution. However, complex dynamics of industrial batch crystallizers cannot be adequately described by a moment model when the knowledge of full crystal size distribution is required, e.g., crystallizers equipped with fines removal or product classification systems. In addition, the moment model merely allows the use of performance objectives expressed in terms of the moments of CSD. The classical performance objectives may lead to conservative operation of a batch crystallizer as the distributed characteristics of crystals cannot be optimized.

With developments in solution methods of the population balance equation, few attempts have recently been made to devise feedback nonlinear controllers that exploit the full population balance modeling framework. Sheikhzadeh et al. (2007) proposed a model-based approach for real-time control of an anti-solvent batch crystallizer by formulating single- and multiple-objective optimal control problems. An in-situ FBRM probe was utilized in combination with ATR-FTIR spectroscopy to provide the dynamic optimizer with online estimations of the crystallization kinetics. This facilitated the feedback implementation of the control approach on a laboratory-scale crystallizer. The experimental results showed that real-time optimization of the process led to improved quality of the crystalline product. Nagy (2009) presented a robust control methodology to achieve the desired shape of CSD. The approach combined the concepts of the direct design approach and the model-based control in a hierarchical framework. The optimizer used solute concentration, temperature, and chord length distribution measurements to repeatedly compute the optimal supersaturation profile. This profile was then applied as the setpoint for the supersaturation controller. The solute concentration and chord length distribution measurements were performed by an ATR-UV spectrometer and an FBRM probe, respectively. Real-time implementation of the control approach on a laboratory-scale cooling crystallizer indicated that the target CSD could be achieved even in the case of a sudden change in the nucleation rate. Hermanto et al. (2009) developed a nonlinear model predictive control strategy for batch polymorphic transformation of L-glutamic acid from the metastable a-form to the stable b-form crystals. The authors expected that solution of the full population balance equation would significantly increase the computation time, prohibiting the application of nonlinear programming. Therefore, a more practical nonlinear model predictive control strategy based on extended predictive self-adaptive control (EPSAC) was adopted. The EPSAC approximates the nonlinear process variables by iterative linearization around future trajectories so that they converge to the same nonlinear optimal solution (Rueda et al. 2005). To implement the proposed NMPC strategy, an unscented Kalman filter was utilized to estimate the unmeasurable states. The robustness of the feedback control approach to parameter perturbations was compared to some established control strategies. The simulation results suggested that the nonlinear model predictive control strategy had good overall robustness for different performance objectives.

In the remainder of this chapter, an output feedback nonlinear model-based control approach for optimal operation of industrial batch crystallizers is developed. The control approach enables us to investigate the effect of the complexity of population balance models on real-time control of batch crystallizers by exploring different direct optimization strategies. In addition, it allows us to study the

influence of model imperfections and process uncertainties on optimal operation of batch crystallizers.

The control approach is first applied to a single-input single-output (SISO) semi-industrial batch crystallizer. The system dynamics are described by a moment model. The performance of various direct optimization strategies is investigated in terms of the real-time feasibility of optimal operation of the batch crystallizer. In addition, the ability of different nonlinear state estimation techniques to cope with model imperfections and process uncertainties is examined. Subsequently, the use of a full population balance model for nonlinear model-based control of the semi-industrial crystallizer is explored. This paved the way for online control of crystallization processes with more complex dynamics. Thus, the control approach is exploited for real-time control of a multi-input multi-output (MIMO) industrial batch crystallizer. The latter case study allows us to illustrate the significance of process actuation in fulfilling the control objectives commonly sought in operation of industrial batch crystallizers.

5.2 The output feedback control approach

The formulation of a model-based control approach for optimal operation of batch crystallizers largely depends on the product quality requirements, the properties of the crystallizing system, and the availability of online measurements. The control objectives sought in operation of batch processes are typically conflicting (Bonvin 1998). This necessitates the formulation of an optimal control problem that pushes the process to its most optimal operating regime as various operational and quality constraints are honored. The optimal control problem to be solved online can be cast as

$$\begin{aligned} \min_{u(t)\in U, t^F} \quad & \Psi(x(t), z(t), u(t), \theta) \\ \text{subject to :} \quad & \text{equation (2.44)} \\ & \mathcal{H}(x(t), z(t), u(t), \theta) \leq 0, \end{aligned} \tag{5.1}$$

where Ψ is the performance objective; t^F is the final time; $\mathcal{H} : \mathbb{R}^{n_x} \times \mathbb{R}^{n_z} \times U \times \Theta \rightarrow \mathbb{R}^c$ is the vector of functions, which describe all linear and nonlinear, time-varying or end time algebraic constraints of the system; c denotes the total number of constraints. In its most general form, the performance objective Ψ consists of two parts

$$\Psi(x(t), z(t), u(t), \theta) = \mathcal{M}(x(t^F), z(t^F), \theta) + \int_t^{t^F} \mathcal{L}(x(\tau), z(\tau), u(\tau), \theta) \mathrm{d}\tau, \tag{5.2}$$

where $\mathcal{M} : \mathbb{R}^{n_x} \times \mathbb{R}^{n_z} \times \Theta \rightarrow \mathbb{R}$ is a terminal cost term and $\mathcal{L} : \mathbb{R}^{n_x} \times \mathbb{R}^{n_z} \times U \times \Theta \rightarrow \mathbb{R}$ is a running cost term. Equation (5.2) expresses a wide range of performance objectives used in model-based control applications, e.g., setpoint tracking, minimization of operation time, etc.

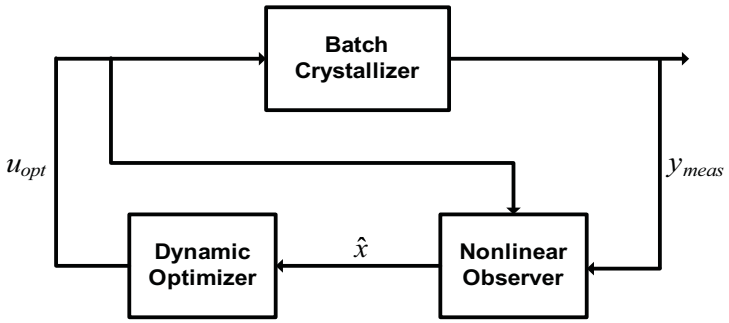

Figure 5.1: The output feedback nonlinear model-based control approach.

To circumvent performance degradation of the optimal operating policies in the presence of model imperfections and process uncertainties, the nonlinear process model should be continuously updated on the basis of new measurements obtained at each sampling time instant. Thus, the control framework depicted in Figure 5.1 is adopted for real-time dynamic optimization of industrial batch crystallizers. In the output feedback control approach, the optimal control problem is solved online in a *receding horizon mode* (Keerthi and Gilbert 1988). The principal idea of the receding horizon control algorithm is illustrated in Figure 5.2. At sampling time instant t_k, the optimal control problem stated in equation (5.1) is solved over a finite time frame $t_k + T_C$, namely the control horizon. The optimal solution of the minimization problem is a sequence of input values, for which the performance objective is minimized over the prediction horizon $t_k^F = t_k + T_P$. The first element of the optimal input sequence is applied to the process. Subsequently, the prediction horizon shifts one sample ahead and the procedure is repeated as soon as new online measurements become available at sampling time instant t_{k+1}.

The output feedback structure of the control approach necessitates recursive initialization of the dynamic optimizer at each sampling time instant. This is performed by a state estimator that utilizes a process model, along with online measurements, to construct the state profiles. The state estimation in combination with the feedback structure of the control approach compensates for model imperfections and process uncertainties to a large extent. In addition, the nonlinear state estimator allows us to estimate process variables, e.g. solute concentration, which may not be measured online due to various technological or economical limitations.

The real-time feasibility of the model-based control approach relies on efficient solution of the optimal control problem. In this thesis, different direct optimization strategies, namely single shooting, multiple shooting, and simultaneous strategies, are exploited to solve the dynamic optimization problem. These strategies convert the original infinite dimensional optimal control problem given in equation (5.1) into a finite dimensional nonlinear programming problem (NLP). Essentially, two different solution strategies for the reformulated problem exist:

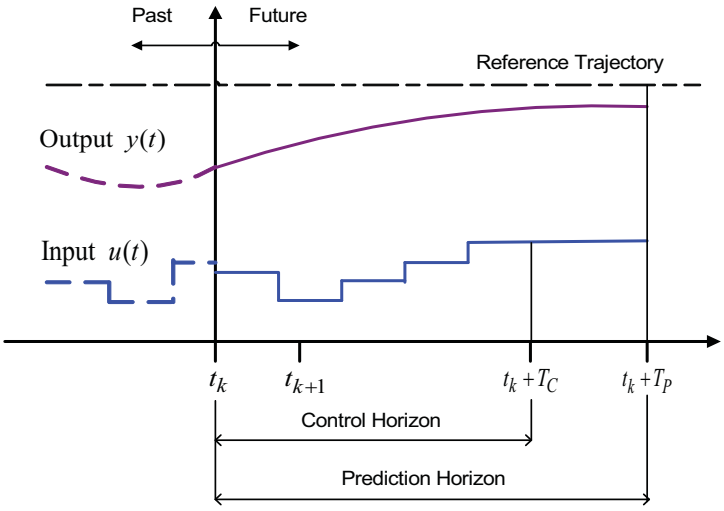

Figure 5.2: The receding horizon principle.

1. Sequential simulation and optimization: In every iteration step of the optimization procedure, the model equations are solved exactly by a numerical integration method for the current values of control inputs.
2. Simultaneous simulation and optimization: The discretized model equations enter the optimization problem as nonlinear constraints.

The multiple shooting optimization strategy can be considered as a hybrid method since the model equations are solved exactly only over the predetermined intervals (Binder et al. 2001).

In the single shooting strategy (Biegler and Cuthrell 1985), the infinitely many degrees of freedom of the control vector are reduced by parameterization. An initial value problem encompassing the model equations is numerically solved in each iteration step of the optimization procedure. The solution is obtained with high accuracy for the current values of the parameterized control vector. Hence, model simulation and optimization are carried out sequentially, guaranteeing the solution feasibility even in the case of premature optimization terminations.

On the other hand, in the simultaneous strategy the model equations are discretized along with the control vector (Cuthrell and Biegler 1989). The discretized differential equations are included in the optimization problem as nonlinear constraints, typically leading to very large NLP problems. Simultaneous model simulation and optimization potentially results in faster computations in comparison with the single shooting strategy. However, feasible state trajectories are obtained only after successful termination of the optimization since the discretized model equations are violated during the optimization procedure.

Contrary to the above discussed optimization strategies, model simulation and optimization are not performed entirely sequentially nor simultaneously in the

Table 5.1: Comparison of the direct optimization strategies (after Binder et al. (2001)).

	Single shooting	Multiple shooting	Simultaneous
General solution approach	sequential	hybrid	simultaneous
Use of DAE solvers	yes	yes	no
Size of nonlinear programming problem	small	intermediate	large
Applicable to highly unstable systems	no	yes	no
DAE model fulfilled in each iteration step	yes	partially	no

multiple shooting strategy (Bock and Plitt 1984; Diehl et al. 2002). In this strategy, the state trajectories and the control vector are parameterized over a predetermined number of intervals. The initial value problems are solved separately on each multiple shooting interval with a prespecified numerical accuracy. This makes the technique well suited for parallel computations. The relatively large number of variables necessitates the use of tailored NLP algorithms, which exploit the special structure of the problem, e.g., sparsity, to yield faster convergence than for the single shooting strategy. However, the continuity of state trajectories is only fulfilled after successful termination of the optimization procedure as with the simultaneous technique. Note that in the direct optimization strategies, the state and the end point constraints are violated at premature optimization terminations. A brief summary of the direct optimization strategies is given in Table 5.1.

The single shooting optimizer is implemented in MATLAB, where the set of model equations and the NLP problem are sequentially solved by the `ODE15s` and `fmincon` functions, respectively. The `ODE15s` solver is chosen due to its ability to efficiently integrate a set of highly stiff differential algebraic equations. The `fmincon` uses a sequential quadratic programming (SQP) algorithm to solve medium-scale optimization problems subject to inequality constraints. The SQP algorithm is one of the most widely used algorithms for constrained optimization of process systems (Edgar et al. 2001). The GAMS algebraic programming environment, in conjunction with the CONOPT3 solver, is utilized to devise the simultaneous dynamic optimizer. CONOPT3 uses a combination of various NLP algorithms, namely sequential linear programming, generalized reduced gradient, and sequential quadratic programming algorithms. This makes CONOPT3 suitable for solving constrained optimization problems. Due to its unconditional numerical stability, the implicit Euler discretization scheme is employed in the simultaneous optimizer to transform the differential equations into algebraic equations (Huesman et al. 2007). The multiple shooting optimizer is implemented in the MATLAB toolbox OptCon (Nagy et al. 2004; Simon et al. 2009), which uses the large-scale nonlinear optimization solver HQP (Franke et al. 2005). The sets of differential algebraic equations on multiple shooting intervals are solved using

the well-known DASPK solver (Brown et al. 1994).

5.3 Case study 1: A single-input single-output semi-industrial crystallizer

5.3.1 Introduction

This case study is intended to demonstrate the real-time feasibility of nonlinear model-based control of industrial batch crystallizers. The control approach is employed for optimal operation of the $75 - liter$ draft tube crystallizer, in which seeded fed-batch evaporative crystallization of ammonium sulphate takes place. The input-output diagram of the semi-industrial crystallizer is shown in Figure 5.3; see Section 2.2.1 for a detailed description of the process. A preceding study on the controllability of the crystallizer revealed that the product CSD could not be controlled by the available process actuators, namely the heat input and the impeller frequency (Kalbasenka et al. 2005). The evolution of CSD is strongly dependent on the initial conditions of state variables. Therefore, a thorough seeding procedure is used to attain the desired product CSD attributes as well as an operational envelop, in which the crystallization phenomena are most sensitive to the heat input.

In general, a trade-off between nucleation and crystal growth is sought in control of batch crystallizers. For crystallizing systems with a relatively large metastable zone, a crystal growth dominant operation is often preferred. Crystal growth rate is a key process variable closely related to product characteristics and batch productivity. A crystal growth dominant operation restricts supersaturation within the metastable zone between the solubility curve and the metastable limit, where no spontaneous nucleation occurs. High crystal growth rates may however adversely affect product quality due to increased impurity uptake, increased liquid inclusions, as well as undesirable attrition and/or agglomeration. Therefore, excessively high crystal growth rates within the metastable zone should be suppressed.

The trade-off between nucleation and crystal growth can be achieved by defining the performance objective in terms of product quality, process productivity or

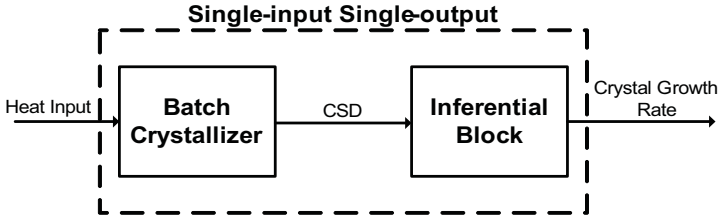

Figure 5.3: The input-output diagram of the semi-industrial batch crystallizer.

batch time (Kalbasenka 2009). The optimal control problem of the semi-industrial batch crystallizer under study is formulated as

$$\begin{aligned} \min_{Q(t)} \quad & \frac{\int_0^{t_f} (100\frac{G(t)-G_{max}}{G_{max}})^2 \mathrm{d}t}{\int_0^{t_f} \mathrm{d}t} \\ \text{subject to :} \quad & \text{equation (2.51)} \\ & Q_{min} \leqslant Q(t) \leqslant Q_{max}, \end{aligned} \tag{5.3}$$

where Q is the parameterized heat input profile; t_f is the fixed batch time; G_{max} is the maximum admissible crystal growth rate, which circumvents the detrimental effects of high supersaturation on the product quality. In equation (5.3), heat input is the manipulated variable exploited to optimize the crystal growth rate profile and consequently control the supersaturation. The heat input's lower bound $Q_{min} = 9kW$ is to ensure a high survival efficiency of seeds at the beginning of the batch run, whereas the upper bound of the heat input $Q_{max} = 13kW$ is due to heat transfer limitations of the process. The optimal seeding not only promotes a crystal growth dominant operational envelop by minimizing secondary nucleation, but also facilitates the achievement of the desired product CSD attributes. Clearly, equation (5.3) maximizes the batch productivity by attaining a maximum admissible crystal growth rate throughout the batch run.

The performance of the control approach is examined when applied to a plant simulator. The simulation platform allows us to evaluate the adequacy of various nonlinear state estimation techniques and dynamic optimization strategies for real-time control of industrial batch crystallizers. The plant simulator simulates the process using exactly the same moment model as the one incorporated in the controller. A description of the moment model is given in Section 2.2.4. The initial conditions, namely the five leading moments of the initial CSD and the initial solute concentration, of the plant model and the controller's model are identical unless otherwise stated. In Section 5.3.4, the system dynamics in the control approach and in the plant simulator are described by a full population balance model. In this section, the impact of the complexity of the population balance model, in terms of the number of state variables, on real-time control of the semi-industrial batch crystallizer is investigated.

5.3.2 Dynamic optimization

To investigate whether direct optimization strategies can ensure online computation of the optimal control problem, the output feedback control approach is applied to the plant simulator. Figure 5.4 demonstrates the simulation results of the control approach when equation (5.3) is solved using different optimization strategies. The optimizers manipulate the heat input to the crystallizer such that the crystal growth rate is kept at its maximum admissible value, viz $G_{max} = 2.5\times10^{-8}$ m/s. G_{max} is a conservatively chosen maximum crystal growth rate to avoid the formation of irregularly shaped crystals and to limit the undesirable effects of high supersaturation. As can be seen in Figure 5.4(a), the optimizers readily reduce the

heat input to the crystallizer when the batch run is initialed at the heat input of 10 kW. This is to suppress the excessively high crystal growth rates at the beginning of the batch run. However, the maximum crystal growth rate cannot be satisfied in the initial phase of the batch run due to the heat input's lower bound, i.e. 9 kW. As the crystals grow larger, the supersaturation in the crystallizer depletes and consequently the crystal growth rate reaches its maximum admissible value. Thereafter, G_{max} is optimally tracked till the heat input hits its upper bound of 13 kW. In the final phase of the batch run, the crystal growth rate starts decaying again. This is due to the heat input's upper bound, making the tracking of G_{max} no longer possible.

Figure 5.4 suggests that the three dynamic optimizers perform similarly in terms of optimal operation of the crystallizer. The similar performance of the optimizers mainly results from their comparable settings as given in Table 5.2. The settings of the simultaneous strategy cannot be defined entirely identical to those

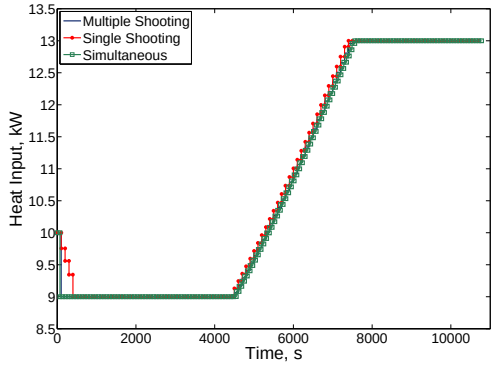

(a) Heat input profiles

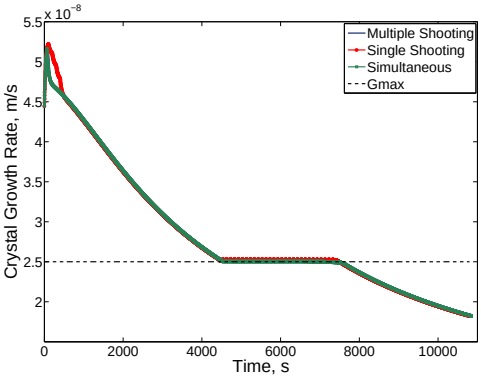

(b) Crystal growth rate profiles

Figure 5.4: Simulation results of the control approach when applied to the semi-industrial crystallizer.

Table 5.2: Settings of the dynamic optimizers applied to the plant simulator.

	Optimization strategy		
	Multiple shooting	Single shooting	Simultaneous
Control horizon	1050 s	1000 s	1000 s
Control vector parameterization [a]	15 elements	15 elements	15 elements
Maximum number of QP iterations	20	20	Not Applicable
Integration tolerance	1×10^{-6}	1×10^{-6}	Not Applicable

[a] Piecewise-constant parameterization.

of the other optimization strategies. This is due to the elimination of the integration solver through discretization of model equations. It was observed that the performance of the dynamic optimizers is largely dependent on the control horizon and the complexity of the control vector parameterization. In addition, the scaling of state variables strongly affects the feasibility of the optimization problem. The initial estimate of the control vector can also have a significant influence on the performance as well as the computational efficiency of the optimization strategies (Costa and Filho 2005).

The computational burden of the optimization strategies is different under approximately the same optimization settings listed in Table 5.2. Figure 5.5 depicts the CPU times of the dynamic optimizers at different sampling time instants along a batch run of $10800\ s$. The single shooting strategy is the most computationally expensive optimization strategy, whereas the multiple shooting and the simultaneous strategies exhibit a much higher computational efficiency. The elimination of the model integration step in the simultaneous strategy drastically improves its numerical efficiency. However, this is achieved at the expense of handling a much larger NLP problem in comparison with the other strategies. The multiple shooting strategy has the lowest computational burden owing to the sparse structure of the NLP problem. In addition, the use of the compiled C++ model and

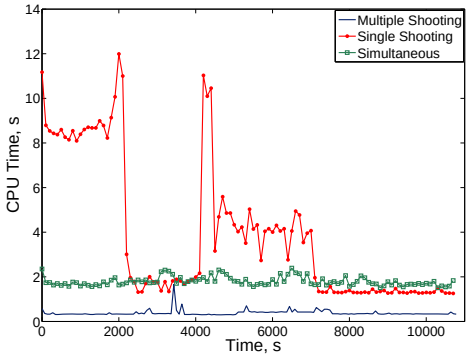

Figure 5.5: CPU times of the dynamic optimizers at different sampling time instants throughout a batch run of $10800\ s$.

Table 5.3: Computation times of the dynamic optimizers corresponding to simulation of a batch run of $10800\ s$.

	Total CPU time[a] over the batch, s	Maximum CPU time of one iteration, s
Multiple shooting	58.97	1.66
Single shooting	424.03	11.97
Simultaneous	194.03	2.39

[a]The reported CPU times correspond to the Microsoft Windows XP (Professional) operating system running on a Genuine Intel(R) T2050 @1.60GHz processor with 1 GB RAM.

solver libraries in the OptCon toolbox significantly improves the computational efficiency of the multiple shooting optimizer. Table 5.3 lists the CPU times of the optimization strategies. It is evident that real-time implementation of the control approach is computationally feasible as the largest optimization CPU time among different sampling time instants along a batch run is considerably less than the measurement sampling time interval, viz $100\ s$.

5.3.3 Nonlinear state estimation

Successful application of an output feedback control approach largely relies on the information about states of the dynamic system. Chapter 4 presented a detailed description of different nonlinear state estimation techniques, whose open-loop estimation adequacy was investigated. In this section, the performance of the nonlinear state observers is evaluated in terms of their closed-loop behavior and their ability to cope with process uncertainties commonly encountered in industrial batch crystallizers. The closed-loop control performance is assessed under the following scenarios:

- nominal scenario, where the measurements y_{meas} are corrupted by random noise sequences having normal distributions;
- uncertain scenario, which aims to examine how well the performance objective, namely the reference crystal growth rate trajectory tracking, is fulfilled in the presence of model imperfections and process uncertainties.

The state estimation errors are expressed in terms of the normalized root mean squared error (NRMSE); see equation (4.18). Similarly, the closed-loop control performance is evaluated in terms of the reference trajectory tracking error defined as

$$\mathtt{NRMSE} = \sqrt{\mathbb{E}\big[\big(\frac{G_{max} - G(t)}{G_{max}}\big)^2\big]}. \tag{5.4}$$

The expected values of the reference trajectory tracking errors are estimated based on 50 simulation runs. To have a fair performance evaluation, the tuning parameters of the observers remain fixed in the two scenarios unless otherwise stated. The tuning parameters are given in Appendix B.

Nominal scenario

Figure 5.6 shows the estimation errors of the five leading moments of CSD under the nominal scenario. It is observed that the error trends are similar to those obtained under the open-loop scenario discussed in Chapter 4. However, the nonlinear observers tend to have somewhat smaller estimation errors and a faster convergence rate under the closed-loop nominal scenario. As can be seen, the stochastic observers, in particular the EKF and the UKF with time-varying process noise covariance matrix, outperform the observers with a deterministic estimation

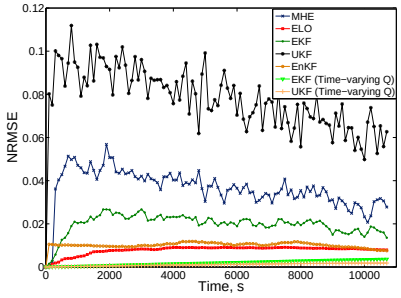

(a) 0^{th} moment

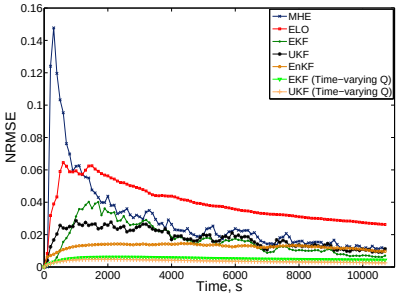

(b) 1^{st} moment

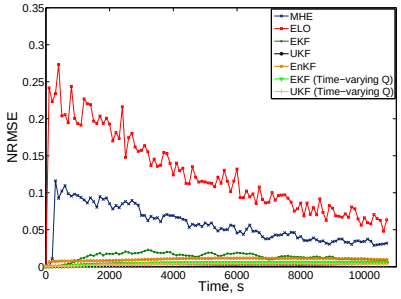

(c) 2^{nd} moment

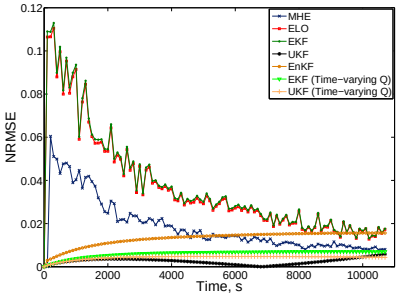

(d) 3^{rd} moment

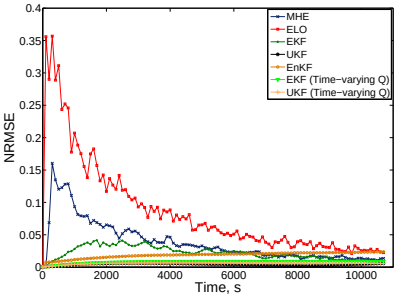

(e) 4^{th} moment

Figure 5.6: State estimation errors under the nominal scenario.

Table 5.4: Computation times of the nonlinear observers.

Nonlinear observer	Average CPU time[a] of one iteration, s
ELO	0.012
EKF	0.012
EKF (Time-varying Q)	0.013
UKF	0.032
UKF (Time-varying Q)	0.033
EnKF (Ensemble size: 10)	0.087
EnKF (Ensemble size: 20)	0.157
EnKF (Ensemble size: 40)	0.297
EnKF (Ensemble size: 80)	0.581
MHE (Estimation horizon: 300 s)	0.610
MHE (Estimation horizon: 500 s)	0.629
MHE (Estimation horizon: 700 s)	0.658

[a]The reported CPU times correspond to the Microsoft Windows XP (Professional) operating system running on a Genuine Intel(R) T2050 @1.60GHz processor with 1 GB RAM.

framework. Table 5.4 lists the computation times of the nonlinear observers under the nominal scenario. The computational burden of all observers is significantly less than the measurement sampling time interval, viz $100\ s$.

To evaluate the effect of state estimation on closed-loop control performance, the reference crystal growth rate trajectory tracking is examined. Figure 5.7(a) displays the normalized root mean squared errors of the crystal growth rate with respect to its maximum admissible value, i.e. the reference trajectory; see equation (5.4). The crystal growth rate is inferred from the solute concentration estimates provided by the observers. Due to lack of actuation, the performance objective can only be fulfilled throughout the limited time interval shown in Figure 5.7(b). A connection between the state estimation quality and the fulfillment of the performance objective can be established by comparing the NRMSE of the crystal growth rate and that of the estimated states. Figure 5.7(b) suggests that the errors in the reference crystal growth rate trajectory tracking follow the same trend as those of the 2^{nd} moment of CSD; see Figure 5.6(c). Therefore, the control performance is more closely connected to the estimation quality of the 2^{nd} moment of CSD amongst the five leading moments of CSD. As can be seen, the relatively poor state estimation by the ELO and the MHE leads to ineffective tracking of the reference trajectory. On the other hand, the stochastic observers allow the controller to follow the reference trajectory more effectively. This is likely to result in a crystalline product with the desired quality attributes.

The estimation horizon of the MHE is varied to study its influence on the closed-loop performance. Figure 5.8 shows the reference trajectory tracking errors for different estimation horizons. It is observed that the state estimation quality of the MHE improves by extending the estimation horizon. However, this is achieved at the expense of slightly higher computational costs; see Table 5.4.

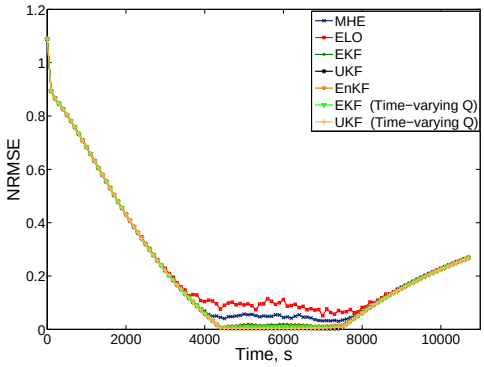

(a) Throughout the batch run

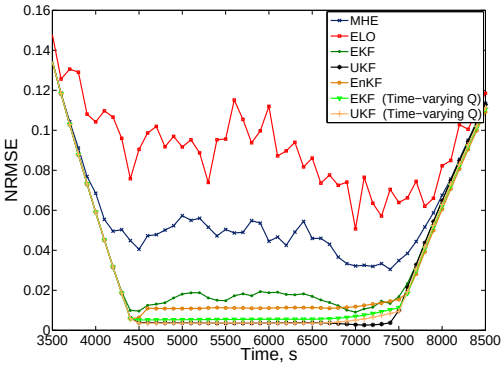

(b) Throughout the time frame over which the performance objective is fulfilled

Figure 5.7: Errors in the reference crystal growth rate trajectory tracking under the nominal scenario.

To enhance the closed-loop performance of the EnKF, the effect of the ensemble size N is investigated. The appropriate number of ensemble members is typically determined on the basis of the state dimension and the nonlinearity of the system. The errors in the reference trajectory tracking in relation to ensemble size $N = 10, 20, 40$ and 80 are shown in Figure 5.9. As can be seen, the errors slightly decrease as the ensemble size is doubled from 10 to 20. However, further improvement in the closed-loop control performance cannot be achieved by increasing the ensemble size N once a threshold size of 20 is reached. Table 5.4 indicates that the computational burden of the EnKF increases approximately linearly with the number of ensemble members.

It follows from the aforementioned analysis that the EKF and the UKF with time-varying process noise covariance matrix have the best closed-loop performance. In comparison with the other two stochastic observers, the EnKF exhibits higher state estimation errors, leading to less effective reference trajectory track-

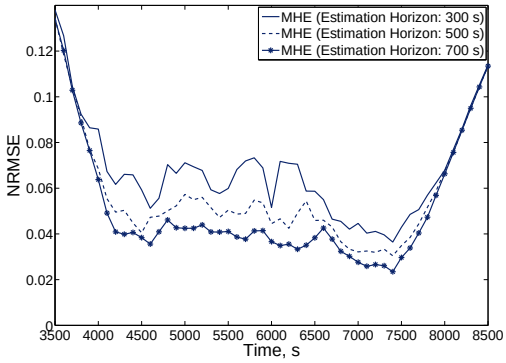

Figure 5.8: Errors in the reference crystal growth rate trajectory tracking in relation to the estimation horizon of the MHE.

ing. This can be due to inadequate filter tuning. It is also observed that the reference trajectory tracking errors of the MHE are larger than those of the stochastic filters. As shown, the closed-loop performance of the MHE can be enhanced by extending the estimation horizon.

Uncertain scenario

Industrial batch crystallizers are often prone to various process uncertainties, mainly arisen from measurement deficiencies and uncertain initial conditions due to improper seeding. In addition, the great degree of uncertainty typically associated with the parameters of crystallization kinetic expressions may not allow the process model to provide an adequate description of the system dynamics. The capability of nonlinear observers to cope with model imperfections and process

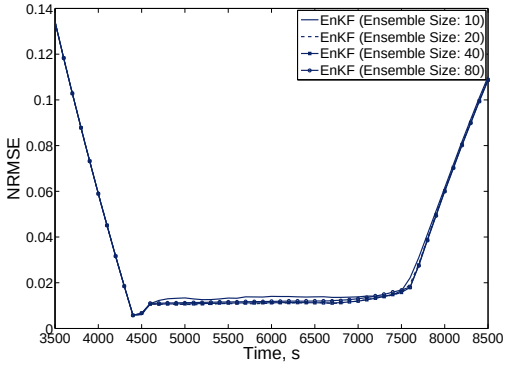

Figure 5.9: Errors in the reference crystal growth rate trajectory tracking in relation to the ensemble size of the EnKF.

disturbances is examined under a scenario with uncertainty specifications given in Table 5.5. In this scenario, the EKF and the UKF with time-varying process noise covariance matrix as well as the EnKF are retuned to avoid divergence, which is primarily caused by the introduction of plant-model mismatch. When more weight is attached to the process model, the observers tend to diverge in the presence of plant-model mismatch due to an inaccurate description of the system dynamics. The divergence can be compensated for by attaching more weight to the information obtained from the plant simulator.

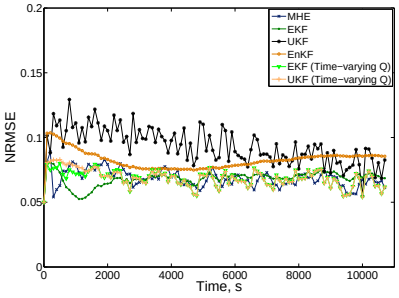

(a) 0^{th} moment

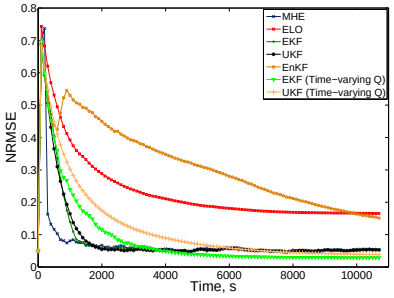

(b) 1^{st} moment

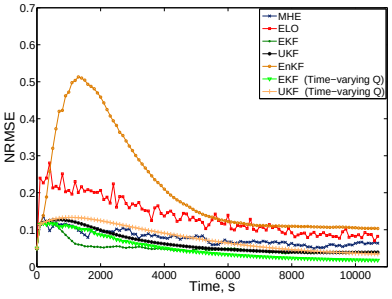

(c) 2^{nd} moment

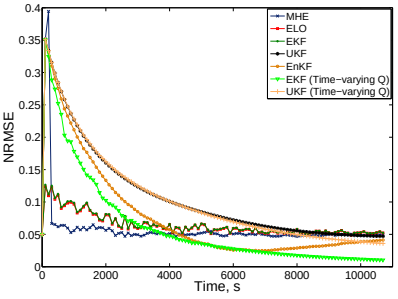

(d) 3^{rd} moment

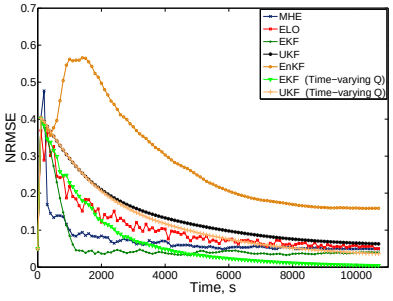

(e) 4^{th} moment

Figure 5.10: State estimation errors under the uncertain scenario.

Table 5.5: Specifications of model imperfections and process uncertainties in the uncertain scenario.

Parametric plant-model mismatch:	$+35.0\%$ error in k_b and k_g
Systematic measurement error:	$+5.0\%$ error in the five leading moments of CSD
Uncertain initial conditions:	$+2.0\%$ error in the initial solute concentration
	$+5.0\%$ error in the five leading moments of the initial CSD

Figure 5.10 shows the estimation errors of the five leading moments of CSD under the uncertain scenario. It is observed that the initial estimation errors are not zero due to the discrepancy between the initial conditions of the process model and those of the plant simulator. In comparison with the nominal scenario, the latter effect leads to larger estimation errors in the initial phase of the batch run. As the process evolves in time, the large initial estimation errors vanish and converge to values comparable to those achieved under the nominal scenario. Figure 5.10 suggests that the estimation errors tend to stabilize around larger values than in the nominal scenario. This is attributed to the systematic measurement error, which introduces a bias in the state estimates. As can be seen, the EKF, the UKF, and the MHE exhibit a better performance compared to the EnKF. Like the nominal scenario, the EKF and the UKF with time-varying process noise covariance matrix have better estimation quality and faster convergence rates, in particular for the higher moments of CSD.

The errors in the reference crystal growth rate trajectory tracking under the uncertain scenario are shown in Figure 5.11. The bias in the state estimates, particularly in the 2^{nd} moment of CSD, has degraded the performance of the controller by introducing an off-set in the reference trajectory tracking. This is due to the inability of the observers to deal with parametric model imperfections and systematic measurement errors effectively. Figure 5.12 depicts the normal distributions of the crystal growth rates inferred under the nominal and the uncertain

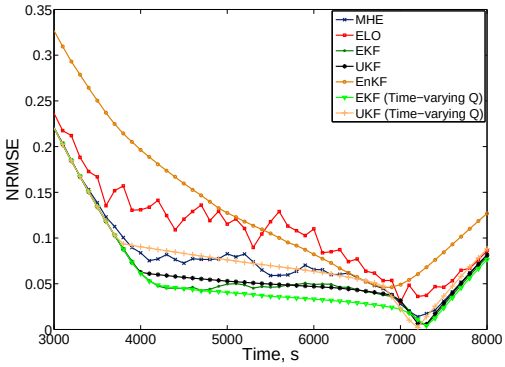

Figure 5.11: Errors in the reference crystal growth rate trajectory tracking under the uncertain scenario.

scenarios around the maximum admissible crystal growth rate, i.e. the dashed line. The crystal growth rate distributions are computed on the basis of 50 system realizations. It is observed that the crystal growth rates obtained under the uncertain scenario exhibit a rather large deviation with respect to the reference trajectory. The violation of the maximum admissible crystal growth rate may significantly degrade the product quality due to, e.g., formation of irregularly shaped crystals, impurity uptakes, etc., even though higher crystal growth rates will result in increased batch productivity. Figure 5.12 indicates that the EKF and the

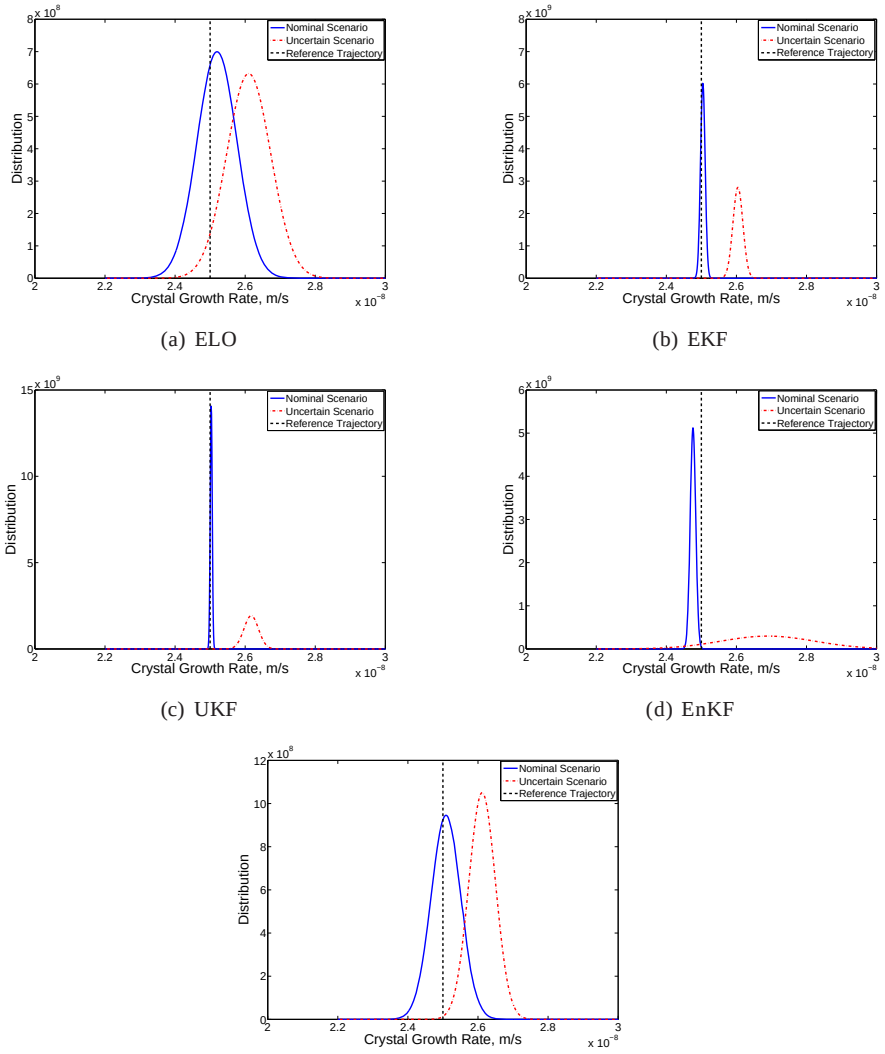

(a) ELO

(b) EKF

(c) UKF

(d) EnKF

(e) MHE

Figure 5.12: The normal probability distribution of the crystal growth rates inferred by the nonlinear observers.

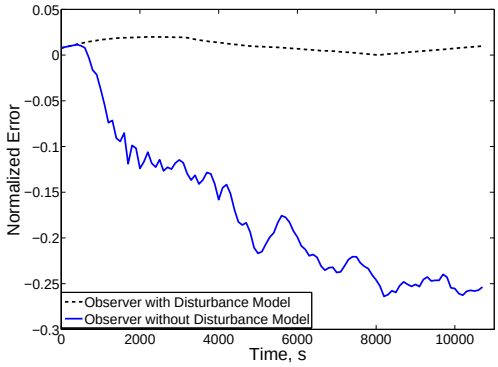

(a) EKF

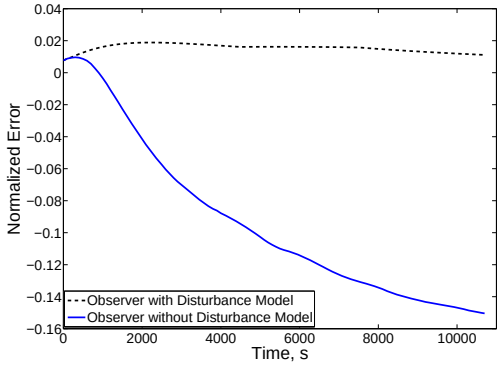

(b) UKF

Figure 5.13: Normalized estimation errors of the 2^{nd} moment of CSD under the uncertain scenario.

UKF have the narrowest distributions under both scenarios. It is evident that the effectiveness of the latter observers in providing accurate state estimates under the nominal scenario enables the controller to satisfactorily fulfill its objective.

The control performance under the uncertain scenario is improved by including a disturbance model into the nonlinear observers. As the performance of the controller is closely connected to the estimation accuracy of the 2^{nd} moment of CSD, the disturbance model is intended to describe the off-set in the estimates of the latter state variable. Hence, an extra state variable with a constant value is augmented to the state vector to estimate and consequently to suppress the disturbances acting on m_2. Figure 5.13 suggests that the disturbance model incorporated into the EKF and the UKF significantly enhances the estimation accuracy of the 2^{nd} moment of CSD. Figure 5.14 depicts the crystal growth rate profiles throughout the batch run. It is evident that the disturbance model adequately describes the disturbances acting on the system and consequently enables effective reference trajectory tracking in the time frame over which the control objective can

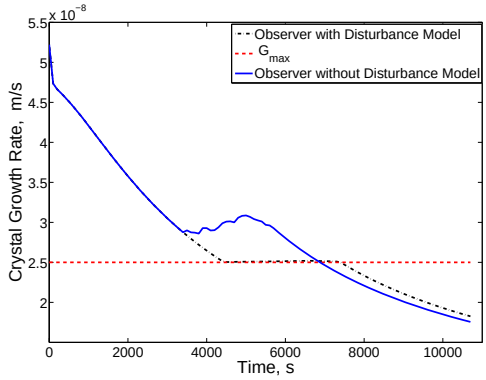

(a) EKF

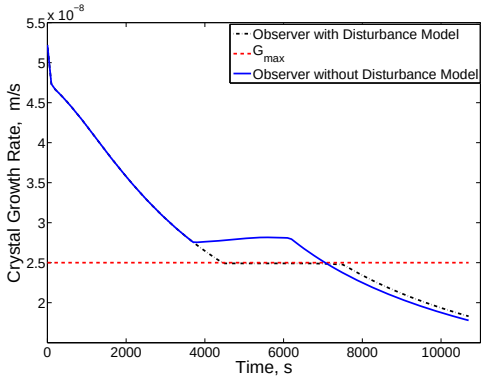

(b) UKF

Figure 5.14: The optimal crystal growth rate profiles under the uncertain scenario.

be fulfilled. As can be seen, the controller fails to tightly follow the reference trajectory when the disturbance model is not included in the EKF and the UKF. Note that the maximum crystal growth rate cannot be maintained in the initial and the final phases of the batch run due to actuation limitations.

5.3.4 Model-based control using a full population balance model

In this section, the effect of the complexity of a population balance model, in terms of the number of state variables, on optimal operation of the semi-industrial batch crystallizer is investigated. The system dynamics in the control approach are described by a full population balance (PB) model. The PB model of the batch crystallizer under study is presented in Section 2.2.3. The control approach is applied to a plant simulator, which simulates the process using a PB model. The closed-loop control performance is examined in the presence of structural and parametric model imperfections as well as process uncertainties. The following scenarios are

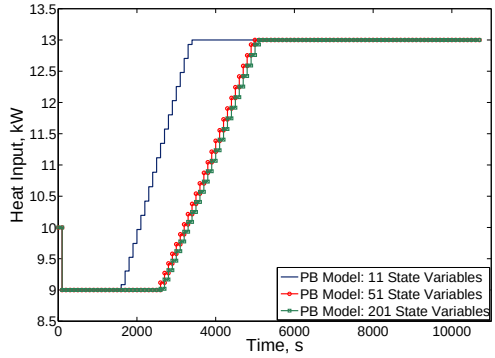

(a) Heat input profiles

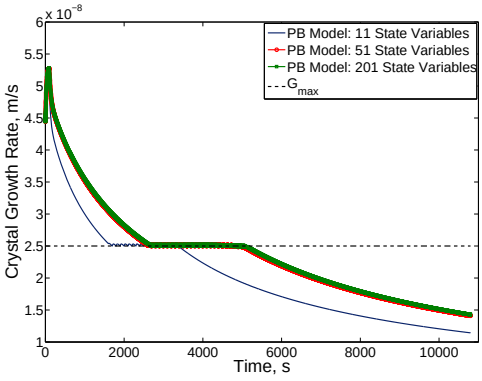

(b) Crystal growth rate profiles

Figure 5.15: Simulation results of the state feedback control approach for different discretization coarseness of the population balance model.

considered:

- state feedback control, where the state estimator is not incorporated in the control approach. Thus, the online measurements are directly fed to the dynamic optimizer. This scenario is intended to examine the real-time feasibility of dynamic optimization of a population balance model;
- output feedback control, in which a moving horizon estimator is used in conjunction with the dynamic optimizer[1]. This is to compensate for the detrimental effects of model imperfections and process uncertainties on optimal operating policies.

In both scenarios, the evolution of crystal size distribution and solute concentration throughout the batch run is measured. The optimal control problem is solved

[1]The choice of the moving horizon estimator was made prior to the nonlinear state estimation study described in Section 5.3.3.

by the multiple shooting optimization strategy. As discussed in Section 5.3.2, the latter strategy exhibits the highest computational efficiency amongst the direct optimization strategies considered in this thesis.

State feedback control

The number of state variables of the PB model is determined by the coarseness of the finite volume grid mesh adopted to discretize the population balance equation. Figure 5.15 demonstrates the optimal profiles of the state feedback control approach obtained on the basis of PB models with different numbers of state variables. The optimizer's model is identical to that of the plant simulator. Again, the maximum crystal growth rate cannot be followed at all times during the batch run; see Section 5.3.2. Figure 5.15 indicates that when the control approach exploits a PB model with 11 state variables, viz the crystal population in 10 crystal cells and the solute concentration, the reference trajectory tracking is attained over a shorter time frame. This can be attributed to large numerical diffusions in predictions of the PB model with 10 crystal cells. On the other hand, Figure 5.15 suggests that the PB models with 51 and 201 state variables allow the controller to fulfill its objective more effectively. Figure 5.16 shows the evolution of crystal size distribution in the course of a batch run of $10800\ s$. It is observed that a coarse

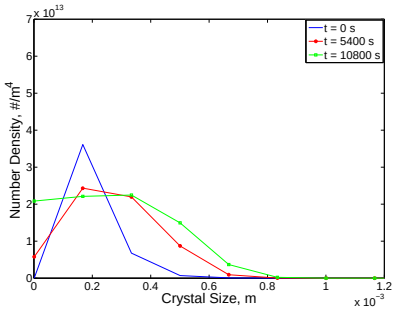

(a) Population balance model with 11 state variables

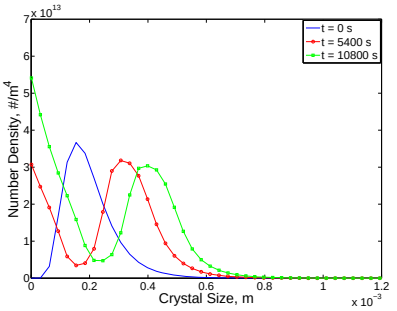

(b) Population balance model with 51 state variables

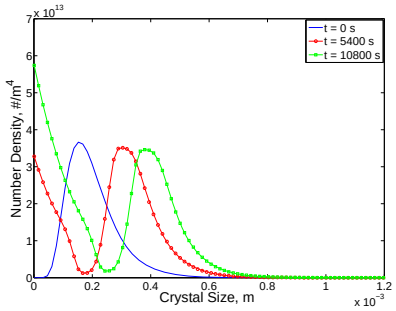

(c) Population balance model with 101 state variables

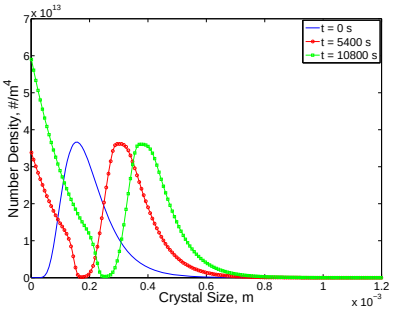

(d) Population balance model with 201 state variables

Figure 5.16: Crystal size distributions at different time instants during the batch run.

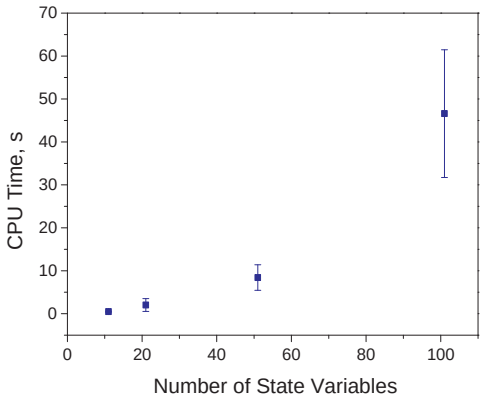

Figure 5.17: Average computation times of one optimization step in relation to the number of state variables of the population balance model. The vertical lines display the standard deviations of computation times around the average values.

grid mesh results in non-smooth crystal size distributions. On the other hand, a sufficiently large number of crystal cells leads to an adequate representation of the crystal size distribution at the expense of a higher optimization burden.

Figure 5.17 depicts the average computation times required for one optimization step in relation to the number of state variables of the PB model. As can be seen, the computational burden of the state feedback control approach seems to increase exponentially with the number of state variables. Table 5.6 lists the computation times of one optimization step in the control approach when different PB models are used. It is observed that the control approach based on the PB model with 201 state variables cannot be used for real-time control of the crystallizer under study. The average computation time of one optimization step is

Table 5.6: Average computation times of one optimization step in the state feedback control approach.

Number of state variables	CPU time[a], s
11	0.48 ± 0.06
21	2.02 ± 0.75
51	8.42 ± 1.48
101	46.59 ± 15.43
201	1204.37 ± 205.79

[a]The reported CPU times correspond to the Microsoft Windows XP (Professional) operating system running on a Genuine Intel(R) T2050 @1.60GHz processor with 1 GB RAM.

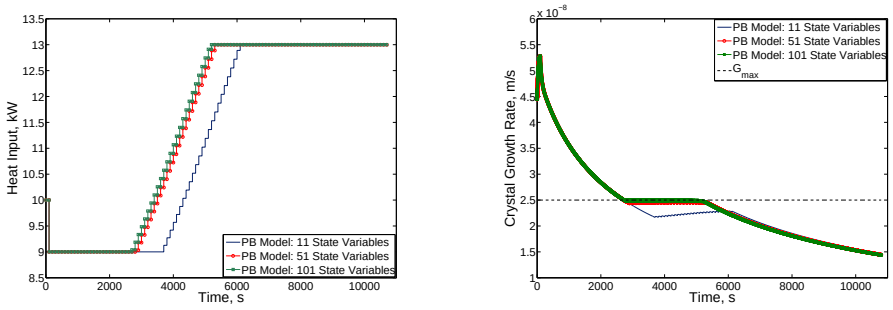

(a) Heat input profiles

(b) Crystal growth rate profiles

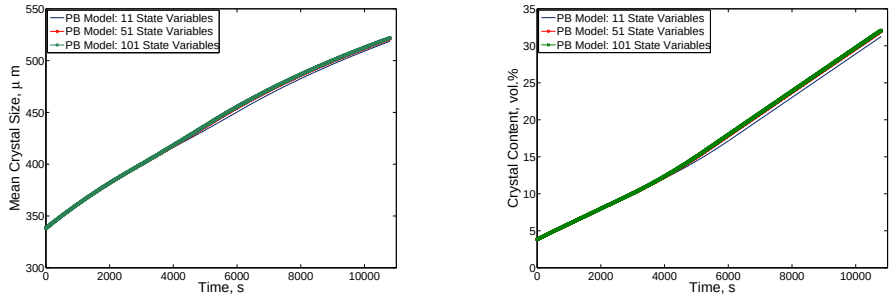

(c) Mean crystal size

(d) Batch crystal content

Figure 5.18: Simulation results of the state feedback control approach in the presence of structural plant-model mismatch.

approximately 120 s, which exceeds the measurement sampling time interval of 100 s.

The ability of the state feedback control approach to cope with the structural plant-model mismatch arisen from a coarse finite volume grid mesh is examined. The control approach is applied to a plant simulator, consisting of the PB model with 201 state variables. It is assumed that the plant simulator provides a true representation of the process dynamics. On the other hand, the control approach adopts a PB model with less state variables, which leads to structural model imperfections with respect to the plant simulator. Figure 5.18 shows the simulation results of the state feedback control approach in the presence of structural plant-model mismatch. As can be seen in Figure 5.18(b), the structural plant-model mismatch results in a poor reference trajectory tracking when the control approach is based on the PB model with 11 state variables. The degradation of the control performance is due to an inadequate representation of the evolution of crystal size distribution, which arises from the coarse grid mesh. Table 5.7 lists the errors in the moments of the product CSD simulated by the different PB models with respect to predictions of the plant simulator. It is evident that the errors of the PB model with 11 state variables are significantly larger than those of the other PB models, particularly in the higher moments. The errors diminish as more

Table 5.7: Normalized root mean squared errors of the moments of the product crystal size distribution.

Number of state variables of the PB model	NRMSE				
	μ_0	μ_1	μ_2	μ_3	μ_4
11	0.039	0.043	0.130	0.318	0.629
21	0.022	0.013	0.042	0.125	0.242
51	0.009	0.008	0.015	0.047	0.088
101	0.004	0.003	0.008	0.023	0.041

crystal cells are used for spatial discretization of the population balance equation. As shown in Figure 5.18(b), the performance objective can be effectively realized when PB models with 51 and 101 state variables are adopted in the control approach. Figure 5.18(c) and Figure 5.18(d) suggest that the more effective reference trajectory tracking will in turn lead to slightly larger crystals and increased batch productivity.

To enhance the effectiveness of the control approach in the presence of structural plant-model mismatch, the optimal control problem is modified as

$$\begin{aligned} \min_{Q(t)} \quad & \frac{\int_0^{t_f} \left(100\frac{G(t)-G_{max}+(G_{meas}-G)}{G_{max}}\right)^2 \mathrm{d}t}{\int_0^{t_f} \mathrm{d}t} \\ \text{subject to :} \quad & \text{equation (2.44)} \\ & Q_{min} \leqslant Q(t) \leqslant Q_{max}, \end{aligned} \tag{5.5}$$

where G_{meas} denotes the measured value of the crystal growth rate that is inferred from concentration measurements. The correction term $G_{meas}-G$ is introduced in the performance objective to suppress the large off-set in the reference trajectory tracking. The correction term aims to diminish the large discrepancy between the predicted crystal growth rate and its measured value. This term confers an integrating action to the optimizer according to the generally used method in linear model predictive control (Muske and Rawlings 1993). The simulation results of the control approach with the modified performance objective are depicted in Figure 5.19. It is observed that the correction term allows us to eliminate the large deviation of the crystal growth rate from its reference trajectory. This illustrates the significance of concentration measurements, whose availability is essential for effective application of the control approach.

Output feedback control

The output feedback control of the semi-industrial batch crystallizer on the basis of a PB model is demonstrated. The PB model with 51 state variables is exploited to devise the output feedback control approach shown in Figure 5.1. A moving horizon estimator is designed to facilitate receding horizon implementation of the dynamic optimizer. The performance of the control approach in the presence of model imperfections and process uncertainties is examined when applied to a plant simulator consisting of the PB model with 201 state variables. A correction term is added to the performance objective to diminish the effects of structural

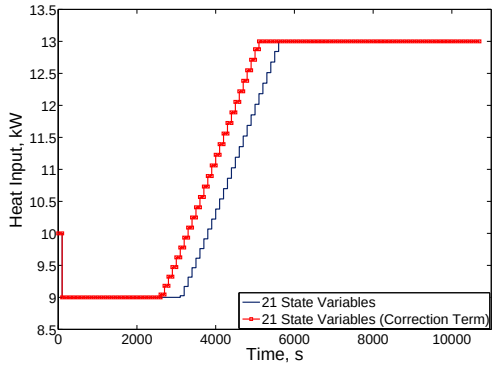

(a) Heat input profiles

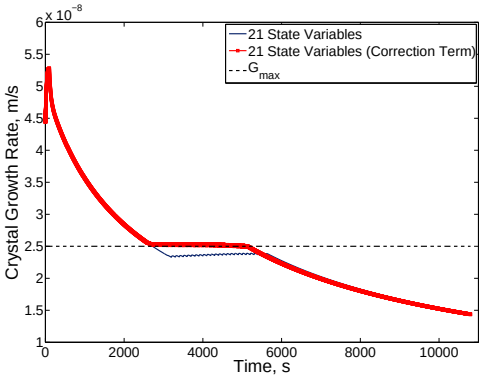

(b) Crystal growth rate profiles

Figure 5.19: Simulation results of the state feedback control approach with the modified performance objective in the presence of structural plant-model mismatch.

plant-model mismatch; see equation (5.5).

A comparison of the simulation results of the state feedback and the output feedback control approaches is shown in Figure 5.20. The specifications of model imperfections and process uncertainties are given in Table 5.8. Figure 5.20(b) suggests that the parametric plant-model mismatch and process uncertainties slightly degrade the performance of the state feedback control approach in terms of the reference trajectory tracking. On the other hand, the output feedback implementation of the dynamic optimizer allows us to follow the reference crystal growth rate trajectory more closely.

Figure 5.20(a) shows that the optimal heat input profile obtained under the output feedback control scenario exhibits a sudden increase at time $300\ s$. This results from the rather long estimation horizon, viz $500\ s$, required to build up information to initialize the moving horizon estimator. Therefore, the estimator

Table 5.8: Specifications of model imperfections and process uncertainties in the output feedback control scenario.

Parametric plant-model mismatch:	$+15.0\%$ error in kinetic parameters
Systematic measurement error:	$+2.0\%$ error in the solute concentration
	$+5.0\%$ error in the crystal size distributions
Uncertain initial conditions:	$+2.0\%$ error in the initial solute concentration
	$+5.0\%$ error in the mean of the initial crystal size distribution

is unable to readily take action against the detrimental effects of uncertain initial conditions. Despite this, once the moving horizon estimator is initialized at time $500\ s$, the recursive state estimation allows us to adequately compensate for model imperfections and process uncertainties. In addition to increased batch productivity, the effective crystal growth rate control will result in slightly larger crystals; see Figure 5.20(c) and Figure 5.20(d).

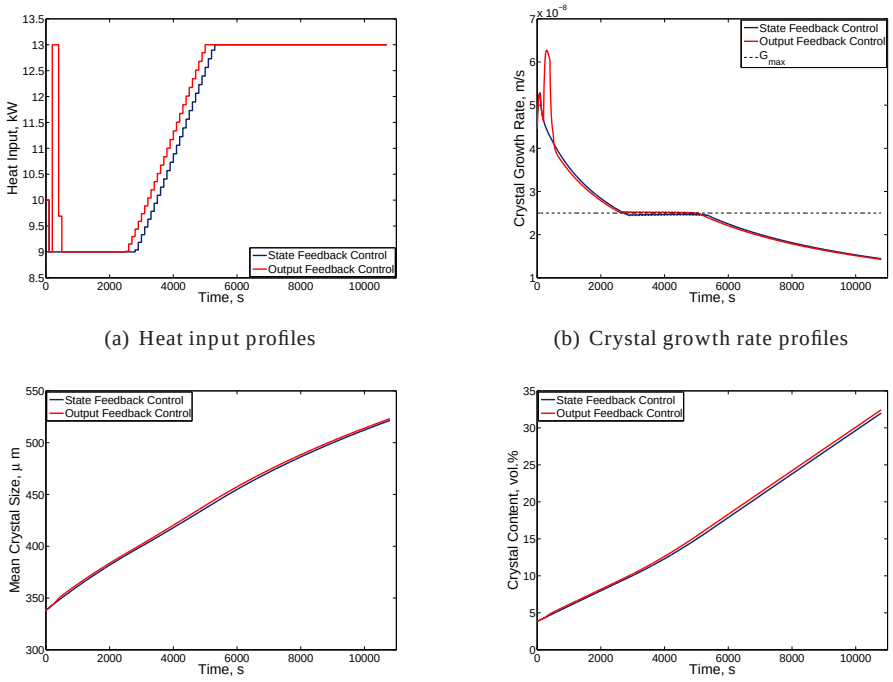

(a) Heat input profiles

(b) Crystal growth rate profiles

(c) Mean crystal size

(d) Batch crystal content

Figure 5.20: A comparison of simulation results of the state feedback control and the output feedback control approaches in the presence of model imperfections and process uncertainties. The control approach exploits the population balance model with 51 state variables, whereas the plant simulator consists of the population balance model with 201 state variables.

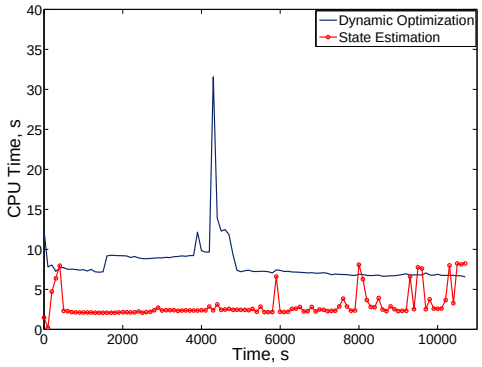

Figure 5.21: CPU time profiles of dynamic optimization and state estimation tasks in the output feedback control approach based on the population balance model with 51 state variables.

The computation time profiles of dynamic optimization and state estimation along a batch run of $10800\ s$ are depicted in Figure 5.21. It is observed that the computational burden of the output feedback control approach is considerably less than the measurement sampling time interval, viz $100\ s$, at all times during the batch run. Therefore, the PB-based control approach can be applied for real-time control of the semi-industrial batch crystallizer under study.

5.4 Case study 2: A multi-input multi-output industrial crystallizer

This case study is intended to investigate the effect of different actuating mechanisms on optimal operation of industrial batch crystallizers. The output feedback control approach presented in Section 5.2 is applied to a $1100-liter$ draft tube baffle crystallizer. The input-output diagram of the industrial crystallizer employed for seeded fed-batch evaporative crystallization of ammonium sulphate is shown in Figure 5.22. The crystallizer is equipped with a fines removal and dissolution system. The fines classification takes place in an annular zone built around the crystallizer body. The annular zone serves as a settling zone, in which fine crystals are separated from coarse crystals as a result of a low upward velocity of the moving liquid and gravitational forces. The fine crystals are collected in a stream, which is passed through a heat exchanger to partially or completely dissolve the fines. The residence time of fine crystals in the external loop is increased by pumping the fines stream through a $220 - liter$ dissolution tank prior to feeding the stream back to the crystallizer. A detailed description of the process can be found in Eek (1995).

The fines removal and dissolution offers a significant degree of freedom in

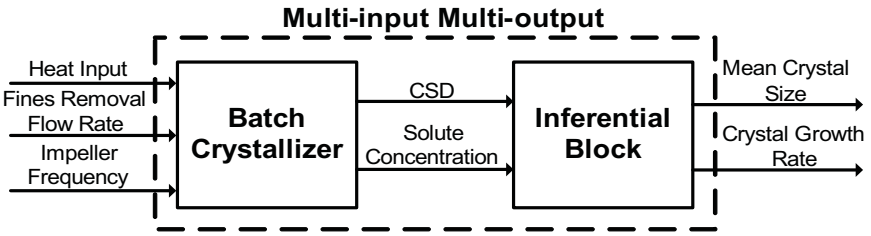

Figure 5.22: The input-output diagram of the industrial batch crystallizer.

industrial batch crystallization to influence the crystal size distribution. It is the only actuating mechanism that can exercise a corrective action against undesirable nucleation processes (Kalbasenka 2009). Fines destruction allows us to obtain a product crystal size distribution with a larger mean size and a narrower width (Myerson 2002).

Next to the heat input and the impeller frequency, the fines removal flow rate serves as an effective process actuator in the industrial crystallizer under study. As depicted in Figure 5.22, the evolution of crystal size distribution and solute concentration is measured in the course of the batch run. The classification of fine crystals in the crystallizer necessitates the use of a full population balance model to describe the system dynamics. In this thesis, the empirical kinetic expression proposed by Ottens et al. (1972) is adopted for secondary nucleation, whereas crystal growth is modeled by a power-law function. The classification of crystals in the annular zone is described by the non-ideal classification function given in Bermingham (2003). It is assumed that the fine crystals are completely dissolved in the dissolution tank.

The optimal control problem of the industrial crystallizer is formulated as

$$\begin{aligned} \min_{Q,\phi_{V,fines},N_{imp}} \quad & w\int_0^{t_f}(100\frac{G(t)-G_{max}}{G_{max}})^2 \mathrm{d}t-(1-w)\frac{\mu_4(t_f)}{\mu_3(t_f)} \\ \text{subject to :} \quad & \text{equation (2.44)} \\ & 40 \leq Q \leq 130 \\ & 0.001 \leq \phi_{V,fines} \leq 0.004 \\ & 300 \leq N_{imp} \leq 380, \end{aligned} \tag{5.6}$$

where Q is the heat input to the crystallizer (kW/m^3); $\phi_{V,fines}$ is the fines removal flow rate (m^3/s); N_{imp} is the impeller frequency (rpm). The performance objective stated in equation (5.6) consists of two parts. The running cost term is intended not only to suppress excessively high crystal growth rates, but also to maximize the batch productivity by tracking the reference crystal growth rate trajectory. On the other hand, the terminal cost term aims to improve the product quality by maximizing the mean crystal size, i.e. $\frac{\mu_4}{\mu_3}$, of the crystalline product. In equation (5.6), w is a weight factor that facilitates a trade-off between the two terms of the performance objective. The optimal control problem is solved by the

multiple shooting optimization strategy.

The control approach is applied to a plant simulator, which simulates the industrial batch crystallizer using a PB model with 201 state variables. The output feedback implementation of the dynamic optimizer is facilitated by means of an unscented Kalman filter. The specifications of model imperfections and process uncertainties are listed in Table 5.8. The control approach uses a PB model with 51 state variables. The effects of structural plant-model mismatch are diminished by incorporating the correction term $G_{meas} - G$ into the running cost part of the performance objective. As described in Section 5.3.4, the correction term gives an integrating action to the dynamic optimizer.

The multi-objective optimal control problem given in equation (5.6) seeks a trade-off between the product quality and the batch productivity. The variations of the mean crystal size and the batch crystal content as a function of the weight factor of the performance objective are shown in Figure 5.23. As expected, increasing the weight factor leads to increased batch productivity at the expense of loss in the product quality, i.e. crystalline products with a smaller mean crystal size.

Figure 5.24 shows the optimal input profiles applied to the plant simulator. The weight factor of the performance objective is set to 0.5. As can be seen, the heat input is readily reduced to its lower bound to suppress the high crystal growth rates at the beginning of the batch run. The crystal growth rate profile throughout the batch run is depicted in Figure 5.25(a). Like the SISO case study, the reference crystal growth rate trajectory cannot be tracked in the initial phase of the batch run due to inadequate process actuation. It is observed that the fines removal flow rate and the impeller frequency exhibit a sudden change at time 200 s; see

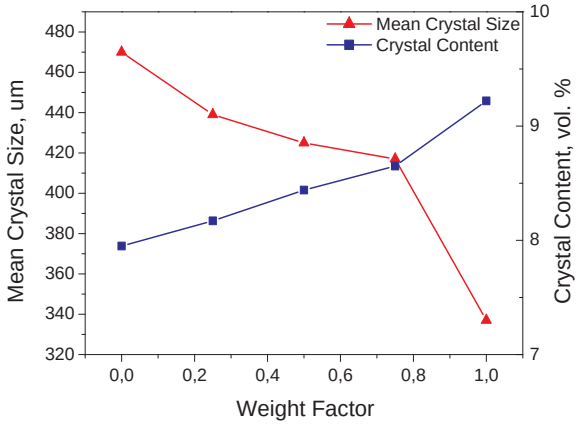

Figure 5.23: The trade-off between product quality and batch productivity in relation to the weight factor of the performance objective.

Figure 5.24(b) and Figure 5.24(c). The aggressive control action is to cope with the uncertainties in the initial conditions.

As the supersaturation depletes, the crystal growth rate reaches its reference trajectory at time $5700\ s$. Figure 5.25(a) suggests that the additional actuating mechanisms of the industrial crystallizer allow us to follow the reference trajectory effectively towards the end of the batch run. Appendix C.1 presents the optimal profiles obtained when different actuating mechanisms are exploited. It is observed that the control objective cannot be fulfilled by only actuating the heat input, whereas the fines removal flow rate facilitates effective control of the reference trajectory towards the end of the batch run. Note that maintaining the maximum crystal growth rate in the course of the batch run leads to increased batch productivity.

It is shown in Figure 5.24(a) and Figure 5.24(b) that the heat input and the fines removal flow rate start increasing at time $5700\ s$ to circumvent further decay of the supersaturation. The increase in the heat input induces more supersaturation due to the evaporation of solvent. On the other hand, the rise in the fines removal flow rate leads to increased destruction of fine crystals, which in turn raises the supersaturation. Figure 5.24(c) indicates that the impeller frequency remains at its upper bound at almost all times during the batch run. High impeller frequen-

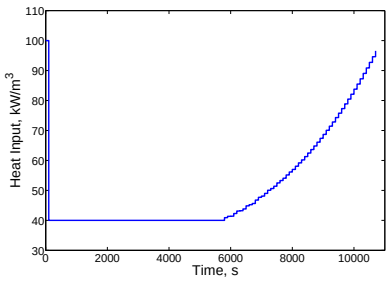

(a) Heat input

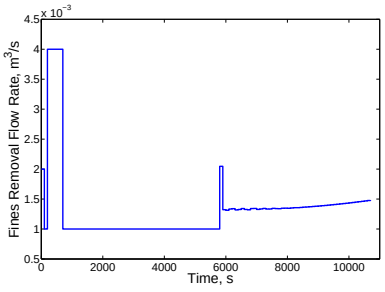

(b) Fines removal flow rate

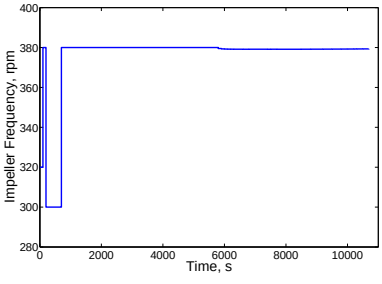

(c) Impeller frequency

Figure 5.24: The optimal input profiles applied to the industrial crystallizer.

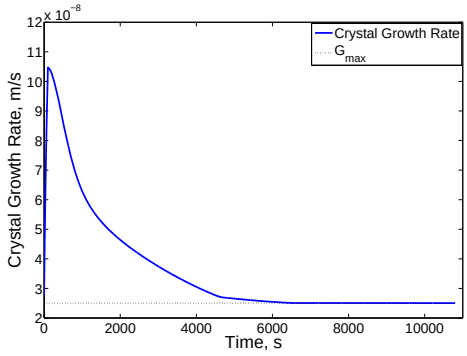

(a) Crystal growth rate profile

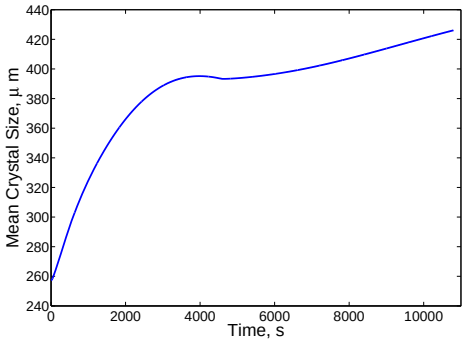

(b) Mean crystal size profile

Figure 5.25: Simulation results of the control approach when applied to the industrial crystallizer.

cies promote secondary nucleation and consequently the formation of crystals of infinitesimal size. Figure 5.25(b) depicts the mean crystal size profile throughout the batch run. Higher levels of supersaturation facilitate the production of crystals with a larger mean size.

To demonstrate the improvements gained by the use of the multi-objective optimal control problem, the fulfillment of the control objectives is examined in relation to different values of w. The optimal input and output profiles in the cases of $w = 0$ and $w = 1.0$ are given in Appendix C.2. It is observed that the reference trajectory is tracked most closely when $w = 1.0$. This leads to a higher batch productivity; see Figure 5.23. On the other hand, the larger crystals in the case of $w = 0$ are obtained at the expense of loss in the batch productivity. The simulation results clearly illustrate the significance of the multi-objective optimal control problem, which allows us to seek a trade-off between increased batch productivity and improved product quality. This can only be accomplished by exploiting the

additional actuating mechanisms of the MIMO crystallizer that facilitate effective supersaturation control.

5.5 Summary

An output feedback nonlinear model-based control approach has been presented for optimal operation of industrial batch crystallizers. A population balance modeling framework is exploited as the cornerstone of the control approach. The population balance model facilitates the use of the control approach for real-time control of a wide range of industrial batch crystallizers. In addition, the modeling framework allows us to optimize the distributed characteristics of crystals.

The control approach is first applied to a semi-industrial single-input single-output batch crystallizer. The online computation of the optimal control problem has been thoroughly investigated. The optimal control problem is solved by several direct optimization strategies, namely single shooting, multiple shooting, and simultaneous strategies. The simulation results indicate that the optimization strategies perform similarly in terms of optimal operation of the batch crystallizer. However, their computational burdens differ significantly under approximately the same optimization settings. It is observed that the multiple shooting optimization strategy has the lowest computational burden. This primarily results from the sparse structure of the nonlinear programming problem. The multiple shooting strategy is particularly suitable for real-time control of industrial batch crystallizers, whose dynamics are described by a full population balance model.

Several nonlinear observers developed under deterministic and Bayesian estimation frameworks have been tested. In agreement with the open-loop analysis, the EKF and the UKF with time-varying process noise covariance matrix exhibit adequate state estimation capability, which in turn ensures the closed-loop control performance. However, the simulation results suggest that the control objective cannot be satisfactorily fulfilled in the presence of model imperfections and process uncertainties. The closed-loop control performance is enhanced by incorporating a disturbance model into the observers.

The output feedback control approach has also been applied to an industrial multi-input multi-output batch crystallizer. In this case study, a multi-objective optimal control problem is formulated to exploit the additional degrees of freedom of the industrial crystallizer. The simulation results suggest that the extra actuating mechanisms enable us to maximize the batch productivity as ensuring improved product quality. It is deemed that the generic output feedback control approach presented in this chapter facilitates real-time control of a wide range of industrial batch crystallizers.

6 CHAPTER

Real-time Implementation of the Control Approach

The true worth of an experimenter consists in his pursuing not only what he seeks in his experiment, but also what he did not seek.

Claude Bernard

The output feedback control approach is implemented on a semi-industrial crystallizer, in which seeded fed-batch evaporative crystallization of ammonium sulphate takes place. This chapter describes the real-time performance of the control approach. First, the system dynamics are represented by the moment model. The effect of different direct optimization strategies on optimal operation of the crystallizer is investigated experimentally. In addition, the real-time performance of the control approach presented in this thesis is compared with that of a model predictive controller. The second section demonstrates the real-time implementation of the control approach when the system dynamics are described by the full population balance model.

6.1 The moment model-based control approach

The real-time feasibility of the output feedback control approach presented in Chapter 5 is examined for fed-batch evaporative crystallization of an ammonium sulphate-water system. The system dynamics are described by the moment model. The crystallization takes place in the $75 - liter$ draft tube crystallizer, which is equipped with a distributed control system (DCS CENTUM CS3000, Yokogawa, Japan). The hierarchical control framework depicted in Figure 6.1 is adopted to apply the optimal operating policies to the semi-industrial crystallizer. The optimal input sequences are implemented using conventional proportional integral derivative (PID) controllers. The PID controllers are embedded in the DCS, which

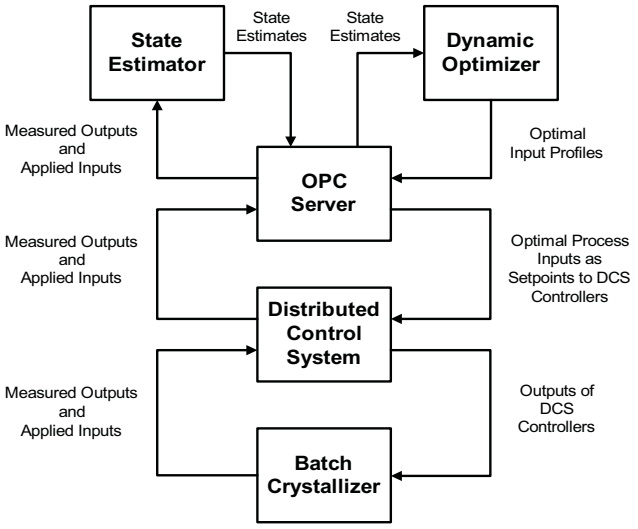

Figure 6.1: The hierarchical output feedback control framework.

forms the lowest control layer. The timed signal exchange among different components of the control approach is facilitated by an OPC (OLE - Object Linking and Embedding - for Process Control) communication interface (IPCOS, The Netherlands). Synchronization and sequencing of tasks are carried out by means of a timer and a scheduler, respectively.

Open-loop control versus closed-loop control

Variations of the crystal growth rate in relation to different heat input profiles are studied. The crystal growth rate largely affects the product quality of the seeded batch runs, whereas the heat input serves as the only driving force for supersaturation generation in the evaporative crystallizer under study. Figure 6.2 depicts the heat input and the crystal growth rate profiles of various seeded batch runs.

Table 6.1: Description of the seeded fed-batch evaporative crystallization experiments.

Experiment	Operating conditions				Seeding conditions	
	Temperature, $^{\circ}C$	Pressure, $mbar$	Impeller frequency, rpm	Heat input, kW	Seed aging time, min	Initial supersaturation
DT_c31	50	100	450	9.0	57	0.01627
DT_c55	50	100	450	Figure 6.2(a)	60	0.00567
DT_c63	50	100	450	Figure 6.2(a)	59	0.00718
DT_c68	50	100	450	Figure 6.3(a)	55	0.00962
DT_c80	50	100	450	Figure 6.2(a)	53	0.01103
DT_c81	50	100	450	4.5	55	0.00705
DT_c82	50	100	450	Figure 6.3(a)	62	0.00683
DT_c89	50	100	450	Figure 6.6(a)	76	0.00953

The experimental settings are given in Table 6.1. In experiment DT_c31, the heat input to the crystallizer is kept constant at $9\ kW$. As a result, the crystal growth rate gradually decays, being unable to follow its maximum admissible value; see Figure 6.2(b). The inability to realize the maximum crystal growth rate necessitates the use of an advanced control strategy that optimally manipulates the heat input. The control approach should systematically push the process to its optimal operating regime as the operational constraints are honored. In experiment DT_c55, the open-loop implementation of the dynamic optimizer presented in Section 5.3 is attempted. In this batch run, the optimal heat input profile is computed off-line and manually applied to the crystallizer as a time-varying set point of a PI controller. Figure 6.2(b) indicates that the crystal growth rate yet again fails to track its reference trajectory.

In experiments DT_c63 and DT_c80, the dynamic optimizer is implemented in

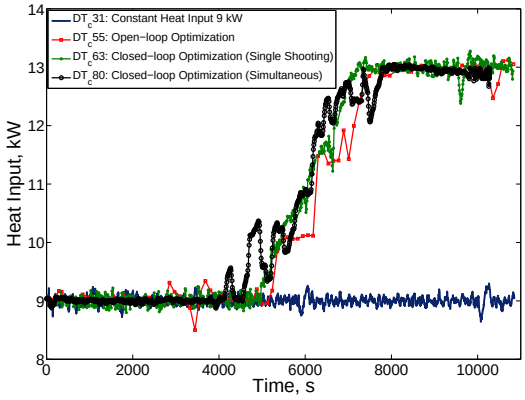

(a) Heat input profiles

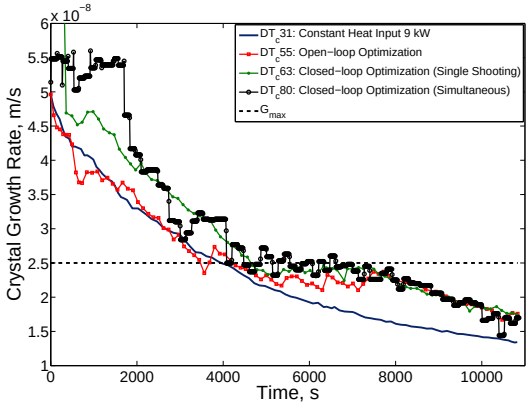

(b) Crystal growth rate profiles

Figure 6.2: Experimental results of the control approach.

a closed-loop mode. It was demonstrated in Chapter 5 that the output feedback structure of the control approach allows us to more effectively fulfill the control objective. Figure 6.2 shows that once the crystal growth rate crosses the reference trajectory, viz G_{max}, the heat input is raised to facilitate tighter tracking of the maximum crystal growth rate. However, the reference trajectory can no longer be closely followed when the heat input reaches its upper bound. The crystal growth rate steadily decreases thereafter, whereas the heat input remains at $13\ kW$.

As expected, the output feedback control approach outperforms the dynamic optimizer when applied in an open-loop mode. The improved performance is due to the feedback of the system states. The closed-loop implementation of the dynamic optimizer not only compensates for model imperfections, but also enables effective disturbance handling through state estimation. Figure 6.2(b) suggests that the simultaneous and the single shooting dynamic optimizers exhibit comparable performance in terms of the reference trajectory tracking. The differences in initial crystal growth rates of various batch runs result from different supersaturation at the seeding point; see Table 6.1.

The effect of the lower heat input bound on optimal process operation

Figure 6.2 indicates that optimal process operation cannot be achieved at all times during a batch run. The reference trajectory is violated at the beginning and towards the end of a batch run due to actuation limitations. In the optimal control problem, the heat input's lower bound is defined as $9\ kW$ to avoid possible dissolution of seeds; see equation (5.3). On the other hand, the heat transfer limitations of the process restrict the heat input to an upper bound of $13\ kW$.

To evaluate the possibility of tracking the maximum crystal growth rate over a wider time horizon, the effect of reducing the lower heat input bound on optimal process operation is investigated. First, it should be examined whether the seeds are dissolved at heat inputs lower than $9\ kW$. In experiment DT_c81, the seeds are inserted into the crystallizer at the conservatively chosen heat input of $4.5\ kW$. As shown in Figure 6.3, the heat input is kept constant throughout experiment DT_c81, resulting in a continuous violation of the maximum crystal growth rate. The evolution of median and width of the measured crystal size distributions is depicted in Figure 6.4. It is observed that the CSD attributes of the first measurement taken at $t = 100\ s$ immediately after seeding remain to a large extent similar to those obtained in experiment DT_c31. Therefore, seeds are unlikely to dissolve when they are exposed to lower heat inputs than $9\ kW$.

Subsequently, the heat input's lower bound in the optimal control problem is decreased to $2\ kW$ in experiment DT_c82. In this batch run, seeds are inserted into the crystallizer at the heat input of $4.5\ kW$. The controller is switched on after obtaining 8 reliable CSD measurements to accurately initialize the simultaneous dynamic optimizer. As can be seen in Figure 6.3(a), the heat input is readily reduced to $3.9\ kW$ to bring the crystal growth rate to the reference trajectory, viz G_{max}. Thereafter, a good reference trajectory tracking is achieved till the heat input reaches its upper bound of $13\ kW$. Figure 6.3(b) indicates that the output feedback control approach enables us to effectively control the crystal growth rate until the lack of actuation hampers the optimal process operation towards the

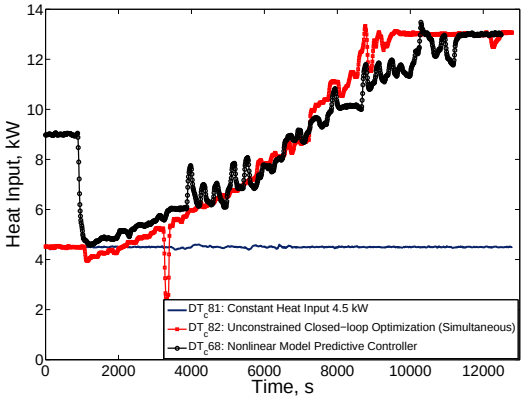

(a) Heat input profiles

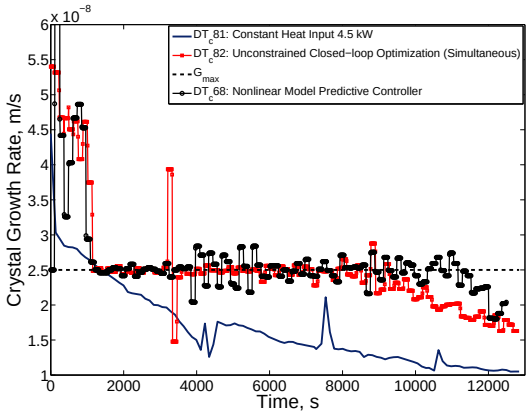

(b) Crystal growth rate profiles

Figure 6.3: Experimental results of the output feedback control approach with relaxed optimization constraint in comparison with a nonlinear model predictive controller.

batch end.

Nonlinear model predictive control

To assess the performance of the control approach presented in this thesis in comparison with that of model predictive control, a commercial nonlinear model predictive controller (IPCOS, The Netherlands) is applied to the semi-industrial crystallizer. The nonlinear model predictive controller (NMPC) differs from the control approach in that it first utilizes the nonlinear moment model to forecast the system behavior over the prediction horizon. Subsequently, a local linear time-variant model is extracted from the original nonlinear model at each sampling point along the operating trajectory. The linear model is used for optimization of the performance objective stated in equation (5.3) (Landlust et al. 2008; Mesbah

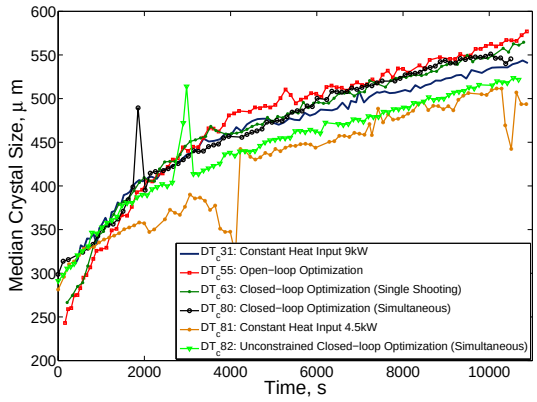

(a) Median crystal size

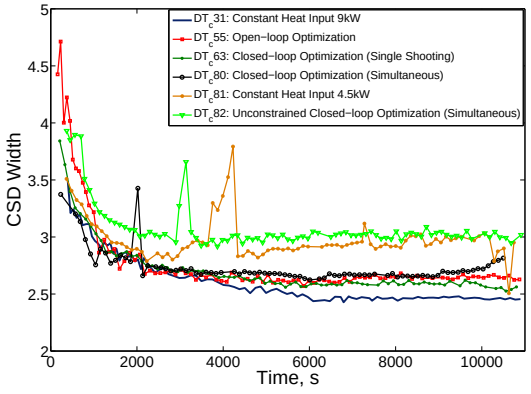

(b) Width of the crystal size distribution

Figure 6.4: The evolution of median and width of the crystal size distribution throughout the batch experiments.

et al. 2010d). The output feedback implementation of the NMPC is facilitated by an extended Luenberger-type observer.

Figure 6.3 depicts the optimal profiles obtained by applying the NMPC in experiment DT_c68. As can be seen, seeding is carried out at the heat input of $9\ kW$ in experiment DT_c68. When the controller is switched on after obtaining 6 CSD measurements, the heat input is reduced to $4\ kW$ to decrease the crystal growth rate. Figure 6.3(b) indicates that the NMPC is able to follow the reference trajectory, i.e. $G_{max} = 2.5 \times 10^{-8}\ m/s$, rather effectively till the heat input reaches its upper bound. It is expected that the fluctuations of the crystal growth rate around the reference trajectory can be diminished to some degree by fine tunning the controller.

Table 6.2: Batch runs in the $75-liter$ draft tube crystallizer.

Experiment	Control approach	Optimization strategy	Results at the batch end ($10800\ s$)		
			Crystal content, $vol.\%$	Median crystal size, μm	CSD width
DT_c31	-	-	24.2	544	2.45
DT_c55	Open-loop	Single shooting	27.3	573	2.62
DT_c63	Closed-loop	Single shooting	28.3	565	2.56
DT_c68	Closed-loop	NMPC	20.2	566	2.91
DT_c80	Closed-loop	Simultaneous	30.8	546	2.82
DT_c81	-	-	12.9	512	2.80
DT_c82	Closed-loop	Simultaneous	20.0	521	3.02
DT_c89	Closed-loop	Multiple shooting	26.6	567	2.73

Product quality and process productivity

The results of online CSD measurements shown in Figure 6.4 suggest that the start-up phase of the batch runs is to a large extent reproducible. This is due to the thorough seeding procedure that largely circumvents uncertain initial conditions (Kalbasenka et al. 2007). Figure 6.4 indicates that the CSD attributes of the product crystals remain almost similar. However, reducing the lower bound of the heat input results in somewhat smaller crystals due to lower crystal growth rates at the beginning of the batch run; see Table 6.2. The broader CSD width in experiment DT_c82 can be attributed to the lower initial supersaturation as listed in Table 6.1. Low initial supersaturation may cause partial dissolution of seeds, leading to product quality degradation.

The evolution of crystal volume content of various batch runs is depicted in Figure 6.5. The spikes in the crystal content measurements are due to regular rinsing of the product line of the crystallizer to prevent blockage. It is evident

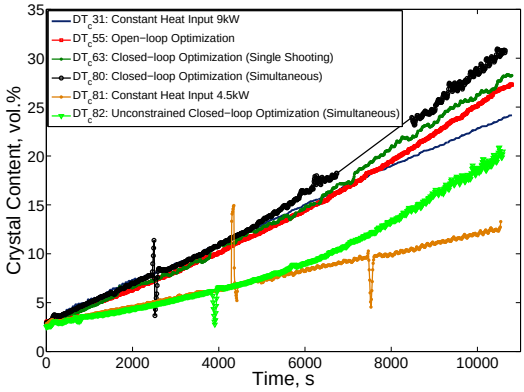

Figure 6.5: The evolution of crystal volume content throughout the batch experiments.

that the application of the control approach leads to a substantial increase, i.e. up to 30%, in productivity as compared to batch runs with constant heat input; see Table 6.2. The larger crystal content at the end of the controlled batch runs results from the higher crystal growth rates. It is observed that the dynamic optimizers yield almost the same productivity, though the simultaneous dynamic optimizer gives a slightly higher crystal content at the batch end. Figure 6.5 suggests that the optimal crystal growth rate profile in experiment DT_c82 is obtained at the expense of reduced batch productivity. This is due to lower crystal growth rates at the beginning of experiment DT_c82. Clearly, achieving the desired product quality requirements attained by effective crystal growth rate control is of greater significance than maximizing the batch productivity.

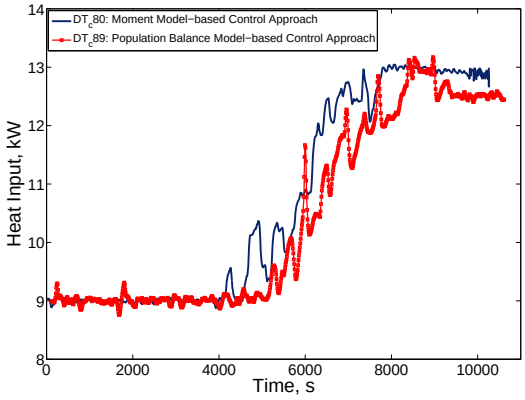

(a) Heat input profiles

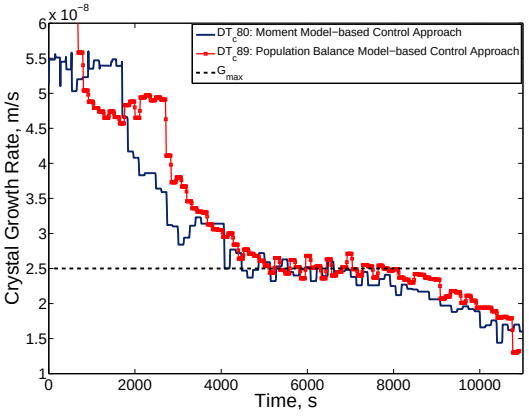

(b) Crystal growth rate profiles

Figure 6.6: Experimental results of the output feedback control approach based on the full population balance model with 51 state variables.

6.2 The population balance model-based control approach

To experimentally verify the real-time feasibility of nonlinear model-based control of industrial batch crystallizers whose dynamics are described by full population balance models, the PB model-based control approach is applied to the $75 - liter$ draft tube crystallizer. Like the previous section, the semi-industrial crystallizer is used for fed-batch evaporative crystallization of an ammonium sulphate-water system. The simulation results presented in Section 5.3.4 indicate that the computation time of the output feedback control approach based on the full population balance model with 51 state variables is less than the measurement sampling time interval.

Figure 6.6 shows the heat input and the crystal growth rate profiles obtained by implementation of the PB model-based control approach in experiment DT_c89. The experimental settings are listed in Table 6.1. As expected, the PB model-based control approach performs similarly to the moment model-based control approach. This results from the ability of the moment model to adequately describe the dynamics of the semi-industrial crystallizer under study. Figure 6.6 indicates that the reference crystal growth rate trajectory cannot be effectively tracked at all times during the batch run due to the heat input constraints. The CSD attributes of the crystalline product and the crystal volume content of batch run DT_c89 are given in Table 6.2. It is observed that the batch characteristics are comparable to those achieved when the optimal operation of the crystallizer is realized by the moment model-based control approach.

6.3 Summary

The output feedback control approach has been applied for optimal operation of a semi-industrial batch crystallizer. The experimental results indicate that real-time implementation of the control approach leads to a significant increase, i.e. up to 30 $\%$, in the batch productivity. The reproducibility of batch runs with respect to size distribution attributes of the crystalline product is achieved by thorough seeding.

It is observed that the direct optimization strategies perform similarly in terms of optimal process operation. In addition, the control approach presented in this thesis has a similar performance to that of a nonlinear model predictive controller. The real-time feasibility of the output feedback control approach when a full population balance model is exploited to describe the system dynamics has also been demonstrated. The experimental results suggest that the moment model-based control approach and the full population balance model-based control approach exhibit comparable performance in terms of optimal operation of the crystallizer under study.

7 CHAPTER

Conclusions and Recommendations

The science of today is the technology of tomorrow.
Edward Teller

In this chapter, the research objective of the thesis is revisited. The primary findings of the presented research are summarized. Finally, recommendations are given for future research.

7.1 Conclusions

The primary research objective of this thesis was to evaluate the opportunities for real-time model-based control to improve product quality and process productivity of industrial batch crystallizers. The model-based control of batch crystallizers is particularly challenging. The distributed characteristics of crystals complicate the modeling of crystallization processes. The validation of process models and performance monitoring is cumbersome due to limitations in measurement of process variables. In addition, the uncertainties inherent in crystallization processes may impair the effectiveness of advanced control strategies. The optimal operation of industrial crystallizers is often hampered by lack of process actuators.

The presented research addresses the challenges of real-time control of existing industrial batch crystallizers by adopting a population balance model-based control approach. Several goals have been set to fulfill the primary research objective of this thesis; see Section 1.4. Accordingly, the main contributions of this research are structured in three major directions:

1. *Population balance modeling*: A full population balance modeling framework has been developed. The generic structure of the population balance model allows us to describe the dynamics of a wide range of industrial batch crystallizers. The inference of model parameters from experimental data has been addressed. In addition, it has been shown how the computational burden of the population balance model can be reduced while its descriptive capability remains intact.

1a. The applicability of the ATR-FTIR spectroscopy for in-situ concentration monitoring of the aqueous ammonium sulphate solution has been demonstrated at semi-industrial scale. A rapid online calibration technique has been developed to arrive at a partial least squares model for concentration predictions. The proposed technique substantially reduces the time required for calibration. The technique needs relatively few spectra, without specifying a test set for the validation of the PLS model. It has been shown that by using the in-situ concentration measurements, a better estimate of the kinetic parameters can be obtained.

— see Chapter 2 and (Kadam et al. 2010a) —

1b. A comprehensive analysis of the most widely used population balance solution methods has been given in terms of the performance requirements essential for online control applications. It has been shown that the high order finite volume methods with flux limiting functions are well capable of capturing the sharp discontinuities and steep moving fronts, which are often encountered in simulation of industrial batch crystallizers. In addition, these schemes benefit from ease of implementation and relatively low computational requirements. The latter feature allows us to utilize a finer grid mesh to further enhance the numerical accuracy of the method at the cost of a reasonable increase in the computational burden.

— see Chapter 3 and (Mesbah et al. 2009) —

2. *Nonlinear state estimation*: The effectiveness of various nonlinear state estimation techniques for output feedback control of industrial batch crystallizers has been investigated. Online adaptation of model predictions by means of state estimation is a prerequisite for compensating for the adverse effect of model imperfections and process uncertainties on the control performance.

2a. It has been shown that the stochastic filters developed under the Bayesian framework provide accurate state estimates, which in turn ensure the adequate fulfillment of control objectives. It has been demonstrated that adopting a time-varying process noise covariance matrix, which is particularly suited for batch processes, further enhances the estimation accuracy of stochastic observers.

— see Chapters 4-5 and (Mesbah et al. 2010a) —

2b. It has been shown that model imperfections and process uncertainties are largely detrimental to the performance of nonlinear model-based controller. The control performance can be improved by incorporating a disturbance model into the state estimator.

— see Chapter 5 and (Mesbah et al. 2010a) —

3. *Real-time dynamic optimization*: The feasibility of real-time dynamic optimization of population balance models has been investigated using different direct optimization strategies. In addition to simulation case studies, the real-time performance of the control approach has been demonstrated experimentally by several implementations on a semi-industrial crystallizer.

3a. It has been shown that the different direct optimization strategies perform similarly in terms of optimal operation of the batch crystallizer under study. However, the direct single shooting strategy has the lowest computational efficiency. The study on the direct optimization strategies has revealed that the multiple shooting strategy is well-suited for online dynamic optimization of population balance models.

— see Chapters 5-6 and (Mesbah et al. 2010b,d,e) —

3b. It has been demonstrated that the lack of actuation may obstruct optimal operation of industrial crystallization processes throughout the entire batch run. It has been shown that the extra degrees of freedom in multi-input multi-output batch crystallization systems allow us to achieve better process control.

— see Chapters 5-6 and (Mesbah et al. 2010c) —

This research has led to the design of an output feedback nonlinear model-based controller, which can be exploited for real-time control of a wide range of industrial batch crystallizers. The distinct contribution of this thesis is the use of a full population balance modeling framework as the cornerstone of the control approach. The modeling framework not only allows us to describe the dynamics of diverse crystallization kinetics of any complexity, but also incorporates the effect of different actuation mechanisms. These modeling features are essential for the applicability of the control approach to a wide range of industrial batch crystallizers.

The use of the population balance modeling framework has certain implications for the model-based control approach. The numerical difficulties of solving the population balance equation can be largely alleviated by the high order finite volume methods combined with a flux limiting function. These numerical techniques ensure efficient model solution, which is a prerequisite for real-time control. Efficient dynamic optimization of the population balance model has been realized by the direct multiple shooting strategy.

Successful application of the control approach for real-time control of industrial batch crystallizers has been demonstrated by several simulation case studies as well as experimental implementations. The effectiveness of the output feedback control approach in the presence of model imperfections and process uncertainties can best be ensured by an extended Kalman filter or an unscented Kalman filter with time-varying process noise covariance matrix. It is deemed that the control approach developed in this thesis will greatly pave the way for real-time control of industrial batch crystallizers. Nonetheless, several challenges yet remain to be addressed in future.

7.2 Recommendations for future research

In light of the research objective sought in this thesis, the following suggestions are given for future research:

- Optimal operation of industrial batch crystallizers may be severely hampered by lack of actuation. This calls for better design of crystallizers, which offer enhanced controllability and process actuation (Huesman et al. 2010). The novel design concepts should not only allow us to fulfill the desired control objectives in one crystallization step, but should also minimize the post-processing of the crystalline product. A key challenge is to improve control over the physical phenomena governing the product quality. It is envisaged that the task-based design approach may bring into existence a new generation of solution crystallization processes with distinct actuation possibilities (Lakerveld 2010).

- With recent advances in the process analytical technology, in-situ measuring sensors are being increasingly exploited for process development and control purposes (Braatz 2002; Birch et al. 2005). Despite the numerous applications reported in the literature, the use of in-situ sensors is mostly investigated at laboratory-scale. It is imperative to examine the precision and robustness of in-situ measuring sensors in harsh industrial crystallization environments. The process analytical technology may offer vast opportunities for advanced control of industrial batch crystallizers. In-situ measuring sensors can be utilized to devise a supersaturation controller, on which a nonlinear model-based controller is mounted. Such hierarchical advanced control approach may allow us to robustify the optimal operating policies against process disturbances.

- Obtaining high-fidelity crystallization process models is a particularly challenging task due to the structural and parametric uncertainties associated with kinetic expressions. There is a wealth of literature on the use of the most common optimal experiment design procedures to arrive at crystallization process models utilized in control applications; see, e.g., (Matthews and Rawlings 1998; Ma and Braatz 2003). However, the reported studies are mostly limited to laboratory-scale batch crystallizers, whose dynamics are described by reduced-order models. More importantly, the commonly used optimal experiment design procedures cannot establish a link between the experiment design criterion and the intended closed-loop control performance. This calls for further research on the development of closed-loop experiment design approaches for nonlinear dynamic systems. It is deemed that these experiment design approaches will enable us to build high-fidelity population balance models for real-time crystallization control applications.

- The unit operation of crystallization seldom exists in isolation. A batch crystallizer is almost always a part of a wider particulate processing system. The practical objectives of the process train, e.g., filterability or stability of the crystalline product, cannot be straightforwardly expressed in terms of crystal size and shape distributions. This has led to widespread use of surrogate performance objectives (Fujiwara et al. 2005). It is expected that dynamic optimization of a batch crystallizer will be most effective if the performance objective relates to practical objectives of the particulate processing system.

- Reproducible start-ups are crucial for advanced control of industrial batch

crystallizers. Extensive research has been conducted to experimentally optimize initial conditions of batch crystallizers; see, e.g., (Lakerveld 2010) and the references therein. The experimental approaches to optimize batch start-ups are often labor-intensive. In addition, they merely lead to near-optimal initial conditions of batch crystallizers. It is deemed that dynamic optimization will offer a rigorous framework to arrive at optimal start-up procedures (Chung et al. 1999). However, a great challenge lies in incorporating the effects of practical uncertainties of start-up procedures into the dynamic optimization problem. This calls for exploration of the use of robust optimization algorithms to minimize uncertainties in optimal start-up procedures of industrial batch crystallizers.

A APPENDIX

Piping and Instrumentation Diagram of the $75-liter$ Crystallizer

This appendix presents the piping and instrumentation diagram (P&ID) of the $75-liter$ draft tube crystallizer. The tag names and their descriptions are listed in Table A.1.

Table A.1: The P&ID tag description of the $75-liter$ draft tube crystallizer.

Tag	Description
	Equipment
M302	Motor of buffer tank stirrer
M303	Motor of feed tank stirrer
M306	Motor of water tank stirrer
P301	Product pump
P302	Dilution pump
P303	Feed pump
P304	Cooling water pump
P306	Crystallizer heating-system pump
P308	Vacuum pump
P309	Condensate-collector pump
FF301	Dilution-line filter
FF302	Feed-line filter
FF303	Dilution-line filter
FF304	Feed-line filter
HE301	Draft-tube jacket
HE302	Electric heater of buffer tank
HE303	Electric heater of feed tank
HE304	Water-tank cooling coil
HE305	Crystallizer jacket
HE306	Electric heater of water tank
HE307	Condenser
HE309	Heat tracing on overflow line between T302 and T303

continued · · ·

Table A.1: The P&ID tag description of the $75-liter$ draft tube crystallizer (continued).

Tag	Description
AF306	Heat tracing on overflow line between T302 and T303
	Process lines
PL301	Product line
PL302	Dilution line
PL303	Sample line
PL304	Feed recycle line
PL305	Feed line
PL306	Product return line
PL307	Vacuum line
	Valves
V301	On product line PL301
V302	On buffer tank discharge to sewage system
V303	On sample line PL303 after HELOS
V304	Product return valve on line PL306
V305	On sample line PL303 after HELOS
V306	On sample line PL303, buffer tank inlet
V307	On feed recycle line PL304, buffer tank inlet
V308	Safety valve on discharge line of pump P306
V309	On suction side of pump P306
V310	On water tank discharge to sewage system
V311	On suction side of pump P302
V312	On inlet of filter FF301
V313	On outlet of filter FF301
V314	On outlet of filter FF303
V315	On inlet of filter FF303
V316	On cold water supply line of water tank
V317	On cold water supply line of buffer tank
V318	On overflow line between tanks T302 and T303
V319	On cooling water supply line of HE304
V320	On suction side of pump P303
V321	On inlet of filter FF302
V322	On outlet of filter FF302
V323	On outlet of filter FF304
V324	On inlet of filter FF304
V325	On feed line PL305
V326	On cooling water discharge line of HE304
V327	On water discharge line of pump P308
V328	On feed recycle line PL304
V329	On suction side of pump P304
V330	On condenser outlet line
V331	On water supply line of pump P308
V332	On discharge line of pump P309 to sewage system
V333	On discharge line of pump P309 to buffer tank

continued · · ·

Table A.1: The P&ID tag description of the $75 - liter$ draft tube crystallizer (continued).

Tag	Description
V334	On outlet line from crystallizer jacket HE305
V335	Condenser de-aeration valve
V336	On outlet line from draft-tube jacket HE301
V337	On water supply line to crystallizer jacket HE305
V338	Air valve of vacuum pump P308 (top valve)
V339	On water supply line to draft-tube jacket HE301
V340	On line between pump P308 and vacuum system (bottom valve)
V341	On drainage line of entrainment trap T304
	Valves of rinse water system
RV301	On product line PL301 on suction side of pump P301
RV302	On product line PL301 after control valve FCV304
RV303	On inlet of water tank
RV304	On feed recycle line PL304, buffer tank inlet
RV305	On sample line PL303, buffer tank inlet
RV306	On discharge line of pump P302
RV307	On outlet of filters FF301 / FF303
RV308	On discharge line of pump P303
RV309	On outlet of filters FF302 / FF304
RV310	On overflow line between tanks T302 and T303 before V318
RV311	On overflow line between tanks T302 and T303 after V318
RV312	On discharge line of pump P303
	Control instrumentation and sensors
DRT301	Crystallizer product densitometer
FCV303	Flow Control Valve (FCV) from product line to sample line
FCV304	FCV from product line to product return or recycle line
FCV305	FCV on water supply line to HE301 and HE305
FCV306	FCV on air inlet to condensate collector T308
FCV307	FCV on condensate discharge line of condensate collector T308
FCV308	FCV on condensate supply line of condensate collector T308
FRC301	Crystallizer product flowmeter
FRC302	A connection to a reserve flowmeter
FR303	Flowmeter of water supply to draft tube
FRC305	Flowmeter of water supply to HE301 and HE305
HELOS	CSD measurement device on sample line
LCV301	Level Control Valve (LCV) on feed line
LRC301	Crystallizer level controller
LS302	Level Switch (LS) on HE302 of buffer tank
LS303	LS on HE303 of feed tank
LS306	LS on HE306 of water tank
LTS301	Level Transmitter / Switch on condensate collector T308
PCV301	Pressure Control Valve (PCV)
PI301	Pressure gauge reading on vacuum line PL307
PI302	Pressure Indicator (PI) on discharge line of pump P306

continued · · ·

Table A.1: The P&ID tag description of the $75-liter$ draft tube crystallizer (continued).

Tag	Description
PRC301	Crystallizer vapor pressure
PRC302	Crystallizer pressure near draft-tube top
PSV302	Pressure Safety Valve on vacuum line PL307
QR301	VEL301: Ultrasonic velocity (a LiquiSonic analyzer measurement)
	TMP301: Temperature (a LiquiSonic analyzer measurement)
SEQ301	Sequence table within Yokogawa DCS
SRC301	Frequency controller of crystallizer impeller
TRC301	Crystallizer temperature controller (at the top)
TRT302	Crystallizer temperature (at the bottom)
TRT303	Crystallizer vapor temperature
TRT304	Feed temperature
TRC305	Temperature of water at outlet of crystallizer jacket HE305
TRC306	Temperature of water at inlet of draft-tube jacket HE301
TRC307	Temperature of water at outlet of draft-tube jacket HE301
TRC308	Temperature of water at inlet of crystallizer jacket HE305
TRT309	Temperature in water tank
TRT310	Temperature in buffer tank
TRT313	Temperature in feed tank
TRT318	Temperature of cooling water at inlet of condenser HE307
TRT319	Temperature of cooling water at outlet of condenser HE307
TRT320	Temperature of condensate at the top of condensate collector T308
TRT321	Temperature of condensate at the bottom of collector T308
TRT323	Temperature of cooling water at inlet of cooling coil HE304
TRT325	Temperature of cooling water at outlet of cooling coil HE304
TRT328	Temperature of heat tracing HE309
XRC301	Heat-input controller

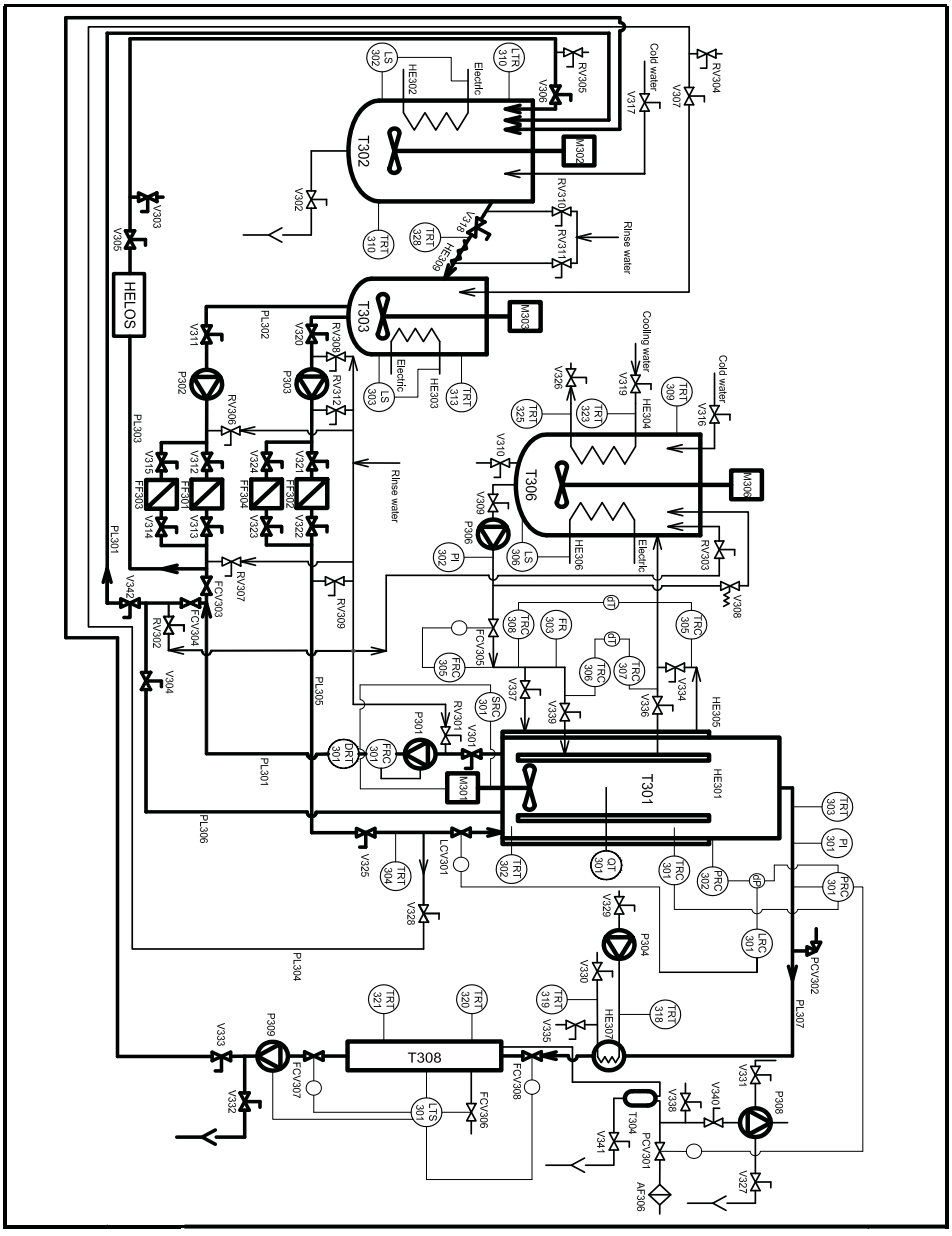

Figure A.1: The piping and instrumentation diagram of the $75 - liter$ draft tube crystallizer.

B APPENDIX

Tuning Parameters of the Nonlinear State Estimators

In Chapter 5, various nonlinear state estimators are used to facilitate output feedback implementation of the control approach. The tuning parameters of the state estimators applied in the nominal scenario are given in this appendix.

Extended Luenberger Observer

Observer gain:

$$\mathbf{K} = \begin{bmatrix} 0 & 0 & 0 & 2.72 \times 10^{-3} & 0 \\ 0 & 0 & 0 & 0 & 8.45 \times 10^{1} \\ 0 & 0 & 1.17 \times 10^{-1} & 0 & 0 \\ 0 & 0 & 0 & 4.41 \times 10^{-1} & 0 \\ 0 & 0 & 0 & 0 & 4.64 \times 10^{-1} \\ 0 & 0 & 0 & 0 & 0 \end{bmatrix} \tag{B.1}$$

Extended Kalman Filter

Process noise covariance matrix:

$$\mathbf{Q} = \begin{bmatrix} 45 \times 10^{20} & 0 & 0 & 0 & 0 & 0 \\ 0 & 27 \times 10^{8} & 0 & 0 & 0 & 0 \\ 0 & 0 & 9 \times 10^{-2} & 0 & 0 & 0 \\ 0 & 0 & 0 & 90 & 0 & 0 \\ 0 & 0 & 0 & 0 & 9 \times 10^{-9} & 0 \\ 0 & 0 & 0 & 0 & 0 & 45 \times 10^{-4} \end{bmatrix} \tag{B.2}$$

Measurement noise covariance matrix:

$$\mathbf{R} = \begin{bmatrix} 45 \times 10^{12} & 0 & 0 & 0 & 0 \\ 0 & 27 \times 10^{2} & 0 & 0 & 0 \\ 0 & 0 & 9 & 0 & 0 \\ 0 & 0 & 0 & 56 \times 10^{-13} & 0 \\ 0 & 0 & 0 & 0 & 63 \times 10^{-16} \end{bmatrix} \tag{B.3}$$

In the extended Kalman filter with time-varying process noise covariance matrix, the measurement noise covariance matrix remains the same as above.

Unscented Kalman Filter

Process noise covariance matrix:

$$\mathbf{Q} = \begin{bmatrix} 45 \times 10^{18} & 0 & 0 & 0 & 0 & 0 \\ 0 & 27 \times 10^{8} & 0 & 0 & 0 & 0 \\ 0 & 0 & 9 \times 10^{-2} & 0 & 0 & 0 \\ 0 & 0 & 0 & 9 \times 10^{-1} & 0 & 0 \\ 0 & 0 & 0 & 0 & 9 \times 10^{-5} & 0 \\ 0 & 0 & 0 & 0 & 0 & 4 \times 10^{-7} \end{bmatrix} \tag{B.4}$$

Measurement noise covariance matrix:

$$\mathbf{R} = \begin{bmatrix} 9 \times 10^{9} & 0 & 0 & 0 & 0 \\ 0 & 81 \times 10^{4} & 0 & 0 & 0 \\ 0 & 0 & 9 \times 10^{-5} & 0 & 0 \\ 0 & 0 & 0 & 9 \times 10^{-1} & 0 \\ 0 & 0 & 0 & 0 & 9 \times 10^{-5} \end{bmatrix} \tag{B.5}$$

In the unscented Kalman filter with time-varying process noise covariance matrix, the measurement noise covariance matrix remains the same as above.

Ensemble Kalman Filter

In the ensemble Kalman filter with 20 ensemble members, the noise added to the observation is drawn from a zero-mean normal distribution with the following variances

$$\mathbf{R} = \begin{bmatrix} 3 \times 10^{17} & 0 & 0 & 0 & 0 \\ 0 & 27 \times 10^{9} & 0 & 0 & 0 \\ 0 & 0 & 3 \times 10^{5} & 0 & 0 \\ 0 & 0 & 0 & 3 \times 10^{4} & 0 \\ 0 & 0 & 0 & 0 & 30 \end{bmatrix}. \tag{B.6}$$

C APPENDIX

Optimal Operation of an Industrial Batch Crystallizer

Chapter 5 describes the output feedback control of a multi-input multi-output industrial batch crystallizer. This appendix shows the effect of different process actuators on optimal operation of the industrial batch crystallizer. In addition, the optimal input and output profiles obtained when the weight factor of the performance objective is set to 0 and 1.0 are presented.

C.1 The effect of process actuators

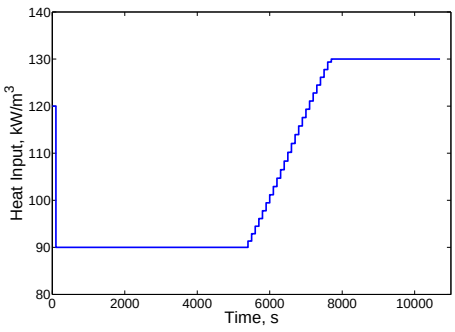

Figure C.1: The optimal heat input profile applied to the industrial crystallizer ($w = 1$). The heat input is the only process actuator.

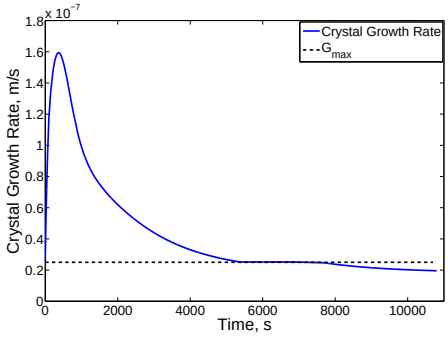

Figure C.2: Simulation results of the output feedback control approach when applied to the industrial crystallizer with one process actuator, viz the heat input; see Figure C.1 ($w = 1$).

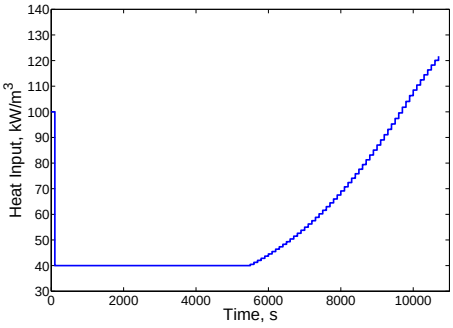

(a) Heat input

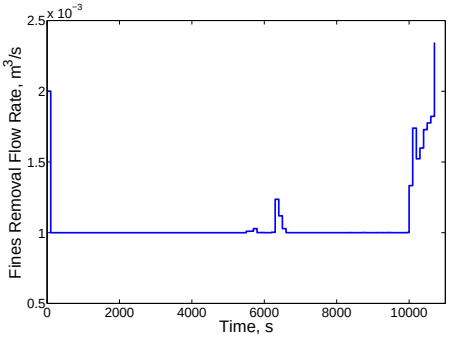

(b) Fines removal flow rate

Figure C.3: The optimal input profiles applied to the industrial crystallizer ($w = 1$).

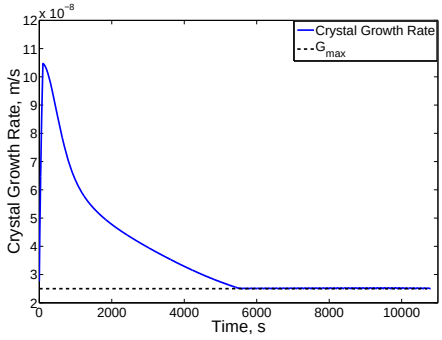

Figure C.4: Simulation results of the output feedback control approach when applied to the industrial crystallizer with two process actuators, viz the heat input and the fines removal flow rate; see Figure C.3 ($w = 1$).

C.2 The effect of performance objective

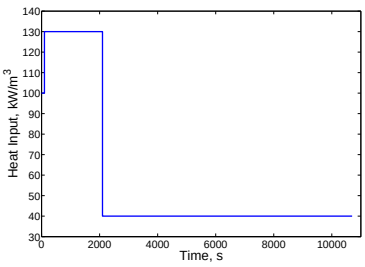

(a) Heat input

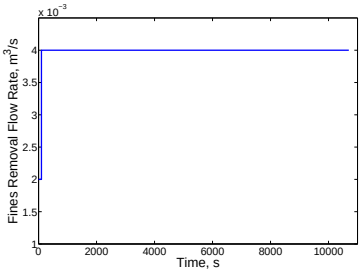

(b) Fines removal flow rate

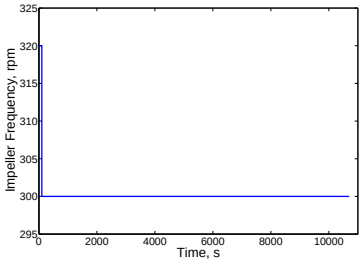

(c) Impeller frequency

Figure C.5: The optimal input profiles applied to the industrial crystallizer ($w = 0$).

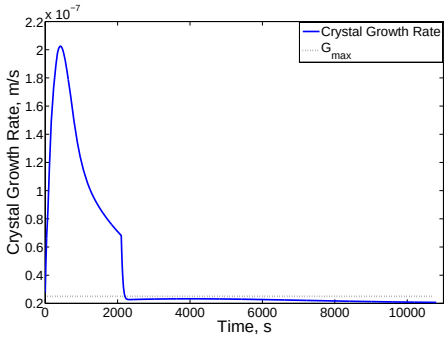

(a) Crystal growth rate profile

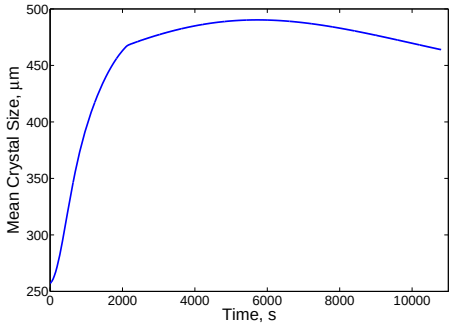

(b) Mean crystal size profile

Figure C.6: Simulation results of the output feedback control approach when applied to the industrial crystallizer ($w = 0$).

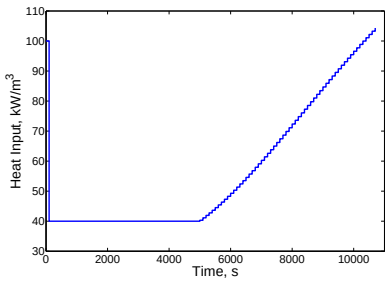

(a) Heat input

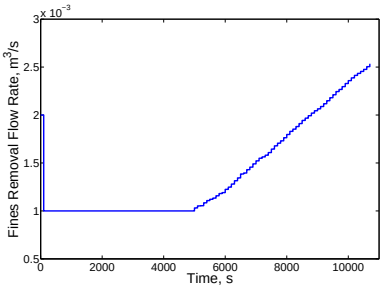

(b) Fines removal flow rate

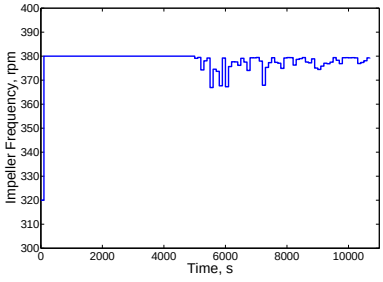

(c) Impeller frequency

Figure C.7: The optimal input profiles applied to the industrial crystallizer ($w = 1.0$).

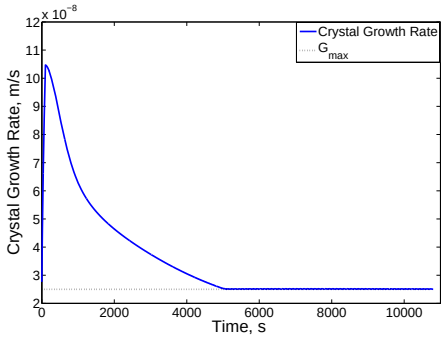

(a) Crystal growth rate profile

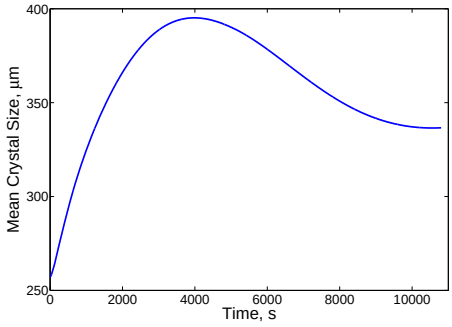

(b) Mean crystal size profile

Figure C.8: Simulation results of the output feedback control approach when applied to the industrial crystallizer ($w = 1.0$).

Bibliography

A. Abbas and J.A. Romagnoli. DCS implementation of optimal operational policies: a crystallisation case study. *International Journal of Computer Applications in Technology*, 25:198–208, 2006.

A.H. Alexopoulos and C.A. Kiparissides. Part II: Dynamic evolution of the particle size distribution in particulate processes undergoing simultaneous particle nucleation, growth and aggregation. *Chemical Engineering Science*, 60:4157–4169, 2005.

A.H. Alexopoulos, A.I. Roussos, and C. Kiparissides. Part I: Dynamic evolution of the particle size distribution in particulate processes undergoing combined particle growth and aggregation. *Chemical Engineering Science*, 59:5751–5769, 2004.

S. Arulampalam, S. Maskell, N. Gordon, and T. Clapp. A tutorial on particle filters for online nonlinear / non-Gaussian Bayesian tracking. *IEEE Transactions on Signal Processing*, 50:174–188, 2002.

T. Bakir, S. Othman, G. Fevotte, and H. Hammouri. Nonlinear observer of crystal-size distribution during batch crystallization. *AIChE Journal*, 52:2188–2197, 2006.

Y. Bard. *Nonlinear Parameter Estimation*. Academic Press, London, United Kingdom, 1974.

S. Barthe and R.W. Rousseau. Utilization of focused beam reflectance measurement in the control of the crystal size distribution in a batch cooled crystallizer. *Chemical Engineering & Technology*, 29:206–211, 2006.

G. Bastin and D. Dochain. *On-line Estimation and Adaptive Control of Bioreactors*. Elsevier, Amsterdam, The Netherlands, 1990.

R.J. Baterham, J.S. Hall, and G. Barton. Pelletizing kinetics and simulation of full scale balling circuits. In *Proceedings of the* 3^{rd} *International Symposium on Agglomeration*, pages A136–A144, Nurnberg, West Germany, 1981.

M.K. Bennett and S. Rohani. Solution of population balance equations with a new combined Lax-Wendroff / Crank-Nicholson method. *Chemical Engineering Science*, 56:6623–6633, 2001.

S. Bermingham. *A Design Procedure and Predictive Models for Solution Crystallization Processes: Development and Application*. Ph.D. Thesis, Delft University of Technology, The Netherlands, 2003.

S. Biagiola and J. Solsona. State estimation in batch processes using a nonlinear observer. *Mathematical and Computer Modelling*, 44:1009–1024, 2006.

S.I. Biagiola and J.L. Figueroa. Application of state estimation based NMPC to an unstable nonlinear process. *Chemical Engineering Science*, 59:4601–4612, 2004.

L.T. Biegler and J.E. Cuthrell. Improved infeasible path optimization for sequential modular simulators II: The optimization algorithm. *Computers and Chemical Engineering*, 9:257–267, 1985.

T. Binder, L. Blank, H.G. Bock, R. Bulirsch, W. Dahmen, M. Diehl, T. Kronseder, W. Marquardt, J.P. Schlöder, and O.V. Stryk. Introduction to model based optimization of chemical processes on moving horizons. Available at: `http://www.mathematik.uni-r.de/Mat8/Blank/Paper/over_01.ps`. Last visited on 21 May 2010, 2001.

M. Birch, S.J. Fussell, P.D. Higginson, N. McDowall, and I. Marziano. Towards a PAT-based strategy for crystallization development. *Organic Process Research & Development*, 9:360–364, 2005.

H.G. Bock and K. Plitt. A multiple shooting algorithm for direct solution of optimal control problems. In *Proceedings of the 9th IFAC World Congress*, Budapest, Hungary, 1984.

Ph. Bogaerts. A hybrid asymptotic-Kalman observer for bioprocesses. *Bioprocess Engineering*, 20:101–113, 1999.

D. Bonvin. Optimal operation of batch reactors - a personal view. *Journal of Process Control*, 8:355–368, 1998.

A. Borissova, S. Khan, T. Mahmud, K.J. Roberts, J. Andrews, P. Dallin, Z. Chen, and J. Morris. In situ measurement of solution concentration during the batch cooling crystallization of l-Glutamic acid using ATR-FTIR spectroscopy coupled with chemometrics. *Crystal Growth & Design*, 9:692–706, 2009.

G.D. Botsaris. *Secondary Nucleation: A Review*. In Industrial Crystallization, J.W. Mullin, Editor, Plenum Press, New York, USA, 1976.

R.D. Braatz. Advanced control of crystallization processes. *Annual Reviews in Control*, 26:87–99, 2002.

R.D. Braatz and S. Hasebe. Particle size and shape control in crystallization processes. In *AIChE Symposium Series: Proceedings of the* 6^{th} *International Conference on Chemical Process Control*, pages 307–327, 2002.

P.N. Brown, A.C. Hindmarsh, and L.R. Petzold. Using krylov methods in the solution of large-scale differential algebraic systems. *SIAM Journal Scientific Computing*, 15:1467–1488, 1994.

G. Burgers, P.J.V. Leeuwen, and G. Evensen. Analysis scheme in the ensemble Kalman filter. *Monthly Weather Review*, 126:1719–1724, 1998.

C.T. Chang and M.A.F. Epstein. Identification of batch crystallization control strategies using characteristic curves. *AIChE Symposium Series*, 78:68–75, 1982.

C.T. Chang and M.A.F. Epstein. Simulation studies of a feedback control strategy for batch crystallizers. *AIChE Symposium Series*, 83:110–119, 1987.

M.Q. Chen, C. Hwang, and Y.P. Shih. A wavelet-Galerkin method for solving population balance equations. *Computers and Chemical Engineering*, 20:131–145, 1996.

T. Chen, J. Morris, and E. Martin. Particle filters for state and parameter estimation in batch processes. *Journal of Process Control*, 15:665–673, 2005.

P.D. Christofides, N. El-Farra, M. Li, and P. Mhaskar. Model-based control of particulate processes. *Chemical Engineering Science*, 63:1156–1172, 2008.

S.H. Chung, D.L. Ma, and R.D. Braatz. Optimal seeding in batch crystallization. *The Canadian Journal of Chemical Engineering*, 77:590–596, 1999.

G. Ciccarella, M. Dalla Mora, and A. Germani. A Luenberger-like observer for nonlinear systems. *International Journal of Control*, 57:537–556, 1993.

C.B.B. Costa and R.M. Filho. Evaluation of optimization techniques and control variable formulations for a batch cooling crystallization process. *Chemical Engineering Science*, 60:5312–5322, 2005.

C.B.B. Costa, M.R.W. Maciel, and R.M. Filho. Considerations on the crystallization modeling: Population balance equation. *Computers and Chemical Engineering*, 31: 206–218, 2007.

J.E. Cuthrell and L.T. Biegler. Simultaneous optimization and solution methods for batch reactor control profiles. *Computers and Chemical Engineering*, 13:49–62, 1989.

S.R. Dash and S. Rohani. Iterative parameter estimation for extraction of crystallization kinetics of potassium chloride from batch experiments. *The Canadian Journal of Chemical Engineering*, 71:539–548, 1993.

P.J. Daudey, G.M. van Rosmalen, and E.I. De Jong. Secondary nucleation kinetics of ammonium sulphate in a cmsmpr crystallizer. *Journal of Crystal Growth*, 99: 1076–1081, 1990.

F. Daum. Nonlinear filters: beyond the Kalman filter. *IEEE A&E Systems Magazine*, 20:57–69, 2005.

R. David, J. Villermaux, P. Marchal, and J.P. Klein. Crystallization and precipitation engineering-IV. Kinetic model of adipic acid crystallization. *Chemical Engineering Science*, 46:1129–1136, 1991.

R. David, A.M. Paulaime, F. Espitalier, and L. Rouleau. Modeling of multiple-mechanism agglomeration in a crystallization process. *Powder Technology*, 130: 338–344, 2003.

F. Deza, D. Bossanne, E. Busvelle, J.P. Gauthier, and D. Rakotopara. Exponential observers for nonlinear systems. *IEEE Transactions on Automatic Control*, 38:482–484, 1993.

M. Diehl, H.G. Bock, J.P. Schloder, R. Findeisen, Z.K. Nagy, and F. Allgower. Real-time optimization and nonlinear model predictive control of processes governed by differential-algebraic equations. *Journal of Process Control*, 12:577–585, 2002.

D. Dochain. State and parameter estimation in chemical and biochemical processes: A tutorial. *Journal of Process Control*, 13:801–818, 2003.

N. Doki, N. Kubota, A. Sato, and M. Yokota. Effect of cooling mode on product crystal size in seeded batch crystallization of potassium alum. *Chemical Engineering Journal*, 81:313–316, 2001.

A.S. Dukhin, P.J. Goetz, and C.W. Hamlet. Acoustic spectroscopy for concentrated polydisperse colloids with low density contrast. *Langmuir*, 12:4998–5003, 1996.

D. Dunuwila and K.A. Berglund. ATR-FTIR spectroscopy for in situ measurement of supersaturation. *Journal of Crystal Growth*, 179:185–193, 1997.

D. Dunuwila, L.B. Caroll, and K.A. Berglund. An investigation of the applicability of attenuated total reflection infrared spectroscopy for measurement of solubility of aqueous citric acid solutions. *Journal of Crystal Growth*, 137:561–568, 1994.

J.W. Eaton and J.B. Rawlings. Feedback control of chemical processes using online optimization techniques. *Computers and Chemical Engineering*, 14:469–479, 1990.

T.F. Edgar, D.M. Himmelblau, and L.S. Lasdon. *Optimization of Chemical Processes*. McGraw-Hill, New York, USA, 2001.

R.A. Eek. *Control and Dynamic Modelling of Industrial Suspension Crystallizers*. Ph.D. Thesis, Delft University of Technology, The Netherlands, 1995.

G. Evensen. Advanced data assimilation for strongly nonlinear dynamics. *Monthly Weather Review*, 125:1342–1354, 1997.

D. Eyre, C.J. Wright, and G. Reuter. Spline-collocation with adaptive mesh grading for solving the stochastic collection equation. *Journal of Computational Physics*, 78:288–304, 1988.

FDA. U.S. Food and Drug Administration. Available at: `http://www.fda.gov/`. Last visited on 24 February 2010.

V.V. Fedorov. *Theory of Optimal Experiments*. Academic Press, New York, USA, 1972.

J.H. Ferziger and M. Peric. *Computational Methods for Fluid Dynamics*. Springer-Verlag, Berlin, Germany, 1996.

G. Févotte. New perspectives for the on-line monitoring of pharmaceutical crystallization processes using in situ infrared spectroscopy. *International Journal of Pharmaceuticals*, 241:263–278, 2002.

B.A. Finlayson. *Nonlinear Analysis in Chemical Engineering*. McGraw-Hill, New York, USA, 1980.

R. Franke, E. Arnold, and H. Linke. HQP: A solver for nonlinearly constrained optimization. *Available at:* `http://www.hqp.sourceforge.net`., Last visited on 10 May 2010, 2005.

M. Fujiwara, P. Shan Chow, D.L. Ma, and R.D. Braatz. Paracetamol crystallization using laser backscattering and ATR-FTIR spectroscopy: Metastability, agglomeration and control. *Crystal Growth & Design*, 2:363–370, 2002.

M. Fujiwara, Z.K. Nagy, J.W. Chew, and R.D. Braatz. First-principles and direct design approaches for the control of pharmaceutical crystallization. *Journal of Process Control*, 15:493–504, 2005.

C. Gahn and A. Mersmann. Theoretical prediction and experimental determination of attrition rates. *Trans IChemE*, 75:125–131, 1997.

C. Gahn and A. Mersmann. Brittle fraction in crystallization processes Part A: Attrition and abrasion of brittle solids. *Chemical Engineering Science*, 54:1273–1282, 1999a.

C. Gahn and A. Mersmann. Brittle fraction in crystallization processes Part B: Growth of fragments and scale-up of suspension crystallizers. *Chemical Engineering Science*, 54:1283–1292, 1999b.

J. Garside. Advances in the characterization of crystal growth. *AIChE Symposium Series*, 80:23–38, 1984.

E. Gatzke and F.J. Doyle. Use of multiple models and qualitative knowledge for on-line moving horizon disturbance estimation and fault diagnosis. *Journal of Process Control*, 12:339–352, 2002.

J.P. Gauthier and A.K. Kupka. Observability and observers for nonlinear systems. *SIAM Journal on Control and Optimization*, 32:975–994, 1992.

F. Gelbard and J.H. Seinfeld. Numerical solution of the dynamical equation for particulate systems. *Journal of Computational Physics*, 28:357–375, 1978.

A. Gerstlauer, A. Mitrovic, S. Motz, and E.D. Gilles. A population model for crystallization processes using two independent particle properties. *Chemical Engineering Science*, 56:2553–2565, 2001.

S. Gillijns, O. Barrero Mendoza, J. Chandrasekar, B.L.R. De Moor, D.S. Bernstein, and A. Ridley. What is the ensemble Kalman filter and how well does it work? In *Proceedings of the American Control Conference*, pages 4448–4453, Minnesota, USA, 2006.

N. Gordon, D. Salmond, and A. Smith. Novel approach to nonlinear / non-Gaussian Bayesian state estimation. *IEE Proceedings F-Radar and Signal Processing*, 140:107–113, 1993.

H. Grön, A. Borissova, and K.J. Roberts. In-process ATR-FTIR spectroscopy for closed-loop supersaturation control of a batch crystallizer producing Monosodium Glutamate crystals of defined size. *Industrial & Engineering Chemistry Research*, 42:198–206, 2003.

R. Gunawan, I. Fusman, and R.D. Braatz. High resolution algorithms for multidimensional population balance equations. *AIChE Journal*, 50:2738–2749, 2004.

T. Gutwald and A. Mersmann. A batch cooling crystallization at constant supersaturation: Technique and experimental results. *Chemical Engineering & Technology*, 13:229–237, 1990.

Y. Hao, Z. Xiong, F. Sun, and X. Wang. Comparison of unscented Kalman filters. In *Proceedings of IEEE International Conference on Mechatronics and Automation*, pages 895–899, Harbin, China, 2007.

E.L. Haseltine and J.B. Rawlings. Critical evaluation of extended Kalman filtering and moving-horizon estimation. *Industrial & Engineering Chemistry Research*, 44: 2451–2460, 2005.

J.E. Helt and M.A. Larson. Effect of temperature on the crystallization of potassium nitrate by direct measurement of supersaturation. *AIChE Journal*, 23:822–830, 1977.

M.W. Hermanto, M.S. Chiu, and R.D. Braatz. Nonlinear model predictive control for the polymorphic transformation of L-Glutamic acid crystals. *AIChE Journal*, 55:2631–2645, 2009.

L. Hlozny, A. Sato, and N. Kubota. On-line measurement of supersaturation during batch cooling crystallization of ammonium alum. *Journal of Chemical Engineering of Japan*, 25:604–606, 1992.

H. Hojjati and S. Rohani. Measurement and prediction of solubility of paracetamol in water-isopropanol mixture. Part 1: Measurement. *Organic Process Research & Development*, 10:1101–1109, 2006.

M.J. Hounslow, R.L. Ryall, and V.R. Marshall. A discretized population balance for nucleation, growth and aggregation. *AIChE Journal*, 34(11):1821–1832, 1988.

P.L. Houtekamer and H.L. Mitchell. Ensemble Kalman filtering. *The Quarterly Journal of the Royal Meteorological Society*, 131:3269–3290, 2005.

Q. Hu, S. Rohani, and A. Jutan. Modelling and optimization of seeded batch crystallizers. *Computers and Chemical Engineering*, 29:911–918, 2005a.

Q. Hu, S. Rohani, and A. Jutan. New numerical method for solving the dynamic population balance equations. *AIChE Journal*, 51(11):3000–3006, 2005b.

Q. Hu, S. Rohani, D.X. Wang, and A. Jutan. Optimal control of a batch cooling seeded crystallizer. *Powder Technology*, 156:170–176, 2005c.

A. Huesman, P. Van den Hof, and A. Stankiewicz. On the essential role of process control in process intensification. In *Proceedings of the* 2^{nd} *European Process Intensification Conference*, pages 1–6, Venice, Italy, 2009.

A. Huesman, O.H. Bosgra, and P. Van den Hof. Towards the systematic design of actuation for process systems. In *Proceedings of the* 9^{th} *International Symposium on Dynamics and Control of Process Systems*, pages 455–460, Leuven, Belgium, 2010.

A.E.M. Huesman, O.H. Bosgra, and P.M.J. Van den Hof. Degrees of freedom analysis of economic dynamic optimal plantwide operation. In *Proceedings of the* 8^{th} *International IFAC Symposium on Dynamics and Control of Process Systems*, pages 165–170, Cancun, Mexico, 2007.

H.M. Hulbert and S. Katz. Some problems in particle technology: A statistical mechanical formulation. *Chemical Engineering Science*, 9:555–574, 1964.

X. Hulhoven, A. Vande Wouwer, and Ph. Bogaerts. Hybrid extended Luenberger-asymptotic observer for bioprocess state estimation. *Chemical Engineering Science*, 61:7151–7160, 2006.

In-Stat. Solid growth in global semiconductor market to continue through 2008. Available at: `http://www.instat.com/index.asp`. Last visited on 15 February 2010.

J.D. Jansen, O.H. Bosgra, and P.M.J. Van den Hof. Model-based control of multiphase flow in subsurface oil reservoirs. *Journal of Process Control*, 18:846–855, 2008.

A.G. Jones. Optimal operation of a batch cooling crystallizer. *Chemical Engineering Science*, 29:1075–1087, 1974.

A.G. Jones. *Crystallization Process Systems*. Butterworth-Heinemann, Oxford, United Kingdom, 2002.

A.G. Jones and J.W. Mullin. Programmed cooling crystallization of potassium sulphate solutions. *Chemical Engineering Science*, 29:105–118, 1974.

S.J. Julier and J.K. Uhlmann. A new extension of the kalman filter to nonlinear systems. In *Proceedings of the* 11^{th} *International Symposium on Aerospace/Defense Sensing, Simulation and Controls*, pages 182–193, Orlando, USA, 1997.

S.J. Julier and J.K. Uhlmann. Unscented filtering and nonlinear estimation. In *Proceedings of the IEEE*, volume 92, pages 401–422, 2004.

S. Kadam, A. Mesbah, E. van der Windt, and H.J.M. Kramer. Rapid online calibration for ATR-FTIR spectroscopy during batch crystallization of Ammonium Sulphate in a semi-industrial scale crystallizer. *Submitted to Chemical Engineering Research and Design*, 2010a.

S. Kadam, E. van der Windt, P.J. Daudy, and H.J.M. Kramer. A comparative study of ATR-FTIR and FT-NIR spectroscopy for the in-situ concentration monitoring during batch cooling crystallization processes. *Crystal Growth & Design*, 10: 2629–2640, 2010b.

A.N. Kalbasenka. *Model-Based Control of Industrial Batch Crystallizers: Experiments on Enhanced Controllability by Seeding Actuation*. Ph.D. Thesis, Delft University of Technology, The Netherlands, 2009.

A.N. Kalbasenka, A.E.M. Huesman, H.J.M. Kramer, and O.H. Bosgra. Controllability analysis of industrial crystallizers. In *Proceedings of the* 12^{th} *International Workshop on Industrial Crystallization*, pages 157–164, Halle, Germany, 2005.

A.N. Kalbasenka, J. Landlust, A.E.M. Huesman, and H.J.M. Kramer. Application of observation techniques in a model predictive control framework of fed-batch crystallization of ammonium sulphate. In *Proceedings of AIChE Spring Meeting*, volume 2, page 227, Orlando, Florida, USA, 2006.

A.N. Kalbasenka, L.C.P. Spierings, A.E.M. Huesman, and H.J.M. Kramer. Application of seeding as a process actuator in a model predictive control framework for fed-batch crystallization of ammonium sulphate. *Particle & Particle Systems Characterization*, 24:40–48, 2007.

R.E. Kalman and R. Bucy. New results in linear filtering and prediction. *Journal of Basic Engineering (ASME)*, 83:98–108, 1961.

R. Kandepu, B. Foss, and L. Imsland. Applying the unscented Kalman filter for nonlinear state estimation. *Journal of Process Control*, 18:753–768, 2008.

S.S. Keerthi and E.G. Gilbert. Optimal infinite-horizon feedback laws for a general class of constrained discrete-time systems: Stability and moving-horizon approximations. *Journal of Optimization Theory and Applications*, 57:265–293, 1988.

B. Koren. A robust upwind discretization method for advection, diffusion and source terms. In C.B. Vreugdenhill and B. Koren, editors, *Numerical methods for advection-diffusion problems*, volume 22, pages 117–138, 1993.

A.D. Krener and A. Isidori. Linearization by output injection and nonlinear observers. *Systems and Control Letters*, 3:47–52, 1983.

A.J. Krener and W. Respondek. Nonlinear observers with linearizable error dynamics. *SIAM Journal on Control and Optimization*, 23:197–216, 1985.

M. Kühberger and A. Mersmann. Improved product quality at a cooling crystallization process by measurement and control of supersaturation. *Trans IChemE*, 75:213–218, 1997.

S. Kumar and D. Ramkrishna. On the solution of population balance equations by discretization-III. Nucleation, growth and aggregation of particles. *Chemical Engineering Science*, 52:4659–4679, 1997.

R. Lakerveld. *Development of a Task-based Design Approach for Solution Crystallization Processes*. Ph.D. Thesis, Delft University of Technology, The Netherlands, 2010.

J. Landlust, A. Mesbah, J. Wildenberg, A.N. Kalbasenka, H.J.M. Kramer, and J.H.A. Ludlage. An industrial model predictive control architecture for batch crystallization. In *Proceedings of the* 17^{th} *International Symposium on Industrial Crystallization*, pages 35–42, Maastricht, The Netherlands, 2008.

Y.D. Lang, A.M. Cervantes, and L.T. Biegler. Dynamic optimization of a batch cooling crystallization process. *Industrial & Engineering Chemistry Research*, 38: 1469–1477, 1999.

L. Lapidus and G.F. Pinder. *Numerical Solution of Partial Differential Equations in Science and Engineering*. Wiley, New York, USA, 1982.

P.A. Larsen, D.B. Patience, and J.B. Rawlings. Industrial crystallization process control. *IEEE Control Systems Magazine*, 26:70–80, 2006.

J.H. Lee and L.N. Ricker. Extended Kalman filter based nonlinear model predictive control. *Industrial & Engineering Chemistry Research*, 33:1530–1541, 1994.

V. Lemesle and J.L. Gouze. A bounded error observer for a class of bioreactor models. In *Proceedings of the* 8^{th} *IFAC Conference on Computer Applications in Biotechnology (CAB8)*, pages 24–27, Quebec, Canada, 2001.

M. Leskens, L.B.M. van Kessel, P.M.J. Van den Hof, and O.H. Bosgra. Nonlinear model predictive control with moving horizon state and disturbance estimation with application to MSW combustion. In *Proceedings of the* 16^{th} *IFAC World Congress*, Prague, Czech Republic, 2005.

R.J. LeVeque. *Finite Volume Methods for Hyperbolic Problems*. Cambridge University Press, New York, USA, 2002.

F. Lewiner, J.P. Klein, F. Puel, and G. Févotte. Online ATR-FTIR measurement of supersaturation during solution crystallization processes. Calibration and applications on three solute/solvent systems. *Chemical Engineering Science*, 56: 2069–2084, 2001.

B.M. Liang, R.W. Hartel, and K.A. Berglund. Growth rate dispersion in seeded batch sucrose crystallization. *AIChE Journal*, 33:2077–2079, 1987.

Y.L.L. Lim, J.M.L. Lann, X.M. Meyer, X. Joulia, G. Lee, and E.S. Yoon. On the solution of population balance equations (PBE) with accurate front tracking methods in practical crystallization processes. *Chemical Engineering Science*, 57: 3715–3732, 2002.

V. Liotta and V. Sabesan. Monitoring and feedback control of supersaturation using ATR-FTIR to produce an active pharmaceutical ingredient of a desired crystal size. *Organic Process Research & Development*, 8:488–494, 2004.

J.D. Litster, D.J. Smit, and M.J. Hounslow. Adjustable discretized population balance for growth and aggregation. *AIChE Journal*, 41:591–603, 1995.

Y. Liu and I.T. Cameron. A new wavelet-based adaptive method for solving population balance equations. *Powder Technology*, 130:181–188, 2003.

I. Livk, M. Gregorka, and C. Pohar. Identification of batch crystallization processes (estimate of kinetic parameters of sodium-perborate precipitation). *Computers and Chemical Engineering*, 19:S241–S246, 1995.

L. Ljung. *System Identification: Theory for the User*. Prentice Hall, Englewood Cliffs, New Jersey, USA,, 1987.

D. Luenberger. Observing the state of a linear system. *IEEE Transactions on Military Electronics*, 8:74–80, 1964.

A. Ma, D.K. Tafti, and R.D. Braatz. High resolution simulation of multidimensional crystal growth. *Industrial & Engineering Chemistry Research*, 41:6217–6223, 2002a.

D.L. Ma and R.D. Braatz. Robust identification and control of batch processes. *Computers and Chemical Engineering*, 27:1175–1184, 2003.

D.L. Ma, S.H. Chung, and R.D. Braatz. Worst-case performance analysis of optimal batch control trajectories. *AIChE Journal*, 45:1469–1476, 1999.

D.L. Ma, D.K. Tafti, and R.D. Braatz. Optimal control and simulation of multidimensional crystallization process. *Computers and Chemical Engineering*, 26: 1103–1116, 2002b.

A. Mahoney and D. Ramkrishna. Efficient solution of population balance equations with discontinuities by finite elements. *Chemical Engineering Science*, 57: 1107–1119, 2002.

A. Maisels, F.E. Kruis, and H. Fissan. Direct Monte Carlo simulations of coagulation and aggregation. *Journal of Aerosol Science*, 30:S417–S418, 1999.

M. Mangold, A. Buck, R. Schenkendorf, C. Steyer, A. Voigt, and K. Sundmacher. Two state estimators for the barium sulfate precipitation in a semi-batch reactor. *Chemical Engineering Science*, 64:646–660, 2009.

P. Marchal, R. David, J.P. Klein, and J. Villermaux. Crystallization and precipitation engineering-I. An efficient method for solving population balances in crystallization with agglomeration. *Chemical Engineering Science*, 43:59–67, 1990.

H.B. Matthews. *Model Identification and Control of batch Crystallization for an Industrial Chemical System*. Ph.D. Thesis, University of Wisconsin-Madison, USA, 1997.

H.B. Matthews and J.B. Rawlings. Batch crystallization of a photochemical: Modeling, control and filtration. *AIChE Journal*, 44:1119–1127, 1998.

B. Mayrhofer and J. Nyvlt. Programmed cooling of batch crystallizations. *Chemical Engineering and Processing*, 24:217–220, 1988.

D. Meimaroglou, A.I. Roussos, and C. Kiparissides. Part IV: Dynamic evolution of the particle size distribution in particulate processes. a comparative study between Monte Carlo and the generalized method of moments. *Chemical Engineering Science*, 61:5620–5635, 2006.

A. Menon. *A Task Based Design Procedure and Modeling Approaches for Industrial Crystallization Processes*. Ph.D. Thesis, Delft University of Technology, The Netherlands, 2006.

A. Mersmann. *Crystallization Technology Handbook*. Marcel Dekker, Inc., New York, USA, 2001.

A. Mersmann, R. Sangl, M. Kind, and J. Pohlisch. Attrition and secondary nucleation in crystallizers. *Chemical Engineering & Technology*, 11:80–88, 1988.

A. Mesbah, H.J.M. Kramer, A.E.M. Huesman, and P.M.J. Van den Hof. A control oriented study on the numerical solution of the population balance equation for crystallization processes. *Chemical Engineering Science*, 64:4262–4277, 2009.

A. Mesbah, A.E.M. Huesman, H.J.M. Kramer, and P.M.J. Van den Hof. A comparison of nonlinear observers for output feedback model-based control of seeded batch crystallization processes. *Submitted to Journal of Process Control*, 2010a.

A. Mesbah, A.E.M. Huesman, H.J.M. Kramer, Z.K. Nagy, and P.M.J. Van den Hof. Real-time control of a semi-industrial fed-batch evaporative crystallizer using different direct optimization strategies. *AIChE Journal (doi 10.1002/aic.12366)*, In Press, 2010b.

A. Mesbah, J. Landlust, A.E.M. Huesman, H.J.M. Kramer, P.J. Jansens, and P.M.J. Van den Hof. A model-based control framework for industrial batch crystallization processes. *Chemical Engineering Research and Design*, 88:1223–1233, 2010c.

A. Mesbah, J. Landlust, C. Versteeg, A.E.M. Huesman, H.J.M. Kramer, J.H.A. Ludlage, and P.M.J. Van den Hof. Model-based optimal control of industrial batch crystallizers. *Computer-Aided Chemical Engineering*, 28:1563–1568, 2010d.

A. Mesbah, Z.K. Nagy, A.E.M. Huesman, H.J.M. Kramer, and P.M.J. Van den Hof. Nonlinear model-based control of a semi-industrial batch crystallizer using a population balance modeling framework. *Submitted to IEEE Transactions on Control Systems Technology*, 2010e.

S.M. Miller and J.B. Rawlings. Model identification and control strategies for batch cooling crystallizers. *AIChE Journal*, 40:1312–1327, 1994.

H. Muhr, R. David, J. Villermaux, and P.H. Jezequel. Crystallization and precipitation engineering-VI. Solving population balance in the case of the precipitation of silver bromide crystals with high primary nucleation rates by using the first order upwind differentiation. *Chemical Engineering Science*, 51:309–319, 1996.

J.W. Mullin. *Crystallization*. Butterworth-Heinemann, Oxford, United Kingdom, 2001.

J.W. Mullin and J. Nyvlt. Programmed cooling of batch crystallizers. *Chemical Engineering Science*, 26:369–377, 1971.

K.R. Muske and J.B. Rawlings. Model predictive control with linear models. *AIChE Journal*, 39:262–287, 1993.

A.S. Myerson. *Handbook of Industrial Crystallization*. Butterworth-Heinemann, Boston, USA, 2002.

Z.K. Nagy. Model based robust control approach for batch crystallization product design. *Computers and Chemical Engineering*, 33:1685–1691, 2009.

Z.K. Nagy and R. Braatz. Robust nonlinear model predictive control of batch processes. *AIChE Journal*, 49:1776–1786, 2003.

Z.K. Nagy and R.D. Braatz. Open-loop and closed-loop robust optimal control of batch processes using distributional and worst-case analysis. *Journal of Process Control*, 14:411–422, 2004.

Z.K. Nagy, F. Allgower, R. Franke, A. Frick, and B. Mahn. Efficient tool for nonlinear model predictive control of batch processes. In *Proceedings of the* 12^{th} *Mediterranean Conference on Control and Automation*, Kusadasi, Turkey, 2004.

Z.K. Nagy, B. Mahn, R. Franke, and F. Allgower. Evaluation study of an efficient output feedback nonlinear model predictive control for temperature tracking in an industrial batch reactor. *Control Engineering Practice*, 15:839–850, 2007.

Z.K. Nagy, J.W. Chew, M. Fujiwara, and R.D. Braatz. Comparative performance of concentration and temperature controlled crystallizations. *Journal of Process Control*, 18:399–407, 2008.

A.M. Neumann. *Characterizing Industrial Crystallizers of Different Scale and Type*. Ph.D. Thesis, Delft University of Technology, The Netherlands, 2001.

A.M. Neumann and H.J.M. Kramer. A comparative study of various size distribution measurement systems. *Particle & Particle Systems Characterization*, 19:17–27, 2002.

M. Nicmanis and M.J. Hounslow. Finite element methods for steady-state population balance equations. *AIChE Journal*, 44:2258–2272, 1998.

H. Nijmeijer and A.J. van der Schaft. *Nonlinear Dynamical Control Systems*. Springer, New York, USA, 1990.

S.M. Nowee, A. Abbas, and J.A. Romagnoli. Optimization in seeded cooling crystallization: A parameter estimation and dynamic optimization study. *Chemical Engineering and Processing*, 46:1096–1106, 2007.

R. Oliveira, E.C. Ferreira, and S. Feyo de Azevedo. Stability dynamics of convergence and tuning of observer-based kinetic estimators. *Journal of Process Control*, 12:311–323, 2002.

R. ÓMeadhra. *Modeling of the Kinetics of Suspension Crystallizers: A New Model for Secondary Nucleation*. Ph.D. Thesis, Delft University of Technology, The Netherlands, 1995.

W. Ostwald. Studien über die bildung und umwandlung fester körper. *Zeitschrift für Physilische Chemie*, 22:289–330, 1897.

E.P.K. Ottens, A.H. Janse, and E.J. de Jong. Secondary nucleation in a stirred vessel cooling crystallizer. *Journal of Crystal Growth*, 13 / 14:500–505, 1972.

W. Paengjuntuek, A. Arpornwichanop, and P. Kittisupakorn. Product quality improvement of batch crystallizers by a batch-to-batch optimization and nonlinear control approach. *Chemical Engineering Journal*, 139:344–350, 2008.

B. Palwe, M. Chivate, and N. Tavare. Growth kinetics of ammonium nitrate crystals in a draft tube baffled batch crystallizer. *Industrial and Engineering Chemistry Process Design and Development*, 24:914–919, 1985.

S. Patankar. *Numerical Heat Transfer and Fluid Flow*. Hemisphere Publishing, New York, USA, 1980.

M. Perrier, S. Feyo de Azevedo, E.C. Ferreira, and D. Dochain. Tuning of observer-based estimators: theory and application to the on-line estimation of kinetic parameters. *Control Engineering Practice*, 8:377–388, 2000.

R. Ploß and A. Mersmann. A new model of the effect of stirring intensity on the rate of secondary nucleation. *Chemical Engineering & Technology*, 11:137–146, 1989.

J. Pohlisch and A. Mersmann. The influence of stress and attrition on crystal size distribution. *Chemical Engineering & Technology*, 11:40–49, 1988.

J. Prakash, S.C. Patwardhan, and S.L. Shah. Constrained state estimation using the ensemble Kalman filter. In *Proceedings of the American Control Conference*, pages 3542–3547, Seattle, USA, 2008.

PRLog. Global pharmaceutical market forecast to 2012. Available at: `http://www.prlog.org/`. Last visited on 15 February 2010.

S. Qamar and G. Warnecke. Numerical solution of population balance equations for nucleation, growth and aggregation processes. *Computers and Chemical Engineering*, 31:1576–1589, 2007.

S. Qamar, M.P. Elsner, I.A. Angelov, G. Warnecke, and A. Seidel-Morgenstern. A comparative study of high resolution schemes for solving population balances in crystallization. *Computers and Chemical Engineering*, 30:1119–1131, 2006.

Y. Qiu and Å.C. Rasmuson. Estimation of crystallization kinetics from batch cooling experiments. *AIChE Journal*, 40:799–812, 1994.

C.C. Qu and J. Hahn. Process monitoring and parameter estimation via unscented kalman filtering. *Journal of Loss Prevention in the Process Industries*, In Press, 2008.

D. Ramkrishna. The status of population balances. *Reviews in Chemical Engineering*, 3(1):49–95, 1985.

D. Ramkrishna. *Population Balances: Theory and Applications to Particulate Systems in Engineering*. Academic Press, San Diego, USA, 2000.

A.D. Randolph and M.A. Larson. *Theory of Particulate Processes*. Academic Press, San Diego, USA, 1988.

C.V. Rao and J.B. Rawlings. Constrained process monitoring: Moving-horizon approach. *AIChE Journal*, 48:97–109, 2002.

C.V. Rao, J.B. Rawlings, and D.Q. Mayne. Constrained state estimation for nonlinear discrete-time systems: Stability and moving horizon approximations. *IEEE Transactions on Automatic Control*, 48:246–258, 2003.

J.B. Rawlings and B.R. Bakshi. Particle filtering and moving horizon estimation. *Computers and Chemical Engineering*, 30:1529–1541, 2006.

J.B. Rawlings, S.M. Miller, and W.R. Witkowski. Model identification and control of solution crystallization processes: A review. *Industrial & Engineering Chemistry Research*, 32:1275–1296, 1993.

S. Rigopoulos and A.G. Jones. Finite-element scheme for solution of the dynamic population balance equation. *AIChE Journal*, 49:1127–1139, 2003.

R.I. Ristić, J.N. Sherwood, and T. Shripathi. Strain variation in the growth sectors of potash alum single crystals and its relationship to growth rate dispersion. *Journal of Crystal Growth*, 102:245–248, 1990.

D.G. Robertson, J.H. Lee, and J.B. Rawlings. A moving horizon-based approach for least-squares state estimation. *AIChE Journal*, 42:2209–2224, 1996.

B. Roffel and B. Betlem. *Process Dynamics and Control: Modeling for Control and Prediction*. John Wiley & Sons Ltd, West Sussex, England, 2006.

A. Romanenko and J.A. Castro. The unscented filter as an alternative to the EKF for nonlinear state estimation: A simulation case study. *Computers and Chemical Engineering*, 28:347–355, 2004.

A. Romanenko, L.O. Santos, and P.A. Afonso. Unscented Kalman filtering of a simulated pH system. *Industrial & Engineering Chemistry Research*, 43:7531–7538, 2004.

A.I. Roussos, A.H. Alexopoulos, and C. Kiparissides. Part III: Dynamic evolution of the particle size distribution in batch and continuous particulate processes: A Galerkin on finite elements approach. *Chemical Engineering Science*, 60:6998–7010, 2005.

D. Rozier, F. Birol, E. Cosme, P. Brasseur, J.M. Brankart, and J. Verron. A reduced order Kalman filter for data assimilation in physical oceanography. *SIAM Review*, 49:449–465, 2007.

A. Rueda, S. Cristea, C.D. Prada, and R.M.C. De Keyser. Non-linear predictive control for a distillation column. In *Proceedings of the* 44^{th} *IEEE Conference on Decision and Control, and the European Control Conference*, pages 5156–5161, Seville, Spain, 2005.

A. Sandu and C. Borden. A framework for the numerical treatment of aerosol dynamics. *Applied Numerical Mathematics*, 45:475–497, 2003.

D. Sarkar, S. Rohani, and A. Jutan. Multi-objective optimization of seeded batch crystallization processes. *Chemical Engineering Science*, 61:5282–5295, 2006.

T.S. Schei. On-line estimation for process control and optimization applications. *Journal of Process Control*, 18:821–828, 2008.

G.A.F. Seber and C.J. Wild. *Nonlinear Regression*. Wiley Series in Probability and Mathematical Statistics, Wiley, New York, USA, 1989.

M. Sheikhzadeh, M. Trifkovic, and S. Rohani. Real-time optimal control of an anti-solvent isothermal semi-batch crystallization process. *Chemical Engineering Science*, 63:829–839, 2007.

M. Sheikhzadeh, M. Trifkovic, and S. Rohani. Adaptive MIMO neuro-fuzzy logic control of a seeded and an unseeded anti-solvent semi-batch crystallizer. *Chemical Engineering Science*, 63:1261–1272, 2008.

D. Shi, P. Mhaskar, N.H. El-Farra, and P.D. Christofides. Predictive control of crystal size distribution in protein crystallization. *Nanotechnology*, 16:S562–S574, 2005.

L.L. Simon, Z.K. Nagy, and K. Hungerbuhler. Model based control of a liquid swelling constrained batch reactor subject to recipe uncertainties. *Chemical Engineering Journal*, 153:151–158, 2009.

T. Söderström and P. Stoica. *System Identification*. Prentice-Hall, New York, USA, 1989.

M. Song and X.J. Qiu. Alternative to the concept of the Interval of Quiescence (IQ) in the Monte Carlo simulation of population balances. *Chemical Engineering Science*, 54:5711–5715, 1999.

M. Soroush. State and parameter estimations and their applications in process control. *Computers and Chemical Engineering*, 23:229–245, 1998.

B. Srinivasan, S. Palanki, and D. Bonvin. Dynamic optimization of batch processes I. Characterization of the nominal solution. *Computers and Chemical Engineering*, 27:1–26, 2003.

M. Srinivasarao, S.C. Patwardhan, and R.D. Gudi. From data to nonlinear predictive control. 2. Improving regulatory performanace using identified observers. *Industrial & Engineering Chemistry Research*, 45:3593–3603, 2006.

M.J. Tenny and J.B. Rawlings. Efficient moving horizon estimation and nonlinear model predictive control. In *Proceedings of the American Control Conference*, pages 4475–4480, Alaska, USA, 2002.

T. Togkalidou, M. Fujiwara, S. Patel, and R.D. Braatz. Solute concentration prediction using chemometrics and ATR-FTIR spectroscopy. *Journal of Crystal Growth*, 231:534–543, 2001.

T. Togkalidou, H.H. Tung, Y. Sun, A. Andrews, and R.D. Braatz. Solute concentration prediction for pharmaceutical crystallization processes using robust chemometrics and ATR-FTIR spectroscopy. *Organic Process Research & Development*, 6:317–322, 2002.

J. Valappil and C. Georgakis. Systematic estimation of state noise statistics for extended Kalman filters. *AIChE Journal*, 46:292–308, 2000.

A.E.D.M. van der Heijden and G.M. van Rosmalen. *Industrial Mass Crystallization*. In Handbook of Crystal Growth, D.T.J. Hurle, Editor, Elsevier, The Netherlands, 1993.

A.E.D.M. van der Heijden, J.P. van der Eerden, and G.M. van Rosmalen. The secondary nucleation rate: A physical model. *Chemical Engineering Science*, 49: 3103–3113, 1994.

R. van der Merwe and E. Wan. The square-root unscented Kalman filter for state and parameter estimation. In *Proceedings of IEEE International Conference on Acoustics, Speech and Signal Processing*, pages 3461–3464, Salt Lake City, USA, 2001.

B. van Leer. Upwind-difference methods for aerodynamic problems governed by the Euler equations. In *Lectures in applied mathematics*, volume 22, pages 327–336, American Mathematical Society, 1985.

H.K. Versteeg and W. Malalasekera. *An Introduction to Computational Fluid Dynamics. The Finite Volume Method*. Longman Group, Malaysia, 1995.

F. Wang and K.A. Berglund. Monitoring pH swing crystallization of nicotinic acid by the use of attenuated total reflection Fourier transform infrared spectroscopy. *Industrial & Engineering Chemistry Research*, 39:2101–2104, 2000.

G.M. Westhoff. *Design and Analysis of Suspension Crystallizers. Aspects of Crystallization Kinetics and Product Quality*. Ph.D. Thesis, Delft University of Technology, The Netherlands, 2002.

D.I. Wilson, M. Agarwal, and D. Rippin. Experiences implementing the extended Kalman filter on an industrial batch reactor. *Computers and Chemical Engineering*, 22:1653–1672, 1998.

J.A. Wojcik and A.G. Jones. Dynamics and stability of continuous MSMPR agglomerative precipitation: Numerical analysis of the dual particle co-ordinate model. *Computers and Chemical Engineering*, 22:535–545, 1998.

M. Wulkow, A. Gerstlauer, and U. Nieken. Modeling and simulation of crystallization processes using PARSIVAL. *Chemical Engineering Science*, 56:2575–2588, 2001.

W. Xie, S. Rohani, and A. Phoenix. Extended Kalman filter based nonlinear geometric control of a seeded batch cooling crystallizer. *Canadian Journal of Chemical Engineering*, 80:167–172, 2002.

Z.Q. Yu, J.W. Chew, P.S. Chow, and R.B.H. Tan. Recent advances in crystallization control - An industrial perspective. *Chemical Engineering Research and Design*, 85: 893–905, 2007.

M. Zeitz. Extended Luenberger observer for nonlinear systems. *Systems and Control Letters*, 9:149–156, 1987.

G.P. Zhang and S. Rohani. Online optimal control of a seeded batch cooling crystallizer. *Chemical Engineering Science*, 58:1887–1896, 2003.

G.X. Zhou, M. Fujiwara, X.Y. Woo, E. Rusli, H.H. Tung, C. Starbuck, O. Davidson, Z. Ge, and R.D. Braatz. Direct design of pharmaceutical antisolvent crystallization through concentration control. *Crystal Growth & Design*, 6:892–898, 2006.

R.C. Zumstein and R.W. Rousseau. Growth rate dispersion by initial growth rate distributions and growth rate fluctuations. *AIChE Journal*, 33:121–129, 1987.

List of Symbols

Roman

B	nucleation rate, $[\#/m^4 s]$
B_0	nucleation rate of crystals of infinitesimal size, $[\#/m^3 s]$
b	nucleation rate exponent
C	solute concentration, $[wt.\%]$
C^*	saturation concentration of solute, $[wt.\%]$
e	measurement error
G	crystal growth rate, $[m/s]$
g	crystal growth rate exponent
H	enthalpy, $[J]$
h	specific enthalpy, $[J/kg]$
h_{cf}	crystal classification function
K_k	observer gain
k	the Boltzmann constant, $[J/K]$
k_b	nucleation rate constant, $[\#/m^4]$
k_g	crystal growth rate constant, $[m/s]$
k_v	volume shape factor
L	crystal characteristic size, $[m]$
L_0	mean of a log-normal distribution, $[m]$
L_m	arithmetic mean of a size class, $[m]$
M	molecular weight, $[kg/mole]$
m	mass, $[kg]$
N	number of ensemble members
N_i	number of inlet streams

N_{imp}	impeller frequency, $[rpm]$
N_m	number of measured variables
N_o	number of outlet streams
N_p	number of parameters
N_s	number of solid phases
N_v	number of measurements
$n(L,t)$	crystal number density, $[\#/m^4]$
n_p	number of nodal points
$\mathbf{O}$	observability space
$\mathbf{O_c}$	observability codistribution
P	asymptotic parameter covariance matrix
Q	net rate of heat addition, $[J/s]$
$\bar{Q}_3$	normalized cumulative volume density distribution, $[m^3/m^3]$
$q_3(L)$	crystal volume density, $[1/m]$
S	supersaturation, $[wt.\%]$
T	temperature, $[K]$
T_C	control horizon
T_P	prediction horizon
t	time, $[s]$
u	input variable
V	crystallizer volume, $[m^3]$
V_θ	parameter covariance matrix
v_k	vector of measurement noise
$\mathsf{W_e}$	covariance matrix of the measurement noise
w	nonnegative weight factor
w_k	vector of process noise
x	state variable
y	measured variable
Z	arrival cost term
z	algebraic variable

Greek

δ	Dirac delta function
σ_g	geometric standard deviation of a log-normal distribution
ϵ	liquid fraction
$\mathcal{L}$	running cost term
μ_i	i^{th} moment of the crystal size distribution, $[m^i/m^3]$
μ_c	chemical potential
$\mathcal{M}$	terminal cost term
$\mathcal{N}$	normal distribution
ν	stoichiometric coefficient
ρ	density, $[kg/m^3]$
θ	vector of model parameters
θ_0	vector of true system parameters
$\phi(r_i^+)$	flux limiting function
ϕ_H	enthalpy flux, $[J/s]$
ϕ_m	mass flow rate, $[kg/s]$
ϕ_{mol}	molar flow rate, $[mole/s]$
ϕ_V	volumetric flow rate, $[m^3/s]$
$\varphi(L)$	basis function
Ψ	performance objective
$\omega(L)$	weight function
χ_p^2	chi-distribution

Subscripts

0	initial value
est	estimated value
$grow$	growth
in	inlet
L	liquid phase
$meas$	measured value
$nucl$	nucleation
opt	optimal value

out	outlet
s	solid phase
V	vapor phase

Abbreviations

ATR-FTIR	Attenuated Total Reflection Fourier Transform InfraRed
CPU	Central Processing Unit
CSD	Crystal Size Distribution
DAE	Differential Algebraic Equation
DCS	Distributed Control System
EKF	Extended Kalman Filter
ELO	Extended Luenberger Observer
EnKF	Ensemble Kalman Filter
EPSAC	Extended Predictive Self-Adaptive Control
FBRM	Focused Beam Reflectance Measurement
FEM	Finite Element Method
FDA	Food and Drug Administration
FVM	Finite Volume Method
GFEM	Galerkin's Finite Element Method
MHE	Moving Horizon Estimator
MIMO	Multi-Input Multi-Output
MOC	Method of Characteristics
NLP	NonLinear Programming
NMPC	Nonlinear Model Predictive Controller
NRMSE	Normalized Root Mean Squared Error
OCFE	Orthogonal Collocation on Finite Elements
ODE	Ordinary Differential Equation
OPC	OLE - Object Linking and Embedding - for Process Control
PB	Population Balance
PBE	Population Balance Equation
PID	Proportional Integral Derivative
PLS	Partial Least Squares
SISO	Single-Input Single-Output

SQP	Sequential Quadratic Programming
UKF	Unscented Kalman Filter
WLS	Weighted Least Squares

List of Publications

Journal papers

A. Mesbah, Z.K. Nagy, A.E.M. Huesman, H.J.M. Kramer, and P.M.J. Van den Hof. Nonlinear model-based control of a semi-industrial batch crystallizer using a population balance modeling framework. Submitted to *IEEE Transactions on Control Systems Technology* (September 2010).

S. Kadam, A. Mesbah, E. van der Windt, and H.J.M. Kramer. Rapid online calibration for ATR-FTIR spectroscopy during batch crystallization of Ammonium Sulphate in a semi-industrial scale crystallizer. Submitted to *Chemical Engineering Research and Design* (May 2010).

A. Mesbah, A.E.M. Huesman, H.J.M. Kramer, and P.M.J. Van den Hof. A comparison of nonlinear observers for output feedback model-based control of seeded batch crystallization processes. Submitted to *Journal of Process Control* (April 2010).

A. Mesbah, A.E.M. Huesman, H.J.M. Kramer, Z.K. Nagy, and P.M.J. Van den Hof (2010). Real-time control of a semi-industrial fed-batch evaporative crystallizer using different direct optimization strategies. *AIChE Journal*, In Press (doi 10.1002 / aic.12366).

A. Mesbah, J. Landlust, A.E.M. Huesman, H.J.M. Kramer, P.J. Jansens, and P.M.J. Van den Hof (2010). A model-based control framework for industrial batch crystallization processes. *Chemical Engineering Research and Design*, 88, 1223-1233.

A. Mesbah, J. Landlust, C. Versteeg, A.E.M. Huesman, H.J.M. Kramer, J.H.A. Ludlage, and P.M.J. Van den Hof (2010). Model-based optimal control of industrial batch crystallizers. *Computer-Aided Chemical Engineering*, 28, 1563-1568.

A. Mesbah, H.J.M. Kramer, A.E.M. Huesman, and P.M.J. Van den Hof (2009). A control oriented study on the numerical solution of the population balance equation for crystallization processes. *Chemical Engineering Science*, 64, 4262-4277.

F. Abdolahi Demneh, A. Mesbah, and A. Jaberi (2008). Comparative evaluation of natural gas pipeline simulators. *PetroMin*, 4, 6-8.

F.A. Demneh and A. Mesbah (2008). The effect of kinetic energy change on flow in gas pipelines. *Journal of Hydrocarbon Processing*, 5, 1-4.

A.N. Ajah, A. Mesbah, J. Grievink, P.M. Herder, P.W. Falcao, and S. Wennekes (2008). On the robustness, effectiveness and reliability of chemical and mechanical heat pumps for low-temperature heat source district heating: A comparative simulation-based analysis and evaluation. *Journal of Energy*, 33, 908-929.

A.N. Ajah, A. Mesbah, J. Grievink, A.C. Patil, P.M. Herder, and R.M. Stikkelman (2007). Conceptual design of a hythane based infrastructure system for combined power and district heat production. *Chemical Engineering Transactions*, 12, 459-464.

F. Abdolahi, A. Mesbah, R.B. Boozarjomehry, and W.Y. Svrcek (2007). The effect of major parameters on simulation results of gas pipelines. *International Journal of Mechanical Sciences*, 49, 989-1000.

A. Mesbah and F. Abdolahi (2006). Natural gas supply cut-off in gas distribution networks. *PetroMin*, 5, 34-36.

Conference proceedings

A. Mesbah, A.E.M. Huesman, H.J.M. Kramer, and P.M.J. Van den Hof (2010). Nonlinear state estimation for closed-loop control of batch crystallization processes. In *Proceedings of the* 9^{th} *International Symposium on Dynamics and Control of Process Systems*, Leuven, Belgium, 371-376.

S. Kadam, A. Mesbah, E. van der Windt, and H.J.M. Kramer (2009). Application of ATR FTIR spectroscopy for in-situ concentration measurements of Ammonium Sulphate on laboratory and pilot plant scales. In *Proceedings of the* 16^{th} *Bremen International Workshop on Industrial Crystallization*, Lappeenranta, Finland, 69-76.

A. Mesbah, A.N. Kalbasenka, A.E.M. Huesman, H.J.M. Kramer, and P.M.J. Van den Hof (2008). Real-time dynamic optimization of batch crystallization processes. In *Proceedings of the* 17^{th} *IFAC World Congress*, Seoul, South Korea, 3246-3251.

A. Mesbah, J. Landlust, A.E.M. Huesman, H.J.M. Kramer, P.M.J. Van den Hof, and P.J. Jansens (2008). Model-based optimal operation of seeded batch crystallization processes. In *Proceedings of the* 17^{th} *International Symposium on Industrial Crystallization*, Maastricht, The Netherlands, 721-728.

J. Landlust, A. Mesbah, J. Wildenberg, A.N. Kalbasenka, H.J.M. Kramer, and J. Ludlage (2008). An industrial model predictive control architecture for batch crystallization. In *Proceedings of the* 17^{th} *International Symposium on Industrial Crystallization*, Maastricht, The Netherlands, 35-42.

A. Mesbah, A.N. Kalbasenka, A.E.M. Huesman, H.J.M. Kramer, P.J. Jansens, and P.M.J. Van den Hof (2007). Real-time dynamic optimization of crystal yield in fed-batch evaporative crystallization of ammonium sulphate. In *Proceedings of the* 14^{th} *Bremen International Workshop on Industrial Crystallization*, CapeTown, South Africa, 81-88.

A.N. Ajah, A. Mesbah, J. Grievink, P.W. Falcao, and S. Wennekes (2006). Comparative simulation-based analysis and evaluation of chemical and mechanical

heat pumps for low temperature heat source upgrading. In *Proceedings of the* 17^{th} *International Congress of Chemical and Process Engineering*, Prague, Czech Republic.

Keynote lectures

Nonlinear state estimation for closed-loop control of batch crystallization processes. *The* 9^{th} *International Symposium on Dynamics and Control of Process Systems*, Leuven, Belgium, July 2010.

Abstracts

A. Mesbah, A.E.M. Huesman, H.J.M. Kramer, and P.M.J. Van den Hof (2010). Real-time control of industrial batch crystallizers: A model-based control approach. *The* 29^{th} *Benelux Meeting on Systems and Control*, Heeze, The Netherlands.

A. Mesbah, A.E.M. Huesman, H.J.M. Kramer, and P.M.J. Van den Hof (2010). Stochastic nonlinear observers for industrial seeded batch crystallization processes. *AIChE Spring Meeting*, San Antonio, USA.

H.J.M. Kramer, A. Mesbah, and R. Lakerveld (2010). Developments in control and design of industrial crystallization processes: Intensification of crystallization processes. *Jahrestreffen des Fachausschusses Kristallisation*, Magdeburg, Germany.

A. Mesbah, I. Mora Moreno, A.E.M. Huesman, H.J.M. Kramer, and P.M.J. Van den Hof (2009). Design of nonlinear observers for model-based control of seeded batch crystallization processes. *Netherlands Process Technology Symposium 2009*, Veldhoven, The Netherlands.

A. Mesbah, I. Mora Moreno, A.E.M. Huesman, H.J.M. Kramer, and P.M.J. Van den Hof (2009). Stochastic observers for industrial seeded batch crystallization processes. *The* 28^{th} *Benelux Meeting on Systems and Control*, Spa, Belgium.

A. Mesbah, M. Teki, H.J.M. Kramer, A.E.M. Huesman, and P.M.J. Van den Hof (2008). Dynamic modeling of downstream units of an industrial crystallization-based separation process. *Netherlands Process Technology Symposium 2008*, Veldhoven, The Netherlands.

A. Mesbah, A.E.M. Huesman, and P.M.J. Van den Hof (2008). Real-time optimal control of a seeded fed-batch evaporative crystallizer. *The* 27^{th} *Benelux Meeting on Systems and Control*, Heeze, The Netherlands.

A. Mesbah, A.E.M. Huesman, H.J.M. Kramer, and P.M.J. Van den Hof (2007). Dynamic optimization of crystal yield in evaporative crystallization of ammonium sulphate. *Netherlands Process Technology Symposium 2007*, Veldhoven, The Netherlands.

A. Mesbah and L.C.P Spierings (2007). Model predictive control of a seeded batch crystallizer. *The* 26^{th} *Benelux Meeting on Systems and Control*, Lommel, Belgium.

Summary

Optimal Operation of Industrial Batch Crystallizers
A Nonlinear Model-based Control Approach

Ali Mesbah

Batch crystallization is extensively employed in the chemical, pharmaceutical, and food industries to separate and purify high value-added chemical substances. Despite their widespread application, optimal operation of batch crystallizers is particularly challenging. The difficulties primarily result from the complexity of process models, uncertainties in crystallization kinetics, sensor limitations for reliable measurement of process variables, and the inherent process uncertainties that may impair the effectiveness of advanced control strategies. In addition, the optimal operation of batch crystallizers is often hampered by lack of process actuators. Nonetheless, advanced control of batch crystallizers offers ample opportunities to effectively respond to the dynamic market demands of crystalline products. This is to realize the stringent product specifications of the consumer-driven market as enhancing the process productivity.

In this thesis, a nonlinear model-based control approach is developed to address the inherent challenges of real-time control of existing industrial batch crystallizers. The primary requirement on the control approach is its applicability to a wide range of industrial batch crystallizers. This calls for a generic modeling framework, which allows us to describe the dynamics of diverse crystallization kinetics of any complexity and to incorporate the effect of different actuating mechanisms. The generic framework of the process model necessitates the use of computationally efficient model solution techniques and optimization strategies to ensure the real-time feasibility of the control approach. In addition, model imperfections, along with process disturbances, make the online adaptation of model predictions a prerequisite for successful application of the control approach.

In pursuit of the research objective, the contributions of this thesis are structured in three major directions:

1. *Population balance modeling*: A full population balance modeling framework is developed as the cornerstone of the control approach. The inference of model parameters from experimental data is discussed. In addition, various population balance solution methods are investigated in terms of the performance requirements essential for online control applications.

2. *Nonlinear state estimation*: The effectiveness of several nonlinear state estimation techniques for output feedback control of industrial batch crystallizers is evaluated. The ability of the state estimators in coping with model imperfections and process uncertainties is examined.

3. *Real-time dynamic optimization*: The feasibility of real-time dynamic optimization of population balance models is explored using different direct optimization strategies.

The research program leads to the design of an output feedback nonlinear model-based control approach. The distinct contribution of this thesis lies in using a full population balance modeling framework, which is essential for the applicability of the control approach to a wide range of industrial batch crystallizers. It is shown that the numerical difficulties of solving the population balance equation can be alleviated by using high order finite volume methods combined with a flux limiting function. These numerical techniques facilitate efficient model solution, which is a prerequisite for real-time control. In addition, it is shown that the multiple shooting strategy is well-suited for online dynamic optimization of population balance models.

Successful application of the control approach is demonstrated by several simulation case studies, viz a single-input single-output semi-industrial crystallizer and a multi-input multi-output industrial crystallizer. It is illustrated that model imperfections and process uncertainties are largely detrimental to the performance of the nonlinear model-based controller. The performance inadequacy can be effectively compensated for by using an extended Kalman filter or an unscented Kalman filter with time-varying process noise covariance matrix. The real-time performance of the control approach is demonstrated experimentally by several implementations on a semi-industrial crystallizer. It is shown that lack of actuation may obstruct the optimal operation of industrial crystallizers throughout the entire batch run.

Samenvatting

Optimale Operatie van Industriële Batch Kristallisatoren
Een Niet-lineaire Modelgebaseerde Regelmethode

Ali Mesbah

Batch kristallisatie wordt intensief gebruikt in de chemische-, farmaceutische- en voedselindustrie om hoogwaardige chemische substanties te scheiden en te zuiveren. Ondanks wijdverspreide toepassing van batch kristallisatoren is de optimale operatie ervan nog steeds bijzonder uitdagend. De moeilijkheden komen vooral voort uit de complexe modellen van het proces, de onzekerheden in de kristallisatiekinetiek, en de beperkingen van sensoren om betrouwbaar procesvariabelen te meten, hetgeen een hoge onzekerheid in de waarde van de procesvariabelen ten gevolge heeft en daarmee de effectiviteit van geavanceerde regeltechnieken kan verminderen. Bovendien wordt soms de optimale operatie van batch kristallisatie belemmerd door het ontbreken van voldoende mogelijkheden om het proces aan te sturen. Desondanks bieden geavanceerde regelstrategieën voor batch kristallisatie voldoende mogelijkheden om effectief te reageren op de dynamische vraag van de markt in kristallijneproducten. Toepassing van een goede regelstrategie is namelijk essentieel om de strikte, door de consument opgelegde, productspecificaties te realiseren of om de productiecapaciteit van het proces te verhogen.

Dit proefschrift richt zich op de uitdagingen die real-time regeling van bestaande industriële batch kristallisatoren met zich mee brengen. Een van de belangrijkste vereisten voor een regelstrategie is de toepasbaarheid op een breed scala aan industriële batch kristallisatoren. Dit vraagt om een generiek raamwerk voor de modelvorming van het proces, die detoepassing van diverse kristallisatie kinetiek modellen toelaat, ongeacht de complexiteit hiervan en die tevens in staat is om de effecten van verschillende aansturingsmechanismen te beschrijven. Deze generieke modelvormingsstructuur van het proces maakt noodzakelijkerwijs gebruik van efficiënte numerieke oplos- en optimalisatiemethoden om de real-time implementatie van de regelstrategie in de praktijk mogelijk te maken. Bovendien zorgen de onvolmaaktheden in het model, evenals verstoringen en onzekerheden in het proces, ervoor dat voor een succesvolle implementatie van de regelmethode de processmodelgebaseerde voorspelling voortdurend moet worden aangepast aan deze veranderingen.

De belangrijkste bijdragen van dit onderzoek aan de realisering van deze onderzoeksdoelstelling kunnen als volgt worden gestructureerd:

1. *Beschrijving van de populatiebalans*: Een robuste en efficiënte oplossingsmethode voor een volledige populatiebalans is ontwikkeld als hoeksteen van de regelstrategie. Tevens wordt aandacht besteed aan het schatten van modelparameters uit gemeten experimentele data. Daarnaast zijn diverse methoden om de populatiebalansvergelijking op te lossen onderzocht met het oog op de prestatie-eisen die van essentieel belang zijn voor toepassing in online regelsystemen.

2. *Niet-lineaire toestandsschatting*: De effectiviteit van meerdere technieken voor niet-lineaire toestandsschatting voor toepassing in terugkoppelregelsystemen voor industriële batch kristallisatoren is geëvalueerd. Naast hun geschiktheid voor toepassing in 'open-loop' werd de geschiktheid van de toestandsschatters onderzocht op hun vermogen om te gaan met modelonvolmaaktheden en procesonzekerheden.

3. *Real-time dynamische optimalisatie*: De haalbaarheid van een real-time dynamische optimalisatie voor op de populatiebalans gebaseerde modellen is onderzocht met verschillende optimalisatiestrategieën.

Het onderzoeksprogramma heeft geleid tot het ontwerp van een niet-lineaire modelgebaseerde uitgangsteruggekoppelde regelmethode. De duidelijk zichtbare bijdrage van dit proefschrift ligt in het gebruik van een raamwerk voor het oplossen van de volledige populatiebalansvergelijking, wat essentieel is voor de toepassing van de regelstrategie voor een breed scala aan industriële batch kristallisatoren. Aangetoond wordt dat numerieke problemen tijdens het oplossen van de populatiebalansvergelijking kunnen worden aangepakt met een eindige volumemethode van hoge orde in combinatie met een functie voor de limitering van de flux. Deze numerieke technieken vergemakkelijken het efficiënt oplossen van het model, wat een eerste vereiste is voor een real-time regeling. Bovendien is aangetoond dat de 'multiple shoot' strategie uitstekend geschikt is voor online dynamische optimalisatie van populatiebalansmodellen.

De succesvolle toepassing van de regelmethode is gedemonstreerd in meerdere simulatiestudies, namelijk met een semi-industriële kristallisator met een 'SISO' (een ingang, een uitgang) regeling en een industriële kristallisator met een 'MIMO' (meerdere ingangen, meerdere uitgangen) regeling. Er wordt duidelijk gehoond dat modelonvolmaaktheden en procesonzekerheden zeer nadelig zijn voor de prestaties van de niet-lineaire modelgebaseerde regelaar. Deze ongeschiktheid kan echter effectief worden gecompenseerd door het gebruik van een uitgebreide Kalman filter of een 'unscented' Kalman filter met een op tijdsafhankelijke procesruis gebaseerde covariantiematrix. De real-time prestaties van de regelmethode zijn experimenteel gedemonstreerd op een semi-industriële kristallisator. Aangetoond is dat door een gebrek aan sturingsmechanismen de optimale operatie van een industrieel kristallisatieproces kan worden belemmerd gedurende de gehele batch run.

Curriculum Vitae

Ali Mesbah was born on April 5, 1983 in Tehran, Iran. After graduating from secondary school in 2000, he started the bachelor's program in Chemical Engineering at University of Tehran. He obtained his B.Sc. degree in 2004 and moved to the Netherlands to follow the master's program in Chemical Engineering at Delft University of Technology. His M.Sc. research work, advised by Professor F. Kapteijn, was done in the field of catalysis engineering. During his master's program, he carried out an internship project at AKZO NOBEL Chemicals Research and Technology in Arnhem, the Netherlands.

In August 2006, Ali started his doctoral research at the Delft Center for Systems and Control and the Process and Energy Laboratory under the supervision of Professor P.M.J. Van den Hof. The primary focus of his research was the investigation of opportunities for optimal operation of industrial batch crystallizers. During his PhD, he received the DISC certificate for following the graduate course program at the Dutch Institute of Systems and Control. He also took a visiting period at Loughborough University, the United Kingdom.

Since August 2010, Ali has been working as a postdoctoral researcher at the Delft Center for Systems and Control. His main research interests are dynamic modeling of chemical processes, dynamic optimization, and identification for control.